Model-Based Building Performance

Evaluation and Diagnosis

Xu Xinhua

A thesis submitted in partial fulfillment of the requirements

for the Degree of Doctor of Philosophy

Department of Building Services Engineering

The Hong Kong Polytechnic University

April 2005

CERTIFICATE OF ORIGINALITY

The research described in this thesis is the original work except the sources quoted. It was carried out at the Department of Building Services Engineering, The Hong Kong Polytechnic University under the supervision of Prof. Shengwei Wang and Dr. Jianlei Niu.

Xu Xinhua

Department of Building Services Engineering

The Hong Kong Polytechnic University

Hong Kong, P.R. China

April 2005

ABSTRACT

Abstract of thesis entitled: Model-Based Building Performance Evaluation and Diagnosis

Submitted by   :   Xu Xinhua

For the degree of   :   Doctor of Philosophy

at The Hong Kong Polytechnic University in April, 2005.

Effective and efficient performance diagnosis and evaluation at the building level is important and practical with easily available measurements at the building level in most contemporary buildings. This thesis presents a systematic methodology for building performance evaluation and diagnosis viewing building system as a whole. This methodology involves the development of a building global performance evaluation tool and practical strategy and approach for practical applications using the evaluation tool. The evaluation tool includes a simplified building energy model and a consolidation AHU model. The simplified building energy model is developed for thermal energy consumption prediction. And the consolidation AHU model is developed to represent all the installed AHU systems for performance prediction of air side systems. With the performance prediction using the tool, a performance signature-based diagnosis strategy is developed for performance diagnosis, and a performance evaluation approach is developed to assess the energy efficiency of alternative strategies for building retrofitting and upgrading.

The simplified building energy model is a hybrid model, which is the compounding of physically described simplified models of building envelopes and a partially data driven simplified model of internal mass which possesses physical meanings. The parameters of the

simplified model of building envelope (3R2C model) are identified using genetic algorithm (GA) method based on frequency response characteristic analysis. The parameters of the simplified model of internal mass (2R2C) are identified using short-term monitoring operation data based on a GA estimator. The validation shows that the simplified building energy model, which was trained with short-term monitoring operation data, can be extended to dynamically and reliably predict the thermal energy consumption under different operation and weather conditions. To make the modeling process and calibration against monitored data much easier, a consolidation AHU model is presented to represent all the installed AHU systems for airside electricity consumption estimation of all AHU systems. The model was validated in a real building system of good accuracy.

Based on the building global performance evaluation tool, a performance signature-based diagnosis strategy is presented for performance diagnosis. Cooling energy consumption is chosen as an important indicator for energy performance diagnosis. The diagnosis process using the strategy shows that the causes resulting in the "measured" cooling energy consumption deviating from the baseline can be identified qualitatively and quantitatively by comparing the observed performance signatures of the "measured" cooling energy consumption with characteristic performance signatures. The diagnosed causes are beneficial for further investigations of building system.

A performance evaluation approach, which is also based on the building global performance evaluation tool, is presented to assess the energy efficiency of alternative control strategies for decision-making of building retrofitting and upgrading measures. The approach uses the building global performance evaluation tool for performance prediction. Then, an enthalpy

bin method is used to divide predicted performance into a series of enthalpy bins to facilitate evaluation for practical applications. The test in a high rising commercial office building in Hong Kong shows that the approach can effectively evaluate the energy performance of alternative fresh air control strategies at different enthalpy bins. The test also shows that the approach can provide the best combination of alternative basis control strategies for maximum electricity consumption saving. In this study, the optimal fresh air control strategy can save electricity consumption significantly than separate basic control strategies. The approach can provide decision making of system retrofitting to exert the maximum potentials of using fresh air efficiently for electricity consumption savings.

ACKNOWLEDGEMENTS

LIST OF FIGURES

LIST OF TABLES

NOMENCALTURE

A,B,C,D	transmission matrix element
A,B,C,D,G ,H	coefficient matrix
ACT	adaptive comfort temperature
A_{pf}	total projected area of a window (m^2)
a	thermal diffusivity or coefficient
b,c,d	CTF coefficients or coefficients
Bin	enthalpy bin (-)
c	air specific heat ($kJ/(kg\ ℃)$) or coefficient
C	thermal capacitance
CPS	characteristic performance signatures (%)
C_P	specific heat ($Jkg^{-1}K^{-1}$)
d_f	difference between the two maximum fitness values
D	design
DCV	demand controlled ventilation
DN	the day number in the year (*DN*=1 for the 1st January)
DVR	minimum fresh air flow rate demanded (l/s)
e	the equation of time (hour)
E	electricity consumption, energy consumption (kWh)
En, h	enthalpy (kJ/kg)
f	fitness function
$f(\lambda)$	polynomial
F	Vector
$g(\lambda)$	polynomial
G	*s*-transfer function
h	heat transfer coefficient ($Wm^{-2}K^{-1}$)
I	solar radiation (Jm^{-2})
I_0	hourly extraterrestrial radiation incident on a horizontal surface (Whm^{-2})
I_{sc}	solar constant (1370 Whm^{-2})
J	objective function

K	thermal transmittance ($Wm^{-2}K^{-1}$) or ratio of diffuse solar radiation to global solar radiation (-)
K_t	ratio of global solar radiation to extraterrestrial radiation
L	thickness (m) or local latitude (degree)
Lamda	matrix
M	transmission matrix
Meas	measured or measurement
M_{ij}	the *i*-th row and *j*-th column element of matrix ***M***
M	matrix
N	power (*kW*) or number of frequency points
OPS	observed performance signature (%)
$p(\lambda)$	polynomial
P	pressure (*Pa*) or actual number of occupants
PL	phase lag (*rad*)
q	heat flow (Wm^{-2})
Q	cooling/ heating load or heat (*kW*)
$Q(\lambda)$	polynomial
R	thermal resistance (m^2KW^{-1}) or parameter
Res	residual
R_p	fresh air requirement per person (*l/s*)
s	Laplace variable or roots
SHGC	solar heat gain coefficient for direct normal radiation (-)
$SHGC_D$	solar heat gain coefficient for diffusive solar radiation (-)
Sign	performance signatures (%)
Sim	Simulation
t	time (second or hour)
T	temperature (℃ or K)
T, ***T****(t)*	temperature state vector
TX1(t)	temperature response function of a unit ramp excitation (℃ or K)
TY1(t)	temperature response function of a unit ramp excitation (℃ or K)
TZ1(t)	temperature response function of a unit ramp excitation (℃ or K)
TX	temperature response factor of a unit triangle pulse (℃ or K)
TY	temperature response factor of a unit triangle pulse (℃ or K)

TZ	temperature response factor of a unit triangle pulse ($°C$ or K)
$\boldsymbol{u}, \boldsymbol{u}(t)$	temperature input vector
U_0	overall coefficient of heat transfer (U-factor), $W/(m^2 K)$
v	volumetric flow rate (m^3/s)
W	Weighting factor
x	location (m)
X	external thermal response factor ($Wm^{-2}K^{-1}$)
Y	cross thermal response factor ($Wm^{-2}K^{-1}$)
Z	internal thermal response factor ($Wm^{-2}K^{-1}$)
$|\bullet|$	amplitude ($Wm^{-2}K^{-1}$) or absolute value
$\sum$	summation or tilt angle of surface from horizontal

Greek symbols

α	coefficient or solar altitude angle at given time (degree)
β_i	the i-th element of coefficient vector
$\boldsymbol{\beta}$	coefficient vector
λ	thermal conductivity ($Wm^{-1}K^{-1}$)
ρ	density (kgm^{-3})
ω	frequency ($rad\ s^{-1}$)
Δ	time interval (*second* or *hour*), enthalpy interval
ε	hemispherical emittance of surface
ε_f	threshold value (-)
η	slope of excitation function, efficiency
ϕ	height of a unit triangle pulse or solar azimuth (degree)
τ	time (s)
φ	dimensionless pressure drop (-)
ψ	dimensionless flow rate (-) or surface azimuth (degree)
δ	solar inclination (degree)
ω	hour angle (degree)
γ	surface solar azimuth (degree)

θ	incident angle (degree)

Subscripts

act	actual
Att	attenuator
CAV	CAV system
Coil	cooling coil
conv	convective heat
D	design
Duct	air duct
ei	associated with exterior wall at the *i*-th orientation
equip	equipments
est	estimated
glob	global
dif	diffusive
dn	direct normal
fr	fresh air
Fil	filter
h	enthalpy (*kJ/kg*)
H	horizontal
i,k,m,n	integer count or time level
im	associated with building internal mass
in	inside or indoor
In	input power, input electricity consumption
la	latent cooling load
light	lighting
mix	mixed air
Me	mechanical output power, mechanical energy consumption
n	associated with thermal comfort
occup	occupants
out	outside
r	associated with radiation
recy	recycle air

rf	associated with roof
rtn	return air
sol	associated with solar air temperature
sup	supply air
sen	sensible cooling load
set	static pressure setpoint
Tol	total
V	vertical
VAV	VAV system
Virtual	irtual AHU, virtual VAV
win	windows
X,Y,Z	associated with external, across and internal heat conduction

Supercripts

'	associated with simplified 3R2C model
AM	associated with amplitude of frequency characteristic
i,j,n,k,N	integer count
in	inside or indoor
PL	associated with phase lag of frequency characteristic
out	outside
T	transpose of matrix

MODEL-BASED BUILDING PERFORMANCE EVALUATION AND DIAGNOSIS

Table of Contents

Page

CHAPTER 1 INTRODUCTION

1.1 Motive

The buildings sector consumes over a third of the total US energy budget [Energy Information Administrative 1991]. Energy audit studies [Yik 1997] show that air conditioning is the dominant energy end-use in commercial buildings in Hong Kong, often responsible for more than 50% of the annual electricity consumption in the buildings.

However, excessive energy is consumed in building system and HVAC systems because they often fail to operate as intended, after a period of operation even with correct commissioning [Deng and Burnett 1997, House and Kelly 1999, Liu and Song et al. 2002]. Comfort problems often occur simultaneously. These failures may be due to inappropriate temperature set points, poor outside air damper control, as well as sensor drifts etc. Proper operation of building system can lead to improved occupant comfort and health, improved energy efficiency, longer life cycle of equipments, reduced maintenance costs, and reduced unscheduled equipment shut down time, etc.

Theoretical studies and experimental investigations have demonstrated that building energy consumption can often be reduced by 20% [Kissock 1993, Claridge and Liu et al. 1996, Claridge and Culp et al. 2000] and sometimes by up to 50% [Liu and Athar et al. 1994], and most of the building comfort problems can be solved simultaneously [Deng and Liu 1998]. Optimizing operation of building energy

systems and correcting system control and mechanical faults is one of the most cost effective engineering practices available.

However, detecting and diagnosing system faults, correcting system faults, and optimizing building system operation have always been a difficult engineering challenge. Many investigators have focused on fault detection and diagnosis methods and development of intelligent optimal control methods for end users [Lee and Park et al. 1996, Liu and Dexter 2001, Yoshida and Kumar et al 2001, Wang and Wang 2002, Norford and Wright et al. 2002, Wang and Xiao 2004, Lee and House et al. 2004]. These methods holds great potential for the next generation of building automation systems and have found very limited in contemporary building systems since they are still very expensive to implement and subsequently identify system faults. In many building systems, there are not enough sensors installed at the component level of the HVAC terminals to provide enough information for these technology implementations. Moreover, some sensors needed to be installed are not used for control purposes. For example, for the supply air temperature control of AHU, the water flow meter is almost unwanted, which provides important assistance for AHU faults detection and diagnosis.

However, at the building level, Kilowatt meter is always needed to measure the total electricity consumption, and the cooling/heating energy consumption can often be measured at the central plant. Therefore, an important step is to develop cost effective technologies for system faults and inefficiency identification at the building

level, and demonstrate the benefits of these technologies to building owners and engineers. These cost effective technologies should make the optimization of system operation and correction of system faults a business as usual practice. For some large complex that includes several major parts for different usage, such as tower buildings for offices, and block building for commercial center, all the parts are served by a centralized HVAC plant [HK-BEAM Society 2003]. To charge the tenants of different part, a sub-metering system is often needed to measure the cooling/heating energy consumption or/and electricity consumption for different parts. For the case, it also provides important information at the sub building/system level for operation optimization and fault detection and diagnosis. Of course, in few building systems, enough sensors are installed at the building system level and the component level of the HVAC terminals to provide enough information for performance evaluation and diagnosis. For the case, it's more meaningful to evaluate and diagnosis building performance at the building system level and then track down to the component levels.

To optimize system operation and diagnose faults, baseline energy consumption is needed for reference. Energy consumption can be outputs of simulation programs, measurements in field sites, or outputs of regression models. Available simulation tools include detailed whole building simulations, such as DOE2 [Lawrence Berkeley Laboratory 1982] and BLAST [Building Systems Laboratory 1999], detailed system simulations HVACSIM+ [Clark 1985], EnergyPlus [Crawley 2000] etc. To estimate energy consumption, those models have to be calibrated accurately. Unfortunately,

Experience of some researchers shows that differences of 50% or more between simulation results based on design data and measured consumption are not unusual [Liu and Claridge et al. 2003]. Some simple regression models are also developed to predict baseline or expected energy consumption [Ruch and Chen et al. 1993, Reddy and Claridge 1994, Yik and Burnett et al. 1995, Katipamula 1996, Reddy and Kissock et al. 1998]. However, the regression models cannot predict the energy performance when the control strategy is changed or operation conditions are different because the regression models cannot represent the dynamic behaviors of the building systems physically.

Therefore, reference models which can predict dynamic energy consumption robustly are highly of desire. Systematic methods are also significantly needed for building performance evaluation and diagnosis with reference models.

1.2 Literature review

1.2.1 Systematic method

Building performance evaluation and diagnosis can be used investigate and analyze problems with systems and equipments that are performed during the everyday operation and monitoring [Claridge and Liu et al. 1999, Haves 1999]. The building system or the facilities can operate as intended a higher percentage of the total run time if operational problems in the systems can be found, located and fixed in time. Properly operating HVAC system in buildings can lead to improved occupant

comfort and health, improved energy efficiency, etc.

Top-down and bottom-up approaches

Top-down and bottom-up approaches are commonly used for diagnostic reasoning [IEA Annex 25 1996, Piette and Gartland et al. 1998, House and Kelly 1999]. Top-down approach is a kind of analysis method to reason possible lower-level causes of malfunction or degradation which lead to the higher-level performance degradation or abnormal performance with the performance measurements from higher levels. On the contrary, bottom-up approach uses performance indices at lower-levels to detect and diagnosis problems and then propagates the problems up to higher levels to determine impacts on the performance of higher levels. If the impacts are considered to be large or potentially large, correcting the problem would be given a high priority. If the impact is considered to be small, the decision may be to do nothing at this time. Performance measurements at intermediate levels can be used in a top-down approach to isolate faults at lower levels, and also in a bottom-up approach to determine impacts of faults at the building level.

Figure 1.1 shows top-down and bottom-up approaches to diagnostic reasoning for whole building system, which specially focus on HVAC system. The whole building is viewed as a large system which provides comfortable, safe and productive environment for occupancy to live, work, shop and entertain, etc. The function of the whole building is carried out by the sub-system comprised of building envelope, facility management, lighting system, central cooling system and conditioned air

distribution system, etc. Air condition system is the core of buildings which can

provide satisfactory indoor air quality to keep occupancy vibrant and productive.

However, it costs most of the total building energy consumption and the initial

investment is also large. Therefore, the problems related to HVAC system can result in

serious consequences including increasing energy costs, occupant discomfort, poor

productivity, health problems and increased maintenance costs etc.
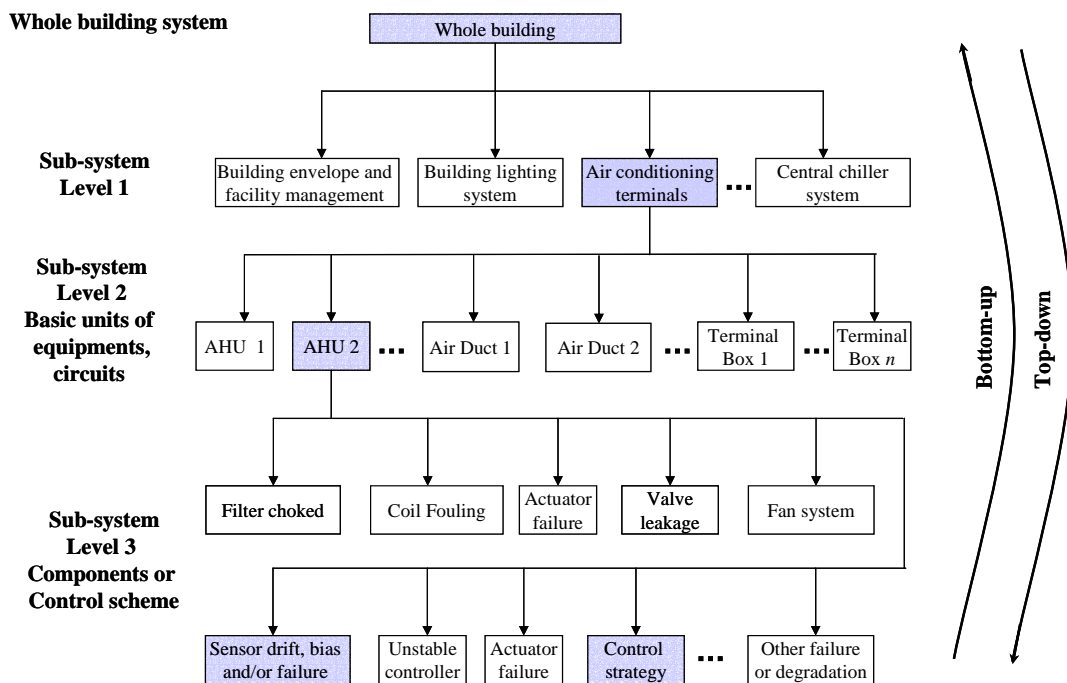
Figure 1.1 Top-down and bottom-up approaches of diagnosis for building system

Diagnosis process

Ordinarily, symptom is viewed as difference or relative difference between the

expected value (prediction) and the actual measurements exceeding a certain

threshold. The representation of symptoms mostly depends on modeling which may

be based on mathematical models which are based on physical laws or empirical or

others. The determination of symptom raises the important issue of how to determine the threshold value when a performance measure exceeds or falls short of expectations. In the case of whole building level or level 1 of the subsystem, the expectation can be the daily, weekly or monthly cooling energy consumption or electricity consumption, etc. For instance, if electricity consumption exceeds 5% of the expectation [Claridge and Liu et al. 1999], then occurs the fault related to the symptom, which indicates the operation of the building system violates one or more rules for normal operating behavior and the system fails to meet expectations.

Models of concern

Measurements on the whole building level, such as heating/cooling energy consumption, electricity consumption, return air temperature, etc, may be examined in an attempt to evaluate building performance or to identify failures in building system and HVAC system [Claridge and Liu et al. 1999, Yu and Paassen 2002, Liu and Claridge et al. 2002]. Measurements at the different level in the subsystem may also provide indices to evaluate different subsystem performance or to identify degradations. Therefore, building energy models and various energy models at different levels play very important roles to provide expected operations as benchmark to evaluate actual operations. In this study, building energy models and AHU energy models are much concerned, which are briefly reviewed as follows.

1.2.2 Building energy reference models

At the building level as a whole process, many researchers have developed various reference models (load models or energy consumption models) for load prediction or cost saving estimations. These models can be categorized into physical models, data driven models, and gray models.

1.2.2.1 Physical models

Physical modeling, also called forward modeling [ASHRAE 1997], begins with a description of the building system or component of interest and defines the building being modeled according to its physical description. Mostly simulation models are based on first principles. The simulation model is necessary to be calibrated according to the previous performance, the parameters of which are adjusted to minimize the difference between the predicted and the measured performance over a selected period. Then the calibrated simulation model is used to calculate the current intended performance of the building. Comparison of the actual and intended performance can be made either during commissioning or during routine operation. The compared variables can be cooling/heating load, energy consumption, peak demand, comfort conditions, etc on time-scales ranging from hours to weeks, or to months/years. The publicly used simulation models are either detailed first principles models, such as DOE-2 [Lawrence Berkeley Laboratory 1982, Ed Kidd et al. 2001], BLAST [Building Systems Laboratory 1999], EnergyPlus [Crawley and Drury 2000], or simplified first principles models, such as HVACSIM+ [NTIS 1986], TRNSYS [Kelin SA *et al* 1990],

AIRMODEL [Giebler and Liu et al. 1998] which was used by Claridge and Liu et al. [1998] to diagnose building malfunction.

However, a large number of parameters are needed as inputs for the simulation models. The process of collecting a physical description is time consuming, labor intensive, and probably does not cost effective, or is almost impossible for some cases (thermal properties of furniture, partitions etc.). In the modeling process, many indefinitive variables are usually assumed as constants. Unsuitable assumptions can make the model deviate, thus decrease the confidence of the model. Furthermore, the calibration process is also labor intensive and not efficient [Rabl 1988]. Experience of some researchers shows that differences of 50% or more between simulation results based on design data and measured consumption are not unusual [Liu and Claridge et al. 2003].

1.2.2.2 Data driven models

Data driven models, also called inverse models [ASHRAE 1997], are based on the empirical behavior of the building as they relate to one or more driving forces or the behavior of similar buildings. They consist of benchmarking models [Akbari and Eto et al. 1993], steady state inverse models [Ruch and Chen et al. 1993; Reddy and Claridge 1994] and dynamic state inverse models [Subbarao and Burch et al. 1990, Minoru and Charles et al. 1995, Kalogirou and Neocleous et al. 1997, Dhar and Reddy et al. 1999]

Benchmarking models

Benchmarking is one type of data driven models. The performance of the building in question is compared to that of similar buildings using a database of the actual performance of a statistically selected sample of comparable buildings. The comparison is usually made in terms of whole building electricity and fuel consumption [Akbari and Eto et al. 1993, EIA 1995, Energy User News 1995, Piette et al. 2001]. The annual energy use per unit floor area in a building, often referred to as the normalized energy consumption (NEC), the energy use intensity (EUI), or the normalized annual consumption (NAC) [Zmeureanu 1990, 1992, Ruch and Claridge 1993], is a commonly used building energy performance indicator.

Although the use of a single control parameter, such as NEC, would be simple and would allow flexibility in design and operation of buildings for compliance with energy performance requirement, it would offer little help to building owners/operators in detecting and diagnosing inefficiency or faults and identifying required improvement measures when buildings fail to comply with the requirement. More limitations of these benchmarking for buildings are that comprehensive comparison data sets have to be established and the reliability of assessment according to the comparison result is reduced greatly if prerequisites such as building type, floor area and geographical location are different, moreover activities in different building differ greatly. For instance, it's meaningless to compare two same supermarket building with more and less customers respectively because the energy

consumptions depend on the situation of business.

Inverse models

Inverse models are based on empirical behaviors of building as they relate to one or more force(s). This approach is commonly referred to as system identification, parameter identification. In this modeling approach, a structure or physical configuration of the building or system is assumed first and then important parameters are identified with operation data by statistical analysis or regression analysis. Such models include steady state and dynamic state.

Steady state inverse models

Many researchers have developed the simplest steady state inverse models, i.e., univariate multiple parameters models by performing regression analysis on monthly utility consumption data against average billing period temperature [Fels 1986, Fels and Goldberg 1986, Ruch and Claridge 1991, Thamilseran and Haberl 1995]. The advantage of these simplest models is that their use can be easily automated and applied to large numbers of buildings where monthly utility billing data and average daily temperature for the building period are available. These simplest models can also be applied to daily data to compensate for differences in weekday and weekend use [Claridge and Haberl et al. 1992]. Multivariable regression techniques allow analysts to investigate the influence of more than one independent variable (such as outdoor air temperature, humidity, solar radiation, etc.) on building energy use [Ruch

and Chen et al. 1993, Reddy and Claridge 1994, Katipamula 1996, Reddy and Kissock et al. 1998]. In fact, multiple regression modeling can lead both to improper interpretation of the relative importance of the various physical regression parameters and to unstable regression coefficients because some variables are intercorrelated (e.g., dry air temperature, solar radiation and humidity). Ruch and Chen [1993], Reddy and Claridge [1994] applied principle component analysis (PCA) method to reduce the collinearities among the regression variables, which can produce a more reliable model than MLR (multiple linear regression) analysis and offer more insights into the environment and operation driving forces that influence energy consumption in commercial buildings.

These steady state inverse models can reflect the influences of outdoor air temperature, humidity, solar radiation, etc., on the energy consumption. However, they cannot be used for performance evaluation when the system control strategy is changed in light of the steady state characteristics. They are also not suitable for performance diagnosis if the control strategy changes or the indoor operation conditions differ.

Dynamic state inverse models

Dynamic inverse models are capable of capturing dynamic such as mass dynamics and better suited to handle intercorrelated forcing functions or independent parameters. Examples of dynamic inverse models include autoregressive moving average (ARMA) models [Reddy [1989, Subbarao and Burch 1990], Fourier series

models [Dhar and Reddy et al. 1998, 1999] and artificial neural networks.

Autoregressive moving average (ARMA) models assume a linear relationship between the present and lagged values of the response variable and those of the driving terms. These models are helpful for only short term predictions based on long term historic data. Therefore, they found a wide use in thermal storage and predictive control applications. Reddy [1989] used multivariate ARMA models (MARMA) to predict the indoor air temperature of three residence in terms of outdoor temperature, solar radiation, and whole-house electricity consumption. Kimbara and Kurosu et al. [1995] developed autoregressive integrated moving average (ARIMA) algorithm for use in the optimal operation of cooling/heating storage systems. Based on the past load data of an air conditioning system, the model predicts load profiles for the next day in order to store the proper amount of energy by utilizing nighttime electric power. The load profiles are updated every hour on the basis of the newly obtained data.

Hourly energy use in commercial buildings shows periodic variations in daily and annual cycles such that the Fourier series functional forms are suitable in modeling this behavior. Dhar and Reddy et al. [1998, 1999] described Fourier series approaches that have been developed for modeling hourly weather dependent and weather independent energy use in commercial buildings and presented the results of application to data collected from many sites. The result showed that Fourier series are very suitable for modeling hourly weather independent energy use unless the daily variation is very irregular. On the other hand, a nonlinear temperature dependent

Fourier series model gave very good prediction in most weather dependent cases examined.

Artificial neural networks (ANN), a family of nonlinear regression techniques, have been used for modeling building energy use. Kawashima and Dorgan et al [1995] proposed an artificial neural network to predict the hourly thermal load. Kalogirou and Neocleous et al [1997] used ANNs to estimate building heating loads with a minimum of input data. Ferrano and Wong [1990] described an artificial neural network model to predict the next day's total thermal load. Kreider and Wang [1991] demonstrated an automated load predictor using the ANN. Anstett and Kreider [1993] examined the accuracy of the ANN for energy predictions.

Appling dynamic regression or ANN techniques above can lead to models. However, it is generally necessary to acquire data over a long period of time with widely varying conditions in order to train the models for accurate predictions under all conditions. Furthermore, it is not known how well the models would perform in predicting building energy use if there were a major change in the control strategies employed, such as there would occur in going from a night setup control to pre-cooling control strategy, because those parameters do not respect the proper physics or the parameters cannot represent the physical properties [Braun and Montgomery et al. 2001, Braun and Chaturvedi 2002].

1.2.2.3 Gray models

A kind of simplified models, which can represent the physical properties of the building system, is preferred for performance evaluation, diagnosis, optimal control etc. These models are called as gray models, which assume that the model structure can describe the behaviors of the concerned system and explain the system physically, and the parameters of model structure are back-out with the measured data. Braun and Chaturvedi [2002] developed an inverse gray-box thermal network model for transient building load prediction. In the approach, second order transfer function was established from a 3R2C thermal network model, which consists of three resistances and two capacitances, to predict building load. All the parameters of 3R2C models for external wall, roof, and internal walls etc., whose values are assumed in certain ranges respectively, are needed to identify by a nonlinear regression algorithm to minimize errors between predictions of the transfer functions and the measured operation data. Liao and Dexter [2004] developed a method to establish a simplified second-order physical model (thermal network model) to simulate the dynamic behavior of existing heating systems of residential building with multi-zone. In the method, the total resistance and capacitance of the envelopes and internal mass contribute to the parameters of a simplified second-order model, and the parameters are commissioned with the monitoring operation data. With the simplified model developed, a soft-sensor was built to estimate the average room temperature for an inferential control scheme for optimizing the boiler controls in multi-zone heating systems [Liao and Dexter 2003]

However, these gray models described above do not use sufficiently the building information which may be easily obtained such as the properties of external wall, roof etc. Therefore, the modeling may lead to much more parameters to be identified [Braun and Chaturvedi 2002] or the model not stable using measured operation data in a short period.

1.2.2.4 Summary

As stated above, the physical modeling entails collecting a physical description, which is time consuming and probably not effective. Moreover, the calibration error can be very large due to the experience of researchers. Data driven modeling entails acquiring data over a long period of time with widely varying conditions in order to train black box models that can provide accurate predictions. Moreover, the data driven models cannot predict the energy consumption correctly if some control strategies change greatly. Gray modeling does not use sufficiently the building information which may be easily obtained, and too many parameters needed to be identified. Therefore, a kind of models, which should use the easily available information as much as possible, identify parameters as less as possible, and predict energy consumption as accurately as possible, is highly of desire.

1.2.3 AHU models

HVAC systems take great part of total building energy consumption. Over the past decades, there have been significant improvements to energy efficiency of HVAC

systems in new and existing buildings, resulting in saving in overall energy consumption and better building performance. For example, VAV is an increasing popular configuration for energy efficient ventilation of commercial buildings [Lorenzetti and Norford 1992, Englander and Norford 1992].

However, they often fails to satisfy the performance expectations or fails with performance degradations, such as poor indoor air quality and more energy consumption, after a period of operation with correct commissioning [House and Kelly 1999]. To detect and locate the causes of fails and to improve the energy performance, various systematic methods and models were developed for building diagnosis [House and Kelly 1999, Piette and Gartland et al. 1998, Claridge and Liu et al. 1999]. AHU systems are an important part of HVAC systems and fans consume significant electricity power. Therefore, the performance prediction and performance evaluation of AHU systems are important. To estimate the electricity consumption of air side of AHUs, many researchers have developed various models for fan energy consumption according to the flow rate or cooling load [DOE 1980, Wang and Yoshida et al. 2004].

DOE-2 is a world wide used energy simulation program. This program uses a black box regression model that produces the fan system power as a function of percentage design air flow using a second-order equation [DOE 1980]. HVACSIM+ is able to simulate fan's energy consumption and pressure head using airflow rate and fan rotate speed by series of equations fitting using manufacture's data [Clark 1985].

The model in the ASHRAE Secondary Toolkit is a gray box fan component model which establishes a fourth-order equation to predict fan efficiency from dimensionless flow parameter [Brandemunehl and Gabel et al. 1993]. Stein and Hydeman [2004] developed a gray model to produce fan efficiency as a function of air flow and fan static pressure. Wang and Yoshida et al. [2004] described a newly total energy consumption model of a fan subsystem, which contain fan, driveline, motor and variable-speed drive. It can accurately simulate the total energy consumption of fan and can be used for automated continuous commissioning during operation. The above models are focus on individual fan performance.

Considering all the air handling units as a whole can facilitate understanding and estimating energy consumption. Reddy and Liu et al. [1998a] developed an ideal dual-duct constant-air-volume (DDCAV system) to deliver the concept of thermal energy delivery efficiency (EDE) as a diagnostic tool to evaluate HVAC retrofit performance and Operation & Maintenance measures. The ideal DDCAV system, which replaced all the installed air handling units to serve for a two zone building, was subject to some of the fundamental restrictions in terms of human comfort and operation under which practical HVAC system operation. The two cooling/heating coils of the system, one for each zone, were assumed to be of infinite capacity to lower the temperatures of the mixed air stream to the appropriate supply air temperature. Reddy and Liu et al. [1998b] further developed an ideal dual-duct variable-air-volume (DDVAV system) with terminal reheat to investigate the energy use and satisfactory zone ventilation under different out door air ventilation strategies.

Liu and Claridge [1998] applied the simplified ideal single dual-duct system to replace all the installed air handling units, along with a simplified building model, for energy consumption calibration for a two-zone building. The calibrated models were developed for HVAC system faults identification and system operation optimization. Liu and Song et al. [2004] reported the application the calibrated models for detecting significantly more outdoor air flow rate than the design value and a lower than necessary cold deck temperature during summer.

However, all these ideal DDCV or DDVAV systems emphasize mainly the cooling/heating energy and consumption. Although Energy Systems Laboratory et al. [2002] stated that air side electricity consumption (fan energy consumption) can be calculated by AIRMODEL [Giebler and Liu et al. 1998], which is used as platform for energy consumption estimation for research [Reddy and Liu et al. 1998a, 1989b, Liu and Claridge 1998, Liu and Song et al. 2004], it seems that no detailed reports about the fundamental to estimate the air side electricity consumption for the ideal duct systems. Therefore, it is highly of value to develop a method for estimating the air side electricity consumption of the ideal air handling systems as energy consumption reference for system performance evaluation and fault diagnosis etc.

1.3 Objective

The objective of this thesis is to develop a systematic methodology for building performance evaluation and diagnosis viewing the building system as a whole. The systematic methodology involves the development of the building global performance

evaluation tool for performance prediction and practical applications of the evaluation tool for building performance diagnosis and evaluation at the building level. Simplified models are the core of the building global performance evaluation tool for performance evaluation and diagnosis.

1.4 Organization of the thesis

This chapter described the motive of this thesis. The motive is to develop robust and dynamic reference models (i.e., evaluation tool) for building energy performance prediction as well as specific strategy and approach for building performance evaluation and diagnosis based on performance prediction using models on the building level. Various models and methods for building performance evaluation and diagnosis are reviewed critically, resulting in an explicit conclusion, also the objective of the thesis.

Chapter 2 presents a systematic methodology for building performance evaluation and diagnosis. This methodology involves the development of a building global performance evaluation tool (i.e., a simplified building energy model and a consolidation AHU model) and practical strategy and approach to apply the evaluation tool for building energy performance evaluation and diagnosis. The fundamental and basis of modeling is specified.

Chapter 3 presents the nodal placement of simplified models of building envelopes, which is part of simplified building energy models. A GA estimator is

developed to optimize the parameters of simplified models of building envelopes by comparing the frequency response characteristics of the simplified models with theoretical frequency response characteristics.

Chapter 4 presents the validation of optimal nodal placement of simplified models of building envelopes. Three representative constructions are used to validate performance of the optimal nodal placement. The validation shows that the simplified model with the optimal nodal placement performs better than the same order simplified models with other configurations.

Chapter 5 presents a simple time domain calculation method for thermal response factors and CTF coefficients of simplified thermal network models. This method can calculate thermal response factors directly in time domain simply while avoiding direct root finding process of traditional methods for thermal response factor calculation. CTF coefficients can be derived easily with the thermal response factors.

Chapter 6 presents the parameter identification of the simplified model of internal mass which is part of the simplified building energy model. A GA estimator is also developed to optimize the parameters of simplified models of internal mass by matching the model prediction with the operation data as close as possible while the simplified models of building envelopes are determined in advance.

Chapter 7 presents the validation of the simplified building energy model using the operation data of a real building. The robustness and accuracy of the simplified

models are emphatically analyzed.

Chapter 8 presents a consolidation AHU model for simplifying the modeling process and making calibration against monitored data much easier. The consolidation AHU represents all the installed AHU systems for accomplishing corresponding functions. The consolidation AHU model is validated in a high-rising commercial office building using the simplified building energy models and monitoring data.

Chapter 9 presents a performance signature-based diagnosis strategy for energy performance evaluation and diagnosis. The strategy is based on the performance prediction using the simplified building energy model. The validation of the diagnosis strategy is presented in a real building.

Chapter 10 presents a performance evaluation approach of alternative control strategies based on the building global performance evaluation tool for performance evaluation of buildings. The approach uses the evaluation tool for performance prediction and employs an enthalpy bin method for energy performance evaluation based on performance prediction. The approach is validated in a real building for energy efficiency of alternative control strategies for building retrofitting and upgrading.

Chapter 11 summaries the main conclusions and achievements of the research reported in this thesis and prospects of the systematic methodology for more applications in practical engineering.

CHAPTER 2 SYSTEMATIC METHODOLOGY

In this chapter, the systematic methodology of building performance evaluation and diagnosis viewing a building system as a whole is illustrated. This methodology involves a few steps from modeling to specific strategy and approach to apply models for performance evaluation and diagnosis. As the basis of the simplified building energy model, thermodynamic control volume is predefined in *Section 2.2*, where all the significant factors accounting for cooling/heating energy consumption will be determined qualitatively. The philosophies of the simplified building energy model and the consolidation AHU model will be presented briefly in *Section 2.3* and *Section 2.4* respectively. Further description and validation will be given in the later chapters.

2.1 Systematic methodology for building performance evaluation and diagnosis

Figure 2.1 illustrates the systematic methodology for building performance evaluation and diagnosis. The methodology includes the development of a building global performance evaluation tool (i.e. simplified building energy modeling, consolidation AHU modeling), a performance signature-based diagnosis strategy and a performance evaluation approach of alternative control strategies for building performance evaluation and diagnosis using the evaluation tool. As the basis of performance evaluation and diagnosis, the evaluation tool is used for building performance prediction.
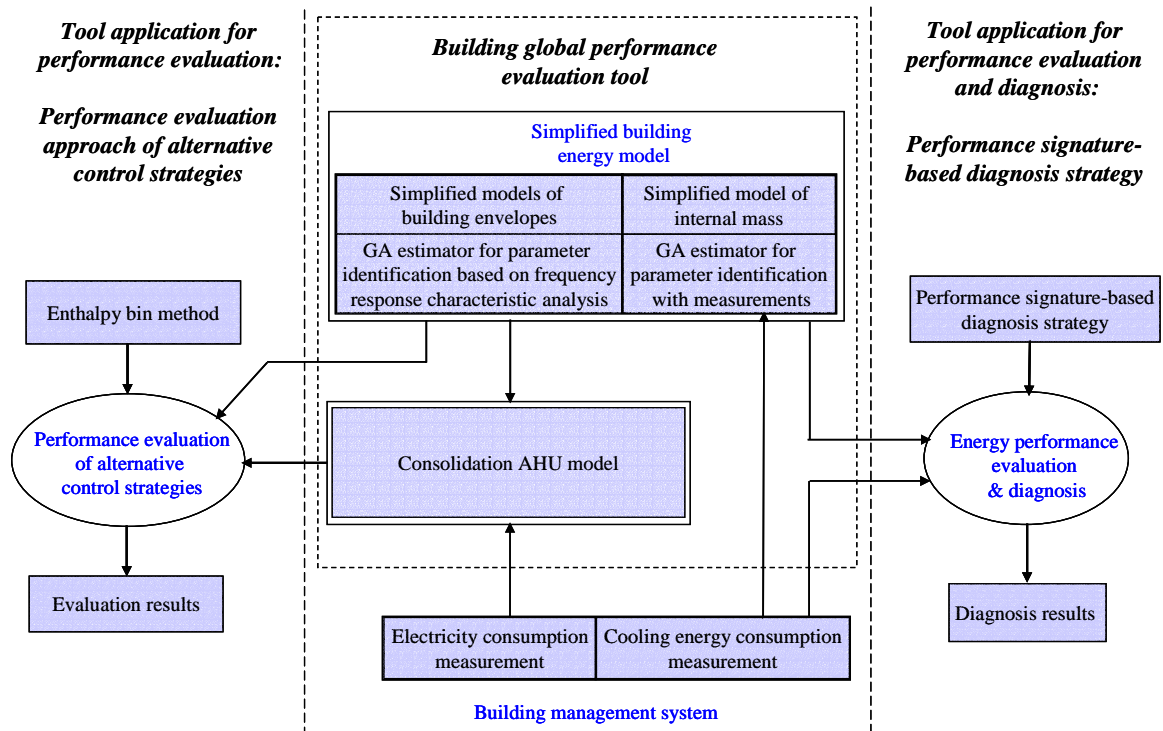
Figure 2.1 Illustration of the systematic methodology

As the core of the evaluation tool, the simplified building energy model is constructed as a hybrid building energy model, which is the compounding of simplified models of building envelopes and internal mass. Although simplified models are used widely, the parameters have great effects on the performance prediction. In this methodology, a GA estimator is developed for parameter optimization for the simplified model of building envelope based on the frequency response characteristic analysis. Another GA estimator is developed for parameter optimization for the simplified model of internal mass using site measurements. The philosophy of the hybrid building energy model is further presented in *Section 2.3*.

As another element of the evaluation tool, the consolidation AHU model is

developed to predict energy performance of air side systems. The consolidation AHU represents all the installed AHU systems. The philosophy of the consolidation AHU model is given in *Section 2.4*.

Taking cooling energy consumption as an important performance indicator, the performance signature-based diagnosis strategy is developed to diagnose the causes that result in cooling energy consumption deviation based on the performance prediction of the evaluation tool. The strategy will be described in *Chapter 9* in detail. Building performance upgrading takes a great role in energy saving and environment performance improvement. The performance evaluation approach of alternative control strategies is developed to evaluate the energy performance of alternative control strategies for decision making of air handling system retrofitting of building system. The approach employs an enthalpy bin method for facilitating evaluation based on the performance evaluation of the evaluation tool. The approach will be presented in detail in *Chapter 10*.

2.2 Thermodynamic control volume

Understanding the basis of building thermal energy consumption models is essential in explaining the characteristics of energy prediction by these models, and also in understanding the source of any possible effects on the predictions. Therefore, it is the first step to consider the thermodynamic control volume representing the thermal phenomena taking place in a building, and their governing thermal transfer force.
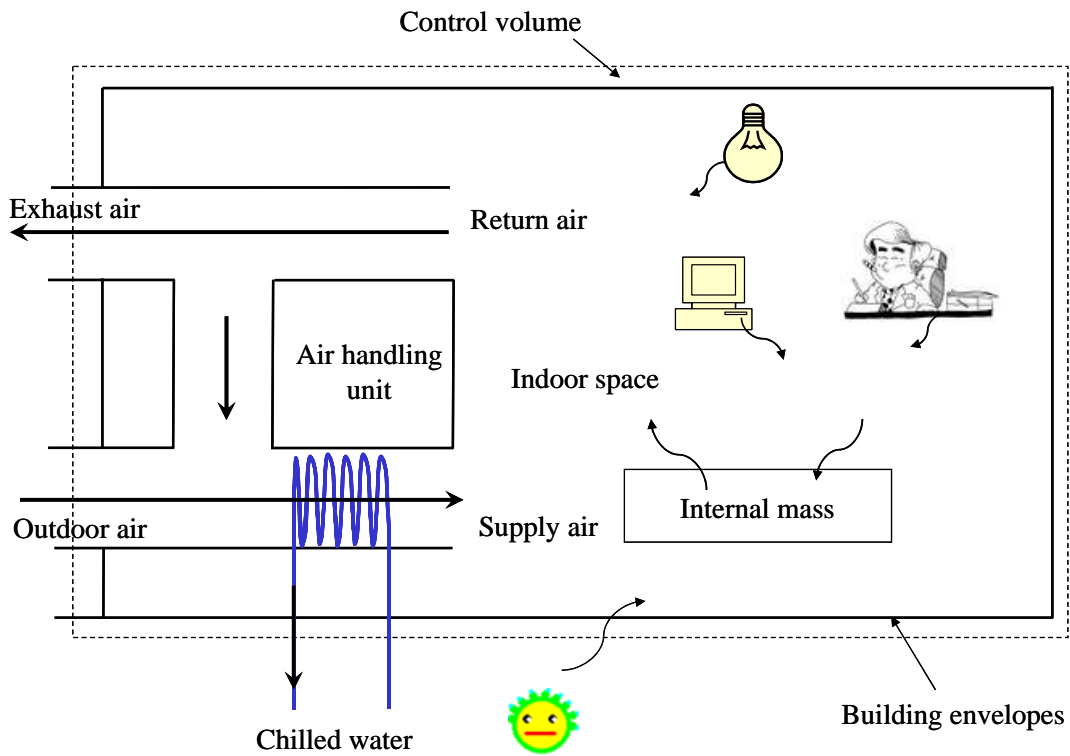
Figure 2.2 Thermodynamic control volume

It is obvious that steady state thermodynamic control volume cannot reflect the effects of thermal storage such as building envelopes and internal mass. For building performance evaluation and faults diagnosis, dynamic energy models are much concerned. The thermodynamic control volume with dynamic state is depicted briefly in Figure 2.2. When dynamic state is considered, there are obvious thermal storage and thermal release process. The substance or structure for the storage and thermal release is building envelope including exterior wall and roofs etc. The internal structure, partitions, carpet and furniture etc. have great effects on the thermal process. To simplify the thermal process, all the substance inside the building, which can store heat, is called as internal mass.

The thermal process is briefed as follows. For the opaque part of the building envelopes, the external face absorbs the solar radiation and convective heat from the outside air, and internal face release gradually these absorbed heat into indoor space as the forms of conductive heat or convective heat which become cooling load instantly. For the transparency part of the building envelopes such as windows, thermal storage can be ignored. The conductive heat because of temperature difference through the transparency becomes cooling load directly. The solar irradiation though the transparency becomes two parts. One is convective heat, which becomes cooling load instantly. The other is radiation heat, which is absorbed by internal mass. For the indoor part of the building, the heat release from lighting and equipments can be divided into convective heat and radiative heat. The heat release from occupants consists of radiative heat, convective heat and latent heat. The latent heat and convective heat becomes cooling load directly. The internal mass absorbs all sorts of radiation, which include that for solar radiation through transparency, that from lighting, equipments, and occupants. Then the internal mass releases them gradually in the form of convective heat becoming cooling load instantly. At the same time, to meet the comfort requirement, appropriate outdoor air is introduced and almost the same amount indoor air is exhausted. The introduced outdoor air also constitutes a part of cooling load, which includes latent load and sensible load. All the cooling loads are taken away simultaneously by the chiller water through cooling coils of air handling units.

The external forces of the cooling load are the introduced fresh air and weather

condition. The internal forces of cooling load are mainly lighting, equipments, and occupants. The internal forces of the cooling load are occupants, lighting, equipments, etc.

2.3 Philosophy of the hybrid building energy model

As the core of the building global performance evaluation tool, the hybrid building energy model is further described in this section.

Building envelopes and internal mass have great effects on cooling energy consumption because of the characteristics of thermal absorption. Therefore, modeling the thermal performance of building envelope and internal mass is important. For the building systems, some information is easy to obtain, such as the building envelopes structures, the density and operation schedule/pattern of lighting, equipments, and occupants. However, the detailed information of internal mass is difficult to obtain, or even impossible to obtain. Improper assumptions can make energy modeling deviate, thus decrease the confidence of energy modeling.

A hybrid energy model is proposed as a simplified building energy model for the energy consumption prediction to be used as the energy consumption reference. The primary goal of introducing a hybrid model is to effectively use the building information which can be obtained easily, and assume a physical structure to handle the building information which may not be obtained easily or even impossible to obtain. The details of the hybrid model are described briefly as follows.

Hybrid is not a new concept in academic field. It is often employed to describe a model which consists of different approaches [Bahai and Esat 1994; Padhy 2001; Wu and Thompson 2002]. Petermeier and Benning et al. [2002] developed a hybrid model for the fouling process in tubular heat exchangers, which incorporate qualitative knowledge and quantitative data. In the study, hybrid modeling is the compounding of both physical modeling and partial data-driven modeling. The hybrid building energy model begins with physical descriptions of some components if their detailed physical characteristics are available and assumption of the physical structures of some components if their detailed physical characteristics are hardly available. The parameters of the assumed physical models are identified with the known physical descriptions and operation data to provide the most accurate representation for the assumed model forms and the data sets. Such model not only describes the behavior or performance of the system, but also can explain the system physically. Therefore, such model can predict robustly the energy performance of the building system.

For building envelope, we can establish simplified model based on detailed physical description. For building internal mass, the physical structures can be assumed, and parameters of the assumed physical models are identified with the known physical descriptions and operation recorded data. Therefore, half of the hybrid model is represented by detailed physical parameters and another half is described by identified parameters using operation data. 3R2C models are utilized to simulate building envelopes. The parameters of 3R2C models can be carried out based on the detailed physical information. Internal mass is represented by a 2R2C

model whose resistances and capacitances are assumed to be constant. The nodal

placement of internal mass is identified with the 3R2C model of building envelopes

and the operation data.
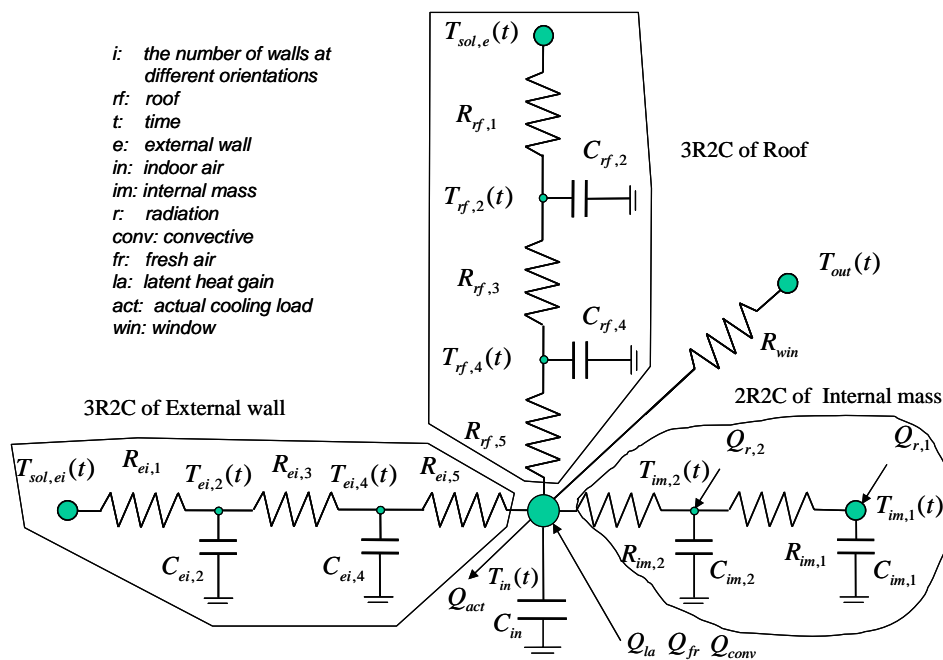
Figure 2.3 Schematics of the thermal network model of building system

Figure 2.3 depicts a schematic representation of an electrical analog for the

thermal network building model (i.e., the simplified building energy model). Because

considering the building as a whole, the fundamental assumption is necessary that the

whole indoor circulated air volume is at a "uniform temperature". The assumption is

fairly common employed by most simulation models. It also corresponds with usual

air temperature measurement in building zones where it is customary to place a few

temperature sensors at representative positions in rooms and determine the average

value.

Four categories are considered: (1) exterior walls, (2) roof(s), (3) windows, and (4) internal mass (ground floor is cooperated into internal mass). Exterior walls should be considered respectively according to the orientations because the dynamic models of the exterior walls at different orientations have different forcing functions due to the changing position of the sun. Exterior walls and ceiling/roof are considered as 3R2C models (three resistances and two capacitances). The windows have negligible energy storage and are represented with pure resistances. Internal mass includes floors, partitions, crawl space in ceiling, internal walls, and furniture etc. It absorbs radiant heat through the windows and that from occupants, lighting, and machine etc., and then releases the heat gradually to the air space. Internal mass is viewed as 2R2C model (two resistances and two capacitances) as shown in Figure 2.3. All resistances and capacitances are assumed to be time invariant. The effect of varying wind velocity on exterior wall convection coefficients is not considered. In this study, the second order model is used because that the accuracy of the first order model is low and the higher order model can not provide significant improvement of accuracy [Braun and Chaturvedi, 2002].

The whole building energy balance can be represented with the following equations.

$$C_{rf,2} \frac{dT_{rf,2}(t)}{dt} = \frac{T_{sol,rf}(t) - T_{rf,2}(t)}{R_{rf,1}} - \frac{T_{rf,2}(t) - T_{rf,4}(t)}{R_{rf,3}} \qquad (2.1)$$

$$C_{rf,4} \frac{dT_{rf,4}(t)}{dt} = \frac{T_{rf,2}(t) - T_{rf,4}(t)}{R_{rf,3}} - \frac{T_{rf,4}(t) - T_{in}(t)}{R_{rf,5}} \qquad (2.2)$$

$$C_{ei,2} \frac{dT_{ei,2}(t)}{dt} = \frac{T_{sol,ei}(t) - T_{ei,2}(t)}{R_{ei,1}} - \frac{T_{ei,2}(t) - T_{ei,4}(t)}{R_{ei,3}} \tag{2.3}$$

$$C_{ei,4} \frac{dT_{ei,4}(t)}{dt} = \frac{T_{ei,2}(t) - T_{ei,4}(t)}{R_{ei,3}} - \frac{T_{ei,4}(t) - T_{in}(t)}{R_{ei,5}} \tag{2.4}$$

$$C_{im,1} \frac{dT_{im,1}(t)}{dt} = Q_{r,1} - \frac{T_{im,1}(t) - T_{im,2}(t)}{R_{im,1}} \tag{2.5}$$

$$C_{im,2} \frac{dT_{im,2}(t)}{dt} = Q_{r,2} + \frac{T_{im,1}(t) - T_{im,2}(t)}{R_{im,1}} - \frac{T_{im,2}(t) - T_{in}(t)}{R_{im,2}} \tag{2.6}$$

$$\begin{aligned} Q_{r,1} + Q_{r,2} &= Q_{r,Total} \\ &= Q_{r,sol} + Q_{r,occup} + Q_{r,light} + Q_{r,equip} \end{aligned} \tag{2.7}$$

$$Q_{win} = \frac{T_{out}(t) - T_{in}(t)}{R_{win}} \tag{2.8}$$

$$Q_{conv} = Q_{conv,sol} + Q_{conv,occup} + Q_{conv,light} + Q_{conv,equip} \tag{2.9}$$

$$\begin{aligned} Q_{est} &= \sum_{i=1}^{n} \left(\frac{T_{ei,4}(t) - T_{in}(t)}{R_{ei,5}} \right) + \frac{T_{rf,4}(t) - T_{in}(t)}{R_{rf,5}} + \frac{T_{im,2}(t) - T_{in}(t)}{R_{im,2}} + Q_{win} \\ &\quad - C_{in} \frac{dT_{in}(t)}{dt} + (Q_{conv} + Q_{fr} + Q_{la,occup}) \end{aligned} \tag{2.10}$$

$$Q_{est} \approx Q_{act} \tag{2.11}$$

Where, *C* and *R* are resistance and capacitance, *T* is temperature, subscript *rf*, *im*, *ei*, *in*, and *win*, indicate roof, internal mass, the *i*-th exterior wall and inside, and windows respectively. Subscript *r*, *Total*, *conv*, *sol*, *occup*, *light* and *equip*, indicate radiation heat, total radiation heat, convective heat, solar radiation, occupants, lighting and equipments respectively.$Q_{r,1}$ and $Q_{r,2}$ absorbed by the nodes $C_{im,1}$ and $C_{im,2}$ respectively are the radiation which includes the radiation from solar radiation through windows, from occupants, lighting and equipments. $Q_{conv,sol}$ and $Q_{r,sol}$ is the convective heat and radiation heat of solar radiation through windows respectively.

Q_{fr} is the heat transfer because of fresh air induction, infiltration (exfiltration). $Q_{la,occup}$

is latent heat gain from occupants. Q_{est} and Q_{act} are the estimated cooling load with

the model and the actual cooling load which can be measured from the central plant.

The model parameters of the building envelope (i.e. exterior walls and roofs) can

be determine with simple configurations or optimized configurations, which will

addressed in *Chapter 3* and *Chapter 4*. The model parameters $C_{im,1}$, $R_{im,1}$, $C_{im,2}$, $R_{im,2}$,

of the building internal mass (i.e. internal structure, furniture, etc.) are identified using

the operation data and a genetic algorithm (GA)-based method in time-domain, which

will addressed in *Chapter 6* and *Chapter 7*, while the simplified models of building

envelopes are obtained in advance.

2.4 Philosophy of the consolidation AHU model

As another element of the building global performance evaluation tool, the

consolidation AHU model is briefly described in this section.

In many real existing building systems, there are not enough sensors installed at

the component level of the HVAC terminals to provide enough information for

performance evaluation or faults diagnosis. It is also very complex to use the

measurement for the purpose of performance evaluation and fault diagnosis even if

enough sensors are installed at component levels. For air handling units, electricity

consumption is an important index for such purpose [Wang and Yoshida et al. 2004].

It is practical to install sub-metering system to monitor the total electricity

consumption of the AHUs. This can provide more useful data for performance

evaluation at the subsystem level.
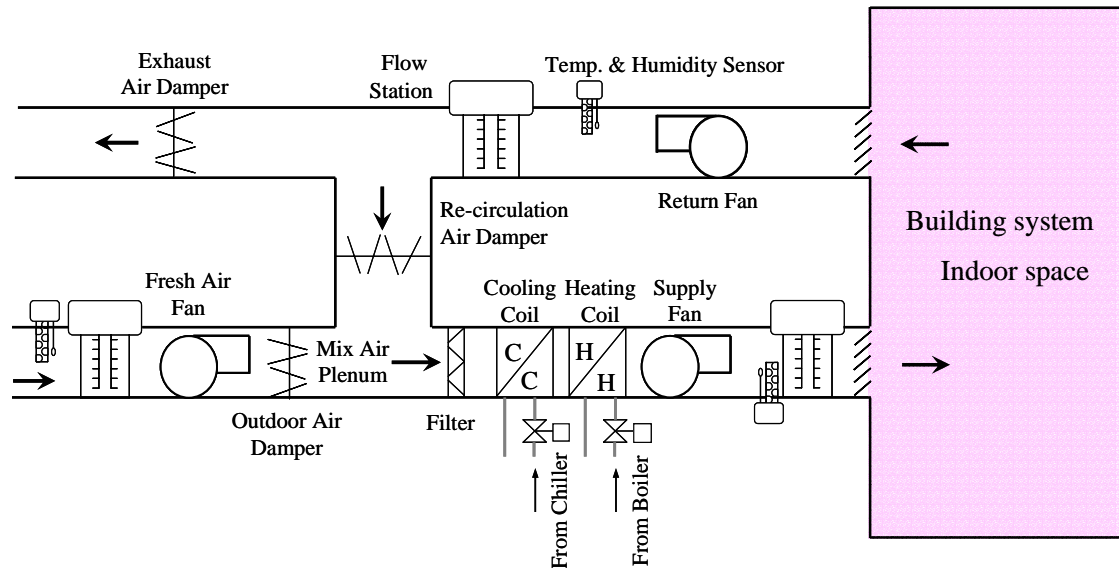
Figure 2.4 Schematics of a consolidation AHU

To consider the air subsystem as a whole, AHU consolidation can be developed

as an ideal AHU model to represent all the practical installed AHU systems. Such

consolidation AHU model can make the modeling process simpler and calibration

against monitored data much easier. Figure 2.4 presents the schematics of a

consolidation AHU which is similar to the practical AHU. It can accomplish the basic

functions of maintaining air temperature and humidity within the building, and

satisfying the indoor air quality with optimized energy consumption at working hours

instead of all the installed AHUs in the building. The difference is that the ideal AHU

is imaginary. The cooling/heating coil of the ideal AHU is assumed to have the

maximum capacity of the total AHU capacity, to lower/raise the temperatures of the

mixed air stream to the appropriate supply air temperature. Fans of the consolidation

AHU have maximum capacities of the corresponding total AHU fan capacities (i.e., fresh air fan capacity, return air fan capacity, and supply air fan capacity) to power the air stream through the system.

Because the consolidation AHU does not exist in reality, how to estimate the supply flow air rate and electricity consumption of the consolidation AHU is the crucial. It is not of purely academic interest, but of interest to practical application. It is assumed that the consolidation AHU has similar pressure loss characteristic as the practical AHU which can be representative for the merged AHUs. The air flow rate can be calculated according to the sensible cooling energy consumption and temperature difference between supply air and return air. Then, the effective mechanical output power can be calculated by multiplying the flow rate and the pressure loss. With the measured electricity consumption of the consolidation AHU from sub-metering system, the experiential relationship is easy to obtain between the electricity consumption and the effective mechanical output power. The details will be delivered in *Chapter 8*.

CHAPTER 3 OPTIMAL NODAL PLACEMENT OF SIMPLIFIED MODELS OF BULDING ENVELOPES

As an important part of the simplified building energy model or the hybrid building energy model, the simplified models of building envelopes are presented in this chapter. This chapter mainly presents the theoretic basis of optimal nodal placement of simplified models of building envelopes based on frequency response characteristic analysis, and the genetic algorithm (GA) estimator developed to identify the optimal parameters to match the frequency response characteristics of simplified models with theoretical frequency response characteristics. The validity of optimal nodal placement will be demonstrated with three typical constructions, which will be presented in *Chapter 4*.

3.1 Introduction

Advanced building and HVAC system simulation techniques provide convenience and low-cost tools for predicting energy and environment performance of building and HVAC system in their design, commissioning, operation, management and diagnosis [Lebrun and Jokela et al. 1999, Kusuda 1999]. They are also important for testing and evaluating the control strategies and algorithms in energy management and control systems [Lebrun and Jokela et al. 1999, Wang 1999]. The heat transfer through the building envelope is the principal component of building thermal loads and energy requirement. Because of the thermodynamic characteristics of the massive

elements of buildings (e.g., concrete or brick walls), it is necessary to conduct transient analysis of heat flow through building envelopes. Many detailed simulation models with response factor method or conduction transfer function, such as EnergyPlus [Crawley and Drury 2000] and DOE-2 [Ed Kidd et al. 2001] have been developed and used successfully. However, for many other applications, such as building performance diagnosis and optimal control, etc., effective, efficient and simple building energy models are necessary [Claridge and Liu et al. 1999, Wang 1999, Wang and Xu 2003].

The current methods for heat flow calculations mainly are response factor method [Stephenson and Mitalas 1967, Mitalas 1968], conduction transfer function (CTF) method [Stephenson and Mitalas 1971], finite difference method and thermal network method. Finite difference method, which can avoid the mathematical difficulties associated with analytical solutions to Fourier continuity equation, is also used to develop dynamic thermal model [Davies 2003]. When this method is utilized, it is necessary to represent the continuous material by thermal networks consisting of thermal resistances and lumped capacitances. However, the process of fine nodal placement for a complete multilayer wall with finite difference method is complicated and tedious. Simplified thermal network models are often used. Seem and Klein et al [1989] applied 3R2C model to calculate heat transfer function equation. In the model, the values of three resistances are outside conductive resistance, wall conduction resistance and inside conductive resistance respectively, the value of individual capacitance is half of the total thermal capacitance. The choice of individual value is

subjective. Braun et al. [2001, 2002] used 3R2C model to establish second order transfer function to predict building load for the evaluation of thermal mass control strategies. The values of individual resistances and capacitances were determined by a regression algorithm in time domain to minimize the errors between the predictions of the simplified model and the detailed finite difference model. The 3R2C model with the configuration that three resistances and two capacitances are distributed evenly was also used for dynamic analysis in the literature [Braun and Chaturvedi 2002]

The study presents a method for optimal nodal placement of 3R2C model in frequency domain. The theoretical frequency characteristics represent exactly the dynamic thermal behaviors of the real system of a building envelope. With reference to system theory [Chen 1994], if the simplified model of a system is equivalent to the real system of a building envelope, they should behave as the equivalent response characteristics in frequency domain. Phase lag and amplitude are two important indices of frequency characteristics. Therefore, it's necessary to find the values of individual resistances and capacitances to ensure the simplified 3R2C model equivalent to the real system of a building envelope. Genetic algorithm (GA) is an advanced search and optimization technique [Mitchell 1997]. The algorithm was ever used in air conditioning fields to search for global optimal solutions [Wang and Jin 2000]. Herein, it's also used to optimize the values of individual resistances and capacitances of the simplified model allowing its frequency responses match the theoretical frequency responses of the real system of a building envelope the best. Validation and comparison were performed in various typical cases which

demonstrated that the optimal nodal placement is much better than other nodal configurations of model simplification in *Chapter 4*. The accuracy of simplified models for constructions of different weights was studied.

3.2 Theoretical frequency characteristics of heat transfer through constructions

To calculate the theoretical frequency characteristics of building envelopes in the frequency range of concern, the transmission matrix of heat transfer should be deduced first. The method to deduce the transmission matrix of heat transfer for one-dimensional homogeneous multilayer plane constructions in Laplace domain is explicitly presented in *Appendix A1*. The deduction process is briefed as follows.

The Fourier continuity equation for heat conduction in one layer of building material is represented by Equation (3.1).

$$\rho C_P \frac{\partial T(x,t)}{\partial t} = \lambda \frac{\partial^2 T(x,t)}{\partial x^2} \tag{3.1}$$

where T is temperature, λ, ρ and C_P are thermal conductivity, density and specific heat respectively. The heat flow q at arbitrary time t and location x in the wall is represented by Equation (3.2).

$$q(x,t) = -\lambda \frac{\partial T(x,t)}{\partial x} \tag{3.2}$$

Assuming that λ, ρ and C_P of each layer are constant and $T(x,0) = 0$, Laplace transform can be applied on Equation (3.1) and (3.2). Then, the transmission equation

(3.3), in terms of Laplace variable *s,* relates the temperatures and heat flows at both

sides of the wall, which includes the surface films at both sides.

$$\begin{bmatrix} T_{in}(s) \\ q_{in}(s) \end{bmatrix} = M(s) \begin{bmatrix} T_{out}(s) \\ q_{out}(s) \end{bmatrix} = \begin{bmatrix} A(s) & B(s) \\ C(s) & D(s) \end{bmatrix} \begin{bmatrix} T_{out}(s) \\ q_{out}(s) \end{bmatrix}$$ (3.3)

where *M(s)* is the total transmission matrix of the entire wall, and also the products of

individual layer transmission matrix including the surface films at both sides as

follows:

$$M(s) = \begin{bmatrix} A(s) & B(s) \\ C(s) & D(s) \end{bmatrix} = M_{in}(s)M_n(s)\cdots M_1(s)M_{out}(s)$$ (3.4)

where,

$$M_i(s) = \begin{bmatrix} A_i(s) & B_i(s) \\ C_i(s) & D_i(s) \end{bmatrix}, (i=1, 2, ..., n)$$ (3.5)

The elements of all the layer transmission matrices can be given in hyperbolic

function forms as shown in Equation (3.6), (3.7) and (3.8).

$$A_i = D_i = \cosh(L_i\sqrt{\frac{s}{a_i}})$$ (3.6)

$$B_i = -\frac{\sinh(L_i\sqrt{\frac{s}{a_i}})}{\lambda_i\sqrt{\frac{s}{a_i}}}$$ (3.7)

$$C_i = -\lambda_i\sqrt{\frac{s}{a_i}}\sinh(L_i\sqrt{\frac{s}{a_i}})$$ (3.8)

where, n is the total layer number of the solid wall, L_i, $a_i (= \dfrac{\lambda_i}{\rho_i C_{Pi}})$ are the thickness and thermal diffusivity of the i-th layer, respectively. When a layer has negligible heat capacitance compared to its thermal resistance (e.g., cavity layer, surface films), its layer transmission matrix (see also Equation (3.5)) becomes,

$$M_i = \begin{bmatrix} 1 & -R_i \\ 0 & 1 \end{bmatrix} \tag{3.9}$$

where R_i is the thermal resistance of the cavity layers or surface films.

Thus, for the inside and outside surface films, the matrices are:

$$M_{in}(s) = \begin{bmatrix} 1 & -R_{in} \\ 0 & 1 \end{bmatrix}, \qquad M_{out}(s) = \begin{bmatrix} 1 & -R_{out} \\ 0 & 1 \end{bmatrix} \tag{3.10}$$

where R_{in} and R_{out} are the thermal resistances of the inside wall and outside wall respectively.

From Equation (3.3), the transmission equation relating temperatures to heat flows on both sides is given by Equation (3.11):

$$\begin{bmatrix} q_{out}(s) \\ q_{in}(s) \end{bmatrix} = \begin{bmatrix} -G_X(s) & G_Y(s) \\ -G_Y(s) & G_Z(s) \end{bmatrix} \begin{bmatrix} T_{out}(s) \\ T_{in}(s) \end{bmatrix} \tag{3.11}$$

where, $G_X(s)$, $G_Y(s)$ and $G_Z(s)$ are the transfer functions of external, cross and internal heat conduction of the construction, respectively. All of them are complicated transcendental hyperbolic functions, especially for a construction of more than two layers. Since $A(s)D(s) - B(s)C(s) = 1$, they can be expressed as Equation (3.12),

(3.13) and (3.14).

$$G_X(s) = \frac{A(s)}{B(s)} \qquad (3.12)$$

$$G_Y(s) = \frac{1}{B(s)} \qquad (3.13)$$

$$G_Z(s) = \frac{D(s)}{B(s)} \qquad (3.14)$$

Substituting s with $j\omega$ ($j = \sqrt{-1}$) in equations (12)-(14), one can yield the complex functions $G_X(j\omega)$, $G_Y(j\omega)$ and $G_Z(j\omega)$, which are the theoretical frequency characteristic of external, cross and internal heat conduction, respectively [Chen and Chen 2000].

These frequency characteristics are represented by the amplitudes and phase lags of these three complex functions representing theoretical frequency characteristics of external, cross and internal heat conduction, which are used as the reference of the frequency characteristics in optimization.

3.3 Frequency characteristics of heat transfer of simplified models

The one-dimensional homogeneous multilayer plane wall is assumed to be a discretised wall with $2N+1$ elements as shown in Figure 3.1.
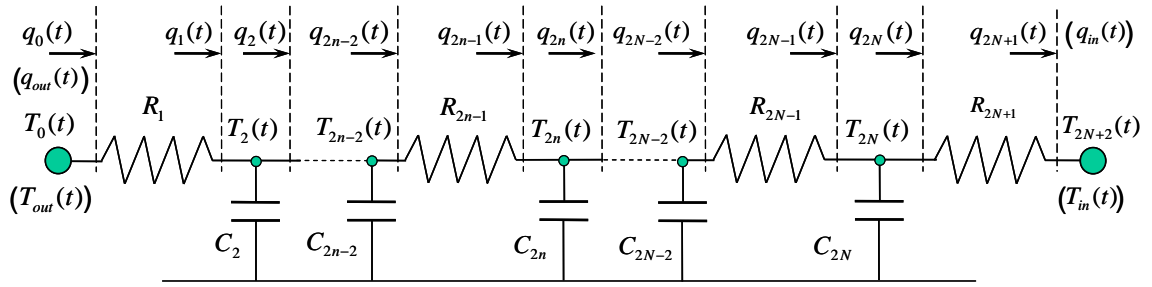
Figure 3.1 Schematics of thermal network for RCs model of building envelope with

2*N*+1 elements

For the *2n-2*, *2n-1*, *2n*th nodes, the relationships among temperatures and heat

flows can be written as follows.

$$q_{2n-1}(t) = q_{2n-2}(t) \tag{3.15}$$

$$q_{2n-1}(t) = \frac{T_{2n-2}(t) - T_{2n}(t)}{R_{2n-1}} \tag{3.16}$$

$$C_{2n}\frac{dT_{2n}(t)}{dt} = q_{2n-1}(t) - q_{2n}(t) \tag{3.17}$$

where, *C*, *R* are thermal capacitance and resistance respectively.

Assuming $T(0) = 0$, Laplace transform can be applied on Equation (3.15), (3.16),

and (3.17). One can obtain the relationships in *s* domain as Equation (3.18).

$$q_{2n-1}(s) = q_{2n-2}(s) \tag{3.18}$$

$$q_{2n-1}(s) = \frac{T_{2n-2}(s) - T_{2n}(s)}{R_{2n-1}} \tag{3.19}$$

$$q_{2n}(s) = -sC_{2n}T_{2n}(s) + q_{2n-1}(s) \tag{3.20}$$

With combining the above three equations, the transmission matrix of the three nodes (*2n-2*, *2n-1*, *2n*th nodes) in terms of Laplace variable *s* relates the temperatures and heat flows as follows:

$$\begin{bmatrix} T_{2n}(s) \\ q_{2n}(s) \end{bmatrix} = M'_{2n}(s) \begin{bmatrix} T_{2n-2}(s) \\ q_{2n-2}(s) \end{bmatrix} = \begin{bmatrix} A'_{2n}(s) & B'_{2n}(s) \\ C'_{2n}(s) & D'_{2n}(s) \end{bmatrix} \begin{bmatrix} T_{2n-2}(s) \\ q_{2n-2}(s) \end{bmatrix} \tag{3.21}$$

where,

$$M'_{2n}(s) = \begin{bmatrix} A'_{2n}(s) & B'_{2n}(s) \\ C'_{2n}(s) & D'_{2n}(s) \end{bmatrix} \tag{3.22}$$

$$A'_{2n}(s) = 1 \tag{3.23}$$

$$B'_{2n}(s) = -R_{2n-1} \tag{3.24}$$

$$C'_{2n}(s) = -C_{2n}s \tag{3.25}$$

$$D'_{2n}(s) = C_{2n}R_{2n-1}s + 1 \tag{3.26}$$

At the *2N+2* node, the transmission equation can be written as follows:

$$\begin{aligned} \begin{bmatrix} T_{in}(s) \\ q_{in}(s) \end{bmatrix} &= M'_{in}(s) \begin{bmatrix} T_{2N}(s) \\ q_{2N}(s) \end{bmatrix} \\ &= \begin{bmatrix} 1 & -R_{2N+1} \\ 0 & 1 \end{bmatrix} \begin{bmatrix} T_{2N}(s) \\ q_{2N}(s) \end{bmatrix} \end{aligned} \tag{3.27}$$

The total transmission equation can be read below.

$$\begin{bmatrix} T_{in}(s) \\ q_{in}(s) \end{bmatrix} = M'_{in}(s)M'_{2N}(s)M'_{2N-2}(s)\cdots M'_2 \begin{bmatrix} T_{out}(s) \\ q_{out}(s) \end{bmatrix}$$

$$= \begin{bmatrix} A' & B' \\ C' & D' \end{bmatrix} \begin{bmatrix} T_{out}(s) \\ q_{out}(s) \end{bmatrix}$$

(3.28)

It is obvious that A', B', C' and D' are polynomials about Laplace variable s.

When the one-dimensional homogeneous multilayer plane wall is assumed to be a discretised wall with 5 elements as shown in Figure 3.2, the building envelope is simplified as 3R2C model. Equation (3.28) can be rewritten as equation (3.29) which describes the relationships between the temperatures and heat flows on both sides in s domain for the 3R2C model as follows.

$$\begin{bmatrix} T_{in}(s) \\ q_{in}(s) \end{bmatrix} = M'_{in}(s)M'_4(s)M'_2(s)\begin{bmatrix} T_{out}(s) \\ q_{out}(s) \end{bmatrix}$$

$$= \begin{bmatrix} 1 & -R_5 \\ 0 & 1 \end{bmatrix}\begin{bmatrix} 1 & -R_3 \\ -C_4 s & C_4 R_3 s + 1 \end{bmatrix}\begin{bmatrix} 1 & -R_1 \\ -C_2 s & C_2 R_1 s + 1 \end{bmatrix}\begin{bmatrix} T_{out}(s) \\ q_{out}(s) \end{bmatrix}$$

$$= \begin{bmatrix} A' & B' \\ C' & D' \end{bmatrix}\begin{bmatrix} T_{out}(s) \\ q_{out}(s) \end{bmatrix}$$

(3.29)

where,

$$A' = 1 + (C_4 R_3 + C_2 R_3 + C_2 R_5)s + C_4 C_2 R_5 R_3 s^2$$

(3.30)

$$B' = -(R_5 + R_3 + R_1) - (C_4 R_3 R_1 + C_2 R_3 R_1 + C_2 R_5 R_1 + C_4 R_5 R_3)s$$
$$- C_4 C_2 R_5 R_3 R_1 s^2$$

(3.31)

$$C' = -(C_4 + C_2)s - C_4 C_2 R_3 s^2$$

(3.32)

$$D' = 1 + (C_4 R_1 + C_4 R_3 + C_2 R_1)s + C_4 C_2 R_3 R_1 s^2$$

(3.33)
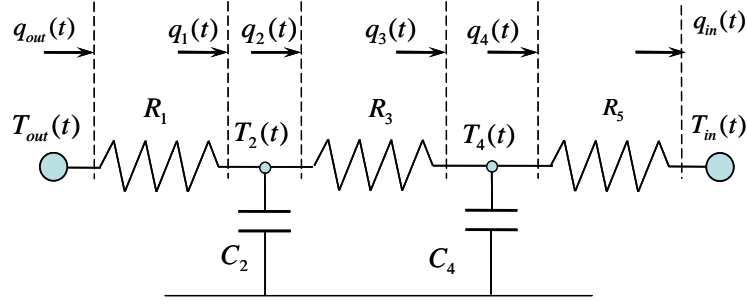
Figure 3.2 Schematics of 3R2C model of building envelope

Equation (3.29) can be rearranged to express the surface heat flows as response and the surface temperatures as excitation as follows.

$$\begin{bmatrix} q_{out}(s) \\ q_{in}(s) \end{bmatrix} = \begin{bmatrix} -G_X^{'}(s) & G_Y^{'}(s) \\ -G_Y^{'}(s) & G_Z^{'}(s) \end{bmatrix} \begin{bmatrix} T_{out}(s) \\ T_{in}(s) \end{bmatrix} \tag{3.34}$$

where $G_X^{'}(s)$, $G_Y^{'}(s)$ and $G_Z^{'}(s)$ are the transfer functions of external, cross and internal heat conduction of the construction, respectively. All of them are the quotients of two polynomials respectively for the thermal network model of multilayer plane construction. Because $A^{'}(s)D^{'}(s) - B(s)^{'}C(s)^{'} = 1$, the elements of the transmission matrix can be expressed as Equation (3.35), (3.36) and (3.37):

$$G_X^{'}(s) = \frac{A'(s)}{B'(s)} \tag{3.35}$$

$$G_Y^{'}(s) = \frac{1}{B'(s)} \tag{3.36}$$

$$G_Z^{'}(s) = \frac{D'(s)}{B'(s)} \tag{3.37}$$

Substituting s with $j\omega$ ($j = \sqrt{-1}$) in Equation (3.35), (3.36) and (3.37), one can yield the complex functions $G'_X(j\omega)$, $G'_Y(j\omega)$ and $G'_Z(j\omega)$, which are the frequency response characteristic of external, cross and internal heat conduction, respectively. These frequency characteristics are generally characterized by their amplitude and phase lag similar to the theoretical frequency characteristics.

These frequency characteristics are represented by the amplitudes and phase lags of these three complex functions representing frequency characteristic of external, cross and internal heat conduction of the simplified model, which are compared with the theoretical frequency characteristics in order to optimize their parameters.

3.4 Objective function of optimization

A thermal network model, which can approximately represent the real system of building envelope, is a good solution for simplicity and convenience of building and HVAC system dynamic simulation and analysis. Substantively, from the points of view of model simplification [Chen 1994], the simplified multi-order thermal network model should behave as the equivalent frequency response characteristics if it can represent the real system of building envelope. Therefore, it is critical to find the proper nodal placement and individual resistances and capacitance of the thermal network model, which make the frequency response characteristic of the thermal network model match that of heat transfer through the real system of building envelope at various frequency points of concern as close as possible. Phase lag and amplitude are two important indices of frequency characteristics.

The parameters to be optimized are the resistances and capacitances of the 3R2C model which give the best fitting with the theoretical frequency characteristics. The objective function of such optimization is expressed in Equation (3.38).

$$J(R_1, R_5, C_4) = \sum_{n=1}^{N} \sum_{m=X,Y,Z} \begin{array}{l} (W_m^{AM} \left\| \left| G_m(j\omega_n) \right| - \left| G_m'(j\omega_n) \right| \right\| \\ + W_m^{PL} \left| PL(G_m(j\omega_n)) - PL(G_m'(j\omega_n)) \right|) \end{array} \tag{3.38}$$

where J is the objective function, PL is phase lag (denoted as $PL(G(j\omega))$), the superscript AM and PL are amplitude and phase lag respectively, W are weighting factors associated with the amplitudes and phase lags of frequency characteristics of the external, cross and internal heat conductions respectively. In this study all the weighting factors were set as 1 as it was found that such value works well. The three parameters constraint to the system of the inequality equations as follows.

$$\begin{cases} 0 < R_1 < R & (a) \\ 0 < R_5 < R & (b) \\ R - R_5 - R_1 > 0 & (c) \\ 0 < C_4 < C & (d) \\ C - C_4 > 0 & (e) \end{cases} \tag{3.39}$$

Where, R and C are the total resistance and capacitance of the construction including air films on both sides. The other two parameters can be solved as follows.

$$\begin{cases} R_3 = R - R_5 - R_1 \\ C_2 = C - C_4 \end{cases} \tag{3.40}$$

Finding the proper values of individual resistances and capacitances is a nonlinear optimization process. There exist many methods for optimization problems. House

and Smith [1991] employed a sequential quadratic programming (SQP) to compute the optimal values. Nizet and Lecomte et al. [1984] used a conjugate gradient method to develop an optimal control method. Both optimization methods as well as other conventional optimization methods have to start from initial guesses of optimal variables and their convergence speed is affected by their initial guesses in most cases. Genetic algorithm (GA) is a better optimization method especially when an optimal problem is not perfectly smooth and unimodal [Mitchell 1997]. It can quickly find a sufficiently good solution. The algorithm was ever used to search for global optimal solutions in HVAC field [Wang and Jin 2000, Wang and Wang 2002]. Herein, GA is utilized to search for the optimal values of individual resistances and capacitance of the simplified model. The details are described in the following sections.

3.5 Brief of genetic algorithm (GA)

GA is an advanced search and optimization technique. It has been developed to imitate the evolutionary principle of natural genetics. GA was developed Holland and his students and colleagues over the course of the 1960s and 1970s [Holland 1975, 1992]. The algorithm was finally popularized by one of his students, Goldberg [1989]. Goldberg [1989], Davis [1991] and Mitchell [1996] provided comprehensive overviews and introductions to GA. Deb [1996] compared the GA search method with traditional methods (the direct exhaustive search method and the gradient-directed search method) for function optimization. One of the main advantages of GA is that it is generally robust in finding global optimal solutions, particularly in multimodal and

49

multi-objective optimization problems [Deb 1996]. Another reason is that GA can find a sufficiently good solution quickly without initialization while other methods have to start from initial guesses of parameter, which have great effect on convergence speed in most cases. Extensive research on the theoretical fundamentals and applications of GA is still going on, aiming at better computation efficiency, improved robustness, and so on [Salomon 1998].

To use GA to solve an optimization problem, a coding system is necessary. Encoding represents a candidate solution (a trial set of the variables) in the search space by a code string called a *chromosome*. Usually, binary coding (0, 1) is used. Decoding is thus required to convert a bit-string into the corresponding set of variables for calculating objective function value. Generally, GA uses three operators (selection, crossover and mutation) to imitate the natural evolution processes. The working procedures of a simple GA using binary coding are summarized as follows.

1) *Initialization*: to create an initial population of bit-strings (chromosomes), randomly, which represent a population of trial solution candidates.

2) *Evaluation*: to calculate the fitness corresponding to each bit-string (each trial solution candidate) in the population. The fitness function is designed such that the better the value of the optimization objective function, the larger the fitness.

3) *GA operations*: to repeat the following operations until a new population of bit strings is formed.

Selection (or *reproduction*): to select a pair of good bit-strings in the current

population (parent population). The probability of a string in the parent population being selected (to mate with other string) is an increasing function of its fitness. Thus, a trial solution candidate that produced better values of objective function is more likely to be selected than those that produced inferior values.

Crossover: to exchange (crossover) randomly chosen portion(s) of the two strings, with certain probability (crossover probability or crossover rate), to form two offspring. Crossover is the dominating operation in GA.

Mutation: to mutate the offspring bit-strings at each locus with a certain probability (the mutation probability or mutation rate). Mutation rate is usually small.

4) *Replacement*: to replace the parent population with the obtained offspring bit-strings.

5) *Evaluation*: the same as step 2.

6) *Termination*: to stop after a pre-specified number of *generations* (one loop from step 3 to step 5 is called a generation) or when a criteria that determines the convergence is satisfied. Otherwise, go to step 3.

The procedures described above form a *run*. They are the basis for most applications of GA. There are a number of details to fill in, such as the size of the population and the probabilities of crossover and mutation.

3.6 Estimation of optimal parameters of simplified models using GA

For optimizing the parameters of simplified thermal network model (3R2C model) in frequency domain, the frequency characteristics of theoretical and simplified models should be calculated first as described in *Section 3.6.1*. A GA estimator is developed to find the optimal parameters of the simplified thermal network model as described in *Section 3.6.2*.

3.6.1 Calculation procedures

The theoretical frequency characteristics are calculated following the procedure as below:

1. The properties (λ, ρ, C_P, L) of individual layers of the calculated walls and the thermal resistance (R_{in} and R_{out}) are provided. The number of frequency points N and the frequency range $(10^{-n_1}, 10^{-n_2})$ of concern are determined. n_1, n_2 and N are generally chosen as 10, 3 and $10(n_1 - n_2) + 1$ respectively [Wang and Chen 2001].

2. N frequency points logarithmically and equally spaced in the frequency range are generated. At the frequency point, ω_k, calculate the complex transmission matrix of individual layers by substituting s with $j\omega_k$ in equations (3.6)-(3.8), and the complex elements $A(j\omega_k)$, $B(j\omega_k)$ and $D(j\omega_k)$ of the total transmission matrix by multiplying the complex transmission matrix of individual layers including the surface films as equation (3.4). The theoretical

frequency characteristics of $G_X(j\omega_k)$, $G_Y(j\omega_k)$ and $G_Z(j\omega_k)$ from Equations (3.12), (3.13) and (3.14) are yielded. The amplitude and phase lag are calculated simultaneously.

The frequency characteristics of simplified 3R2C models can be calculated as follows. With assigned values of individual resistances and capacitances, and the frequency points, the complex elements $A'(j\omega_k)$, $B'(j\omega_k)$ and $D'(j\omega_k)$ of the total transmission matrix are calculated as Equation (3.30), (3.31) and (3.33). The frequency characteristics of $G'_X(j\omega_k)$, $G'_Y(j\omega_k)$ and $G'_Z(j\omega_k)$ as Equation (3.35), (3.36) and (3.37) are yielded. The amplitudes and phase lags are calculated simultaneously.

3.6.2 GA estimator

Figure 3.3 shows schematically the optimization procedure of the GA estimator developed. It starts with random estimates of the individual capacitances and resistances with the constraints as shown in Equation (3.39). The component with grey background represents the procedures of a GA *run*. Multiple *runs* are allowed. Equation (3.41) represents the fitness function (*f*), which is the reciprocal of the objective function of the minimization problem as Equation (3.38).

$$f = f(R_1, R_5, C_4) = \frac{1}{J(R_1, R_5, C_4)} \tag{3.41}$$

In the genetic algorithm, the three parameters (*R₁, R₅, C₄*) constitute the

chromosome of an individual, Equations 3.39(*a*), 3.39(*b*) and 3.39(*d*)) are the search space for (R_1, R_5, C_4). Initializing the three parameters produce the initial population to start a GA *run*. In initializing process, the values of (R_1, R_5, C_4) are checked to meet the constraints of Equation 3.39(*c*) and 3.39(*e*). In the crossover and mutation processes, the values of (R_1, R_5, C_4) are also checked to meet the constraints of Equations 3.39(*c*) and 3.39(*e*). If the constraints are not met, crossover and mutation processes will repeat till the constraints are met.

A GA *run* is terminated if the number of the current generation is equal to a predefined maximum number. At least two *runs* of the GA processes are necessary when running the GA optimizer. The criterion to stop the GA optimizer is based on the comparison of the best fitness values of two consecutive *runs*. When the relative difference between the two maximum fitness values (d_f) reaches a threshold value (ε_f, 0.0001 was chosen in this study), the GA estimator stops. The GA driver developed by Carroll [2001] was revised for use in this study. The control parameters of the GA estimator are given in Table 3.1.

Start GA Estimator: *run=0*

Randomly initializing the Values of R_1, R_5, C_4

No — Satisfy the Constraints?

Yes

GA Population Initialization
$i_{gen} = 1, [R_1, R_5, C_4]$

Calculate the frequency characteristics of the simplified 3R2C model

Theoretical frequency characteristics

Calculate the objective function $J(R_1, R_5, C_4)$

Fitness Evaluation – the i_{gen} generation
1. Calculate the fitness function $f(R_1, R_5, C_4)$
2. Record the elitist and the best fitness $f_{best}(run)$

Stop GA run? i_{gen} = Max generation — Yes

No

GA operation: Selection

GA operation: Crossover Mutation

No — Satisfy the constraints

Yes

Generating new generation $[R_1, R_5, C_4]^{gen}$

$i_{gen} = i_{gen} + 1$

No — Stop GA run? $d_f = \varepsilon_f$

Yes

Stop & Output R_1, R_5, C_4

Figure 3.3 Optimization procedure of the developed GA estimator

Table 3.1 Control parameters of the GA Estimator

Selection	Tournament scheme and elitism
Crossover	Single-point; one child from a pair of parents for next
Mutation	Both creep and jump mutations enabled (creep mutation rate is 0.04; jump mutation rate is 0.02)
Maximum generation of a GA run	100
Population size	20
Length of chromosome	30 bits (10 bits for each of the searching variables)
Threshold value	$\varepsilon_f = 0.0001$

3.7 Thermal load model through constructions

The differential equations of the simplified model of building envelope can be solved numerically to calculate heat gains and loss. The simplified model can also be developed using response factor method to calculate the heat gains and loss with fixed time step, particularly for the hourly record weather data. It is easy to find the negative real roots ($-s_i, i = 1,2,...,m$) of $B'(s)$ because the s-transfer functions $G'(s)$ of the simplified models are polynomial. The periodical response factor of a unit triangle pulse of the cross and internal heat conduction can be read as follows (the period is 24 hours).

$$Y(0) = K + \sum_{i=1}^{m} \frac{K_{yi}}{\Delta s_i} (1 - e^{-\Delta s_i}) \frac{1 - e^{-23\Delta s_i}}{1 - e^{-24\Delta s_i}} \tag{3.42}$$

$$Y(k) = -\sum_{i=1}^{m} \frac{K_{yi}}{\Delta s_i} \frac{(1 - e^{-\Delta s_i})^2}{1 - e^{-24\Delta s_i}} 1 - e^{-(k-1)\Delta s_i} \qquad (k \geq 1) \tag{3.43}$$

$$Z(0) = -K + \sum_{i=1}^{m} \frac{K_{zi}}{\Delta s_i}(1 - e^{-\Delta s_i})\frac{1 - e^{-23\Delta s_i}}{1 - e^{-24\Delta s_i}} \tag{3.44}$$

$$Z(k) = -\sum_{i=1}^{m} \frac{K_{zi}}{\Delta s_i} \frac{(1 - e^{-\Delta s_i})^2}{1 - e^{-24\Delta s_i}} 1 - e^{-(k-1)\Delta s_i} \qquad (k \geq 1) \tag{3.45}$$

where, subscript i denotes the component of ith root, k denotes kth step, and

$Y =$ The periodical response factor of a unit triangle pulse of the cross heat conduction ($Wm^{-2}K^{-1}$);

$Z =$ The periodical response factor of a unit triangle pulse of the internal heat conduction ($Wm^{-2}K^{-1}$);

$\Delta =$ Time interval (3600s);

$$K_{yi} = \left.\frac{-1}{s \cdot dB'(s)\Big/ds}\right|_{s=-s_i} ;$$

$$K_{zi} = \left.\frac{D'(s)}{s \cdot dB'(s)\Big/ds}\right|_{s=-s_i} ;$$

$K =$ Total thermal transfer coefficient of the construction ($Wm^{-2}K^{-1}$).

The total periodical heat gain or loss through a construction can be calculated by the summation of two discrete convolutions as follows.

$$q(k) = \sum_{k=0}^{23} Y(n)T_{sol}(23-n) + \sum_{k=0}^{23} Z(n)T_{in}(23-n) \tag{3.46}$$

where T_{sol} and T_{in} are the solar air temperature and indoor air temperature.

3.8 Summary

Efficient and effective method for optimal nodal placement of simplified models is important in practical applications. This chapter presented a method for optimizing the parameters of the simplified dynamic model of building envelope based on frequency domain analysis. The genetic algorithm (GA) provides an efficient solution for the nonlinear optimization problem for the model nodal placement.

CHAPTER 4 VALIDATION OF OPTIMAL NODAL PLACEMENT OF SIMPLIFIED MODELS OF BULDING ENVELOPES

In the previous chapter, optimal nodal placement method for simplified models of building envelopes based on frequency characteristic analysis is presented. In the chapter, results of case studies are presented to validate the optimal nodal placement method of simplified models. The accuracy of the simplified models with parameters identified by the optimal nodal placement method was studied by comparing with the models of other parameters configurations.

4.1 Different configurations of simplified models

The outputs of the 3R2C model with optimal nodal placement are compared in frequency response domain and time domain with those of the theoretical model and two simplified 3R2C models with typical configurations normally used in application. The two simplified models are named as 3R2C model (a) and 3R2C model (b) in this study as below.

Model (a): three resistances are outside conductive resistance, wall conduction resistance and inside conductive resistance respectively, the value of individual capacitance is half of the total capacitance.

Model (b): three resistances and two capacitances are distributed evenly.

The results of studies using three typical external walls are presented below. They are a light construction, a medium construction and a heavy construction according to the mass classification [ASHRAE 1997]. The transient thermal load analysis was also conducted on the medium construction.

4.2 Wall group 2

Wall group 2 was selected from the *ASHRAE Handbook of fundamentals* [ASHRAE 1997]. The wall, which is mainly the insulation layer, is a typical light weighted wall with the density 90 *Kg/m²*. The detailed properties of the wall in SI unit are given in Table 4.1. With the GA estimator, the parameters of the optimal simplified 3R2C model were obtained. The parameters of the three simplified models are shown in Table 4.2.

Table 4.1 Details of Wall Group 2 of light construction

Description	Thickness and thermal properties				
	$L(mm)$	$\lambda(Wm^{-1}K^{-1})$	$\rho(kgm^{-3})$	$C_p(Jkg^{-1}K^{-1})$	$R(m^2KW^{-1})$
Outside surface film					0.059
Stucco	25	0.692	1858	840	0.03613
Insulation	125	0.043	91	840	2.90697
Plaster or gypsum	20	0.727	1602	840	0.02751
Inside surface film					0.121

Table 4.2 Parameters of simplified 3R2C models of Wall Group 2

Model	Parameters of resistance and capacitance $R(m^2 KW^{-1})$ $C(Jm^{-2}K^{-1})$						
	R_1	C_2	R_3	C_4	R_5	R (total)	C (total)
Theoretical model	-	-	-	-	-	3.1498	75487
Simplified model (a)	0.0586	37743	2.9706	37743	0.1206	3.1498	75487
Simplified model (b)	1.0499	37743	1.0499	37743	1.0499	3.1498	75487
Optimal simplified model	0.0732	42175	2.9394	33312	0.1372	3.1498	75487

Numerical comparisons between the frequency responses of heat conduction of the theoretical model and those of the three simplified models respectively were made within the frequency range of normal concern (10^{-10} to 10^{-3} $rads^{-1}$). Among the frequency responses of the external, cross, and internal heat conduction of three simplified models, Model (b) of the wall produces great deviation from the frequency responses of the theoretical model, as shown in Figure 4.1, 4.2 and 4.3. Therefore, the model can produce large errors in transient thermal calculation. Figures 4.1, 4.2 and 4.3 also show that there are good agreements among model (a), the optimal model and the theoretical model in amplitudes and phase lags of the external, cross, and internal heat conduction.

However, Figure 4.1 indicates the amplitude and phase lag of external heat conduction of the optimal model are closer to those of the theoretical model compared with those of Model (a). Figure 4.2 also shows that the optimal model matches much better with the theoretical model compared with the Model (a) in high frequency regions in term of amplitude and phase lag. As shown in Figure 4.3, the optimal model and Model (a) have similar agreements with the theoretical model in term of

amplitudes and phase lags in the frequency ranges of normal concern.

Results show that the simplified Model (b) cannot produce satisfied results because the dynamic frequency responses of the model deviate greatly from that of theoretical model. When simplified 3R2C models are used to carry out transient thermal calculation or simulation for light constructions mainly with insulation, Model (a) is good choice as the simplified model for simulating light walls. However, the simplified model with optimal nodal placement is even more accurate than Model (a).
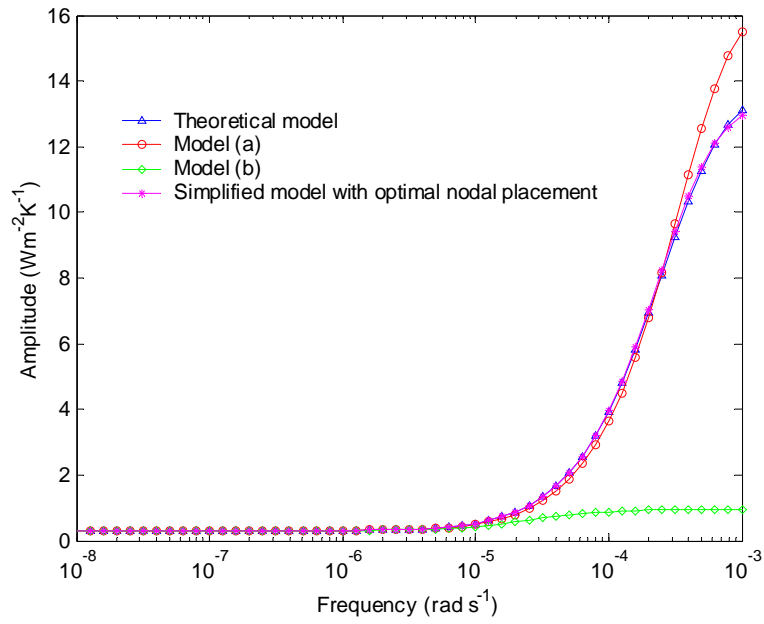
(a) Amplitude
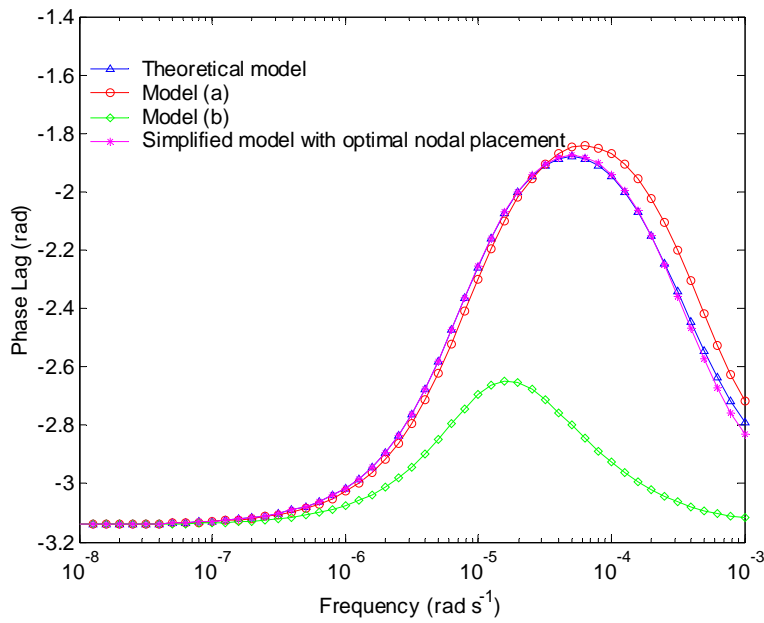
(b) Phase Lag

Figure 4.1 Frequency responses of external heat conduction for Wall group 2
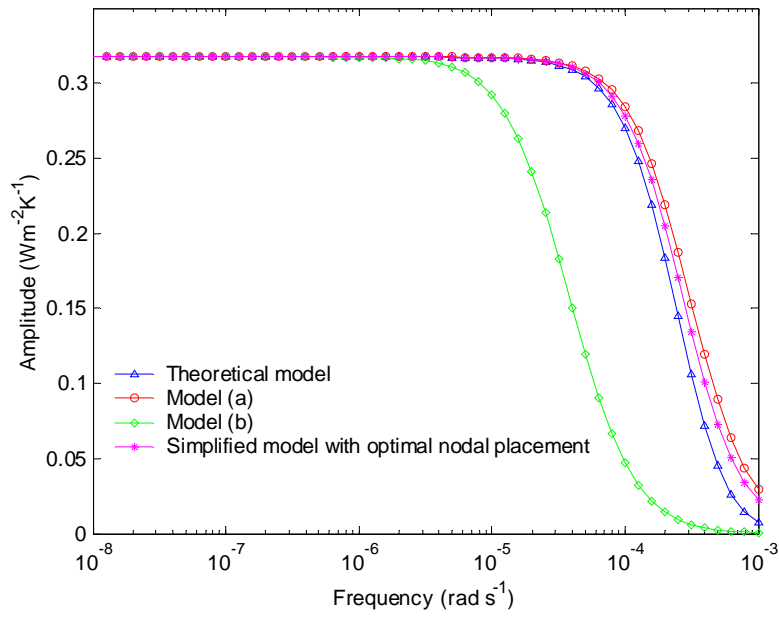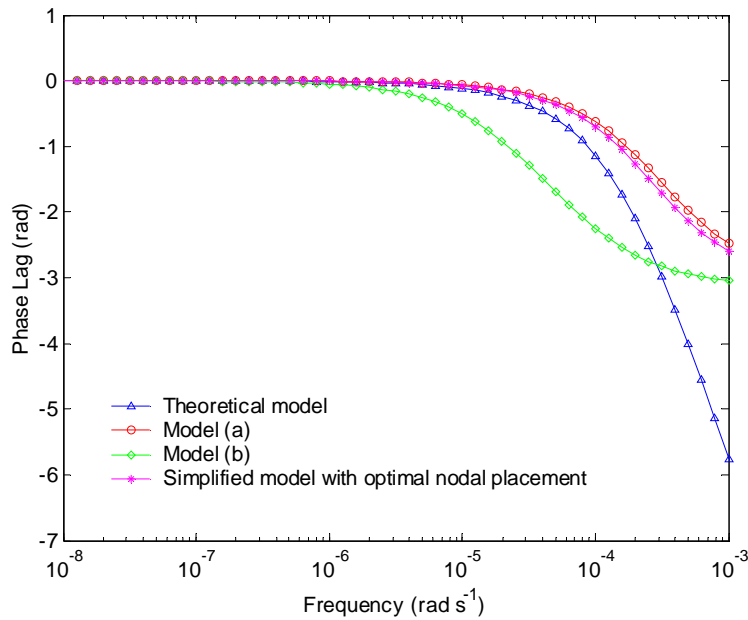
(a) Amplitude

(b) Phase Lag

Figure 4.2 Frequency responses of cross heat conduction for Wall group 2
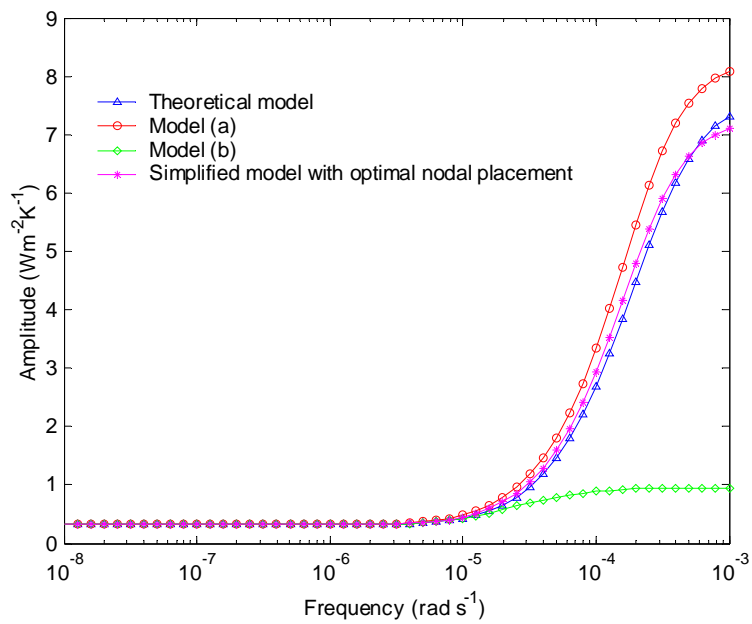
(a) Amplitude
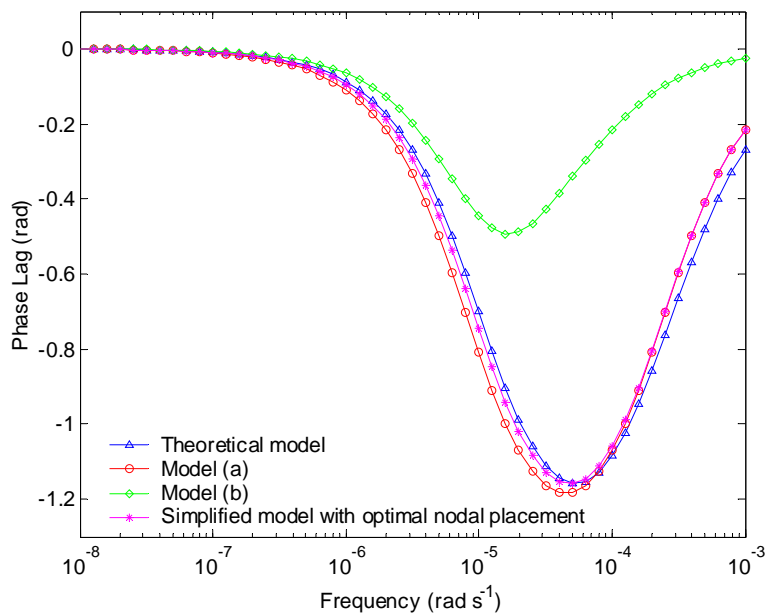
(b) Phase Lag

Figure 4.3 Frequency responses of internal heat conduction for Wall group 2

4.3 A brick/cavity wall

A brick/cavity wall, which is a medium weighted construction with the density 409 Kg/m^2 (details are given in Table 4.3). Using time-domain methods, Davies [1996] provided all its CTF coefficients, also list in Table 4.3. These coefficients provide a convenient reference to calculate the transient thermal transfer of the theoretical model, which can be used to evaluate the calculated transient thermal transfer of various simplified models of the wall with variable sol-air temperature and indoor air temperature. With the GA estimator, the parameters of the optimal simplified 3R2C model were obtained. The parameters of the three simplified models are shown in Table 4.4.

Table 4.3 Details and CTF coefficients of a brick/cavity wall of medium construction

Description	Thickness and thermal properties					
	$L(mm)$	$\lambda(Wm^{-1}K^{-1})$	$\rho(kgm^{-3})$	$C_p(Jkg^{-1}K^{-1})$	$R(m^2KW^{-1})$	
Outside surface film					0.060	
Brickwork	105	0.840	1700	800	0.125	
Cavity					0.180	
Heavyweight concrete	100	1.630	2300	1000	0.06135	
Inside surface film					0.120	
k	0	1	2	3	4	5
$b_k(Wm^{-2}K^{-1})$	0.000179	0.013915	0.043460	0.018036	0.001034	0.000005
$c_k(Wm^{-2}K^{-1})$	6.953625	-12.223156	5.985915	-0.660046	0.020334	-0.000044
d_k	1.000000	-1.620834	0.726131	-0.065025	0.001594	0.000000

The frequency responses of the four models have similar characteristics in low frequency region as shown in Figure 4.4, 4.5 and 4.6 Figure 4.4 shows that the amplitudes and phase lags of external heat conduction of the simplified model of optimal nodal placement well agree with those of the theoretical model in high

frequency region, while the frequency characteristics of model (a) and model (b) deviate greatly from the theoretical frequency characteristics in opposite directions in the high frequency region.

Table 4.4 Parameters of simplified 3R2C models of a brick/cavity wall

Model	Parameters of resistance and capacitance $R(m^2KW^{-1})$ $C(Jm^{-2}K^{-1})$						
	R_1	C_2	R_3	C_4	R_5	R (total)	C (total)
Theoretical model	-	-	-	-	-	0.5455	372800
Simplified model (a)	0.0586	186400	0.3663	186400	0.1206	0.5455	372800
Simplified model (b)	0.1818	186400	0.1818	186400	0.1818	0.5455	372800
Optimal simplified model	0.0929	122420	0.3111	250380	0.1415	0.5455	372800

For the frequency response characteristics of the cross heat conduction, Figure 4.5(b) indicates that the three simplified models have similar phase lags deviating from the theoretical phase lag in the high frequency region. However, the amplitudes of the simplified model with optimal nodal placement almost overlap with those of the theoretical model, while the amplitudes of the simplified Model (a) are greater than those of the theoretical model and the amplitudes of simplified model (b) less than those of the theoretical model in the high frequency region (Figure 4.5(a)).

For the frequency response characteristics of the internal heat conduction, Figure 4.6(a) and (b) indicate that the amplitudes and phase lags of the optimal simplified model agree with those of the theoretical model while the frequency characteristics of simplified model (a) and (b) deviate greatly from the theoretical frequency characteristics in the high frequency region. Same results can be observed when studying the calculated heat gains of those models.
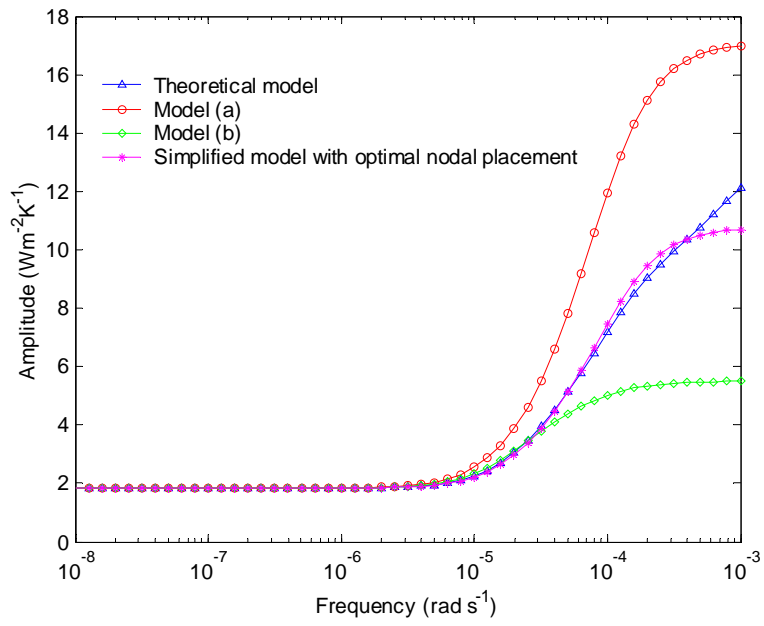
(a) Amplitude
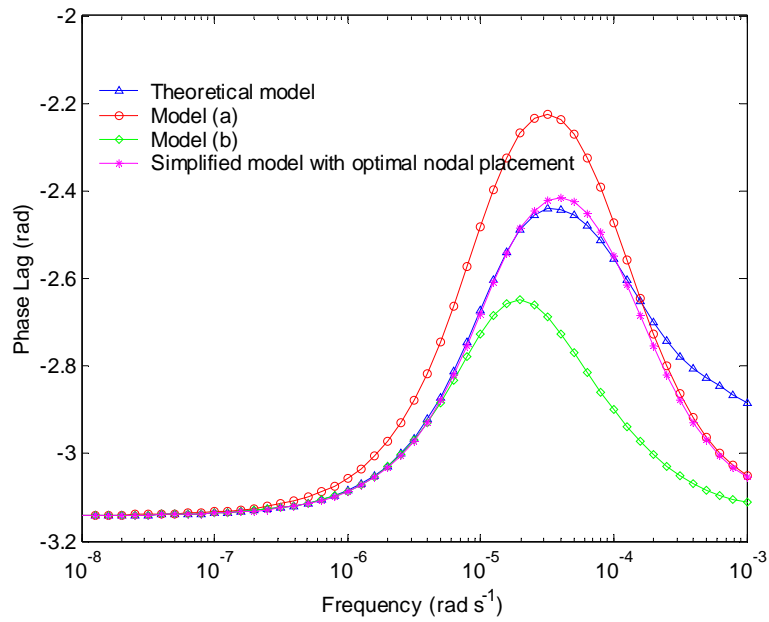
(b) Phase Lag

Figure 4.4 Frequency responses of external heat conduction for Brick/cavity wall
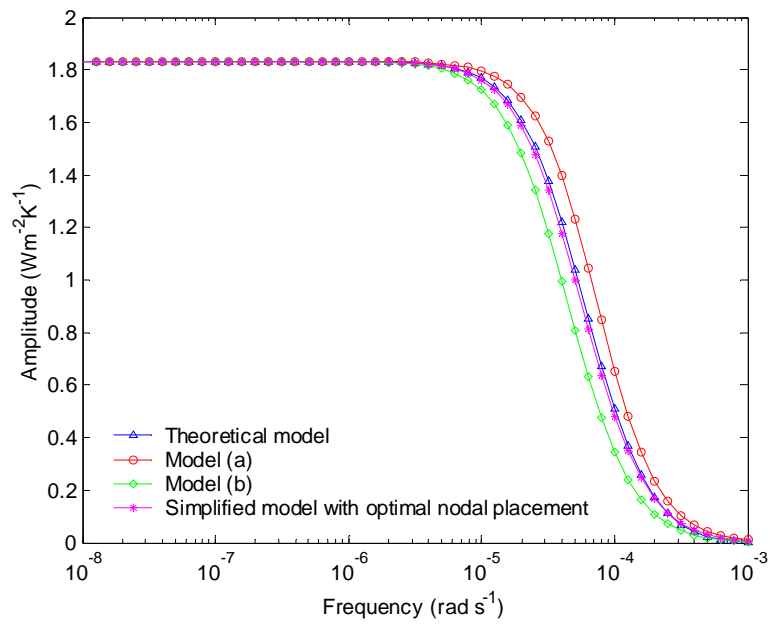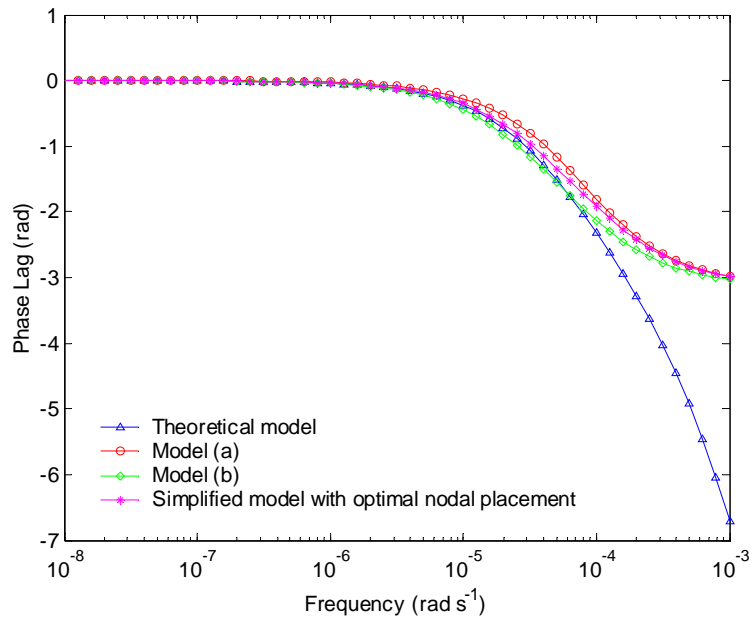
(a) Amplitude

(b) Phase Lag

Figure 4.5 Frequency responses of cross heat conduction for Brick/cavity wall
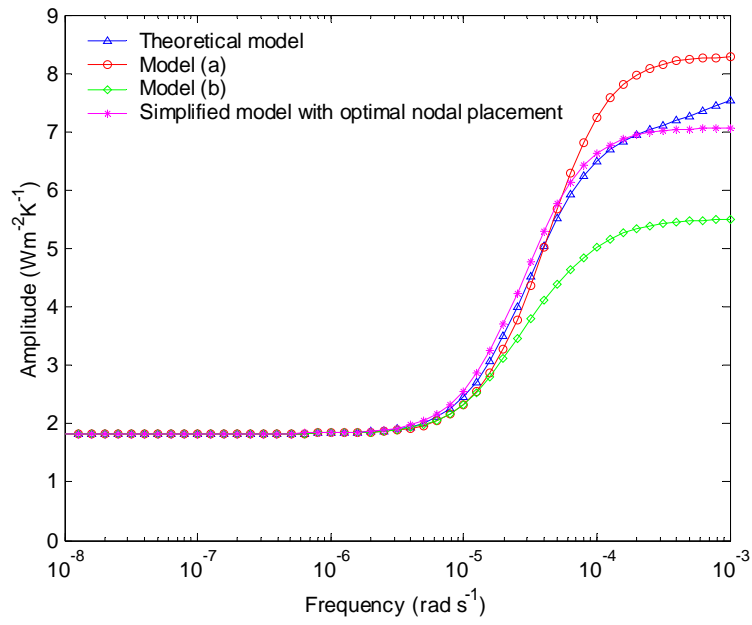
(a) Amplitude
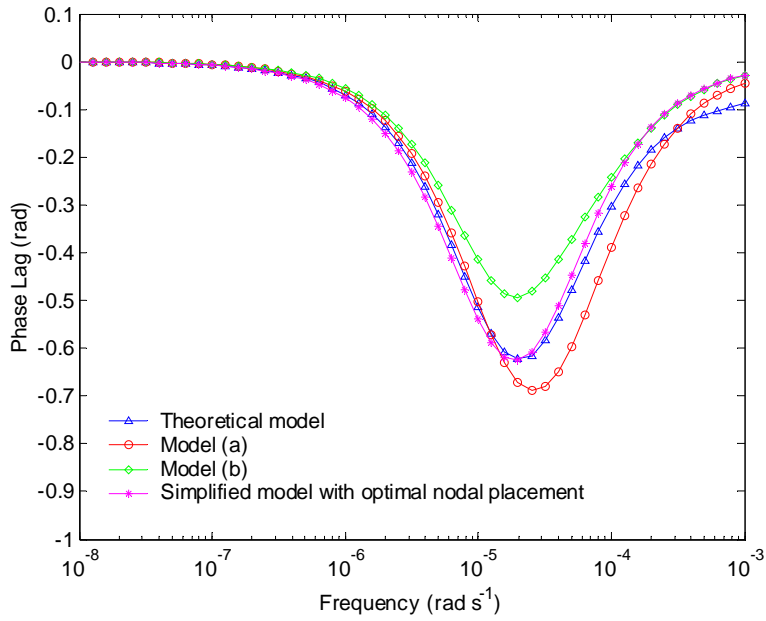
(b) Phase Lag

Figure 4.6 Frequency responses of internal heat conduction for Brick/cavity wall

In real applications, the indoor air temperature changes continuously. Therefore, it's necessary to consider the effects of the change of indoor air temperature when monitoring the whole building energy performance, diagnosing the whole building, evaluating various thermal mass control strategies, and predicting retrofit energy saving, etc. For an intermittent air-conditioned building with the brick/cavity external wall, the daily sol-air temperature and indoor air temperature on a typical summer day are selected for heat gain calculation as shown in Figure 4.7. The heat gains of simplified models are calculated using response factor method with the parameter in Table 4.4, while the heat gain of the theoretical model is calculated using CTF method with the coefficients in Table 4.3. In fact, it is very easy to find the negative real roots ($-s_i, i = 1,2,...,m$) of $B'(s)$ of 3R2C models because they are polynomial. Consequently, the response factor of a unit triangle pulse (of height 1 K and base $2\varDelta$) of the cross and internal heat conduction can be easily calculated as Equation (3.42~3.45).

The heat gains of simplified models are compared with that of the theoretical model as shown in Figure 4.8. The average errors of hourly heat gains of the Model (a), Model (b) and the simplified model of optimal nodal placement (compared with that of the theoretical model) are 6.1%, 10.7% and 3.4% respectively. These results further confirm again that the simplified model with optimal nodal placement agrees better with the theoretical model compared with other configuration of the same order simplified model.
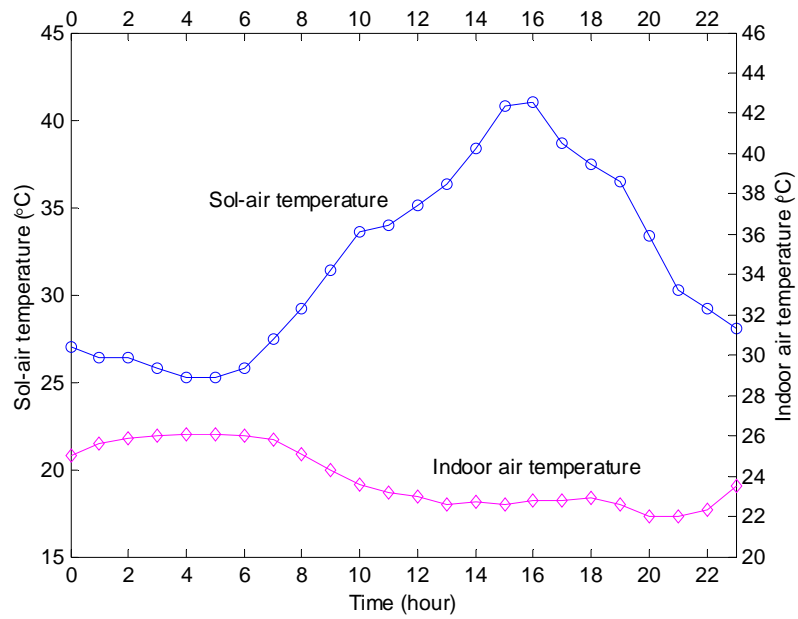
Figure 4.7 Profiles of sol-air temperature and indoor air temperature
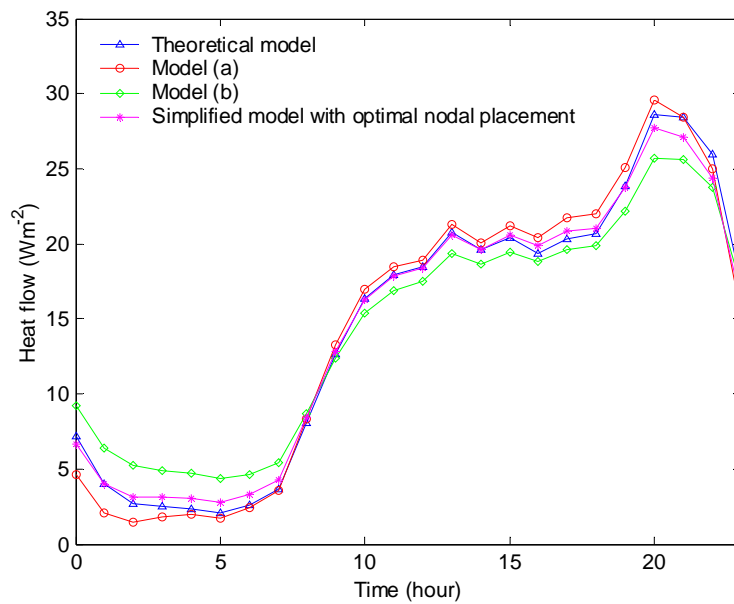
Figure 4.8 Hourly heat gains through the brick/cavity wall

For medium weighted construction, when simplified 3R2C models are used to calculate the transient thermal transfer, the simplified models with optimal nodal placement is the best choice while acceptable results might be produced using other simplified models. Concerning the accuracy of heat transfer calculation, simplified model with optimal nodal placement has obvious advantage. If accuracy of heat transfer calculation is very important in an application, higher order thermal network models are necessary.

4.4 Wall group 41

Wall group 41 was selected from *ASHRAE Handbook of fundamentals* [ASHRAE 1997]. The wall, mainly composed of insulation and high density concrete, is a typical heavy weighted wall with the density 917 Kg/m^2. The details of properties in SI unit are shown in Table 4.5.

Table 4.5 Details of Wall Group 41 of heavy construction

Description	Thickness and thermal properties				
	$L(mm)$	$\lambda(Wm^{-1}K^{-1})$	$\rho(kgm^{-3})$	$C_p(Jkg^{-1}K^{-1})$	$R(m^2KW^{-1})$
Outside surface film					0.059
Face brick	100	1.333	2002	920	0.07502
Insulation	125	0.043	91	840	2.90698
High density concrete	300	1.731	2243	840	0.17331
Plaster or gypsum	20	0.727	1602	840	0.02751
Inside surface film					0.121

Table 4.6 Parameters of simplified 3R2C models of Wall Group 41

Model	Parameters of resistance and capacitance $R(m^2 KW^{-1})$ $C(Jm^{-2}K^{-1})$						
	R_1	C_2	R_3	C_4	R_5	R (total)	C (total)
Theoretical model	-	-	-	-	-	3.362	785889
Simplified model (a)	0.0586	392945	3.1828	392945	0.1206	3.362	785889
Simplified model (b)	1.1207	18640	1.1207	186400	1.1207	3.362	785889
Optimal simplified model	0.0813	183543	3.0985	602346	0.1822	3.362	785889

The frequency responses of the external, cross, and internal heat conduction of the four models are shown in Figure 4.9, 4.10 and 4.11. The results show that the frequency characteristics of Models (a) and Model (b) have great disagreements with the theoretical frequency characteristics even in low frequency region. Figure 4.9 shows the frequency characteristics of external heat conduction of model (a) and (b) deviate greatly from the theoretical frequency characteristics in wide frequency range. For the frequency response characteristics of cross heat conduction, Figure 4.10(b) shows that the phase lags of Model (a) and Model (b) are far from the theoretical phase lags, while amplitudes of simplified Model (a) are greater than those of the theoretical model and the amplitudes of simplified Model (b) much smaller than those of the theoretical model in the high frequency region (Figure 4.10(a)). For the frequency response characteristics of the internal heat conduction, Figure 4.11(a) shows that the amplitudes of Model (a) and Model (b) deviate from the theoretical amplitudes in wide frequency range, while the deviation of phase lags occur in almost all the frequency region (Figure 4.11(a)).

The frequency responses of the external heat conduction of the model with

optimal nodal placement match much better with those of the theoretical model (Figure 4.9). The amplitudes of the cross heat conduction of the model with optimal nodal placement are also very close to those of the theoretical model (Figure 4.10(a)). The phase lags of the cross heat conduction of the model with optimal nodal placement deviates significantly from the theoretical phase lags in a wide range at high frequency (Figure 4.10(b)) and the frequency responses of the internal heat conduction of the model also do not well match those of the theoretical model in the high frequency range (about from 10^{-5} to 10^{-3} rads^{-1}) (Figure 4.11).

Further analysis on these results shows that the amplitude of heat transfer calculation using the simplified model with optimal nodal placement is acceptable and has much better accuracy compared with other simplified models. The dynamics of the model outputs presents significant error even thought it is much better than other simplified models. Therefore, when the accuracy on the prediction of dynamics is of concern, higher order thermal network models should be used for heavy weighted constructions if model simplification is needed.
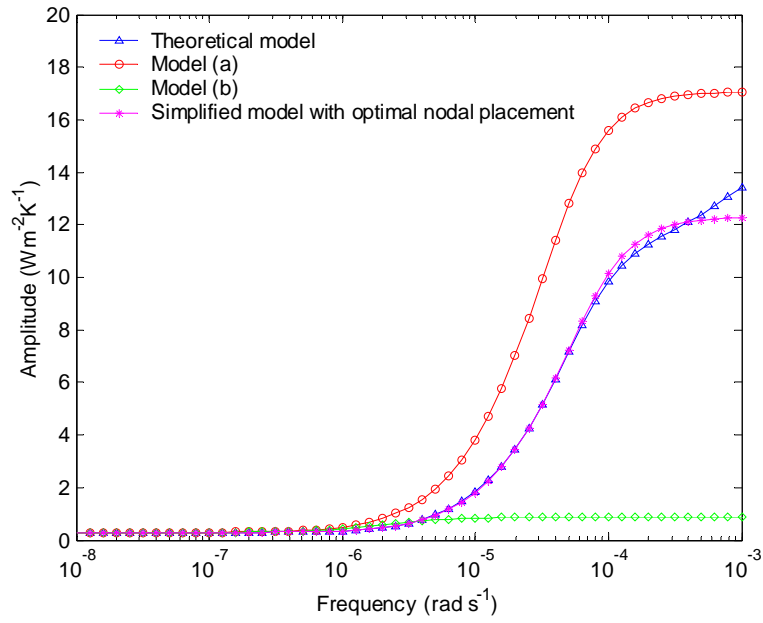
(a) Amplitude
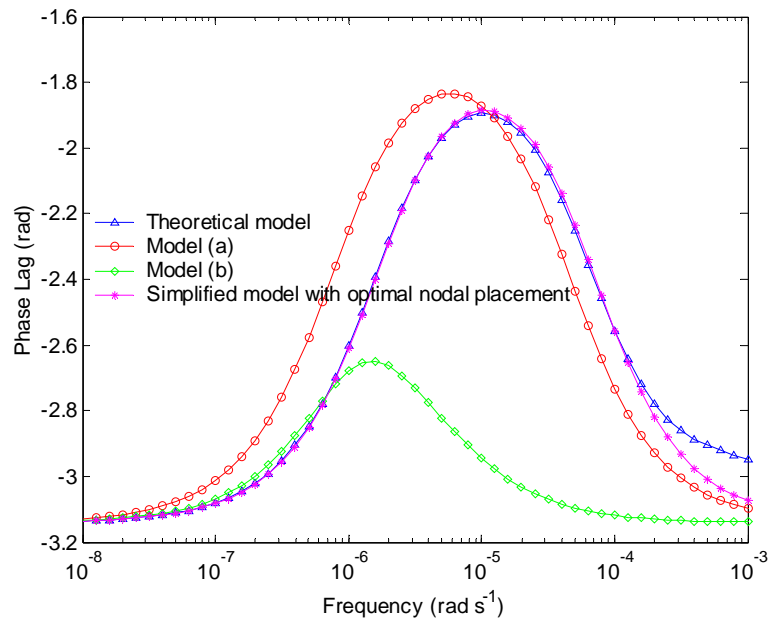
(b) Phase Lag

Figure 4.9 Frequency responses of external heat conduction for Wall group 41
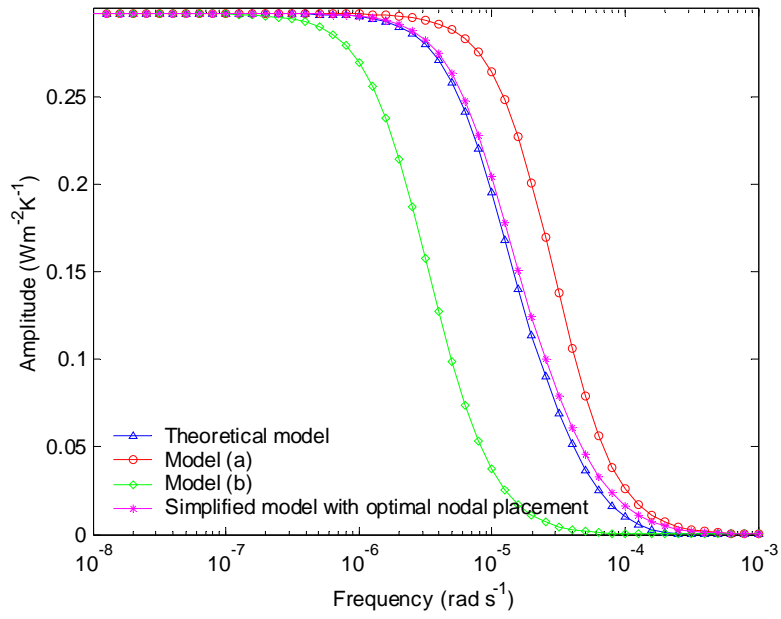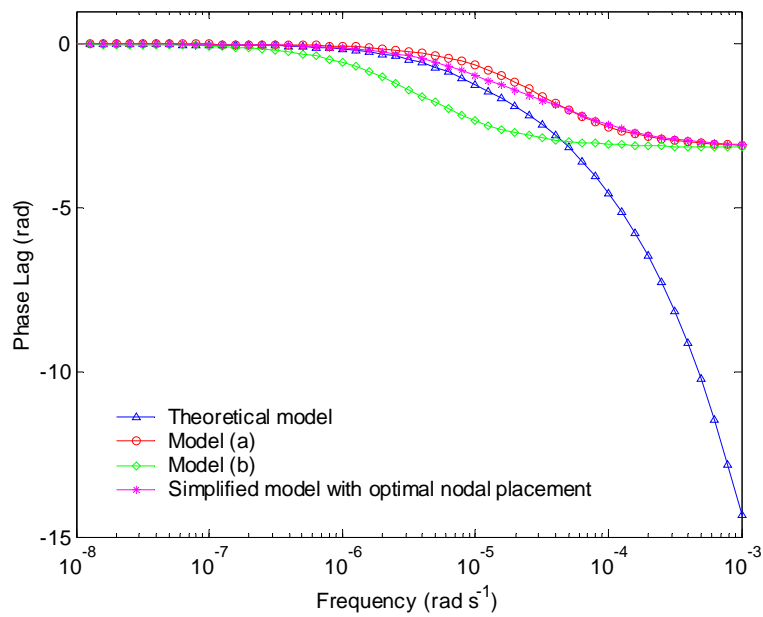
(a) Amplitude

(b) Phase Lag

Figure 4.10 Frequency responses of cross heat conduction for Wall group 41
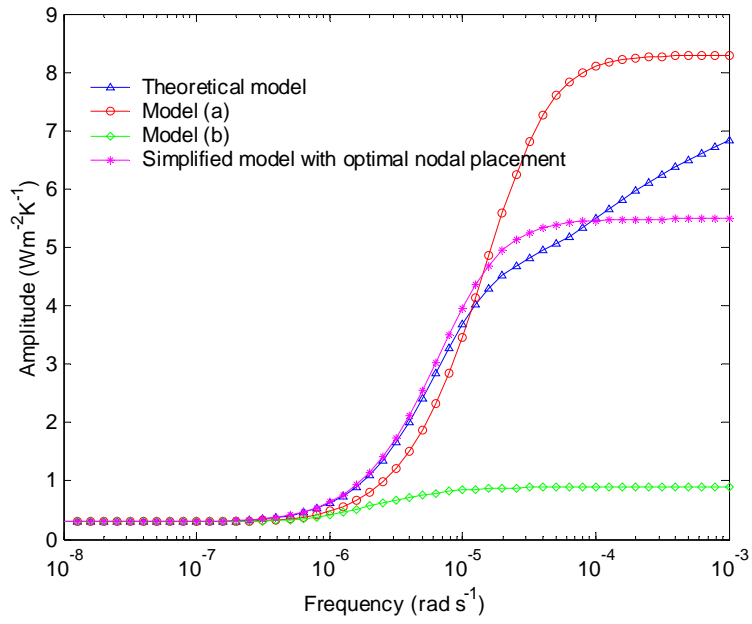
(a) Amplitude
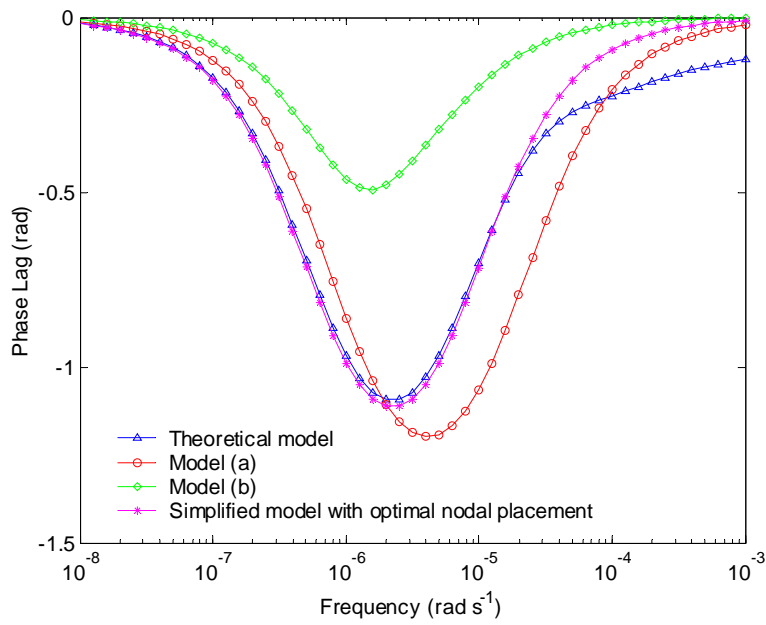
(b) Phase Lag

Figure 4.11 Frequency responses of internal heat conduction for Wall group 41

4.5 Summary

To simplify the dynamic simulation of light weighted walls, the 3R2C model with optimal nodal placement provides dynamic heat transfer calculation of very high accuracy while some other configuration of 3R2C model might provide calculation of reasonable accuracy. For medium weighted constructions, the 3R2C model with optimal nodal placement provides calculations of good accuracy, and the other simplified models have much lower accuracy. When the accuracy of dynamic simulation is of concern, the optimization of nodal placement is important. For heavy weighed constructions, the simplified model with optimal nodal placement can provide results of acceptable accuracy. However, if the accuracy (particularly the time delay of dynamic response) of simulation is of concern, higher order thermal network models should be used if model simplification is needed.

CHAPTER 5 A SIMPLE TIME DOMAIN CALCULATION METHOD FOR THERMAL RESPONSE FACTORS

Although the simplified models of building envelopes are used to estimate building cooling energy consumption in the form of differential equations, how to simply calculate the thermal response factors and CTF (conduction transfer function) coefficients of those simplified thermal network models for practical applications is great of value as the extension of simplified models. This chapter presents a new method to derive thermal response factors of thermal network models (finite differential models) for estimating transient heat transfer through building structures. The derived response factors can be used to easily develop CTF (conduction transfer function) coefficients directly which is also used for transient heat transfer calculations.

5.1 Introduction

Heat transfer models of building structure are of primary importance for building and HVAC design and simulation programs. The heat transfer models through building walls and roofs represent the heat transfer through composite medium consisting of several layers of different physical properties in contact. There are various ways to calculate the heat transfer of building structures. The methods currently used are mainly the response factor method, finite differential method (thermal network method) and the combination of the two methods.

Response factor method [Stephenson et al. 1967, Mitalas 1968] and conduction transfer function (CTF) method [Stephenson and Mitalas 1971] are often used to calculate the space load. Both methods are involved in a computationally lengthy, tedious and inefficient process of finding the poles of hyperbolic s-transfer function and computing their residues [Kusuda 1969] and occasionally may lead to miscalculation due to missing a root, particularly in the case where two adjacent roots are close together [Ouyang and Haghighat 1991]. Researchers were concerned in developing methods to simplify the calculation of the response factors. For example, to avoid finding the poles of hyperbolic s-transfer function, Chen and Wang [2001] developed the frequency-domain regression method to estimate polynomial s-transfer functions whose frequency responses are equivalent to the theoretical frequency responses of the building constructions. With the estimate polynomial s-transfer functions, the response factors and CTF coefficients can be calculated with the inverse Laplace transform.

Finite differential method simplifies the heat conduction problem [Myers 1971] by discretizing the building structure using a set of n nodal points corresponding to a system of n simultaneous first-order ordinary differential equations to be solved for the temperature-time history at each of the n nodal points. Many studies concerned with the problem of nodal placement (thermal network generation). Butler and Letherman [1980], Waters and Wright [1985], and European standard [1995], et al., studied significantly on the nodal placement of the finite differential models (thermal network models). The solution of these differential equations is typically

approximated using the Eluer and Crank-Nicolson technique for moving ahead step by step in time. However, using these numerical techniques, a critical time is needed and the internal temperature distribution is needed to be calculated [Myers 1980, Seem et al 1989]. Furthermore, if it is desired to determine the response of the same structure to another input time history, it is necessary to solve the complete problem over again [Myers 1980].

Based on the finite differential and thermal network concept, a state space method [Myers 1980, Seem et al. 1989, Ouyang and Haghighat 1991] and a time-domain method [Davies 1997] are developed to calculate the thermal response factors and CTF coefficients of finite differential model (thermal network model). Using this method, a large number of iterations might be needed to evaluate the delay times. The sate space method developed by Ouyang and Haghighat [1991] needs to obtain rational fractions of s transfer function from simple series expansion. Some measures are also required to improve the rate of convergence. Simpler and accurate methods are desired for thermal response factor calculation.

This chapter presents a simple method in time-domain to calculate thermal response factors and conduction transfer function coefficient of transient heat transfer models which are used to simulate heat transfer of building structures. This method in time-domain has the advantages of both finite differential models and the thermal response factor method. The method begins with a set of established finite differential equations of a finite differential model. First, the state equation is generated from the

finite differential equations and matrix exponential function is transferred to matrix polynomial. Secondly, the temperature response function of the system forcing by the defined ramp excitation is solved in time domain, which is easy since the matrix exponential function can be derived easily. Then, the temperature response factors of the system forcing by the unit triangle excitation is easily deduced because the unit triangle pulse is the combination of ramp pulses with different intercepts and slopes. Finally, the thermal response factors are calculated easily with simple arithmetic by dividing the temperature response factors with the corresponding resistances. With the thermal response factors, the CTF coefficients can be deduced easily. Validation and comparison are carried out in various cases which show that the method can work well and provide thermal response factors with sufficient accuracy for practical applications.

5.2 State space formulation of simplified models

The heat transfer of building structure can be represented by finite differential models when discretizing the process spatially as shown in Figure 5.1. The differential equations of the thermal network model are as follows.

$$
\begin{cases}
C_2 \dfrac{dT_2}{dt} = \dfrac{T_0 - T_2}{R_1} - \dfrac{T_2 - T_4}{R_3} & (1) \\[2mm]
C_4 \dfrac{dT_4}{dt} = \dfrac{T_2 - T_4}{R_3} - \dfrac{T_4 - T_6}{R_5} & (2) \\[2mm]
\quad \cdots\cdots \\[2mm]
C_{2(n-1)} \dfrac{dT_{2(n-1)}}{dt} = \dfrac{T_{2(n-2)} - T_{2(n-1)}}{R_{2n-3}} - \dfrac{T_{2(n-1)} - T_{2n}}{R_{2n-1}} & (n-1) \\[2mm]
C_{2n} \dfrac{dT_{2n}}{dt} = \dfrac{T_{2n-2} - T_{2n}}{R_{2n-1}} - \dfrac{T_{2n} - T_{in}}{R_{2n+1}} & (n)
\end{cases}
\qquad (5.1)
$$

Heat transfer at the inside surface and out side can be described in the following.

$$q_{in} = \frac{T_{2n} - T_{in}}{R_{2n+1}} \tag{5.2}$$

$$q_{out} = \frac{T_{out} - T_2}{R_1} \tag{5.3}$$
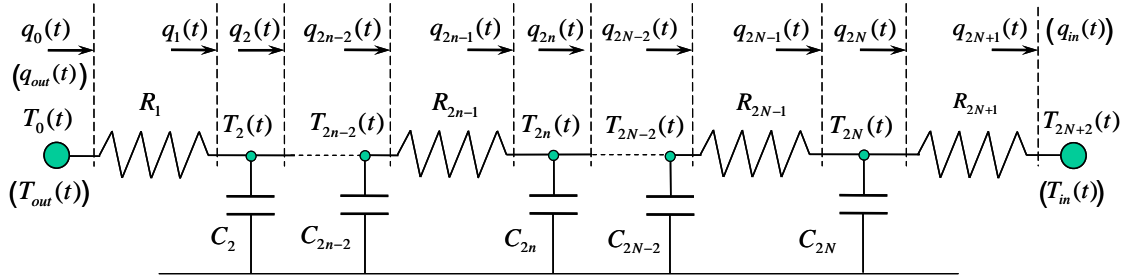
Figure 5.1 Schematics of a finite differential model

Such model can be easily transferred into a state space formulation which is traditionally used to analyze linear systems that have many inputs and outputs as follows. Equation (5.4) is called state equation, and Equation (5.5) and (5.6) is called output equation in a state space formulation.

$$\frac{d\boldsymbol{T}}{dt} = \boldsymbol{A}\boldsymbol{T} + \boldsymbol{B}\boldsymbol{u} \tag{5.4}$$

$$q_{in} = \boldsymbol{C}\boldsymbol{T} + \boldsymbol{D}\boldsymbol{u} \tag{5.5}$$

$$q_{out} = \boldsymbol{G}\boldsymbol{T} + \boldsymbol{H}\boldsymbol{u} \tag{5.6}$$

Where, $\boldsymbol{T}$ and $\boldsymbol{u}$ are the temperature state vector and input vector respectively as shown in Equation (5.7) and (5.8). q is heat flow. $\boldsymbol{A}$, $\boldsymbol{B}$, $\boldsymbol{C}$, $\boldsymbol{D}$, $\boldsymbol{G}$, and $\boldsymbol{H}$ are coefficient matrix as shown in Equation (5.9) ~ (5.14).

$$\boldsymbol{T}^T = \begin{bmatrix} T_2 & T_4 & \cdots & T_{2n} \end{bmatrix}_{1 \times n} \tag{5.7}$$

$$\boldsymbol{u}^T = \begin{bmatrix} T_{out} & 0 & \cdots & 0 & T_{in} \end{bmatrix}_{1 \times n} \tag{5.8}$$

$$A = \begin{bmatrix} \dfrac{-(R_1 + R_3)}{R_1 C_2 R_3} & \dfrac{1}{C_2 R_3} & 0 & 0 & \cdots & 0 & 0 & 0 \\[2mm] \dfrac{1}{R_3 C_4} & \dfrac{-(R_3 + R_5)}{R_3 C_4 R_5} & \dfrac{1}{C_4 R_5} & 0 & \cdots & 0 & 0 & 0 \\[2mm] \cdots & & & \ddots & & & & \cdots \\[2mm] 0 & 0 & 0 & 0 & \cdots & \dfrac{1}{R_{2n-3} C_{2n-2}} & \dfrac{-(R_{2n-3} + R_{2n-1})}{R_{2n-3} C_{2n-2} R_{2n-1}} & \dfrac{1}{C_{2n-2} R_{2n-1}} \\[2mm] 0 & 0 & 0 & 0 & \cdots & 0 & \dfrac{1}{R_{2n-1} C_{2n}} & \dfrac{-(R_{2n-1} + R_{2n+1})}{R_{2n-1} C_{2n} R_{2n+1}} \end{bmatrix}_{n \times n} \tag{5.9}$$

$$B = \begin{bmatrix} \dfrac{1}{R_1 C_2} & 0 & \cdots & 0 & 0 \\[2mm] 0 & 0 & \cdots & 0 & 0 \\[2mm] \cdots & & \ddots & & \cdots \\[2mm] 0 & 0 & \cdots & 0 & 0 \\[2mm] 0 & 0 & \cdots & 0 & \dfrac{1}{C_{2n} R_{2n+1}} \end{bmatrix}_{n \times n} \tag{5.10}$$

$$C = \begin{bmatrix} 0 & \cdots & 0 & \dfrac{1}{R_{2n+1}} \end{bmatrix}_{1 \times n} \tag{5.11}$$

$$D = \begin{bmatrix} 0 & \cdots & 0 & \dfrac{-1}{R_{2n+1}} \end{bmatrix}_{1 \times n} \tag{5.12}$$

$$G = \begin{bmatrix} \dfrac{-1}{R_1} & 0 & \cdots & 0 \end{bmatrix}_{1 \times n} \tag{5.13}$$

$$H = \begin{bmatrix} \dfrac{1}{R_1} & 0 & \cdots & 0 \end{bmatrix}_{1 \times n} \tag{5.14}$$

Where, T, C, and R are the nodal temperature, thermal capacitance and resistance respectively.

The solution to the state vector of the system of first-order differential equations with constant coefficients is given by the formula shown in Equation (5.15).

$$\boldsymbol{T}(t) = e^{At} \boldsymbol{T}(0^-) + \int_{0^-}^{t} e^{A(t-\tau)} \boldsymbol{B} \boldsymbol{u}(\tau) d\tau \tag{5.15}$$

The first term on the right-hand side of Equation (5.15) is called zero-input response, and the second term on the right-hand side of the equation is called zero-state response. The zero-input response of a system involves the response of the state variable to the conditions at time zero. The zero-state response is the convolution integral, which integrates the response of the state variables to the input between time 0 and t. To calculate the integral, it is necessary to calculate the matrix exponential function $e^{A(t-\tau)}$ correctly. It can be given in the following format as shown in Equation (5.16). The deduction of the equation is given in *Appendix B*. The coefficients of the matrix polynomial are determined as Equation (5.17).

$$e^{A(t-\tau)} = \beta_{n-1}A^{n-1} + \beta_{n-2}A^{n-2} + \ldots + \beta_1 A + \beta_0 I \qquad (5.16)$$

$$\beta = Lamad^{-1} \cdot F^T \qquad (5.17)$$

Where,

$$\beta = [\beta_0 \ \beta_1 \ \cdots \ \beta_{n-1}]^T \qquad (5.18)$$

$$F = [e^{\lambda_1(t-\tau)} \quad e^{\lambda_2(t-\tau)} \quad \ldots \quad e^{\lambda_n(t-\tau)}]^T \qquad (5.19)$$

$$Lamda = \begin{bmatrix} 1 & \lambda_1 & \cdots & \lambda_1^{n-1} \\ 1 & \lambda_2 & \cdots & \lambda_2^{n-1} \\ \cdots & \cdots & \cdots & \cdots \\ 1 & \lambda_n & \cdots & \lambda_n^{n-1} \end{bmatrix} \qquad (5.20)$$

Where, $\{\lambda_1, \lambda_2, \cdots, \lambda_n\}$ are the eigenvalues of matrix A and distinct.

When inverse of the matrix *Lamad* is represented by M, as shown in Equation (5.21), the terms of vector β (in Equation (5.18)) can be rewritten in the format, as

shown in Equation (5.22). It is obvious that the coefficients are the functions of time t and τ.

$$M = Lamad^{-1} = \begin{bmatrix} M_{11} & M_{12} & \cdots & M_{1n} \\ M_{21} & M_{22} & \cdots & M_{2n} \\ \cdots & & \ddots & \cdots \\ M_{n1} & M_{n2} & \cdots & M_{nn} \end{bmatrix}_{n \times n} \quad (5.21)$$

$$\beta_{i-1} = M_{i1}e^{\lambda_1(t-\tau)} + M_{i2}e^{\lambda_2(t-\tau)} + \cdots + M_{in}e^{\lambda_n(t-\tau)}, \quad 1 \le i \le n \quad (5.22)$$

5.3 Analytical solution of nodal temperatures forced by defined ramp excitation on the out side of wall

A ramp excitation is defined as an increase at time $t=0$ with a slope of $\eta = \dfrac{1}{\Delta}$ (Kh^{-1}) in the outside air temperature of a wall. The outside air temperature of the wall is at zero temperature everywhere before time $t=0$. The inside air temperature is subsequently maintained at zero. Supposing that the wall is imposed on by such a ramp excitation ($\eta = \dfrac{1}{\Delta}$), the solution of Equation (5.15) forced by the defined ramp excitation actually becomes the format shown in Equation (5.23) as the zero-input response is zero. Equation (5.8) becomes the formula as shown in Equation (5.24).

$$T(t) = \int_{0^-}^{t} e^{A(t-\tau)} B u(\tau) d\tau \quad (5.23)$$

$$u = \begin{bmatrix} \dfrac{1}{\Delta}\tau & 0 & \cdots & 0 & 0 \end{bmatrix}_{1 \times n}^{T} \quad (5.24)$$

Then, the product of B and u can be represented by Equation (5.25).

$$\boldsymbol{B}\,\boldsymbol{u} = \left[\frac{1}{\varDelta R_1 C_2}\tau \quad 0 \quad \cdots \quad 0\right]_{1\times n}^{T} \tag{5.25}$$

We care about the first column of matrix function $e^{\boldsymbol{A}(t-\tau)}$ in Equation (5.23) because the elements of $\boldsymbol{B}\,\boldsymbol{u}$ are zero except the first element as shown in Equation (5.25). The temperature at the n-th node T_{2n}, with which heat flux can be calculated directly, can be calculated as follows.

$$
\begin{aligned}
T_{2n}(t) &= \int_{0^-}^{t} e^{\boldsymbol{A}(t-\tau)}(n,:)\boldsymbol{B}\boldsymbol{u}(\tau)d\tau \\
&= \int_{0^-}^{t} e^{\boldsymbol{A}(t-\tau)}(n,1)[\boldsymbol{B}\boldsymbol{u}(\tau)](1,1)d\tau \\
&= [M_{11}\boldsymbol{I}(n,1) + M_{21}\boldsymbol{A}(n,1) + \cdots + M_{n1}\boldsymbol{A}^{n-1}(n,1)]\frac{1}{\varDelta R_1 C_2}\int_{0^-}^{t} e^{\lambda_1(t-\tau)}\tau d\tau \\
&\quad + [M_{12}\boldsymbol{I}(n,1) + M_{22}\boldsymbol{A}(n,1) + \cdots + M_{n2}\boldsymbol{A}^{n-1}(n,1)]\frac{1}{\varDelta R_1 C_2}\int_{0^-}^{t} e^{\lambda_2(t-\tau)}\tau d\tau \\
&\quad + \cdots \\
&\quad + [M_{1n}\boldsymbol{I}(n,1) + M_{2n}\boldsymbol{A}(n,1) + \cdots + M_{nn}\boldsymbol{A}^{n-1}(n,1)]\frac{1}{\varDelta R_1 C_2}\int_{0^-}^{t} e^{\lambda_n(t-\tau)}\tau d\tau
\end{aligned}
\tag{5.26}
$$

With simple integral, Equation (5.26) can be rewritten as follows.

$$
\begin{aligned}
T_{2n}(t) &= [M_{11}\boldsymbol{I}(n,1) + M_{21}\boldsymbol{A}(n,1) + \cdots + M_{n1}\boldsymbol{A}^{n-1}(n,1)]\frac{e^{\lambda_1 t} - 1 - \lambda_1 t}{\varDelta R_1 C_2 \lambda_1^2} \\
&\quad + [M_{12}\boldsymbol{I}(n,1) + M_{22}\boldsymbol{A}(n,1) + \cdots + M_{n2}\boldsymbol{A}^{n-1}(n,1)]\frac{e^{\lambda_2 t} - 1 - \lambda_2 t}{\varDelta R_1 C_2 \lambda_2^2} \\
&\quad + \cdots \\
&\quad + [M_{1n}\boldsymbol{I}(n,1) + M_{2n}\boldsymbol{A}(n,1) + \cdots + M_{nn}\boldsymbol{A}^{n-1}(n,1)]\frac{e^{\lambda_n t} - 1 - \lambda_n t}{\varDelta R_1 C_2 \lambda_n^2} \\
&= \sum_{i=1}^{n}\left\{\frac{e^{\lambda_i t} - 1 - \lambda_i t}{\varDelta R_1 C_2 \lambda_i^2}\sum_{j=1}^{n}(M_{ji}\boldsymbol{A}^{j-1}(n,1))\right\}
\end{aligned}
\tag{5.27}
$$

Representing the temperature response function at the n-th node by *TY1(t)* (when

the defined ramp excitation is imposed on the outside of the wall), the equation can be shown as follows.

$$TY1(t) = T_{2n}(t)$$

$$= \sum_{i=1}^{n} \left\{ \frac{e^{\lambda_i t} - 1 - \lambda_i t}{\Delta R_1 C_2 \lambda_i^2} \sum_{j=1}^{n} (M_{ji} A^{j-1}(n,1)) \right\} \tag{5.28}$$

The temperature at the 1-st node (T_2) when the defined ramp excitation is imposed on the outside of the wall can be calculated as Equation (5.29).

$$T_2(t) = \int_{0^-}^{t} e^{A(t-\tau)}(1,:)Bu(\tau)d\tau$$

$$= \int_{0^-}^{t} e^{A(t-\tau)}(1,1)[Bu(\tau)](1,1)d\tau$$

$$= [M_{11}I(1,1) + M_{21}A(1,1) + \cdots + M_{n1}A^{n-1}(1,1)]\frac{1}{\Delta R_1 C_2}\int_{0^-}^{t} e^{\lambda_1(t-\tau)}\tau d\tau$$

$$+ [M_{12}I(1,1) + M_{22}A(1,1) + \cdots + M_{n2}A^{n-1}(1,1)]\frac{1}{\Delta R_1 C_2}\int_{0^-}^{t} e^{\lambda_2(t-\tau)}\tau d\tau \tag{5.29}$$

$$+ \cdots$$

$$+ [M_{1n}I(1,1) + M_{2n}A(1,1) + \cdots + M_{nn}A^{n-1}(1,1)]\frac{1}{\Delta R_1 C_2}\int_{0^-}^{t} e^{\lambda_n(t-\tau)}\tau d\tau$$

With simple integral, Equation (5.29) can be rewritten as follows.

$$T_2(t) = [M_{11}I(1,1) + M_{21}A(1,1) + \cdots + M_{n1}A^{n-1}(1,1)]\frac{e^{\lambda_1 t} - 1 - \lambda_1 t}{\Delta R_1 C_2 \lambda_1^2}$$

$$+ [M_{12}I(1,1) + M_{22}A(1,1) + \cdots + M_{n2}A^{n-1}(1,1)]\frac{e^{\lambda_2 t} - 1 - \lambda_2 t}{\Delta R_1 C_2 \lambda_2^2} \tag{5.30}$$

$$+ \cdots$$

$$+ [M_{1n}I(1,1) + M_{2n}A(1,1) + \cdots + M_{nn}A^{n-1}(1,1)]\frac{e^{\lambda_n t} - 1 - \lambda_n t}{\Delta R_1 C_2 \lambda_n^2}$$

TX1(t), the temperature response function at the 1-st node (T_2) when the defined

ramp excitation is imposed on the outside of the wall, can be expressed using Equation (5.31).

$$TX1(t) = T_2(t)$$

$$= \sum_{i=1}^{n} \left\{ \frac{e^{\lambda_i t} - 1 - \lambda_i t}{\Delta R_1 C_2 \lambda_i^2} \sum_{j=1}^{n} (M_{ji} A^{j-1}(1,1)) \right\} \tag{5.31}$$

5.4 Analytical solution of nodal temperatures forced by defined ramp excitation on the inside of wall

To calculate the temperature response function at the n-th node (T_{2n}) when a similar ramp excitation is imposed on the inside of the wall, a ramp excitation is defined as an increase at time $t=0$ with a slope of $\eta = \dfrac{1}{\Delta}$ (Kh^{-1}) in the inside air temperature of a wall. The inside air temperature of the wall is at zero temperature everywhere before time $t=0$. The outside air temperature is subsequently maintained at zero. Supposing that the wall is imposed on by such a ramp excitation ($\eta = \dfrac{1}{\Delta}$), the solution of Equation (5.15) forced by the defined ramp excitation actually becomes the format shown in Equation (5.32) as the zero-input response is zero. Equation (5.8) becomes the formula as shown in Equation (5.33).

$$T(t) = \int_{0^-}^{t} e^{A(t-\tau)} B\, u(\tau) d\tau \tag{5.32}$$

$$u^T = \begin{bmatrix} 0 & 0 & \cdots & 0 & \dfrac{1}{\Delta}\tau \end{bmatrix}_{1 \times n} \tag{5.33}$$

Then, the product of B and u can be represented by Equation (5.34).

$$\boldsymbol{Bu} = \left[0 \quad \cdots \quad 0 \quad \frac{1}{\Delta C_{2n} R_{2n+1}} \tau \right]_{1 \times n}^{T} \tag{5.34}$$

We care about the last column of matrix function $e^{\boldsymbol{A}(t-\tau)}$ in Equation (5.32) because the elements of $\boldsymbol{B u}$ are zero except the last element as shown in Equation (5.34). The temperature at the n-th node T_{2n}, can be calculated as follows.

$$
\begin{aligned}
T_{2n}(t) &= \int_{0^-}^{t} e^{\boldsymbol{A}(t-\tau)}(n,:)\boldsymbol{Bu}(\tau)d\tau \\
&= \int_{0^-}^{t} e^{\boldsymbol{A}(t-\tau)}(n,n)[\boldsymbol{Bu}(\tau)](n,1)d\tau \\
&= [M_{11}\boldsymbol{I}(n,n) + M_{21}\boldsymbol{A}(n,n) + \cdots + M_{n1}\boldsymbol{A}^{n-1}(n,n)]\frac{1}{\Delta C_{2n} R_{2n+1}}\int_{0^-}^{t} e^{\lambda_1(t-\tau)}\tau d\tau \\
&\quad + [M_{12}\boldsymbol{I}(n,n) + M_{22}\boldsymbol{A}(n,n) + \cdots + M_{n2}\boldsymbol{A}^{n-1}(n,n)]\frac{1}{\Delta C_{2n} R_{2n+1}}\int_{0^-}^{t} e^{\lambda_2(t-\tau)}\tau d\tau \\
&\quad + \cdots \\
&\quad + [M_{1n}\boldsymbol{I}(n,n) + M_{2n}\boldsymbol{A}(n,n) + \cdots + M_{nn}\boldsymbol{A}^{n-1}(n,n)]\frac{1}{\Delta C_{2n} R_{2n+1}}\int_{0^-}^{t} e^{\lambda_n(t-\tau)}\tau d\tau
\end{aligned}
\tag{5.35}
$$

With simple integral, Equation (5.35) can be rewritten as follows.

$$
\begin{aligned}
T_{2n}(t) &= [M_{11}\boldsymbol{I}(n,n) + M_{21}\boldsymbol{A}(n,n) + \cdots + M_{n1}\boldsymbol{A}^{n-1}(n,n)]\frac{e^{\lambda_1 t} - 1 - \lambda_1 t}{\Delta C_{2n} R_{2n+1}\lambda_1^2} \\
&\quad + [M_{12}\boldsymbol{I}(n,n) + M_{22}\boldsymbol{A}(n,n) + \cdots + M_{n2}\boldsymbol{A}^{n-1}(n,n)]\frac{e^{\lambda_2 t} - 1 - \lambda_2 t}{\Delta C_{2n} R_{2n+1}\lambda_2^2} \\
&\quad + \cdots \\
&\quad + [M_{1n}\boldsymbol{I}(n,n) + M_{2n}\boldsymbol{A}(n,n) + \cdots + M_{nn}\boldsymbol{A}^{n-1}(n,n)]\frac{e^{\lambda_n t} - 1 - \lambda_n t}{\Delta C_{2n} R_{2n+1}\lambda_n^2}
\end{aligned}
\tag{5.36}
$$

$TZ1(t)$, the temperature response function at the n-th node (T_{2n}) when the defined ramp excitation is imposed on the inside of the wall, can be calculated using equation (5.37).

$$TZ1(t) = T_{2n}(t)$$

$$= \sum_{i=1}^{n} \left\{ \frac{e^{\lambda_i t} - 1 - \lambda_i t}{\Delta R_{2n} C_{2n+1} \lambda_i^2} \sum_{j=1}^{n} (M_{ji} A^{j-1}(n,n)) \right\} \tag{5.37}$$

5.5 Calculation of thermal response factors

The fundamental thermal response functions are the surface heat flow responses against the unit triangle pulse of the surface temperature excitation. When taking the values of function at the same time interval, i.e. one hour in the case, the response function of heat flow can be expressed in the form of a time series. The values of the series obtained are called thermal response factors. The convolution expression of the thermal response factors and temperature series with the same time interval allows for the calculation of the surface heat flow. The equations developed in this study to calculate the thermal response factors and their deduction process are briefed as follows.

A unit triangular pulse, which is of height $\phi = 1$ K and base 2Δ at time $t = 0$, can be formed by a $\eta = \dfrac{1}{\Delta}$ ramp (at time $t = -\Delta$), a $\eta = -\dfrac{2}{\Delta}$ ramp (at time $t = 0$) and a $\eta = \dfrac{1}{\Delta}$ ramp (at time $t = \Delta$). Therefore, the temperature on the n-th node due to a unit triangular pulse on the outside surface is calculated by Equation (5.38).

$$TY(t) = TY1(t + \Delta) - 2TY1(t) + TY1(t - \Delta)$$

$$= \sum_{i=1}^{n} \left\{ \frac{e^{\lambda_i(t + \Delta)} - 1 - \lambda_i(t + \Delta)}{\Delta R_1 C_2 \lambda_i^2} \sum_{j=1}^{n} (M_{ji} A^{j-1}(n,1)) \right\}$$

$$+ 2 \sum_{i=1}^{n} \left\{ \frac{e^{\lambda_i t} - 1 - \lambda_i t}{\Delta R_1 C_2 \lambda_i^2} \sum_{j=1}^{n} (M_{ji} A^{j-1}(n,1)) \right\} \qquad (t \geq \Delta) \quad (5.38)$$

$$\sum_{i=1}^{n} \left\{ \frac{e^{\lambda_i(t - \Delta)} - 1 - \lambda_i(t - \Delta)}{\Delta R_1 C_2 \lambda_i^2} \sum_{j=1}^{n} (M_{ji} A^{j-1}(n,1)) \right\}$$

It can be rearranged as follows.

$$TY(t) = \sum_{i=1}^{n} \left\{ \frac{(1 - e^{\lambda_i \Delta})^2 e^{\lambda_i(t - \Delta)}}{\Delta R_1 C_2 \lambda_i^2} \sum_{j=1}^{n} (M_{ji} A^{j-1}(n,1)) \right\} \qquad (t \geq \Delta) \quad (5.39)$$

The temperature response factors, $TY(j)$ ($j = 0, 1, 2, 3, \cdots$), are the values of $TY(t)$ at time $t = j\Delta$ ($j = 0, 1, 2, 3, \cdots$). Conventionally, $\Delta = 3600$ seconds. The value of the first factor, $TY(0)$, is derived from a single ramp ($\eta = \frac{1}{\Delta}$) at time $t = 0$, as shown in Equation (5.40).

$$TY(0) = TY1(\Delta)$$

$$= \sum_{i=1}^{n} \left\{ \frac{e^{\lambda_i \Delta} - 1 - \lambda_i \Delta}{\Delta R_1 C_2 \lambda_i^2} \sum_{j=1}^{n} (M_{ji} A^{j-1}(n,1)) \right\} \qquad (5.40)$$

Eventually, the cross thermal response factors can be calculated using equations (5.41) and (5.42), which is the ratio of the temperature difference (between the temperature response factors at the n-th node and the indoor air temperature) to the resistance R_{2n+1}.

$$Y(0) = \sum_{i=1}^{n} \left\{ \frac{e^{\lambda_i \varDelta} - 1 - \lambda_i \varDelta}{\varDelta R_1 C_2 \lambda_i^2} \sum_{j=1}^{n} (M_{ji} \boldsymbol{A}^{j-1}(n,1)) \right\} \bigg/ R_{2n+1} \tag{5.41}$$

$$Y(k) = \sum_{i=1}^{n} \left\{ \frac{(1 - e^{\lambda_i \varDelta})^2 e^{\lambda_i \varDelta (k-1)}}{\varDelta R_1 C_2 \lambda_i^2} \sum_{j=1}^{n} (M_{ji} \boldsymbol{A}^{j-1}(n,1)) \right\} \bigg/ R_{2n+1} \quad (k \geq 1) \tag{5.42}$$

Similarly, the thermal response factors $X(k)$ at the 1-st node and $Z(k)$ at the n-node can be calculate using Equation (5.43), (5.44) and (5.46).

$$X(0) = \left(1 - \sum_{i=1}^{n} \left\{ \frac{e^{\lambda_i \varDelta} - 1 - \lambda_i \varDelta}{\varDelta R_1 C_2 \lambda_i^2} \sum_{j=1}^{n} (M_{ji} \boldsymbol{A}^{j-1}(1,1)) \right\} \right) \bigg/ R_1 \tag{5.43}$$

$$X(k) = \left(-\sum_{i=1}^{n} \left\{ \frac{(1 - e^{\lambda_i \varDelta})^2 e^{\lambda_i \varDelta (k-1)}}{\varDelta R_1 C_2 \lambda_i^2} \sum_{j=1}^{n} (M_{ji} \boldsymbol{A}^{j-1}(1,1)) \right\} \right) \bigg/ R_1 \quad (k \geq 1) \tag{5.44}$$

$$Z(0) = \left(1 - \sum_{i=1}^{n} \left\{ \frac{e^{\varDelta \lambda_i} - 1 - \lambda_i \varDelta}{\varDelta C_{2n} R_{2n+1} \lambda_i^2} \sum_{j=1}^{n} (M_{ji} \boldsymbol{A}^{j-1}(n,n)) \right\} \right) \bigg/ R_{2n+1} \tag{5.45}$$

$$Z(k) = \left(-\sum_{i=1}^{n} \left\{ \frac{(1 - e^{\lambda_i \varDelta})^2 e^{\lambda_i \varDelta (k-1)}}{\varDelta C_{2n} R_{2n+1} \lambda_i^2} \sum_{j=1}^{n} (M_{ji} \boldsymbol{A}^{j-1}(n,n)) \right\} \right) \bigg/ R_{2n+1} \quad (k \geq 1) \tag{5.46}$$

5.6 Calculation of conduction transfer function (CTF) coefficients

With the thermal response factors, the conduction transfer function (CTF) coefficients can be deduced easily. The thermal response factors can be rewritten as follows.

$$Y_0 = \sum_{i=1}^{n} \left\{ \frac{e^{\lambda_i \Delta} - 1 - \lambda_i \Delta}{\Delta R_1 C_2 R_{2n+1} \lambda_i^2} \sum_{j=1}^{n} (M_{ji} A^{j-1}(n,1)) \right\}$$

(5.47)

$$= \sum_{i=1}^{n} WY0_i$$

$$Y(k) = \sum_{i=1}^{n} \left\{ \frac{(1 - e^{\lambda_i \Delta})^2 e^{-\lambda_i \Delta} e^{\Delta \lambda_i k}}{\Delta R_1 C_2 R_{2n+1} \lambda_i^2} \sum_{j=1}^{n} (M_{ji} A^{j-1}(n,1)) \right\} \quad (k \geq 1) \quad (5.48)$$

$$= \sum_{i=1}^{n} WY_i e^{\Delta \lambda_i k}$$

$$X_0 = \frac{1}{R_1} - \sum_{i=1}^{n} \left\{ \frac{e^{\lambda_i \Delta} - 1 - \lambda_i \Delta}{\Delta R_1 C_2 R_1 \lambda_i^2} \sum_{j=1}^{n} (M_{ji} A^{j-1}(1,1)) \right\}$$

(5.49)

$$= \frac{1}{R_1} - \sum_{i=1}^{n} WX0_i$$

$$X(k) = -\sum_{i=1}^{n} \left\{ \frac{(1 - e^{\lambda_i \Delta})^2 e^{-\Delta \lambda_i} e^{\Delta \lambda_i k}}{\Delta R_1 C_2 R_1 \lambda_i^2} \sum_{j=1}^{n} (M_{ji} A^{j-1}(1,1)) \right\}$$

(5.50)

$$= -\sum_{i=1}^{n} WX_i e^{\Delta \lambda_i k}$$

$$Z_0 = \frac{1}{R_{2n+1}} - \sum_{i=1}^{n} \left\{ \frac{e^{\Delta \lambda_i} - 1 - \lambda_i \Delta}{\Delta C_{2n} R_{2n+1}^2 \lambda_i^2} \sum_{j=1}^{n} (M_{ji} A^{j-1}(n,n)) \right\}$$

(5.51)

$$= \frac{1}{R_{2n+1}} - \sum_{i=1}^{n} WZ0_i$$

$$Z(k) = -\sum_{i=1}^{n} \left\{ \frac{(1 - e^{\lambda_i \Delta})^2 e^{-\lambda_i \Delta} e^{\Delta \lambda_i k}}{\Delta C_{2n} R_{2n+1}^2 \lambda_i^2} \sum_{j=1}^{n} (M_{ji} A^{j-1}(n,n)) \right\}$$

(5.52)

$$= -\sum_{i=1}^{n} WZ_i e^{\Delta \lambda_i k}$$

Where,

$$WY0_i = \frac{e^{\lambda_i \Delta} - 1 - \lambda_i \Delta}{\Delta R_1 C_2 R_{2n+1} \lambda_i^2} \sum_{j=1}^{n} (M_{ji} A^{j-1}(n,1))$$

(5.53)

$$WY_i = \frac{(1 - e^{\lambda_i \Delta})^2 e^{-\lambda_i \Delta}}{\Delta R_1 C_2 R_{2n+1} \lambda_i^2} \sum_{j=1}^{n} (M_{ji} A^{j-1}(n,1))$$

(5.54)

$$WX0_i = \frac{e^{\lambda_i \Delta} - 1 - \lambda_i \Delta}{\Delta R_1 C_2 R_1 \lambda_i^2} \sum_{j=1}^{n} (M_{ji} A^{j-1}(1,1)) \tag{5.55}$$

$$WX_i = \frac{(1 - e^{\lambda_i \Delta})^2 e^{-\Delta \lambda_i}}{\Delta R_1 C_2 R_1 \lambda_i^2} \sum_{j=1}^{n} (M_{ji} A^{j-1}(1,1)) \tag{5.56}$$

$$WZ0_i = \frac{e^{\Delta \lambda_i} - 1 - \lambda_i \Delta}{\Delta C_{2n} R_{2n+1}^2 \lambda_i^2} \sum_{j=1}^{n} (M_{ji} A^{j-1}(n,n)) \tag{5.57}$$

$$WZ_i = \frac{(1 - e^{\lambda_i \Delta})^2 e^{-\lambda_i \Delta}}{\Delta C_{2n} R_{2n+1}^2 \lambda_i^2} \sum_{j=1}^{n} (M_{ji} A^{j-1}(n,n)) \tag{5.58}$$

Heat conduction z-transfer function of the wall equals to the Z-transforms of response factors $Y(k)$, $X(k)$, and $Z(k)$, ($\Delta = 3600$ is the sampling time). For the z-transforms of cross response factors, $Y(k)$, it's represented as follows.

$$
\begin{aligned}
G_Y(z) &= Y_0 + Y(1)z^{-1} + Y(2)z^{-2} + Y(3)z^{-3} + \cdots Y(n)z^{-n} + \cdots \\
&= Y_0 - Y(0) + Y(0) + Y(1)z^{-1} + Y(2)z^{-2} + Y(3)z^{-3} + \cdots Y(n)z^{-n} + \cdots \\
&= Y_0 - Y(0) + Z\left[\sum_{i=1}^{n} \left\{ WY_i e^{\lambda_i \Delta k} \right\} \right] \\
&= \sum_{i=1}^{n} [WY0_i - WY_i] + Z\left[\sum_{i=1}^{n} \left\{ WY_i e^{\lambda_i \Delta k} \right\} \right] \\
&= \sum_{i=1}^{n} [WY0_i - WY_i] + \sum_{i=1}^{n} \left\{ WY_i \frac{1}{1 - e^{\lambda_i \Delta} z^{-1}} \right\}
\end{aligned} \tag{5.59}
$$

Equation (5.59) can be rewritten in the form of fraction as follows.

$$
\begin{aligned}
G_Y(z) &= \sum_{i=1}^{n} [WY0_i - WY1_i] + \sum_{i=1}^{n} \left\{ WY1_i \frac{1}{1 - e^{\lambda_i \Delta} z^{-1}} \right\} \\
&= \frac{B(Z)}{\prod_{n=1}^{n} \left(1 - e^{\lambda_i \Delta} z^{-1} \right)} \\
&= \frac{b_0 + b_1 z^{-1} + b_2 z^{-2} + \cdots + b_r z^{-r}}{1 + d_1 z^{-1} + d_2 z^{-2} + \cdots + d_m z^{-m}}
\end{aligned} \tag{5.60}
$$

Where, *B(z)* is an r-order polynomial in z^{-1} , the coefficients d_k and b_k are CTF coefficients

For the z-transforms of internal response factors, *X(k)*, it's represented as follows.

$$
\begin{aligned}
G_X(z) &= X_0 + X(1)z^{-1} + X(2)z^{-2} + X(3)z^{-3} + \cdots X(n)z^{-n} + \cdots \\
&= X_0 - X(0) + X(0) + X(1)z^{-1} + X(2)z^{-2} + X(3)z^{-3} + \cdots X(n)z^{-n} + \cdots \\
&= X_0 - X(0) + Z\left[-\sum_{i=1}^{n}\left\{ WX_i e^{\lambda_i \Delta k} \right\} \right] \\
&= \frac{1}{R_1} - \sum_{i=1}^{n} WX0_i + \sum_{i=1}^{n} WX_i + Z\left[-\sum_{i=1}^{n}\left\{ WX_i e^{\lambda_i \Delta k} \right\} \right] \\
&= \frac{1}{R_1} - \sum_{i=1}^{n}[WX0_i - WX_i] - \sum_{i=1}^{n}\left\{ WX_i \frac{1}{1 - e^{\lambda_i \Delta}z^{-1}} \right\}
\end{aligned}
\tag{5.61}
$$

Equation (5.61) can be rewritten in the form of fraction as follows.

$$
\begin{aligned}
G_X(z) &= \frac{1}{R_1} - \sum_{i=1}^{n}[WX0_i - WX_i] - \sum_{i=1}^{n}\left\{ WX_i \frac{1}{1 - e^{\lambda_i \Delta}z^{-1}} \right\} \\
&= \frac{C(Z)}{\prod_{n=1}^{n}\left(1 - e^{\lambda_i \Delta}z^{-1} \right)} \\
&= \frac{c_0 + c_1 z^{-1} + c_2 z^{-2} + \cdots + c_r z^{-r}}{1 + d_1 z^{-1} + d_2 z^{-2} + \cdots + d_m z^{-m}}
\end{aligned}
\tag{5.62}
$$

Where, *C(z)* is an r-order polynomial in z^{-1} , the coefficients d_k and c_k are CTF coefficients.

5.7 Validation Tests and Results

Although thermal response factors and CTF are deduced, only thermal response factors calculated by the simple method is validated. The developed simple method to

calculate thermal response factors in time domain not only has the advantage of the finite differential models to avoid complex root-finding process, but also has the advantage of the thermal response factor method to avoid the computation of all the internal temperature by relating the desired outputs at any time to the previous inputs through a set of response-factor coefficients.

Many case studies were conducted to validate the method developed for calculating the thermal response factors in time domain. The accuracy of the method was also studied by compared with the results available using other methods. Results of two typical structures are presented below. In the study, fifth order and ninth order differential models are used to test two structures (walls).

The geometry, construction material and properties of the two structures used in the tests are given in Table 5.1. Wall I is a multilayer construction, consisting of an outside surface film, a layer of face brick, a layer of a common brick and an inside surface film. Kusuda [1969] provided the properties of thickness, thermal conductivity and thermal diffusivity of individual layer in imperial unit. For nodal placement of the finite differential model, the thermal diffusivity is decomposed to density and heat specific as list in Table 5.1 in SI unit. Using traditional Laplace transforms and the direct root-finding method, Kusuda [1969] provided a list of external, cross, and internal thermal response factors for the wall, which is in Table 5.2 for comparison.

Table 5.1 Detailed properties of Wall I and Wall II

Wall No.	Description	Thickness and thermal properties				
		$L(mm)$	$\lambda(Wm^{-1}K^{-1})$	$\rho(kgm^{-3})$	$C_p(Jm^{-3}K^{-1})$	$R(m^2KW^{-1})$
Wall I	Outside surface film					0.0587
	Face brick	101.5	1.333	2005	920	0.0762
	Common brick	101.5	0.727	1765	840	0.1396
	Inside surface film					0.1468
Wall II	Outside surface film					0.05
	Concrete	89	1.73	2235	1106	0.0514
	Insulation	127	0.0744	24	992	1.707
	Concrete	89	1.73	2235	1106	0.0514
	Inside surface film					0.16

Wall II is a multilayer construction consisting of 5 layers of homogeneous materials including insulation between two layers of concrete with inside and outside air films as shown in Table 5.1. Ouyang and Haghighat [1991] provided also a list of the cross thermal response factors for the wall with the state space method and the direct root-finding method as shown in Table 5.3 for comparison.

With the developed method in this study, the external, cross, and internal thermal response factors for Wall I were calculated for finite differential models of different orders. For case $n=5$ and $n=9$ ($\Delta=3600$s) presented in this paper, the three sets of the thermal response factors are showed in Table 5.2. The thermal response factors given in the table demonstrate that the time domain calculation method for thermal response factors developed in this study works well. Comparisons show that the accuracy increases when higher order finite differential models are used. The comparisons also show that the cross thermal responses of the finite differential models at the first two hours are a little faster than the traditional root-finding method. Although the first two

terms of the thermal response factors, when *n=9*, deviate a little from the results given by the direct root-finding method, the effect of these two factors on the load calculation is very and very small. The rest of the thermal response factors are almost identical to the results given by the direct root-finding method. Therefore, the time domain method developed in this study can provide sufficient accuracy for engineering applications.

Table 5.2 Comparisons of the thermal response factors ($(Btu)(ft^{-2})(h^{-1})(\,{}^\circ F^{-1})$) for Wall I

	By time-domain method (n=5)			By time-domain method (n=9)			By Kusuda [1969]		
	X(k)	Y(k)	Z(k)	X(k)	Y(k)	Z(k)	X(k)	Y(k)	Z(k)
k									
0	0.90832	0.00109	1.97950	0.92926	0.00042	1.96900	0.91949	0.00013	1.98340
1	-0.14222	0.01480	-0.47853	-0.16994	0.01023	-0.48980	-0.16678	0.00812	-0.51260
2	-0.07116	0.03381	-0.24469	-0.08134	0.03101	-0.24283	-0.07950	0.03112	-0.23226
3	-0.05194	0.04233	-0.17163	-0.05214	0.04312	-0.15730	-0.05150	0.04482	-0.15634
4	-0.04012	0.04322	-0.12695	-0.03761	0.04512	-0.11577	-0.03715	0.04658	-0.11690
5	-0.03182	0.04044	-0.09735	-0.02889	0.04209	-0.09083	-0.02816	0.04304	-0.09216
6	-0.02571	0.03621	-0.07676	-0.02313	0.03728	-0.07369	-0.02292	0.03784	-0.07482
7	-0.02105	0.03161	-0.06175	-0.01896	0.03222	-0.06086	-0.01877	0.03250	-0.06173
8	-0.01738	0.02720	-0.05040	-0.01574	0.02750	-0.05075	-0.01556	0.02761	-0.05137
9	-0.01444	0.02319	-0.04154	-0.01316	0.02333	-0.04253	-0.01298	0.02333	-0.04294
10	-0.012.3	0.01966	-0.03446	-0.01105	0.01972	-0.03573	-0.01086	0.01965	-0.03598
11	-0.01006	0.01662	-0.02871	-0.00929	0.01665	-0.03007	-0.00911	0.01653	-0.03018
12	-0.00842	0.01400	-0.02398	-0.00782	0.01404	-0.02532	-0.00764	0.01389	-0.02533
13	-0.00706	0.01179	-0.02007	-0.00658	0.01184	-0.02132	-0.00642	0.01167	-0.02126
14	-0.00592	0.00992	-0.01682	-0.00555	0.00998	-0.01796	-0.00539	0.00980	-0.01786

Table 5.3 gives the cross thermal response factors for Wall II for the case *n=9*, which are calculated using the time domain method developed in this study. The thermal response factors are compared with the results given by Ouyang and Haghighat [1991] using state space method and the direct root-finding method. The results confirm above conclusion again that the time domain method developed in this

study can calculate thermal response factors with sufficient accuracy for practical applications.

Table 5.3 Comparisons of the cross thermal response factors $((W)(m^{-2})(^{\circ}C^{-1}))$ for

Wall II

k	By time-domain method (n=9)	By state space method [Ouyang and Haghighat 1991]	By direct root-finding method [Ouyang and Haghighat 1991]
0	0.00006064	0.00001771	0.00001549
1	0.00195333	0.00164078	0.00164541
2	0.00805260	0.00852682	0.00852884
3	0.01508031	0.01606351	0.01605804
4	0.02049180	0.02132861	0.02132482
5	0.02400185	0.02458189	0.02458376
6	0.02596580	0.02634117	0.02634535
7	0.02678065	0.02701426	0.02701681
8	0.02677065	0.02690951	0.02690827
9	0.02618410	0.02625774	0.02625429
10	0.02520751	0.02523350	0.02523131
11	0.02397968	0.02397017	0.02397118
12	0.02260300	0.02256861	0.02257155
13	0.02115220	0.02110207	0.02110402
14	0.01968105	0.01962103	0.01962030
15	0.01822756	0.01815949	0.01815708
16	0.01681787	0.01674130	0.01673967
17	0.01546929	0.01538425	0.01538486
18	0.01419260	0.01410104	0.01410310
19	0.01299375	0.01289871	0.1290017

5.8 Summary

Using the time domain calculation method developed in this study, the thermal response factors can be derived from the state space equation when the matrix exponential function is converted to matrix polynomial. This method combines the

advantages and discards the disadvantages of different methods. It can not only avoid the time-consuming and complex root-find process used by traditional response factor method, but also avoid a critical time required by the Eluer and Crank-Nicolson technique when the finite differential model is used. It has the advantage of the thermal response factors to avoid the computation of all the internal temperatures by relating the desired outputs at any moment of concern to the previous inputs through a set of response-factor coefficients.

Studies show that the method can be used efficiently and effectively to carry out the thermal response factors for practical applications. The case studies also show that the method can provide the thermal response factors of finite differential models with satisfactory accuracy. In practical application, if the order of the finite differential model is sufficiently high or optimized nodal placement of the finite differential model is provided, the simple time domain calculation method can provide the thermal response factors for building structure transient heat transfer calculation of satisfactory accuracy. With the derived thermal response factors, CTF coefficients can also be deduced very easily for transient heat transfer calculation.

CHAPTER 6 IDENTIFICATION OF THERMAL PARAMETERS OF THE SIMPLIDFIED MODEL OF INTERNAL MASS

The simplified models of building envelopes, i.e., the first part of the simplified building energy model (namely, hybrid building energy model), have been described and validated in *Chapter 3* and *Chapter 4*. In this chapter, the second part of the hybrid building energy model, i.e., the simplified model of internal mass (namely, simplified internal mass model) is presented. The simplified model of internal mass is partially data-driven with the physically meaningful structure of 2R2C. The methods of simplifying the internal mass model and identification of the parameters of the simplified model with a GA estimator are specifically depicted. The validations of the methods were conducted using the operation data in next chapter.

6.1 Introduction

The cooling energy consumption of a space depends on the magnitude and the nature of the sensible heat gain (i.e., heat conduction through walls, direct and diffusive solar radiation, energy input to lights, etc.), and mass of room objects that can absorb radiant heat. The latent heat gain is considered to become cooling load instantaneously. The building envelope absorbs solar radiation on the external surface and transfers the heat gradually into the indoor air in the form of conductive heat which becomes instantaneous cooling load. In this study, it is assumed that the

building envelope does not absorb radiation heat from occupants, lights, etc., on its interior surface. Solar radiation transmitted through windows, and the radiation from occupants, lights, etc., are absorbed by the mass of room objects which are capable of heat storage, and are released gradually as the form of convective heat by the mass of room objects to become instantaneous cooling load. Thus, the mass of room objects play a very important role to convert radiation heat into cooling load.

The mass of room objects that absorbs the radiant heat as well as release heat to indoor air, is called building internal mass. They can also emit radiant heat to indoor air and absorb heat from indoor air by convection. As stated above, the mass of room objects (internal mass) does not include building envelope. Typically, in commercial office buildings, internal mass includes internal walls, floors, interior partitions, ceilings, carpets and rubber pads floor covering, floor tiles, furniture etc. In a word, building internal mass refers to every thing in a building (excluding building envelope) that can absorb radiation heat and release it gradually.

Obviously, it is unimaginable to describe the building internal mass piece by piece physically for cooling energy consumption estimation especially in large commercial office building. Therefore, methods to quantify the effects of building internal mass of converting radiation into cooling load are desired in practical applications. RTF (Room transfer function) is often used to relate heat gain to the corresponding cooling load and its coefficients to evaluate the thermal storage performance of a given space [Stephenson and Mitalas 1967, Kimura and Stephenson

1968]. This method can be applied in design process based on the essential similarity of enclosing surfaces, special geometry, and related characteristics of the concerned space, to corresponding parameters of the space for which that data were calculated. ASHRAE research projects 359-RP [Chiles and Sowell 1984, Sowell and Chiles 1984(a), Sowell and Chiles 1984(b)], 472-RP [Harris and McQuiston 1988, Sowell 1988(a, b, c)] 626-RP [Falconer and Sowell et al. 1993, Spitler and McQuiston et al 1993(a, b)] investigated the unexpected sensitivity of such attributes and other counterintuitive phenomena regarding apparent responsiveness of relative masses in the storage and reject of heat. These projects also identified 14 discrete screening parameters with two to five levels of characterization each by which to select representative data and modify factors appropriately for specific applications.

The coefficients of RTF method provided by the above research projects are significant to estimate the cooling load for equipment sizing. However, the parameter selection is based on the actual building configuration which should be similar to the specified configurations of reference building including enclosing surfaces, special geometry, and related characteristics of building space. The estimation of cooling load may deviate greatly if the actual building configuration of concern differs greatly from the specified configuration of reference building. As a matter of fact, such situation occurs often.

For building energy performance evaluation or control strategy assessment etc., calibrated (simulation) models are often an important tool to estimate cooling load or

energy consumption. The measured cooling load and other measured parameters can indicate some contrails of the effects of building internal mass on converting radiation to cooling load. The coefficients of RTF method provided by the above research projects may not be a good solution because of building diversity. Therefore, a simple and practical model of building internal mass is highly desired.

In this study, a method to simplify the building internal mass model is developed. Viewing the building internal mass as a whole, the simplified thermal network structure is assumed to consider the effects of mass on converting thermal energy into cooling load. The structure of the simplified model is second order as 2R2C which can interpret the physical meaning explicitly. Second order models are usually accurate enough for cooling energy consumption calculation. It is different from 3R2C model to avoid more parameters to be identified. A GA estimator is also developed to find the optimal parameters of the simplified internal mass model with measured cooling energy consumption. The method was validated in real buildings, which will be presented in next chapter.

6.2 Simplified internal mass model

For building cooling load or energy consumption estimation, an appropriate order of the thermal network structure should be taken after trading off between the complexity and accuracy of the model. Braun and Chaturvedi [2002] investigated the effects of the models with different orders on the estimation error. They concluded that the first-order model is not good because of large error while the third-order does

not provide significant improvement over the secondary-order model. Therefore, the secondary-order model may be a good choice. A secondary order model of thermal network structure is therefore selected to model the building internal mass. As shown in Figure 6.1, a 2R2C model is used.
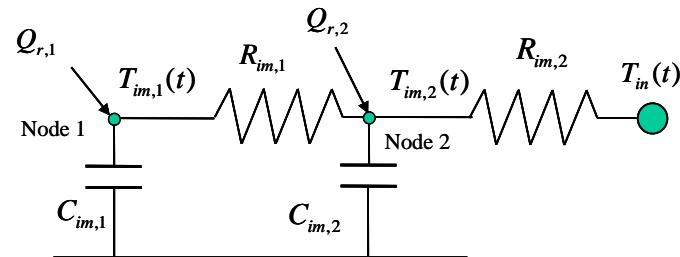
Figure 6.1 2R2C model of building internal mass

The 2R2C model (Two-node model) has two resistances and two capacitances. The resistances and capacitances are assumed to be time invariant. It is worth to note that the resistance of the air film between the surface of mass and indoor air is incorporated into the resistances of the 2R2C model. The radiation on the building internal mass includes the radiant part of heat gain from occupants, lights and equipment etc. It also includes the solar radiation through windows and glass curtain. All the radiation is split into two parts evenly. Half of the radiation is absorbed by *node 1*, stored in the capacitance $C_{im,1}$, and released gradually through the resistance $R_{im,1}$ later. *Node 2* absorbs another half of the radiation and the conductive heat through $R_{im,1}$, stores them in capacitance $C_{im,2}$, and then release them gradually through the resistance $R_{im,2}$ into the indoor air to become instant cooling load. The physical process of the heat absorption and heat release can be represented by

Equation (6.1) and (6.2) as follows.

$$C_{im,1} \frac{dT_{im,1}(t)}{dt} = Q_{r,1} - \frac{T_{im,1}(t) - T_{im,2}(t)}{R_{im,1}} \tag{6.1}$$

$$C_{im,2} \frac{dT_{im,2}(t)}{dt} = Q_{r,2} + \frac{T_{im,1}(t) - T_{im,2}(t)}{R_{im,1}} - \frac{T_{im,2}(t) - T_{in}(t)}{R_{im,2}} \tag{6.2}$$

Where, C and R are capacitance and resistance, T is temperature, subscript $_{im}$ and $_{in}$ indicate internal mass and inside respectively. $T_{im,1}$ and $T_{im,2}$ are the temperatures at *Node 1* and *Node 2* respectively, $Q_{r,1}$ and $Q_{r,2}$ are the radiations absorbed by *Node 1* and *Node 2* respectively, which are half of total radiation heat, $Q_{r,Total}$, as Equation (2.7).

The instant cooling load because of heat release from internal mass can be calculated as Equation (6.3) bellow.

$$Q_{im} = \frac{T_{im,2}(t) - T_{in}(t)}{R_{im,2}} \tag{6.3}$$

Where, Q_{im} is the cooling load because of internal mass heat release.

The parameters of the 2R2C model to be identified are the two resistances and two capacitances. In practical application, the measured cooling load consists of the conductive heat of building envelope, the conductive (convective) heat resulting from building internal masses, and fresh air or infiltration/exfiltration etc. Therefore, to identify the parameters of the simplified model, the whole building energy model should be considered together as described in the next section.

6.3 Hybrid building energy model for energy estimation

As stated in the *Chapter 2*, the hybrid building energy model to estimate the building cooling load is the compounding of both physical simplified models and data-driven simplified model. A schematic of the thermal network structure of hybrid building model is shown in Figure 2.3. As far as building envelope such as external walls and roofs is concerned, the physical information can be easily obtained from design information or site survey. The parameters of the simplified external wall and roof models can be identified when comparing the frequency characteristics of the simplified models and the corresponding theoretical model which is established with the detailed physical information. The parameter identification of simplified 3R2C model has been presented in detail in *Chapter 3* and *Chapter 4*.

The thermal transfer process of the roof can be represented with the following equations.

$$C_{rf,2} \frac{dT_{rf,2}(t)}{dt} = \frac{T_{sol,rf}(t) - T_{rf,2}(t)}{R_{rf,1}} - \frac{T_{rf,2}(t) - T_{rf,4}(t)}{R_{rf,3}} \qquad (6.4)$$

$$C_{rf,4} \frac{dT_{rf,4}(t)}{dt} = \frac{T_{rf,2}(t) - T_{rf,4}(t)}{R_{rf,3}} - \frac{T_{rf,4}(t) - T_{in}(t)}{R_{rf,5}} \qquad (6.5)$$

Where, subscripts *sol* and *rf* indicate solar and roof respectively.

The heat transfer into indoor air because of heat conduction of roof mass, Q_{rf}, can be calculated as follows.

$$Q_{rf} = \frac{T_{rf,4}(t) - T_{in}(t)}{R_{rf,5}} \tag{6.6}$$

Where, Q is heat flow.

Because the external walls at different orientations have different forcing functions due to solar radiation on the wall surface, the external walls should be considered respectively according to the orientations. The thermal transfer process of the simplified 3R2C models of external walls is described with Equations (6.7) and (6.8) as follows.

$$C_{ei,2} \frac{dT_{ei,2}(t)}{dt} = \frac{T_{sol,ei}(t) - T_{ei,2}(t)}{R_{ei,1}} - \frac{T_{ei,2}(t) - T_{ei,4}(t)}{R_{ei,3}} \tag{6.7}$$

$$C_{ei,4} \frac{dT_{ei,4}(t)}{dt} = \frac{T_{ei,2}(t) - T_{ei,4}(t)}{R_{ei,3}} - \frac{T_{ei,4}(t) - T_{in}(t)}{R_{ei,5}} \tag{6.8}$$

Where, subscript ei indicates the i-th external wall.

The heat transfer into indoor air because of heat conduction of the external walls, Q_{ei}, can be calculated as follows.

$$Q_{ei} = \frac{T_{ei,4}(t) - T_{in}(t)}{R_{ei,5}} \tag{6.9}$$

The windows and glass curtains are assumed to have negligible energy storage and be represented with pure resistances. The conductive heat through these transparencies can be calculated as Equation (6.10) as follows.

$$Q_{win} = \frac{T_{out}(t) - T_{in}(t)}{R_{win}} \tag{6.10}$$

Where, subscripts *out* and *win* indicate outside and window respectively.

The sensible cooling energy and latent cooling energy because of fresh air introduced into indoor or infiltration/exfiltraion can be calculates as Equation (6.11) and (6.12). The infiltration/exfiltraion is treated as fresh air.

$$Q_{sen,fr} = c_{air}\rho v_{fr}(T_{out}(t) - T_{in}(t)) \tag{6.11}$$

$$Q_{la,fr} = \rho v_{fr}(h_{out}(t) - h_{in}(t)) - Q_{sen,fr} \tag{6.12}$$

Where, *sen* and *la* indicate sensible and latent cooling loads, v_{fr} is the fresh air flow rate, h_{out} and h_{in} are the enthalpy of outdoor air and indoor air respectively, c_{air} is the air specific heat, ρ is the air density.

The heat transfer through roof, external walls, windows, and the heat release from internal mass is instantaneous heat gain which can become cooling load directly. The convective heat from occupants, equipment and lights etc. also becomes cooling load. The convective heat of solar radiation into indoor space also becomes cooling load instantaneously. The indoor air absorbs some conductive and convective heat gain to raise the temperature. The latent heats because of introduced fresh air and occupants also become cooling load directly. Thus, the sensible and latent cooling energy consumption, the estimated total cooling energy consumption of the building can be calculated as Equation (6.13), (6.14), and (6.15) as follows. It is noted that the

sensible cooling energy consumption is separated from the total cooling energy consumption for the use in *Chapter 8* to calculate supply air flow rate.

$$Q_{sen} = Q_{rf} + \sum_{i=1}^{n} Q_{ei} + Q_{im} + Q_{win} + Q_{sen,fr} + Q_{conv} - C_{in} \frac{dT_{in}(t)}{dt} \tag{6.13}$$

$$Q_{la} = Q_{la,fr} + Q_{la,occup} \tag{6.14}$$

$$Q_{est} = Q_{sen} + Q_{la} \tag{6.15}$$

Q_{conv} is the convective heat from convective part of solar radiation through windows, occupants, lighting and equipments, as shown in Equation (2.9).

Equation (6.15) can be written as follows when substituted with Equations (6.3), (6.6), (6.9~6.14).

$$\begin{aligned} Q_{est} = {} & \frac{T_{rf,4}(t) - T_{in}(t)}{R_{rf,5}} + \sum_{i=1}^{n} \frac{T_{ei,4}(t) - T_{in}(t)}{R_{ei,5}} + \frac{T_{im,2}(t) - T_{in}(t)}{R_{im,2}} + \frac{T_{out}(t) - T_{in}(t)}{R_{win}} \\ & + v_{fr}(h_{out}(t) - h_{in}(t)) + Q_{la,occup} + Q_{conv} - C_{in} \frac{dT_{in}(t)}{dt} \end{aligned} \tag{6.16}$$

When the actual cooling energy consumption and the related variables are measured, the parameters of internal mass can be found to make the estimated cooling energy consumption match the measurement as close as possible.

To calculate the heat transfer of roof, external walls, and internal mass, the nodal temperature should be calculated first. The equations to represent the thermal transfer process of roof, external walls or the internal mass are the secondary order equations. They can be solved numerically with explicit Runge-Kutta algorithm (*Appendix C*).

6.4 Objective function of optimization

The estimated cooling energy consumption with the hybrid building model with Equation (6.13) is used to compare with the measured cooling load to back out the parameters of the simplified model of internal mass. The parameters to be optimized are the resistances and capacitances ($C_{im,1}$, $R_{im,1}$, $C_{im,2}$, $R_{im,2}$) of the simplified 2R2C model of building internal mass, which should give the best fitting with the operation data. The objective function (J) of such optimization uses the integrated root-mean-square error defined in Equation (6.17).

$$J(C_{im,1}, R_{im,1}, C_{im,2}, R_{im,2}) = \sqrt{\frac{\sum_{k=1}^{N}(Q_{act,k} - Q_{est,k})^2}{N-1}} \qquad (6.17)$$

Where, Q is the cooling/ heating load, the subscripts *act* and *est* denote the measured and estimated cooling/heating energy consumption respectively, $C_{im,1}$, $R_{im,1}$, $C_{im,2}$, $R_{im,2}$ are the parameters of the simplified 2R2C model needed to identify. This is a typical nonlinear optimization problem. GA (genetic algorithm) is employed to search for the optimal values. A GA estimator is developed for this optimization as described in next section.

The measured cooling/heating load is calculated using *the return and supply water temperature difference and the water flow rate* retrieved from BMS. To predict the building cooling/heating load using the building thermal network model, *indoor air temperature and humidity, outdoor air temperature and humidity, fresh air flow rate, solar radiation, occupancy and internal gains* are needed.

6.5 GA estimator for parameter identification

Fitness function in GA is used to evaluate the optimization objective function. Ordinarily, the fitness function is designed so that the better the value of the optimization objective function, the larger the fitness function. In this study, the fitness function is designed to be the reciprocal of the objective function as Equation (6.17). The fitness function is shown in Equation (6.18).

$$f = f(C_{im,1}, R_{im,1}, C_{im,2}, R_{im,2}) = \frac{1}{J(C_{im,1}, R_{im,1}, C_{im,2}, R_{im,2})} \qquad (6.18)$$

Equation (6.18) indicates that the fitness will be larger when the estimated cooling energy consumption is more close to the measure cooling energy consumption.

Figure 6.2 shows schematically the flowchart of the GA estimator developed for the parameter identification of the simplified model of internal mass. It starts with the initial estimates of the individual capacitances and resistances of internal mass within assumed ranges. The component with grey background represents the procedures of a GA *run*. Multiple *runs* are allowed.

In the genetic algorithm, the four parameters ($C_{im,1}$, $R_{im,1}$, $C_{im,2}$, $R_{im,2}$) constitute the chromosome of an individual, the assumed ranges of these parameters are the search space for these parameters. Initializing the four parameters produces the initial population to start a GA *run*.
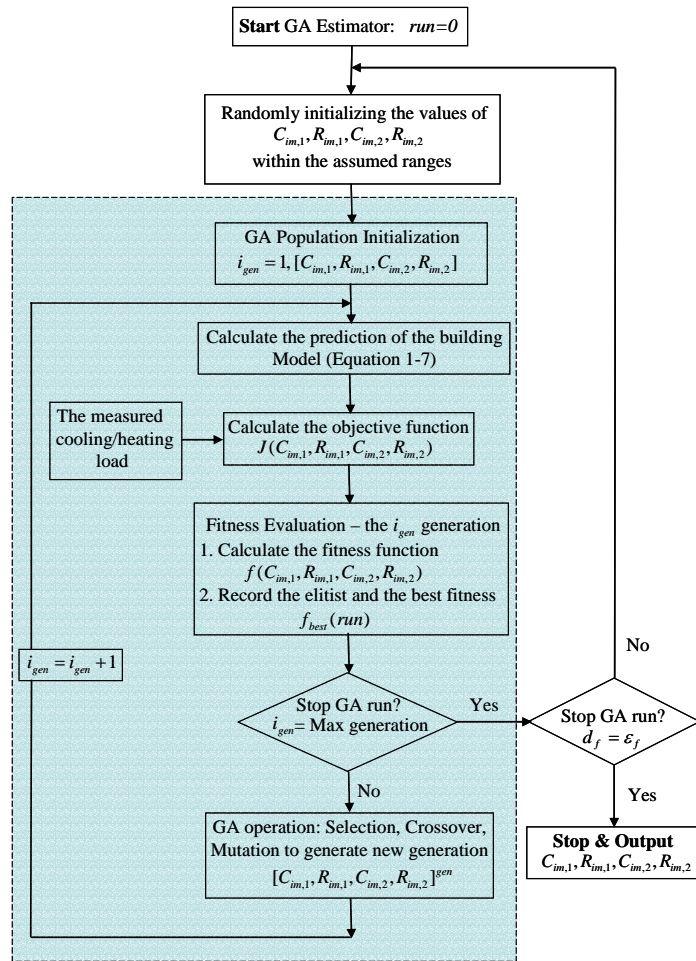
Figure 6.2 GA estimator for parameter estimation of the simplified 2R2C model

Termination of a GA *run* is decided if the number of the current generation is equal to a predefined maximum number. At least two *runs* of the GA processes are necessary when running the GA Estimator. The criterion to stop the GA Estimator is based on the comparison of the best fitness values of two consecutive *runs*. If the relative difference between the two maximum fitness values (d_f) is less than a threshold value (ε_f, e.g., equals to 0.0001), then, the GA Estimator is stopped. The GA driver developed by Carroll [2001] is revised and used.

6.6 Indoor air temperature prediction

With the identified parameters of the simplified model of building internal mass, the hybrid building energy model can also be used to estimate the average indoor air temperature with the given cooling energy consumption. The estimated average indoor air temperature can be compared with the measured average indoor air temperature to further demonstrate the validity of the hybrid building energy model.

6.7 Summary

The chapter presents a method to simplify the internal mass model and identify the parameters of the simplified model of internal mass. It is assumed that all the heat storage materials inside the building including floors and internal walls etc. are described as a simplified lumped thermal network model with 2R2C structure. A GA estimator is developed to find the optimal lumped thermal parameters of building internal mass model (2R2C) by comparing estimated cooling energy consumption with measured cooling energy consumption in a short period. Such model has good robustness to predict thermal performance because its structure can be interpreted physically and the parameters can be identified with the measurements.

CHAPTER 7 VALIDATION OF THE HYBRID BUILDING ENERGY MODEL WITH REAL BUILDINGS

In this chapter, the parameter of the simplified model (2R2C) of internal mass is identified and the hybrid building energy model (the simplified building energy model) is validated in real buildings. The building system and HVAC system of concern are firstly described. Then, the internal heat gains and solar radiation etc. are presented. The result and analysis are given at the end.

7.1 Building system description

The buildings in consideration, China Resources Buildings as shown in Figure 7.1, located at 26th Harbor Road, Hong Kong, were placed in service 1983. The buildings consist of a main building of 50 floors with 180 meter high, an attached building of 7 floors with about 28 meter high, and a basement of 3 floors.

For the main building, the 1st and 2nd floors are served as shopping center with open corridors at the perimeter connecting different buildings. The 3rd, 4th and 5th floors are Chinese restaurants. The 6th floor is chiller plant. The commercial offices are located from the 7th to 49th floors with 2262 m^2 (58 by 39 m) per floor except that the 15th, 31st, 48th floors are for refuge use. The 50th floor is used for banquet hall with 6 meters high.

Figure 7.1 China Resources Buildings

For the attached building, the 1st and 2nd floors are also served as shopping center for selling Chinese art crafts with open corridors at the perimeter connecting different buildings. The 3rd and 4th is an exhibition hall with an atrium in the center. The 5th, 6th and 7th floors are used for commercial offices with 1738 m^2 (22 by 79 m) per floor, and the roof is covered with a swimming pool. The basements are used as garage

The whole buildings are constructed primarily of heavy weight steel concrete with transportation systems and AHU plants are in the cores. The exterior walls above the 2nd floor are a multilayer construction consisting of 5 layers of homogeneous materials including 300*mm* high density concrete between 13*mm* face brick and about 13mm plaster with outside and inside air films. The physical properties of the wall construction are shown in Table 7.1. The floors are 150*mm* high density concrete with an about 50*mm* refurbishment layer. The physical properties of concrete floor are given in Table 7.2.

Table 7.1 Properties of exterior wall construction

Description	Thickness and thermal properties				
	$L(mm)$	$\lambda(Wm^{-1}K^{-1})$	$\rho(kgm^{-3})$	$C_p(Jkg^{-1}K^{-1})$	$R(m^2KW^{-1})$
Outside surface film					0.059
Face brick	13	1.333	2002	920	0.00975
High density concrete	300	1.731	2243	840	0.17331
Plaster or gypsum	13	0.727	1602	840	0.01788
Inside surface film					0.121

Table 7.2 Properties of floors

Description	Thickness and thermal properties				
	$L(mm)$	$\lambda(Wm^{-1}K^{-1})$	$\rho(kgm^{-3})$	$C_p(Jkg^{-1}K^{-1})$	$R(m^2KW^{-1})$
High density concrete	150	1.731	2243	840	0.0867

For the office floors, the ratio of window to wall is about 25%. For restaurant floors and exhibition hall, there are almost no exterior windows. The exterior of the 1st and 2nd of the main building and the attached building are mostly glass curtains and mostly shaded outside. Most of the windows are fixed with aluminum frame without

thermal break (Thermal break: a non-metal component that separates the metal frame exposed to the outside from the surfaces exposed to the inside). The overall coefficient of heat transfer (U_0) of the windows is about 6.42 $W/(m^2K)$ with 3.2 *mm* clean glass as the single glazing material. The coefficient of heat transfer of the glass curtain with 6.0 *mm* toughened glass is about 5.60 $W/(m^2K)$.

7.2 HVAC system description

All the buildings are air conditioned with the chiller plant on the 6th floor except that the banquet hall on the 50th floor is supplied with a separate air-cooled package unit 120 *Ton* (400 *kW*) and the basements are almost not conditioned. The condensing heat is taken away by a sea water cooling system. The plant is equipped with three centrifugal chillers with each 1100 *Ton* (3866 *kW*) cooling capacity, two with each 300 *Ton* (1055 *kW*) cooling capacity and one with 900 *Ton* (3164 *kW*) cooling capacity. Therefore, the cooling capacity is approximately 137 W/m^2 (Gross area 123000 m^2 not including the 50th floors and basements).

A schematic of the chiller water system are shown in Figure 7.2. The water system consists of high zone (all the floors above the 31st floor) and low zone (all the floors bellow the 31st floor including the attached building) to avoid excessive high water pressure on equipments. The high zone is supplied with secondary chilled water through heat exchangers which are located in the 31st floor (refuge floor). In summer season, the cooling source of the heat exchanger (number 7 and 8 shown in the figure) is supplied by primary water circuit of high zone indicated as B in the figure. In other

seasons when cooling energy consumption decreases greatly, the cooling source of high zone is supplied by low zone water circuit denoted as C in the figure while chillers with 300 and 900 *Ton* are shut down.
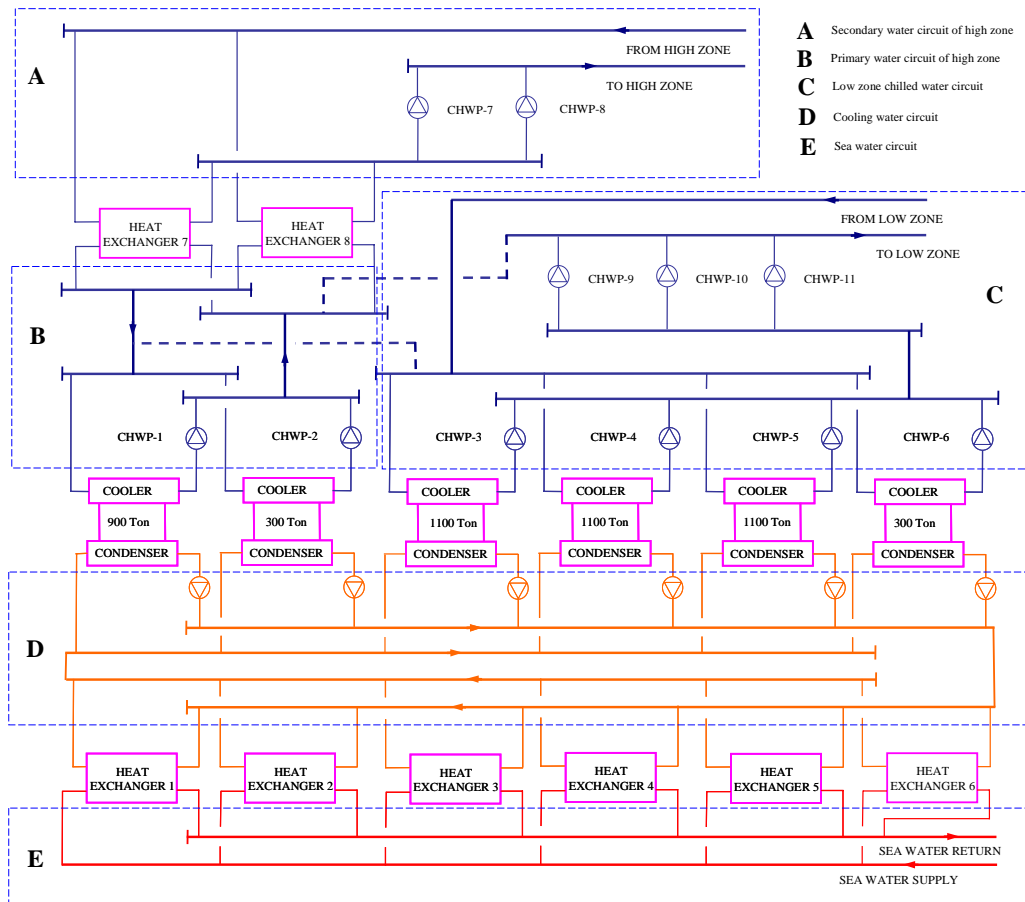
Figure 7.2 Schematics of chiller water system

The low zone is supplied by the secondary water circuit where the pumps (CHWP-9, CHWP-10, CHWP-11) are equipped with variable frequency drivers (VFDs) to regulate the circulated water flow rate to keep the temperature difference between supply water and return water in the main pipes. The condensing heat from chillers is taken away by sea water indirectly through cooling water circuits denoted as D and E.
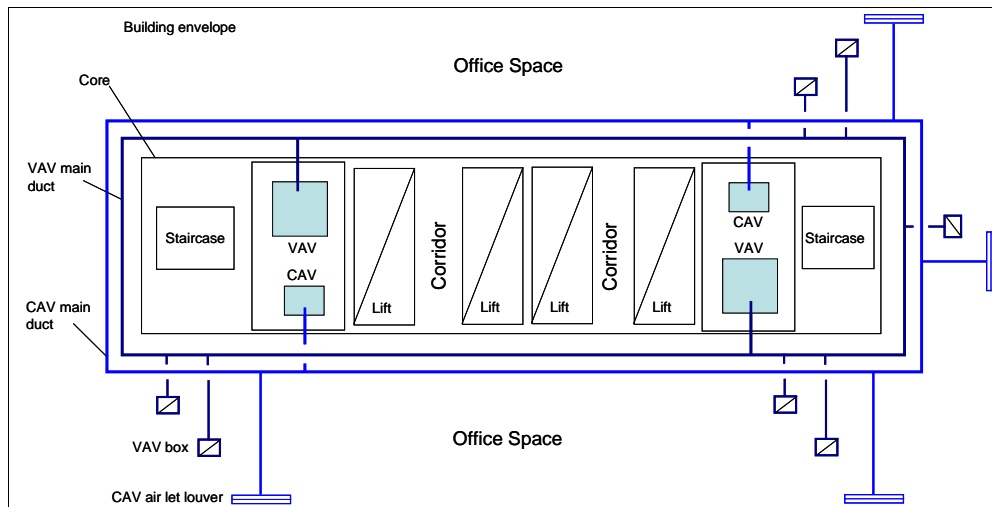
Figure 7.3 Schematics of HVAC layout on the standard floor.

Most of the air conditioning terminals are AHUs. In some floors, FCUs (fan coil units) are separately installed to provide cooling load for communication rooms or computer rooms to keep the temperature at set point when AHUs are shut down at night, on weekends and public day. For the office floors of the main building, AHUs are located in the core areas. Basically, two CAV AHUs service for the perimeter zone and two or three VAV AHUs service for the inner zone. Figure 7.3 shows the schematic HVAC layout of the standard floor. All the VAV boxes are connected to the oval VAV main duct while all the CAV air outlet louvers are connected to the round CAV main duct. All the fresh air of the main building is supplied through the shafts in the core of the main building with fresh air fans installed on the refuge floors

7.3 Internal heat gains and fresh air

Internal heat gains mainly come from occupancy, lighting and equipments etc. According to the site survey and original design information as well as other research achievements [HK-BEAM Society 2003], occupancy and internal heat gain are described as follows. These gains are described to as a design or peak level with a pattern (schedule) that specifies a fraction of the peak for each hour. The normal occupancy period of office, shopping center and restaurant is from 8:00am to 7:00pm, from 10:30am to 20:00pm, and from 6:30am to 22:00pm or late respectively. The design densities of occupancy for the three places are 9, 4.5 and 2 m^2 per person respectively. The design equipment powers for the three places are 25, 30 and 55 W/m^2 respectively. The design lighting powers for the three places are 25, 70 and 35 W/m^2 respectively. The normal patterns of occupancy, equipment load and lighting load for office on weekdays, weekend and public holiday are shown in Table 7.3, Table 7.4 and Table 7.5. It is noted that occupancy, light load and equipment load pattern are in factions of their respective peak values. The normal patterns of occupancy, equipment load and lighting load for shopping center and restaurants on all days are shown in Table 7.6 and Table 7.7.

Table 7.3 Default daily patterns of occupancy, fresh air supply, infiltration, lighting

load and equipment load for office on weekdays

Hour from	To	Occu-pancy	Fresh air supply	Infiltration Rate (ach)	Lighting (Perimeter)	Lighting (Interior)	Equipment
0	6	0.00	Off	0.50	0.05	0.05	0.10
6	7	0.00	Off	0.50	0.05	0.05	0.10
7	8	0.05	Off	0.50	0.10	0.10	0.15
8	9	0.40	On	0.10	0.50	0.50	0.50
9	10	0.95	On	0.10	0.90	1.00	1.00
10	11	0.95	On	0.10	0.90	1.00	1.00
11	12	0.95	On	0.10	0.90	1.00	1.00
12	13	0.95	On	0.10	0.90	1.00	1.00
13	14	0.45	On	0.10	0.80	0.90	0.80
14	15	0.95	On	0.10	0.90	1.00	1.00
15	16	0.95	On	0.10	0.90	1.00	1.00
16	17	0.95	On	0.10	0.90	1.00	1.00
17	18	0.50	On	0.10	0.80	0.80	0.60
18	19	0.25	On	0.10	0.50	0.50	0.40
19	20	0.10	Off	0.50	0.30	0.30	0.20
20	21	0.05	Off	0.50	0.20	0.20	0.15
21	22	0.00	Off	0.50	0.05	0.05	0.10
22	23	0.00	Off	0.50	0.05	0.05	0.10
23	24	0.00	Off	0.50	0.05	0.05	0.10

Table 7.4 Default daily patterns of occupancy, fresh air supply, infiltration, lighting

load and equipment load for office on Saturdays

Hour from	To	Occu-pancy	Fresh air supply	Infiltration Rate (ach)	Lighting (Perimeter)	Lighting (Interior)	Equipment
0	7	0.00	Off	0.50	0.05	0.05	0.05
7	8	0.05	Off	0.50	0.10	0.10	0.15
8	9	0.30	On	0.10	0.50	0.50	0.50
9	13	0.60	On	0.10	0.75	0.80	0.80
13	17	0.10	Off	0.50	0.20	0.20	0.20
17	18	0.05	Off	0.50	0.10	0.10	0.10
18	24	0.00	Off	0.50	0.05	0.05	0.00

Table 7.5 Default daily patterns of occupancy, fresh air supply, infiltration, lighting

load and equipment load for office on Sundays and public holidays.

Hour from	To	Occu-pancy	Fresh air supply	Infiltration Rate (ach)	Lighting (Perimeter)	Lighting (Interior)	Equipment
0	9	0.00	Off	0.50	0.05	0.05	0.05
9	17	0.05	Off	0.50	0.10	0.10	0.10
17	24	0.00	On	0.50	0.05	0.05	0.05

Table 7.6 Default daily patterns of occupancy, fresh air supply, infiltration, lighting

load and equipment load for shopping center on all days

Hour from	To	Occu-pancy	Fresh air supply	Infiltration Rate (ach)	Lighting	Equipment
0	9	0.00	Off	0.50	0.00	0.05
9	10	0.00	Off	0.50	0.00	0.05
10	11	0.25	On	0.10	0.95	0.75
11	12	0.25	On	0.10	0.95	0.75
12	13	0.75	On	0.10	0.95	0.75
13	14	0.75	On	0.10	0.95	0.75
14	15	0.25	On	0.10	0.95	0.75
15	16	0.25	On	0.10	0.95	0.75
16	17	0.25	On	0.10	0.95	0.75
17	18	0.25	On	0.10	0.95	0.75
18	19	0.75	On	0.10	0.95	0.75
19	20	0.75	On	0.10	0.95	0.75
20	21	0.75	On	0.10	0.95	0.75
21	22	0.75	On	0.10	0.95	0.75
22	23	0.00	Off	0.50	0.00	0.05
23	24	0.00	Off	0.50	0.00	0.05

Table 7.7 Default daily patterns of occupancy, fresh air supply, infiltration, lighting

load and equipment load for restaurants on all days

Hour from	To	Occu-pancy	Fresh air supply	Infiltration Rate (ach)	Lighting	Equipment
0	5	0.00	Off	0.50	0.10	0.10
5	6	0.00	Off	0.50	0.10	0.10
6	7	0.60	On	0.10	0.90	0.75
7	8	0.60	On	0.10	0.90	0.75
8	9	0.60	On	0.10	0.90	0.75
9	10	0.60	On	0.10	0.90	0.75
10	11	0.60	On	0.10	0.90	0.75
11	12	0.90	On	0.10	0.90	0.75
12	13	0.90	On	0.10	0.90	0.75
13	14	0.90	On	0.10	0.90	0.75
14	15	0.05	On	0.10	0.90	0.60
15	16	0.05	On	0.10	0.50	0.60
16	17	0.05	On	0.10	0.50	0.60
17	18	0.05	On	0.10	0.50	0.60
18	19	0.75	On	0.10	0.95	0.75
19	20	0.75	On	0.10	0.95	0.75
20	21	0.75	On	0.10	0.95	0.75
21	22	0.75	On	0.10	0.95	0.75
22	23	0.05	Off	0.10	0.75	0.10
23	24	0.05	Off	0.10	0.25	0.10

The internal heat gain from occupancy, lighting and equipments can be split into convective and radiant components (Occupancy heat gains: latent heat 40%, convective 20% and radiant 40%; lighting heat gains: convective 50% and radiant 50% (mostly fluorescent lights); equipment heat gains: convective 80~20% and radiant 20~80%) as shown in Table 7.8.

Table 7.8 Decomposition of sensible internal heat gains and solar radiation heat gains

Heat Gain Source	Radiant Heat, %	Convective Heat, %
Window solar, no inside shade	100	-
Window solar, with inside shade	58	42
Fluorescent lights	50	50
Incandescent lights	80	20
Occupants	33	67
Infiltration and ventilation	-	100
Machinery and appliances	20 to 80	80 to 20

Office, shopping center and restaurant are supplied with constant fresh air of 6 (high density open office), 7 and 7 *L/s* per person in the occupancy periods. Although the building is tight most with fixed windows, the infiltration rate is considered as 0.1 *ach* (air change time) in the occupied periods and 0.5 *ach* in the unoccupied periods.

7.4 Uniform indoor air temperature

The return air temperature of AHUs can be measured and recorded with the building automation management system. The measurement points are in the chamber of AHU plant instead of office area. The average return temperature is taken as the "uniform indoor air temperature" as Equation (7.1) as follows.

$$T_{in} = \sum_{i=1}^{N} \frac{A_i}{A_0} T_{rtn}(i) \tag{7.1}$$

Where, T_{in} and $T_{rtn}(i)$ is uniform indoor air temperature and the return air temperature of the i-th AHU. A_i and A_0 are the served area of the i-th AHU and the total served area. However, when AHUs are shut down, the measurement can not represent the real indoor air temperature because the air is stagnant.

7.5 Solar radiation and window heat flow

Solar radiation can not be measured directly at the site. However, the horizontal global (combined direct and diffuse) solar radiation can be obtained from Hong Kong Royal Observatory. It can be decomposed into direct normal solar radiation and diffuse solar radiation with the relationship established by Lam and Li [1996] or by Yik and Chung et al. [1995] for Hong Kong. The decomposition process is given in *Appendix D*. With the decomposed solar radiation, the calculations of solar air temperature and window heat flow are given in *Appendix E* and *Appendix F* respectively.

7.6 Validation result and analysis

For convenient modeling, the following simplification measures are made. (1) The refuge floors are air open with open window orifices. The heat transfer from refuge floors to the adjacent floors are calculated through the structure of 150*mm* high density concrete with simplified 3R2C models. (2) The ceiling of the 49th floor is considered as adiabatic because the 50th floor is air conditioned with a separate unit. (3) The ceiling of the 7th floor of the attached building is also considered as adiabatic because the roof is covered with a swimming pool. (4) The ground floor is merged into internal mass without special considerations.

The parameters of 2R2C model of the building internal mass were identified using operation data in consecutive fourteen days (two weeks) of summer season. The

needed operation data are as follows. The measured cooling/heating load is calculated using *the return and supply water temperature difference and the water flow rate* retrieved from BMS. To predict the building cooling/heating load using the building thermal network model, *indoor air temperature and humidity, outdoor air temperature and humidity, fresh air flow rate, solar radiation, occupancy and internal gains* are needed. The sampling time for the operation data of the cooling energy consumption and indoor air temperature etc. was half of an hour. The interval time of simulation was also half of an hour.

The indoor air temperature was also estimated with the identified parameters and the measured cooling energy consumption. The operation data in different seasons were also collected to assess the accuracy and stability of the hybrid building energy model with the identified parameters of the simplified model of internal mass to estimate the cooling energy consumption and the indoor air temperature separately. The details are presented as follows.

7.6.1 Identified parameters of the simplified model (2R2C) of internal mass

For the concerned buildings, the basic structure of the floor layer is 150mm high density concrete. Because the internal mass includes the basic structure of the floor layer, the partitions, the internal walls, and furniture, etc., the searching scopes of the parameters of the building internal mass with the GA estimator should be a little larger than the capacitance and resistance of the basic structure of the floor layer. The searching scopes of the two resistances of the simplified model of internal mass were

taken as the resistance of the indoor air film plus three times the resistance of the floor basic structure. The searching scopes of the two capacitances of the simplified model of internal mass was taken as three times the capacitance of the floor basic structure.

The operation data of the building for consecutive fourteen days in typical summer season are used to estimate the parameters of the simplified model of internal mass. The outdoor air temperature and horizontal global solar radiation for identification case are shown in Figure 7.4. Most of the days were sunny and cloudy. Some days were in sunny periods with a few showers.
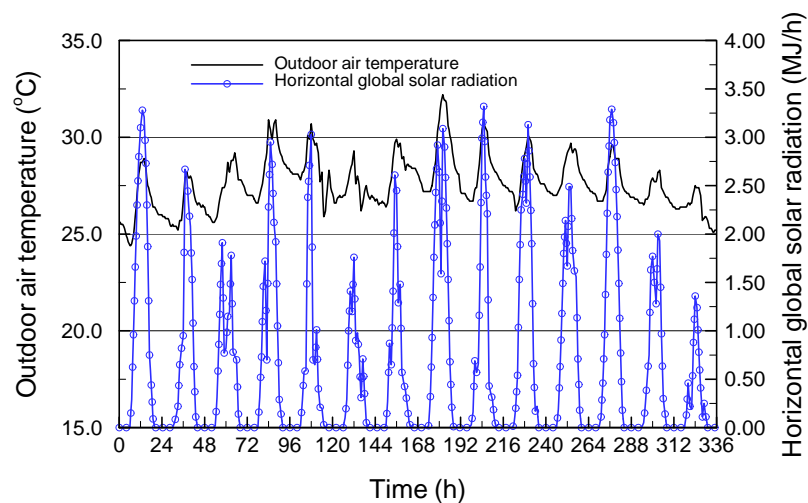
Figure 7.4 Outdoor air temperature and horizontal global solar radiation

(Identification case)

The air conditioning systems in offices were shut down except from 8:00am to 17:00pm of office hours. The air conditioning systems in restaurants and shopping center were shut down a little later. Almost each office floor has fan coils to supplied cooling load to communication or computation rooms for non office hours such as

night time and holidays. The cooling energy consumption in these hours was just a very small part of the total building cooling energy consumption in the normal office hours. The temperatures measured in non office hours did not represent the indoor air temperature because the sensors installed in air chamber (in inner zones) and the most air in offices were stagnant. Therefore, only the operation data in office hours were used to identify the parameters of the simplified model of internal mass model. It is worth notice that the operation data in non-office hours are preferably used in the fittings for parameter identification when reliable measurements in that period are available.

The internal heat gain was described in the previous section. The identified parameters with the GA estimator are as follows. $C_{im,1}$=648729 $J/(m^2K)$, $C_{im,2}$=73793 $J/(m^2K)$, $R_{im,1}$=0.299 m^2K/W, $R_{im,2}$=0.0282 m^2K/W.

Figure 7.5 shows that the estimated cooling energy consumption with the given indoor temperature (actual uniform indoor air temperature) and the identified parameter of the simplified model of internal mass agreed well with the measured cooling energy consumption for identification case. The relative error (the ratio of the sum of the absolute difference between prediction and measurement to the sum of measurement) was 7.8% for the data points of office hours from 8:00am ~ 17:00pm. If all the data points were calculated including office hours and non office hours, the error was obviously high of 18.5% because the model trends to over-predict cooling energy consumption greatly for non office hours. It can be explained that the

calculated uniform indoor air temperature, as Equation (7.1), is lower than the actual temperature which will be described later.
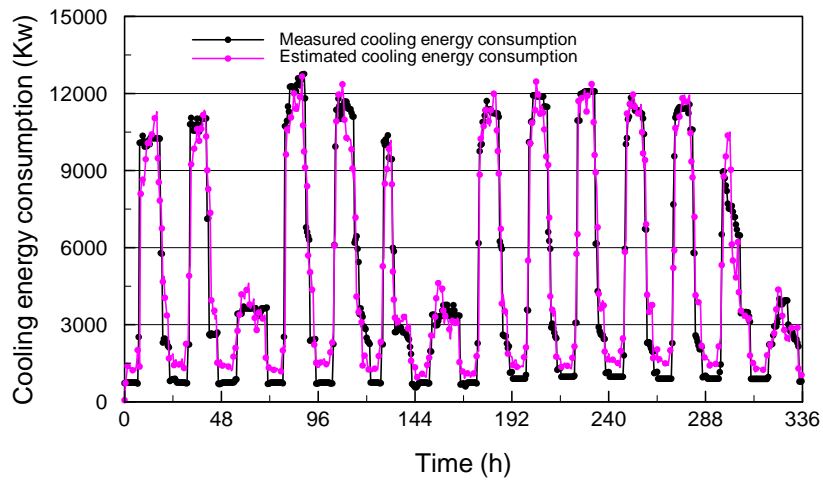
Figure 7.5 Measured and estimated cooling energy consumption (Identification case)
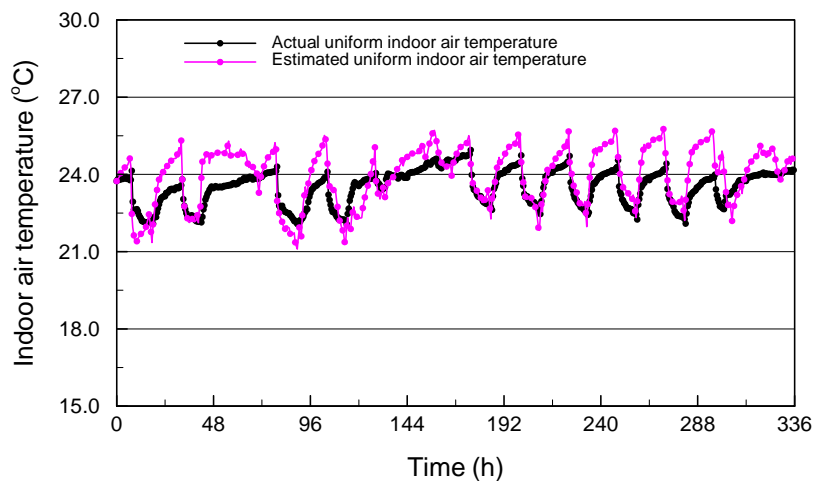
Figure 7.6 Actual and estimated uniform indoor air temperature (Identification case)

Figure 7.6 presents the estimated uniform indoor air temperature with the measured cooling energy consumption and the identified parameters. The estimated uniform indoor air temperature is compared with the actual uniform indoor air temperature averaging the measurements as Equation (7.1). It shows that the estimated indoor air temperature in the office hours with the model approached the

132

actually calculated uniform indoor air temperature with measured return air temperatures. In the other hours, the estimated indoor air temperature was a little higher than calculated uniform indoor air temperature with the measured return air temperatures. In office hours, the air was circulated and the measured return air temperature in the return air chamber was considered as the indoor air temperature. However, In non office hours, the air was stagnant and the measured return air temperature in the return air chamber (in inner area) almost did not affected by the outside weather condition (i.e., heated up), and was obviously lower than the real indoor air temperatures in summer season. Therefore, the estimated indoor air temperature with the hybrid building energy model can represent the uniform indoor air temperature more accurately than the calculated uniform indoor air temperature with the measured return air temperatures in the non office hours.

7.6.2 Validation of the building model

To validate the applicability, the developed hybrid building energy model consisting of the simplified models of building envelopes and the simplified model of internal mass was used to predict the cooling energy consumption in other two operation periods. One was also in summer season lasting for two weeks, the other was in winter season lasting for one week. The same building model was also used to predict the uniform indoor air temperature with the given cooling load. The internal heat gains kept unchanged in the two cases.

In the summer case, the weather condition for validation is shown in Figure 7.7,

which is similar to that used for the training process as shown in Figure 7.4. Figure 7.8 presents the estimated cooling energy consumption profile with the developed hybrid building energy model and the measured cooling energy consumption. The error was 9.7% when the data points in non-office hours were excluded. The average error was 22.0% if all the data points (both in non-office hours and office hours) were included. It shows that the building model can predict the cooling load with acceptable accuracy for practical application.

The estimated uniform indoor air temperatures in the office hours were close to the calculated uniform indoor air temperatures with the measured return air temperature as shown in Figure 7.9. However, the estimated uniform indoor air temperatures in the non office hours (at night and weekend days) were slightly higher than the calculated indoor air temperatures with the measured return air temperature. The situation is the same as that in parameter identification case.
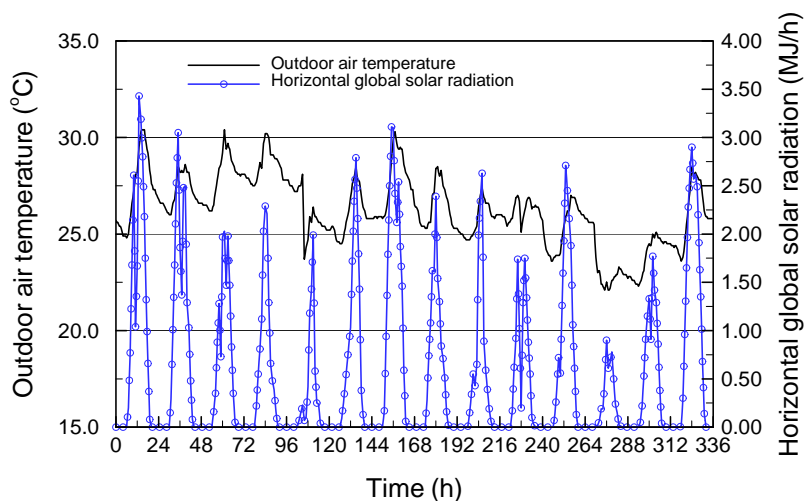
Figure 7.7 Outdoor air temperature and horizontal global solar radiation

(Validation-summer case)
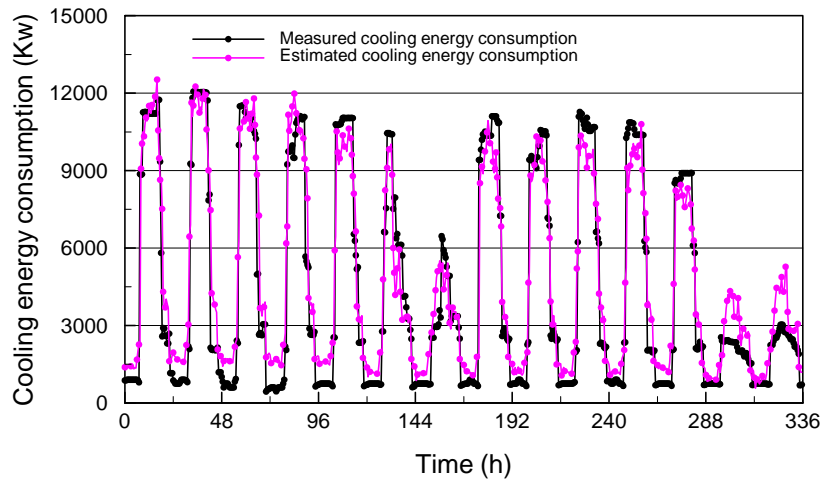
Figure 7.8 Measured and estimated cooling energy consumption

(Validation-summer case)
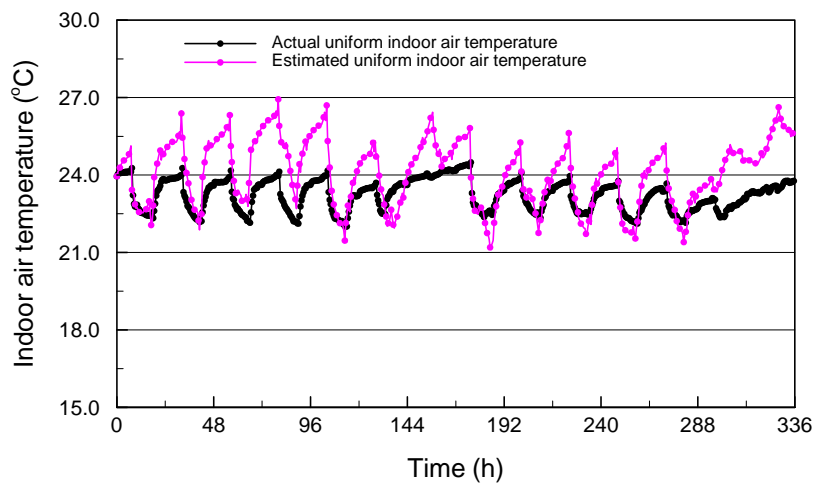
Figure 7.9 Actual and estimated uniform indoor air temperature

(Validation-summer case)

The developed hybrid building energy model was also validated with a week long

operation data in a winter case, which is significantly different from the identification

case. Figure 7.10 shows the outdoor air temperature profile and horizontal global solar

radiation profile (Validation-winter case). The outdoor air temperature was much low

than that in summer season. Most of the days were sunny and the intensities of the solar radiation were a little lower than that used for the training process.

Figure 7.11 presents the cooling energy consumption profiles measured and estimated with developed hybrid building energy model respectively. The estimated cooling energy consumption agreed with the recorded one in office hours with the error 12.0%. The total error including all the data points was higher as 20.1% because there was great deviation in the 7th day (Sunday). The calculated uniform indoor air temperature profile was also shown in Figure 7.12 for comparison.
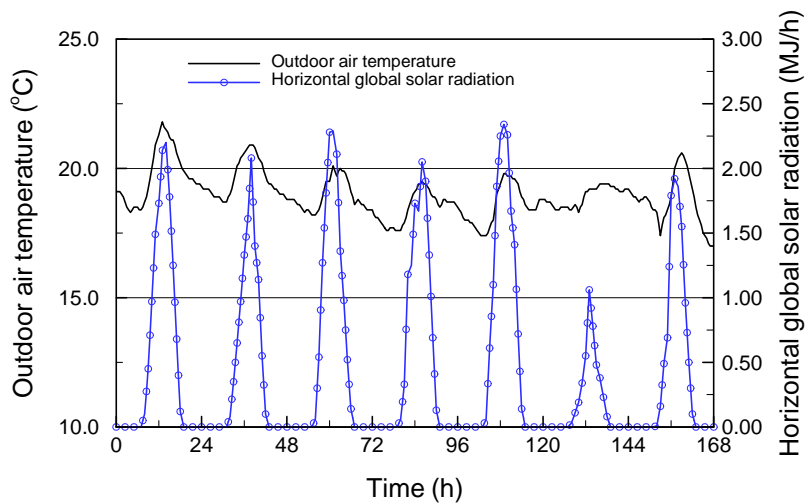
Figure 7.10 Outdoor air temperature and horizontal global solar radiation

(Validation-summer case)
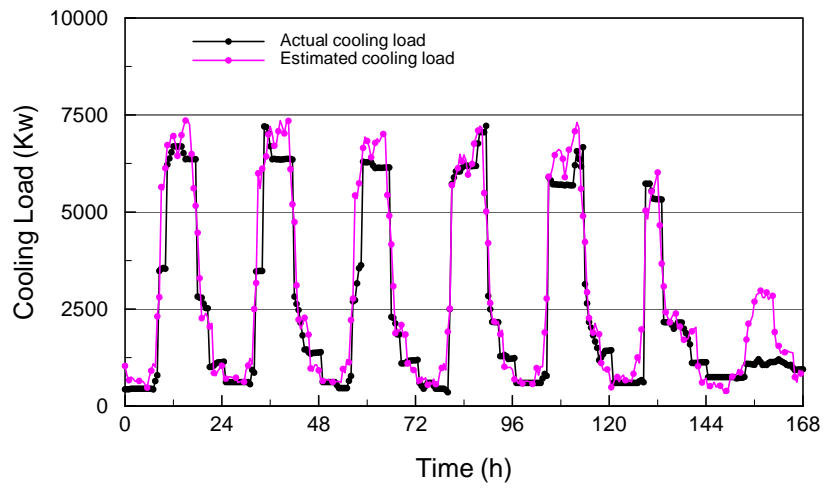
Figure 7.11 Measured and estimated cooling energy consumption

(Validation-winther case)
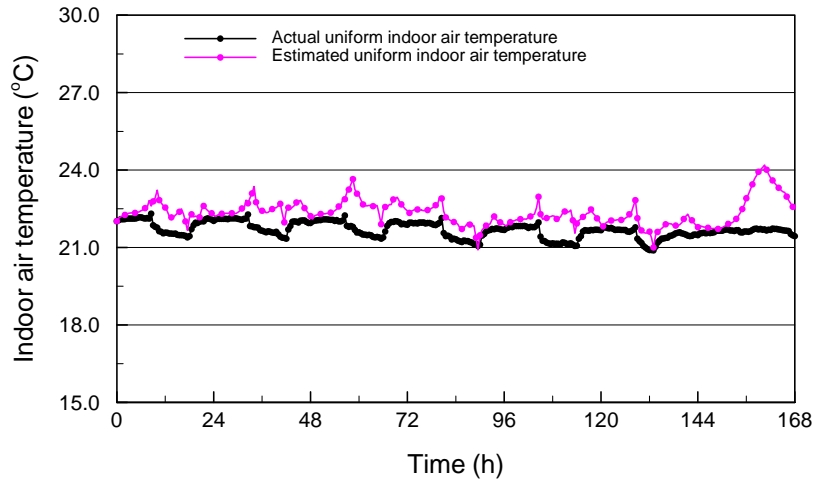
Figure 7.12 Actual and estimated uniform indoor air temperature

(Validation-winter case)

7.7 Summary

In this chapter, the method to identify the parameters of the simplified model of internal mass is validated in real commercial building system with the operation data. The applicability of the developed hybrid building energy model is also demonstrated with various weather conditions. The validation shows that the hybrid building energy model consisting of the simplified models of building envelopes and the simplified model of internal mass can predict the cooling energy consumption with good accuracy under different weather conditions for practical applications. It can also predict the indoor air temperature of acceptable accuracy with the measured cooling energy consumption.

The good stability of the hybrid building energy model should owe to that the simplified models not only can describe the behavior or performance of building envelopes and internal mass, but also can explain them physically.

CHAPTER 8 CONSOLIDATION AHU MODELS

In this chapter, consolidation AHU models are developed to represent all the installed AHUs to simulate the performance of air side systems. At first, the necessity and concept of AHU consolidation are described. Then, the method to estimate the electricity consumption of consolidation AHU models is described in detail. Finally, the consolidation AHU model is validated in a real building system.

8.1 Introduction

Building performance evaluation and diagnosis are important means to determine whether operation problems occur and find what causes result in the problems when they happen [House and Kelly 1999, Liu and Song et al. 2002]. Then, the corresponding measures are taken to fix the problems for proper operation. Proper operation of building system can lead to improved occupant comfort and health, improved energy efficiency, longer life cycle of equipments, reduced maintenance costs, and reduced unscheduled equipment down time, etc. Building performance evaluation is also important means to determine what alternative control strategies can be applied for building performance upgrading.

In component level, various fault detection and diagnosis methods as well as intelligent optimal control methods for end users have been developed [Lee and Park et al. 1996, Liu and Dexter 2001, Yoshida and Kumar et al 2001, Wang and Wang 2002, Norford and Wright et al. 2002, Wang and Xiao 2004, Lee and House et al.

2004]. However, these applications are not easily employed in contemporary building systems because of high expenditure to install enough sensors for such purposes and the complexity of these applications.

At the building level, Kilowatt meter is needed to measure the total electricity consumption or the electricity consumption by HVAC system. The cooling/heating energy consumption can often be measured at the plant. It's also practical to install sub-meter system to measure the electricity consumption in the central plant and the air side electricity consumption of AHU systems respectively. Therefore, it is valuable to predict electricity consumption of AHU systems and chiller system using the measured cooling/heating energy consumption at the building level for performance evaluation or low efficiency detection of building system. Although various methods were developed to estimate energy consumption performance [DOE 1980, Clark 1985, Brandemunehl and Gabel et al. 1993, Wang and Yoshida H et al. 2004] with the "measurements" of individual AHU system, they are not suitable to estimate the total electricity consumption of all the AHUs with the building level's measurement for performance evaluation.

Modeling AHU systems viewing them as a whole is a good solution for building performance evaluation and diagnosis. Considering all the air handling units as a whole can simplify modeling and calibrating with the available monitoring data at the building level. Many researchers developed consolidation AHU to represent all the installed air handling units for practical applications [Reddy and Liu et al. 1998a,

1998b, Liu and Claridge 1998]. However, the consolidation AHU emphasized mainly the cooling/heating energy consumption. Although Energy Systems Laboratory, et al. [2002] stated that air side electricity consumption (fan energy consumption) can be calculated by AIRMODEL [Giebler and Liu et al. 1998] based on the consolidation AHU, it seems that no detailed reports about the principle to estimate the air side electricity consumption for consolidation AHUs.

This study presents a consolidation AHU model, which represents all the installed real AHU systems, and develops a method to estimate the electricity consumption of the model. In the consolidation AHU model, the electricity consumption of the consolidation fans with constant flow rate is the sum of motor powers of the corresponding individual real fans with constant flow rate. The electricity consumption of the consolidation AHU VAV system is simplified to calculate the quotient of the predicted effective mechanical output power of consolidation AHU VAV system and its efficiency. The efficiency of the consolidation AHU VAV system indicates the simple relationship of the predicted effective mechanical output power and actual electricity consumption. The effective mechanical output power is the product of the supply air flow rate and equivalent pressure drop of the consolidation AHU VAV system. Flow rate can be measurement or calculated based on the model predicted sensible cooling load if site measurement is not available. The equivalent pressure drop is represented directly by a typical real AHU VAV system with dimensionless representation. The consolidation AHU model is validated in a real building.

8.2 AHU consolidation for building system

To consider the air subsystem as a whole, a consolidation AHU model represents all the practical installed AHUs. AHU consolidation can make the modeling process simpler and calibration against monitored data much easier. Consolidation AHU is similar to the practical AHU when functions are of concern. The difference is that the consolidation AHU is imaginary. The cooling/heating coil of the consolidation AHU has the maximum capacity of the total AHU capacity. Fans of the consolidation AHU have maximum capacities of the corresponding total AHU fan capacities (i.e., fresh air fan capacity and supply air fan capacity, etc.) to power the air stream through the system. Consolidation AHU can be also called as virtual AHU because it's imaginary and does not exist in reality. To consolidate AHU systems as a whole, some rules were given by Liu and Song et al. [2004].

Usually, large building can be divided to interior zone and exterior zone. In interior zone, cooling is required almost in the all season. In exterior zone, cooling is required in summer season and heating or cooling is needed in winter season depending on the whether condition where the building located. In Hong Kong, heating is almost not needed in winter. According to the practical applications of AHUs in Hong Kong and the practical layout of AHU systems in typical building systems, some basic configurations of consolidation AHU(s) are described as follows.

Figure 8.1 illustrates a consolidation AHU system which contains CAV and VAV systems. The CAV system delivers conditioned supply air of fixed amount flow rate to

the perimeter zone (exterior zone) of the building to provided basic cooling load. The VAV system provides variable flow rate to satisfy variable cooling load for the building. Static pressure set point can be used to control the supply fan operation. The VAV supply air fan can be variable speed with a variable frequency driver (VFD) or with variable pitch angle. The fresh air is supplied by a fresh air fan. An exhaust air fan is used to extract air from indoor to keep suitable pressurization. In high rise buildings or super high rise buildings, it's common that all the fresh air is supplied through the shafts in the core of the building with fresh air fans installed on the refuge floors for the reasons of architecture constrain and architecture aesthetics.

TC-1: *CAV temperature controller*
TC-2: *VAV temperature controller*
M-1:   *Variable frequency driver motor of VAV supply fan*

V-1: *Cooling coil valve*
V-2: *Cooling coil valve*
PC-1: *Static pressure controller*
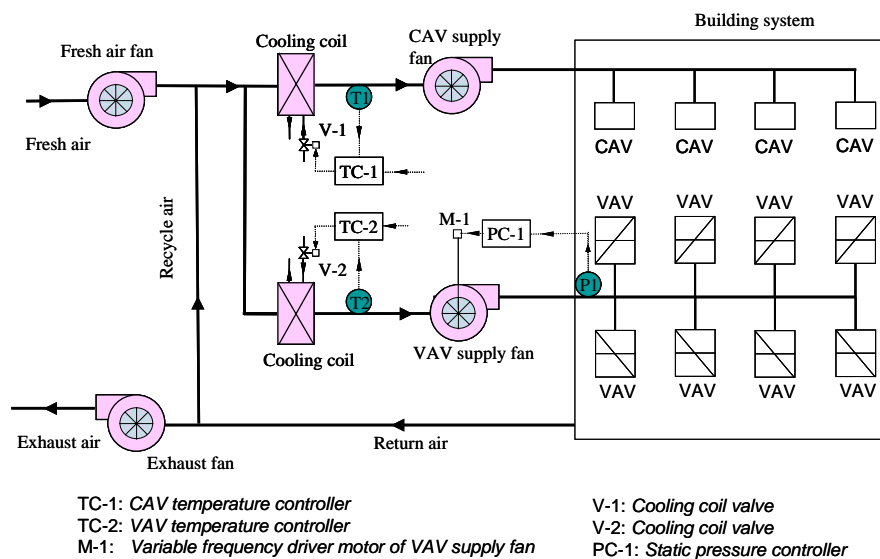
Figure 8.1 Schematics of a consolidation AHU containing CAV and VAV systems with exhaust and fresh air fans

The fresh air fan and exhaust air fan can also be variable speed. The configuration can use economizer control to introduce more fresh air in transit seasons to saving

cooling energy consumption. The flow rate of CAV system of the consolidation AHU

is the sum of the flow rate of all the real CAV systems. Similarly, the flow rate of VAV

system of the consolidation AHU is the sum of the flow rate of all the real VAV

systems.

TC-1: *CAV temperature controller*
M-1:　*Variable frequency driver motor of VAV supply fan*

V-1: *Cooling coil valve*
PC-1: *Static pressure controller*
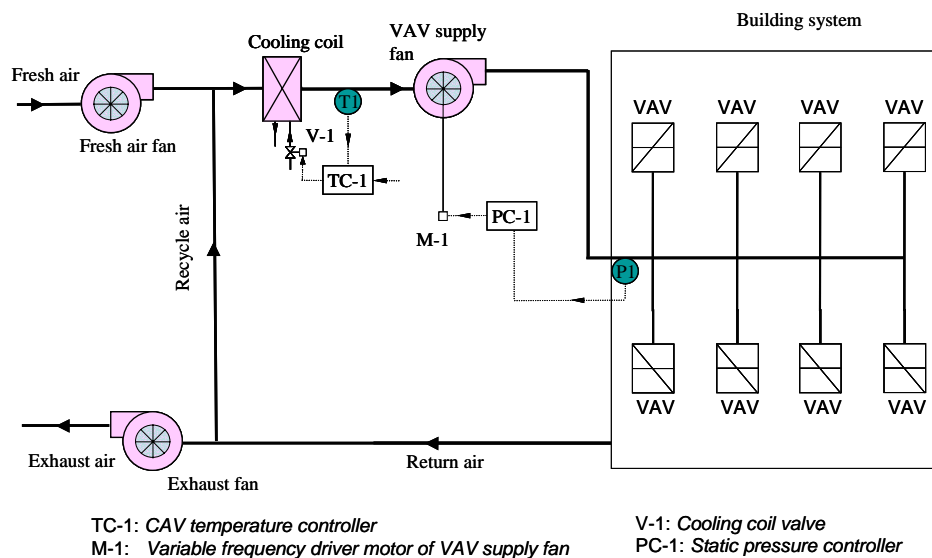
Figure 8.2 Schematics of a consolidation AHU containing VAV system with exhaust

and fresh air fans

In some office buildings, CAV systems are not used. All the cooling energy is

provided by VAV systems. In these buildings, a consolidation AHU system only

containing VAV system can be used to represent all the real VAV system for

simplification. Figure 8.2 illustrates a consolidation AHU system only containing

VAV system with independent fresh air fan and exhaust fan. The exhaust fan and fresh

air fan can be constant or variable speed. It is also common configuration in high rise

buildings or super high rise buildings.

There are some other basic configurations of consolidation AHU(s). For complex buildings which may include block building and tower building, combination of basic configurations can be used to represent all the real AHU systems for simplification consideration. For tower building, simplifying all the real AHUs with a consolidation AHU system is practical because the configurations of the real air conditioning system on different floor are almost the same or similar.

8.3 Electricity consumption of the consolidation AHU model

In this section, the method to estimate the electricity consumption of consolidation AHU models is presented. As shown in Figure 8.1, the air side electricity consumption of the consolidation AHU model includes the consumptions of fresh air fan, exhaust air fan, CAV supply air fan, and VAV supply air fan. The energy consumption of fresh air fan, exhaust fan, and CAV supply fan is relatively easy to calculate by the product of the operation time and the sum of the motor power as Equation (8.1), (8.2), and (8.3). The fresh air fan and exhaust air fan are constant speed.

$$E_{Virtual,fr} = t_{fr} \sum_{i=1}^{n} N_{fr,i} \tag{8.1}$$

$$E_{Virtual,ex} = t_{ex} \sum_{i=1}^{n} N_{ex,i} \tag{8.2}$$

$$E_{Virtual,CAV} = t_{CAV} \sum_{i=1}^{n} N_{CAV,i} \tag{8.3}$$

Where, E is the consolidation fan electricity consumption, t is the operation time of

fans, *N* is the real fan motor power, subscripts *Virtual*, *fr*, *ex*, and *CAV* are associated with the consolidation system (virtual system), fresh air fan, exhaust air fan, CAV supply air fan respectively.

The electricity consumption of the VAV supply fan of the consolidation model is not easy to calculate because the fan power consumption is changed with the supply air flow rate. However, we can approximately calculate the effective mechanical output power of the consolidation AHU VAV system which will be presented in the next two sections. The simple relationship between the effective mechanical output power and the input power (electricity consumption power) of the consolidation AHU VAV system can be established, as Equation (8.4), with site collected operation data. The electricity consumption of the consolidation AHU VAV system can be calculated as Equation (8.5).

$$N_{Virtual,VAV,Me} = \eta\, N_{Virtual,VAV,In} \tag{8.4}$$

$$E_{Virtual,VAV} = \frac{1}{\eta} \int_{\tau=0}^{\tau=t} N_{Virtual,VAV,Me}\, d\tau \tag{8.5}$$

Where, $N_{Virtual,VAV,Me}$ is the effective mechanical output power of the consolidation AHU VAV system, $N_{Virtual,VAV,In}$ is the input power of the consolidation AHU VAV system, η is efficiency of the consolidation AHU VAV system which can be identified from the site data, $E_{Virtual,VAV}$ is the air side total electricity consumption of the consolidation AHU VAV system in the time duration of *t*.

The air side total electricity consumption of the consolidation AHU model, as

shown in Figure 8.1, is calculated as Equation (8.6) when combining Equations (8.1), (8.2), (8.3), and (8.5).

$$E_{Virtual,Total} = E_{Virtual,fr} + E_{Virtual,ex} + E_{Virtual,CAV} + E_{Virtual,VAV} \qquad (8.6)$$

Where, $E_{Virtual,Total}$ is the total electricity consumption of the consolidation AHU model.

8.4 Supply air flow rate of consolidation AHU VAV system

The effective mechanical output power of the consolidation AHU VAV system is the product of the flow rate of the consolidation AHU VAV system and the pressure drop provided by the consolidation VAV supply fan. Therefore, the flow rate and pressure drop should be available first. In some cases, the flow rate can be measured with BMS. When the flow rate is not available, air flow rate can be estimated with cooling/heating energy consumption at the building level, which may be measured on site or calculated with calibrated building energy models as developed in previous chapters. This section presents the air flow rate calculation with cooling energy consumption. The calculation of pressure drop is described in next section.

The flow rate of the consolidation AHU system is directly related to the sensible cooling load although the latent heat also is needed to remove. Equation (8.7) relates the sensible cooling load and the total supply air flow rate of the consolidation AHU, as shown in Figure 8.1.

$$Q_{sen} = c_{air}\rho\, v_{Virtual,CAV}(T_{Virtual,mix} - T_{sup,CAV}) + c_{air}\rho\, v_{Virtual,VAV}(T_{Virtual,mix} - T_{sup,VAV}) \quad (8.7)$$

Where, Q_{sen} is the total sensible cooling load handled by the consolidation AHU model, subscripts *sup*, *mix* are associated with supply air and mixed air respectively, v is the volumetric flow rate.

The flow rate of the consolidation AHU CAV system is the summation of the flow rate of the real consolidated CAV systems as Equation (8.8). The mixed air temperature can be calculated as Equation (8.9). The recycle air flow rate, fresh air flow rate, supply air flow rate have the relationship as Equation (8.10). Combining Equation (8.7-8.10), the flow rate of the consolidation AHU VAV system can be calculated as Equation (8.11).

$$v_{Virtual,CAV} = \sum_{i=1}^{n} v_{CAV,i} \quad (8.8)$$

$$T_{Virtual,mix} = \frac{v_{Virtual,recy}T_{rtn} + v_{fr}T_{out}}{v_{Virtual,recy} + v_{fr}} \quad (8.9)$$

$$v_{Virtual,CAV} + v_{Virtual,VAV} = v_{Virtual,recy} + v_{fr} \quad (8.10)$$

$$v_{Virtual,VAV} = \frac{Q_{sen} - c_{air}\rho\, v_{Virtual,CAV}(T_{rtn} - T_{sup,CAV}) - c_{air}\rho\, v_{fr}(T_{out} - T_{rtn})}{c_{air}\rho(T_{rtn} - T_{sup,VAV})} \quad (8.11)$$

Where, subscripts *recy*, *rtn*, and *in* are associated with recycle air, return air and indoor air respectively.

8.5 Pressure flow characteristic of VAV system

In this section, pressure drop estimation of the consolidation AHU VAV system is

described in detail. AHU consolidation is for practical application and not pure theoretical. Therefore, reasonable simplification is made to calculate the relevant variables of the consolidation AHU VAV system. The pressure drop of the consolidation AHU VAV system is represented directly by a typical real AHU VAV system with dimensionless representation. To calculate the pressure drop of consolidation AHU VAV system, non-dimensional pressure flow characteristic is developed for a typical real AHU VAV system. The consolidation AHU VAV system has the same non-dimensional pressure flow characteristic as the real AHU VAV system. With the non-dimensional pressure flow characteristic and the flow rate, the pressure drop of the consolidation AHU VAV system can be calculated.

8.5.1 Pressure drop of a representative real AHU VAV system

For VAV system, static pressure points are typically placed at two-third of the main duct length before VAV boxes. The supply fan provides pressure to overcome friction loss and dynamic loss to deliver conditioned air to air conditioning zones. Simple schematics, as shown in Figure 8.3, can describe the pressure drops at different parts of VAV duct system of a real AHU. The real AHU system has the same layout as shown in Figure 8.1. The total pressure supplied by the supply air fan to overcome friction loss and dynamic loss can be calculated as Equation (8.12).

$$P_{Tot} = P_{Duct,Rtn} + P_{Att} + P_{Fil} + P_{Coil} + P_{Duct,Sup} + P_{Set} \tag{8.12}$$

Where, P_{Tot} is the pressure head of the supply fan, $P_{Duct,Rtn}$, is the pressure drop of return air duct, P_{Att}, P_{Fil}, P_{Coil}, are the pressure drops across the attenuator, filter, and

coil(s), $P_{Duct,Sup}$ is the pressure drop of VAV duct from the outlet of supply fan to the static pressure set-point, P_{Set} is the static pressure set-point which replaces the total pressure at this point because the dynamic pressure therein is much less than the static pressure set-point. Ordinarily, the design velocity of air flow is several meter per second, and the corresponding dynamic pressure is also very small.
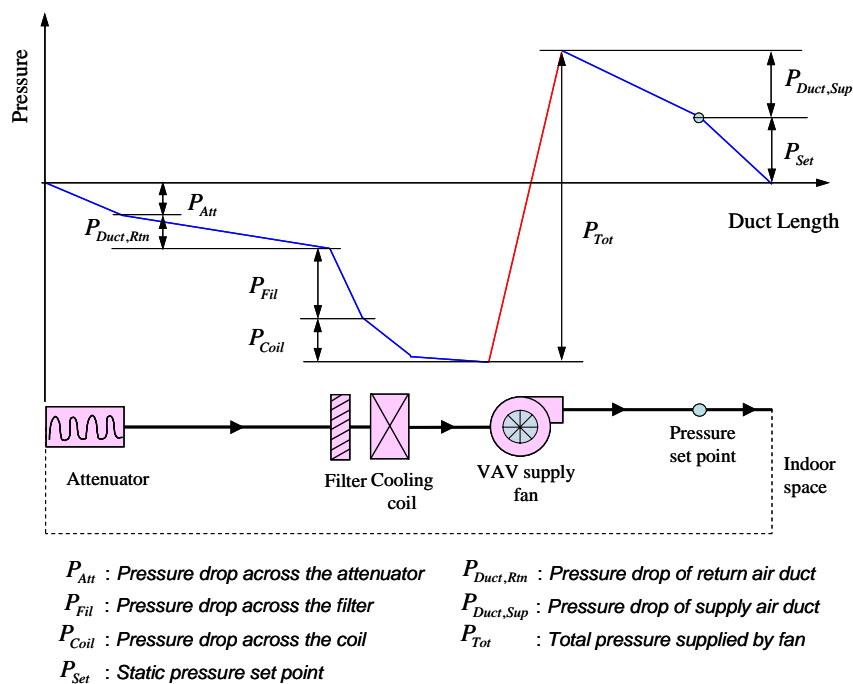
Figure 8.3 Schematics of pressure drops of a real AHU VAV duct system

The pressure drop P because of friction loss or dynamic loss before the static pressure set-point varies with the VAV flow rate, which is almost not dependent on the static pressure set point. (*It's noted that the pressure drop P before the static pressure set-point refers to the sum of pressure drops cross return air duct, the attenuator, filter, coil, and the pressure drop of VAV duct from the outlet of supply fan to the static pressure set-point*) Therefore, the pressure drop P before the static pressure set-point

is of great concern. It can be written as Equation (8.13).

$$P = P_{Duct,Rtn} + P_{Att} + P_{Fil} + P_{Coil} + P_{Duct,Sup}$$
$$= P_{Tot} - P_{Set} \tag{8.13}$$

8.5.2 Non-dimensional pressure flow characteristic

Non-dimensional representation is a common approach in practical applications [Brandemunehl and Gabel et al. 1993, Choi and Kim et al. 2004]. To apply the pressure flow characteristic of a typical real VAV system for consolidation AHU VAV system to calculate the pressure drop, non-dimensional pressure flow characteristic is developed. The non-dimensional variables are defined as Equation (8.14).

$$\varphi = \frac{P}{P_D} \qquad \psi = \frac{v}{v_D} \tag{8.14}$$

Where, φ is dimensionless pressure, P is the actual pressure drop before the static pressure set-point of a real VAV system, P_D is the difference between the design pressure head of supply fan and the static pressure set point, ψ is dimensionless flow rate, v and v_D are the actual and design flow rates respectively of a real VAV system. Simple relationship between the dimensionless pressure and flow rate is described as Equation (8.15).

$$\varphi = a + b\psi + c\psi^2 \tag{8.15}$$

Where, a, b and c are coefficients. They can be easily identified by monitoring a real VAV system, which is described in *Section 8.6*.

8.5.3 Pressure drop of consolidation AHU VAV system

According to the definition of non dimensional pressure and flow, the non-dimensional pressure and flow of consolidation AHV VAV system are described as Equation (8.16).

$$\psi_{Virtual,VAV} = \frac{v_{Virtual,VAV}}{v_{Virtual,VAV,D}} \, , \quad \varphi_{Virtual,VAV} = \frac{P_{Virtual,VAV}}{P_{Virtual,VAV,D}} \tag{8.16}$$

Where, $v_{Virtual,VAV}$ is the actual volumetric flow rate of the consolidation AHU VAV system, which can be measured or calculated with Equation (8.11). $v_{Virtual,VAV,D}$ is the "design" volumetric flow rate of the consolidation AHU VAV system, which is the summation of the design flow rates of consolidated individual AHU VAV systems. $P_{Virtual,VAV}$ is the pressure drop of consolidation AHU VAV system before static set point. $P_{Virtual,VAV,D}$ is the design pressure drop of consolidation AHU VAV system before the static pressure set-point which can be considered similar to (or same as) the design pressure drop of a typical real VAV system before the static pressure set-point.

To calculate the pressure drop of the consolidation AHU VAV system, the non-dimensional pressure flow characteristics of consolidation AHU VAV system is taken as the same to that of a real AHU VAV system as Equation (8.17). The pressure drop of the consolidation AHU VAV system before static pressure set point is calculated as Equation (8.18). The total pressure drop of the consolidation AHU VAV system is calculated as Equation (8.19). The effective mechanical output power of the consolidation AHU VAV system can be calculated easily as Equation (8.20).

$$\varphi_{Virtual} = a + b\,\psi_{Virtual} + c\,\psi_{Virtual}^2 \tag{8.17}$$

$$P_{Virtual,VAV} = \varphi_{Virtual,VAV}\, P_{Virtual,VAV,D} \tag{8.18}$$

$$P_{Virtual,VAV,Tot} = P_{Virtual,VAV} + P_{Virtual,VAV,Set} \tag{8.19}$$

$$N_{Virtual,VAV,Me} = P_{Virtual,VAV,Tot}\; v_{Virtual,VAV} \tag{8.20}$$

Where, $P_{Virtual,VAV,Set}$ is the static pressure set-point of the consolidation AHU VAV system.

With the calculated effective mechanical output power as Equation (8.20), the electricity input power of the consolidation AHU VAV system can be calculated as Equation (8.5) when the efficiency of the consolidation AHU VAV system is identified using monitoring operation data as Equation (8.4).

8.6 Real VAV system performance monitoring

The non-dimensional pressure flow characteristic relationship may be determined according to the characteristics of the components of AHU VAV (such as attenuators, filters, and coiling coils) given in manufacturer catalogues and/or determined according to empirical correlations given in handbook using system geometry configuration parameters. In the study, the VAV system performance data needed for establishing the dimensionless relationship were obtained by monitoring an AHU VAV system on site. The design air flow rate is 6 m^3/s. The design pressure head of the supply fan is about 1600 Pa, where the design pressure set point is about 400 Pa.

The air handling unit of the VAV system is positioned in a separate air chamber.

An attenuator is installed on the partition between the air chamber and an office space to reduce the noise from the supply fan. Fresh air is supplied to the air chamber directly by fresh air duct with separate fresh air fan. The supply fan introduces the mixed air from the air chamber, passes them through the filter and cooling coil, and then distributes them to air conditioning zones through the VAV boxes which simultaneously act as attenuators.

The supply flow rate which is the mixture of return air and fresh air, the pressure drops across the attenuator, the filter, and the coil respectively are measured under various flow rates by manually changing the supply fan pitch angle. The pressure drops on the VAV ductwork from the outlet of supply fan to approximately two third of the VAV ductwork length (at the static pressure set point) under various flow rates are also measured.

Figure 8.4 shows the pressure drops across the filter and cooling coil under various flow rates. Figure 8.5 presents the pressure drops across the attenuator and the pressure flow characteristics of VAV ductwork from the outlet of supply fan to the static pressure set-point which is at about two third of the duct length. It can be seen that the pressure drops over the filter and coil take a great part of the overall pressure drop. The pressure drop across the attenuator is about several dozen *pa* because the air velocity in the attenuator can not be too high.
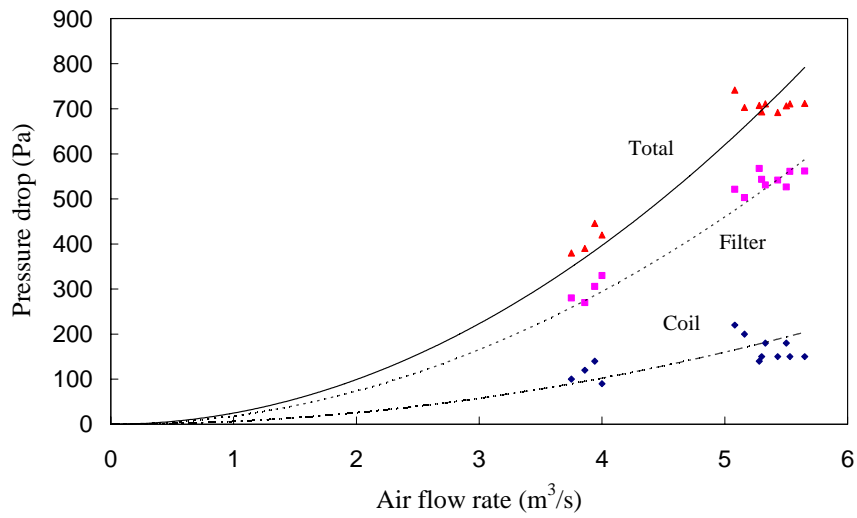
Figure 8.4 Pressure flow characteristics of VAV filter and cooling coil
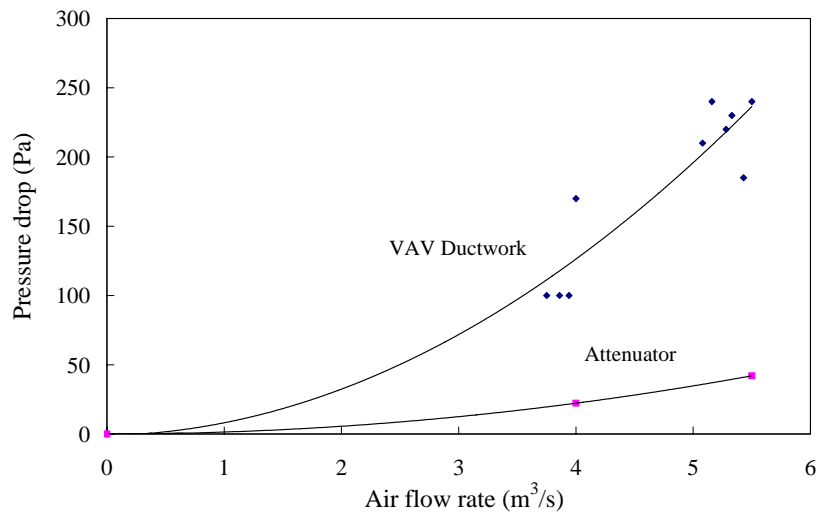
Figure 8.5 Pressure flow characteristics of VAV ductwork and attenuator

Figure 8.6 shows the overall pressure flow characteristics before static pressure set point. The overall pressure drop includes the pressure drop across the attenuator which connects the office and the air chamber, the pressure drops across the components of AHU, i.e., the filter and cooling coil, the pressure drop of VAV

ductwork between the supply air fan outlet and the static pressure set point at about

two third of the duct length.
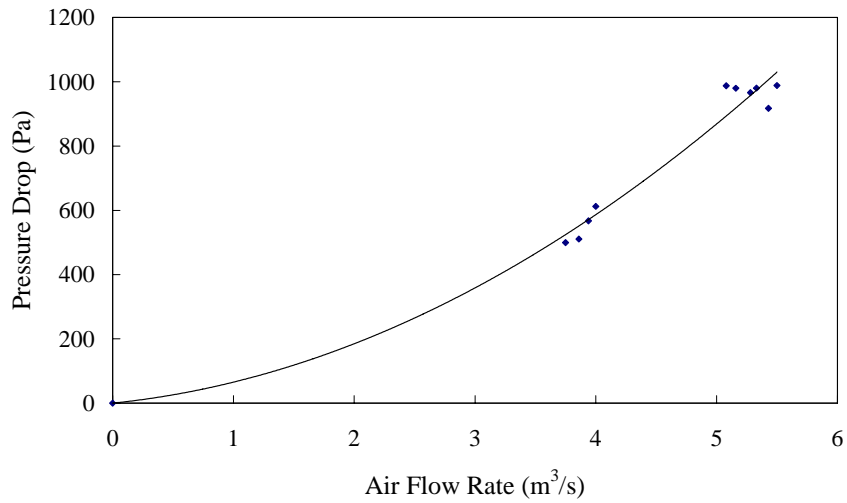
Figure 8.6 Overall pressure flow characteristics before static pressure set point

$$\psi = 0.8044\varphi^2 + 0.1985\varphi - 0.0031$$
$$R^2 = 0.9753$$
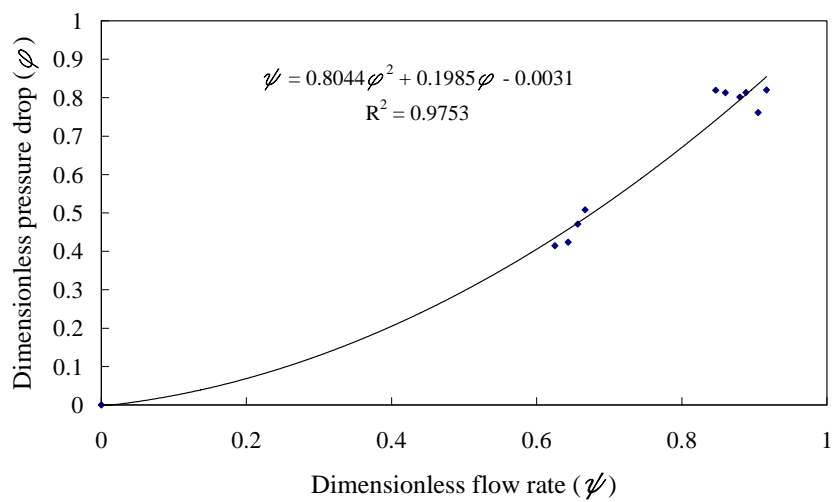
Figure 8.7 Non dimensional pressure flow characteristics

Figure 8.7 presents the non dimensional pressure flow characteristics before static

pressure set point. The second order polynomial as Equation (8.21) is used to describe

the non-dimensional pressure flow characteristics with the coefficient of

determination of $R^2=0.9753$ which is defined as Equation (8.22). The closer to unity the R^2 value, the better the regression model is deemed to be.

$$\varphi = 0.8044\psi^2 + 0.1985\psi - 0.0031 \tag{8.21}$$

$$R^2 = 1 - \frac{\sum(\varphi_i - \hat{\varphi}_i)^2}{\sum(\varphi_i - \overline{\varphi}_i)^2} \tag{8.22}$$

Where, $\hat{\varphi}$ is the dimensionless pressure drop predicted by the model of Equation (8.21), and $\overline{\varphi}$ is the average value of the dimensionless pressure drop calculated with Equation (8.14).

It is noted that the parameters for non-dimensional representation are identified for the system with low velocity ducts. It can be used for similar building with similar AHU VAV system. If high velocity duct is considered, the parameters are needed to be re-identified.

8.7 Description of investigated AHU systems

A typical floor of the tower building of China Resources Buildings is used to validate the consolidation AHU model, as shown in Figure 8.1. The building information was described in *Chapter 7*. The air handling systems are described in more detail for the AHU consolidation.

Two CAV AHUs and two VAV AHUs are designed to service this floor. The layout of these systems is shown in Figure 7.3. Two air chambers in the core are used to accommodate these AHUs. Each air chamber accommodates one CAV AHU and one VAV AHU. Attenuators are installed on the wall between office space and air

chamber to induce return air into air chamber. Return air duct is not needed. The fan powers the mix of return air and fresh air through the filter, cooling coil, and duct. The cooled air is finally delivered to office space.

Two CAV AHUs are used to provide cooled air of constant flow rate to service the perimeter zone. The design flow rate of each CAV AHU is 1.8m^3/s. The main duct of CAV system is around the perimeter of the core and the branch duct is connected to the main duct and delivers the cooled air to the perimeter zone directly with double-layer louver. Two VAV AHUs are used to provide cooled air of variable flow rate to service the inner zone to satisfy the variable cooling load. The design flow rate of each VAV AHU is 4.42m^3/s. The main duct of VAV system is also around the perimeter of core. VAV boxes are connected to the VAV main duct with branch and then regulate the flow rate according to the change of cooling load. The cooled air is finally distributed to the inner zone through diffusers. The total design pressure drop of the two VAV systems is about 1400 Pa.

The air handling systems on this floor can be consolidated as Figure 8.1. The consolidation fresh air flow is 1.5 m^3/s while the power of the consolidation fresh air fan is 1.9 kW. The consolidation exhaust air is 1.3 m^3/s while the power of the consolidation exhaust air fan is 1.5 kW. The flow rate of the consolidation CAV system is 3.6 m^3/s, and the power of the consolidation CAV fan is 4.4 kW. The "design" flow rate of the consolidation VAV is 8.84 m^3/s. The "design" power of the consolidation VAV fan is 26 kW.

8.8 Validation of the consolidation AHU model

The validation of the consolidation AHU model, as shown in Figure 8.1, is presented in this section. The electricity consumption of the consolidation fresh air fan, CAV fan and exhaust fan is relatively easy to estimate. This section mainly focuses on the electricity consumption of the consolidation AHU VAV supply fan. The efficiency of the consolidation AHU VAV system, as Equation (8.4) was identified in *Section 8.8.1*. The validation of electricity consumption of the consolidation AHU model is presented in *Section 8.8.2*.

8.8.1 Efficiency of the consolidation AHU VAV system

To estimate the electricity consumption based on the effective mechanical output power consumption, the efficiency of the consolidation AHU VAV system needs to be determined in advance with monitoring operation data in site. To identify the efficiency of the consolidation AHU VAV system, the electricity consumption of the two individual VAV supply fans needs to be measured, and the effective mechanical output power can be calculated by the product of the flow rate of the consolidation AHU VAV system and the equivalent pressure drop, which can calculated based on the flow rate and dimensionless pressure-flow characteristic as Equation (8.21).

It is favorable that the flow rate of the consolidation AHU VAV system is calculated as the sum of the measured flow rates of individual AHU VAV systems by BMS. However, in this study, no devices were installed to measure the flow rates of

individual AHU VAV systems continuously. The flow rate of the consolidation AHU

VAV system is calculated using the predicted sensible cooling load, as Equation (8.11).

The simplified building energy model developed in previous chapters is used to

predict the cooling energy consumption of this floor.

The available measurements for the efficiency identification of the consolidation

AHU VAV system are as follows. The operation time and the electricity consumption

of the two real VAV supply fan were monitored by BMS. The return air temperatures

of AHUs were measured and recorded with BMS. The average of the measured return

air temperatures were taken as the return air temperature of the consolidation AHU.

The supply air temperature of the real individual VAV and CAV systems were

measured and recorded by BMS, about 13℃. The Indoor air temperature, humidity,

out door air temperature and relative humidity were also measured and recorded with

BMS. The solar radiation was obtained from The Hong Kong Observatory. The last

four measurements were used to predict sensible cooling energy consumption using

the simplified building energy model.

About two weeks' data in summer season were collected to identify the efficiency

of the consolidation AHU VAV system. The predicted sensible, latent, and total

cooling loads in the office hours are shown in Figure 8.8. The third day (Wednesday)

was public holiday and the air conditioning systems were shut down. The cooling load

profiles show that the sensible cooling load was more than two third of the total

cooling load.
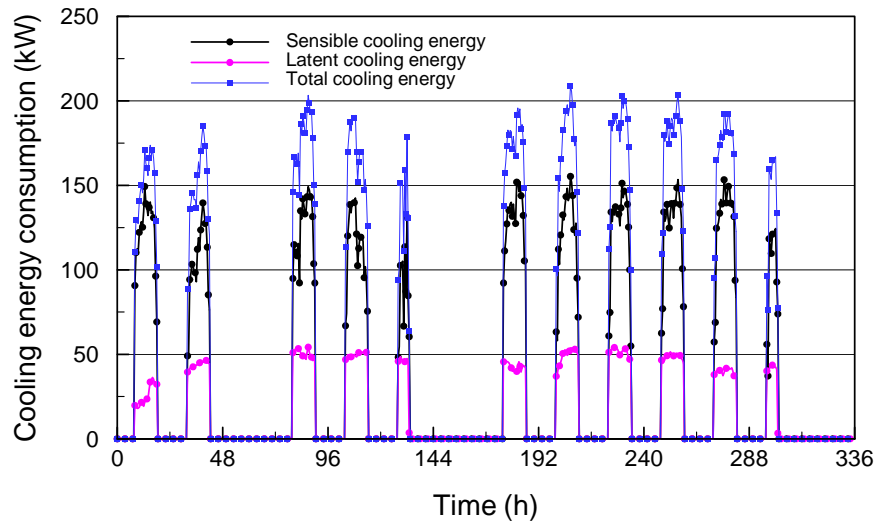
Figure 8.8 Model predicted cooling energy consumption

(Efficiency identification case)

The total fan electricity consumption and the total operation time of the two real VAV systems were collected at 15:30 pm daily. Figure 8.9 presents the recorded daily electricity consumption (previous 15:30pm to current 15:30pm) and the predicted daily effective mechanical output power consumption (previous 15:30pm to current 15:30pm) of the consolidation AHU VAV system. It's obvious that rough linear relationship existed between the recorded daily electricity consumption and predicted daily effective mechanical output power consumption. It is worth to note that the efficiency of the consolidation AHU VAV system is not constant. The efficiency is variable with the supply air flow rate of the consolidation AHU VAV system. However, when the building is exposed to similar weather condition and the daily internal heat gains are similar, the supply air flow rate of the consolidation AHU VAV system to

cool down the building should not vary greatly. At this situation, the efficiency can be considered as constant for practical applications.
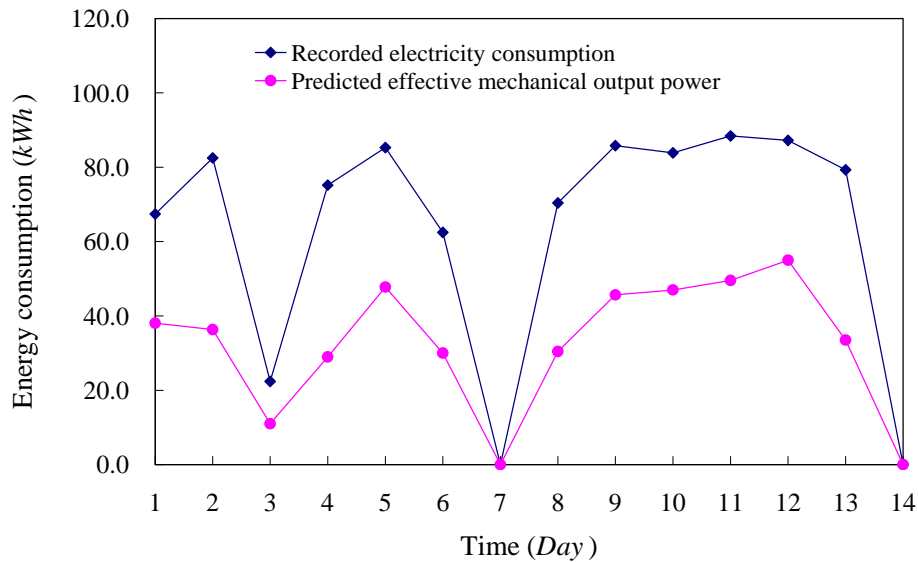
Figure 8.9 Recorded daily fan electricity consumption and predicted daily effective mechanical output power consumption (Efficiency identification case)

At this study, the efficiency of the consolidation AHU VAV system is considered as constant at similar summer weather conditions. Figure 8.10 illustrates the approximate linear relationship between the recorded electricity consumption and the predicted effective mechanical output power consumption of the consolidation AHU VAV system. The efficiency was identified as $\eta = 0.5128$ with the coefficient of determination of $R^2=0.9048$. The closer to unity the R^2 value, the better the regression model is deemed to be.
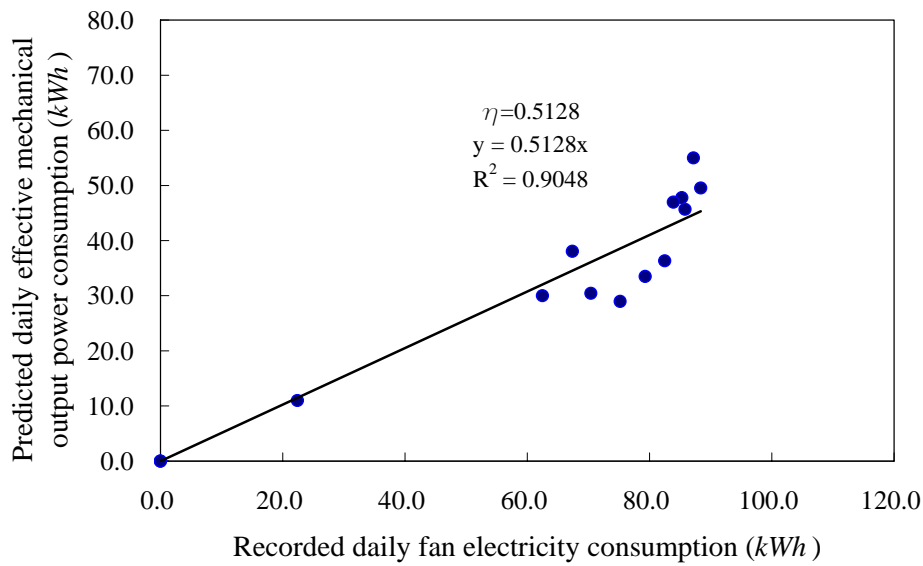
Figure 8.10 Relationship between recorded daily fan electricity consumption and

predicted daily effective mechanical output power consumption

(Efficiency identification case)

8.8.2 Validation of the consolidation AHU model

The measurements in other eleven days in summer season were used to validate

electricity consumption estimation of the consolidation AHU model. The available

measurements were the same as that for efficiency identification case. The identified

efficiency was used to calculate the electricity consumption of the consolidation AHU

VAV system because the summer weather condition for the validation case was

similar to that used for the above efficiency identification case. Figure 8.11 shows the

simulated sensible and latent cooling energy consumption, and total cooling energy

consumption in the office hours for the validation case. The cooling energy

consumption was a little less than that for the efficiency identification case because

the weather was a little cooler. The profiles also show that the sensible cooling energy

consumption is more than two third of the total cooling energy consumption. The

predicted sensible cooling energy consumption was also used to calculate the supply

air flow rate of the consolidation AHU VAV system because of the flow rates of the

individual AHU VAV systems were not measured.
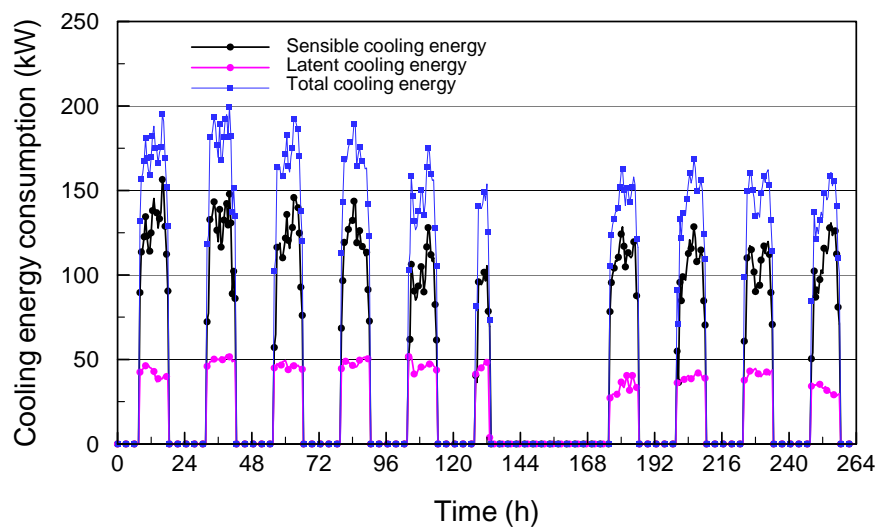
Figure 8.11 Model predicted cooling energy consumption (Validation case)

Figure 8.12 illustrates the recorded daily electricity consumption and the

predicted daily electricity consumption of the consolidation AHU VAV system. The

predicted electricity consumption of the consolidation AHU VAV system was the

quotient of the effective mechanical output power consumption and the above

identified efficiency. The total fan electricity consumption and the total operation time

of the two real VAV systems were also collected at 15:30 pm daily. Therefore, the

recorded daily electricity consumption was also from previous 15:30pm to current

15:30pm. So did the predicted daily effective mechanical output power consumption of the consolidation AHU VAV system.
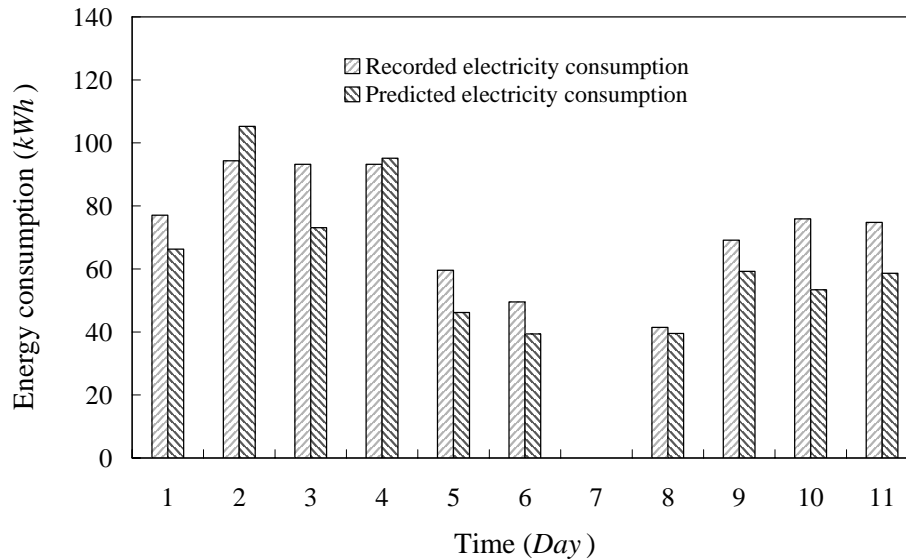
Figure 8.12 Recorded and predicted daily electricity consumptions of the consolidation AHU VAV system (Validation case)

Comparison shows that the predicted electricity consumption basically agreed with recorded accumulated electricity consumption of the consolidation AHU VAV system. The first day was Monday. The electricity consumption for the first day was from 8:00am to 15:30pm because the previous day was Sunday and all the air handling systems were shut down. The seventh day was Sunday, and the electricity consumption was zero. The comparison also shows that the model underestimated the electricity consumption of the consolidation AHU VAV system from the fifth day to eleventh day. It can be explain as follows. The sensible cooling energy consumption was lower than that for the efficiency identification case. Therefore, the supply air

flow rate was also less, which may indicate that the consolidation AHU VAV fan system operated with lower efficiency than the above identified efficiency. However, the identified efficiency was used to calculate the electricity consumption, which led to underestimation.

Anyway, AHU consolidation can simplify modeling process and calibration process with the available monitoring data at the building level. The developed method can predict the electricity consumption of the consolidation AHU VAV system with acceptable accuracy when the efficiencies of the consolidation AHU VAV system are identified under different typical weather conditions or different typical supply air flow rate conditions.

8.9 Summary

To simplify the modeling process and use the monitoring data more efficient, a consolidation AHU model is presented to represent all the real AHU systems in a building for performance prediction of air side systems. The electricity consumptions of consolidation fresh air fan, exhaust air fan, CAV supply air fan are easy to obtain. The electricity consumption of the consolidation AHU VAV system is complicate because it changes with the variable flow rate. This study developed a method to predict the electricity consumption using the model predicted effective mechanical output power consumption.

The efficiency of the consolidation AHU VAV system was identified with the

monitoring electricity consumption and the model predicted effective mechanical output power consumption in a real building. The validation of the consolidation AHU model demonstrates that the consolidation AHU model can predict the electricity consumption of all the AHU VAV systems at the building level with acceptable accuracy. Consolidation AHU model can be used in design process to estimate the air side electricity consumption of all the AHU systems for budget. It also can be used practically to estimate the energy consumption of the whole all-air systems for performance evaluation as well as for cost saving estimation in retrofitting process.

CHAPTER 9 BUILDING ENERGY PERFORMANCE EVALUATION AND DIAGNOAIS

A performance signature-based diagnosis strategy is presented in this chapter for building cooling energy consumption evaluation and diagnosis at building level, which is based on the building global performance evaluation tool as described in *Chapter 2*. Performance signature, which is a unique graphical representation of performance difference of a system under different conditions, is employed for this purpose. By comparing the observed performance signatures of the measured cooling energy consumption with the characteristic performance signatures, the causes resulting in cooling energy consumption deviation from baseline can be diagnosed qualitatively and quantitatively. The reference building energy model to predict cooling energy consumption is the simplified building energy model developed in *Chapter 7*. The "measured" cooling energy consumption from a real office building to be diagnosed is generated using EnergyPlus simulation program.

9.1 Introduction

Diagnosing the problems (faults) leading to more energy consumption at building level is more practical that on equipment/component levels because of limited measurement in many buildings. Whole building electricity utilities and/or cooling/heating energy consumption can provide useful information about the performance of a building. They might indicate whether serious problems or faults

occur in the buildings in light of global views. To detect and diagnose the faults of building system at the building level, three steps may be included [Energy Systems Laboratory 2002]. The first step is to evaluate the building performance. A quantitative evaluation of performance requires a baseline or reference, against which to compare the actual performance. The second step is to identify whether faults occur in buildings by comparing the intended performance with the actual performance. The third step is to diagnose the possible faults when the actual performance deviated from the intended performance with a certain degree.

At building system level, electricity consumption is an important indicator for performance. The electricity consumption in a building consists of lighting, equipment, chiller system, air side fan system etc. Therefore, the causes contributing to electricity consumption are too much and many causes are inter-action. Electricity consumption at building level can give definitive evaluation when compared with the reference. However, it cannot provide effectual information for fault diagnosis.

Cooling energy consumption at the building level not only gives definitive evaluation but also provide important information for diagnosis when compared with the reference cooling energy consumption. It is because mass and energy balance principle tells that the difference between the measured and reference cooling energy consumption must have been due to: fresh air flow rate change, or indoor air temperature deviation, internal heat gains change for a given air tighten building. Therefore, when the cooling/heating energy consumption can be measured in the

central plant or from the branch, it may be more fundamental than electricity utility to be used as building performance index for fault detection and diagnosis at the building level. In this study, cooling energy consumption is used as the important indicator for fault diagnosis at the building level and the faults refer to the causes which result in the cooling energy consumption deviation from the baseline.

With model prediction and site measurement, high effective and efficient performance diagnosis is significantly desired. Signature can be used to indicate a distinguishing or identifying feature of a system. The distinguishing or identifying feature may form an image or a figure for system identification or fault detection etc. Amin and Zhang [2000] used time-frequency signatures to construct the subspaces for improve estimates of the signal and noise subspaces. Li and Weis et al. [2004] developed a large database of random decrement signatures for diagnosis of unknown damage of a fiber reinforced composite beam, together with pattern recognition algorithms. In HVAC field, Wei and Liu et al. [1998] found the cooling and heating energy consumption are affected greatly by changing certain parameters of the building simulation model and created the characteristic signatures for building energy model calibration. In this study, based on the concept of signature, a performance signature-based diagnosis strategy is put forward to diagnose the causes, which may result in building cooling energy consumption deviating from baseline.

9.2 Performance signature-based diagnosis strategy

To diagnose the cooling energy consumption, the possible causes resulting in its

deviation from baseline (reference) is identified first. For a given building, the external elements affecting cooling energy consumption are outdoor air condition and solar radiation. The reference building cooling energy model shares the same external elements with the real building. The internal elements are mainly introduced fresh air flow rate, indoor air temperature, and internal heat gains including lighting, equipments, and occupants etc. In practical operation of the building system, the fresh air flow rate may change due to system fault such as fresh air control. Indoor air temperature and internal gain also may change. These changes can result in cooling energy consumption performance deviating from baseline energy consumption. Therefore, *fresh air flow rate, indoor air temperature, and internal heat gains are identified as building operation parameters for diagnosis*. The baseline values of these building operation parameters need to be determined for calculation of the reference (baseline) cooling energy consumption and for performance comparison (addressed in *Section 9.3*).
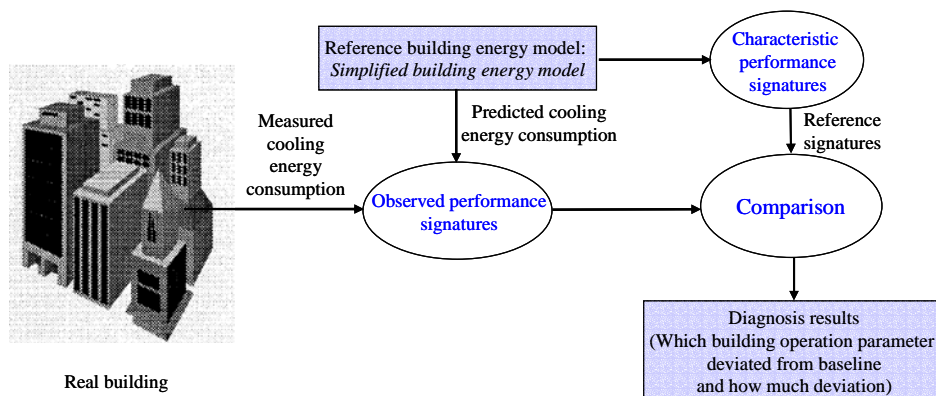
Figure 9.1 The performance signature-based diagnosis strategy based on the building global performance evaluation tool

To diagnose the causes resulting in cooling energy consumption deviation, a performance signature-based diagnosis strategy is presented as Figure 9.1. The strategy is based on the performance prediction of the simplified building energy model, which is the core of the building global performance evaluation tool. The simplified building energy model, as developed in *Chapter 7*, is used as the reference building energy model for performance prediction. By comparing the observed performance signatures with the characteristic performance signatures associated with these three different building operation parameters (i.e., indoor air temperature, fresh air flow rate, and internal heat gains), the causes resulting in the deviation of the cooling energy performance can be found. The observed performance signatures and characteristic performance signatures are described as follows.

For building system or HVAC system, there is a unique graphical representation of the difference between the baseline or predicted performance and the measured performance of a building. The graphical representation of the performance difference can be plotted against the outdoor air temperature. In this study, the performance of the building system refers to cooling energy consumption as stated before. The baseline performance is the output of the simplified building energy model with baseline values of building operation parameters, i.e., indoor air temperature, fresh air flow rate, and internal heat gains. The measured performance of a building is the continuous measurement on site. The unique graphical representation of the difference performance is referred as performance signature as Equation (9.1).

$$OPS(T) = \frac{E_{measured}(T) - E_{simulated}(T)}{Max\{E_{measured}(T)\}} \times 100\% \qquad (9.1)$$

Where, *OPS(T)* is the observed performance signature of cooling energy consumption, which is a function of outdoor air temperature, $E_{measured}(T)$ is the measured cooling energy consumption at difference outdoor air temperature, $E_{simulated}(T)$ is the predicted cooling energy consumption using the simplified building energy model with baselines or changed values of those building operation parameters at difference outdoor air temperature.

For a given building and climate, the graph of the difference of building performance has characteristic shapes that depends on the reasons or causes for the difference. The characteristic shapes refers to the characteristic performance signatures which can be produced for a given building (or a given system) and climate. The characteristic performance signatures are used as reference to diagnose the causes resulting in the deviation of the performance. Characteristic performance signatures are created by the difference of the baseline performance and the output performance of the simplified building energy model with changed values of these three building operation parameters, as Equation (9.2). The changed values of these building operation parameters are defined to deviate from the baseline values by a given amount.

$$CPS_i(T) = \frac{E_i(T) - E_{baseline}(T)}{Max\{E_i(T)\}} \times 100\% \qquad (9.2)$$

Where, *CPS_i(T)* is the characteristic performance signature which is associated

with the *i*-th parameter, i.e., one out of the three building operation parameters (indoor air temperature, fresh air flow rate and internal heat gains). $E_i(T)$ is the output cooling energy consumption of the simplified building energy model with the *i*-th parameter deviating a certain amount from the baseline value while the other two parameters keep as baseline unchanged. $E_{baseline}(T)$ is the baseline cooling energy consumption predicted using the simplified building energy model with these three building operation parameters as baselines.

9.3 Characteristic performance signatures for the building of concern

The tower building of China Resources Buildings in Hong Kong, as described in *Chapter 7*, is used as building prototype for performance evaluation and diagnosis. To provide reference for the cooling energy consumption diagnosis, the characteristic performance signatures for the building is developed. Weather condition has great effects on the characteristic performance signatures. Therefore, the weather condition of Hong Kong is briefed in *Section 9.3.1*. *Section 9.3.2* gives the characteristic performance signatures for these three building operation parameters for the real building in Hong Kong.

9.3.1 Weather condition of Hong Kong

It's obvious that the performance signature at one temperature point is not unique because there are many sets of air state and solar radiation corresponding to a dry bulb temperature value. Generally, typical Meteorological Year type data sets obtained

from observed meteorological records is the usual data source when evaluating thermal performance of buildings through numerical simulation [Chow and Fong 1997]. In this study, the weather data for Hong Kong in 1989 (typical weather year) as shown in Figure 9.2 is used. Outdoor dry-bulb temperatures in the data set range mainly from 10 to 33℃. The dew-point temperature decreases basically with the dry-bulb temperature while the global solar radiation scatters greatly against the dry-bulb temperature.
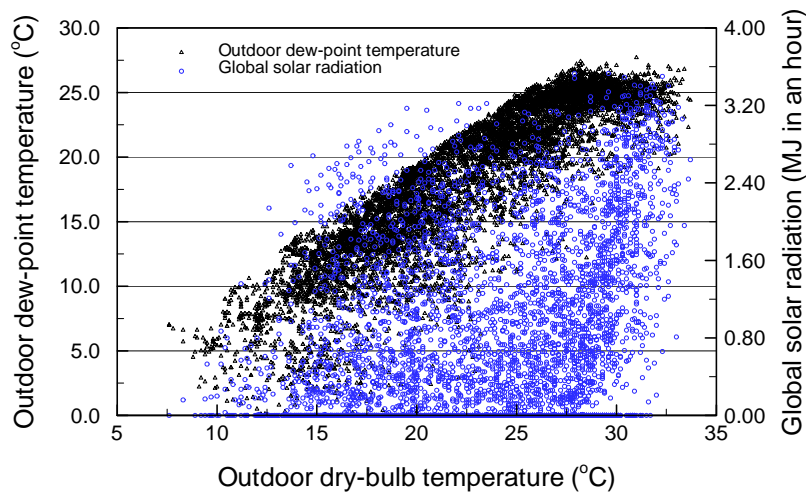
Figure 9.2 Weather data for Hong Kong (1989)

9.3.2 Characteristic performance signatures

To calculate the baseline cooling energy consumption for characteristic performance signatures, the baseline values of these three building operation parameters are determined in detail as follows. The set point of indoor air temperature is 24℃. The design fresh air flow rate is 59.6 m^3/s (0.659 $L/s/m^2$). The total floor area of the tower office building is 90480m^2. The design peak occupancy, equipment, and

lighting power in the office building are 10050 *persons*, 2262 *kW*, 2262 *kW* respectively. The pattern profiles of the internal gain (Lighting, equipment, occupants) in the weekday are shown in Table 7.3, 7.4, 7.5. These values are used as baselines, i.e., the baseline of indoor air temperature is 24℃, the baseline of fresh air flow rate is 59.6 *m³/s*, the baseline of internal heat gains is that occupants 10050 *persons*, lighting power 2262 *kW*, equipment power 2262 *kW*. These baselines are list in Table 9.1.

To obtain the characteristic performance signatures, one of these three building operation parameters is assumed to deviate from the baseline value by a certain amount while the other two keep as baseline values. The detailed deviation of the parameters is as follows. The temperature set point decreases 2℃ from the baseline 24℃ to 22℃. The fresh air flow rate decreases and increases 20% from the baseline value respectively (i.e., 0.8 and 1.2 times the baseline fresh air flow rate). The internal heat gains decrease and increase 20% from the baseline value respectively (i.e., 0.8 and 1.2 times the baseline internal heat gains). The output cooling energy consumption is calculated using the simplified building energy model with changed value of one parameter while others keep baseline values. The characteristic performance signatures for *i*-th building operation parameter are calculated with Equation (9.2) by comparing the output cooling energy consumption and the baseline cooling energy consumption

Figure 9.3 shows the comparison of the baseline cooling energy consumption and

the output cooling energy consumption with the indoor air temperature changing from the baseline 24℃ to 22℃. The cooling energy consumption scatters against the outdoor dry-bulb temperature because the solar radiation and dew-point temperature, which also scatter greatly against the outdoor dry-bulb temperature, are important elements affecting cooling energy consumption. The simulation result shows that heating is needed occasionally when the outdoor temperature is lower than about 15℃. It's noted that the heating is rarely needed in practice in Hong Kong although the outdoor temperature is much low in winter season such as in January and February.
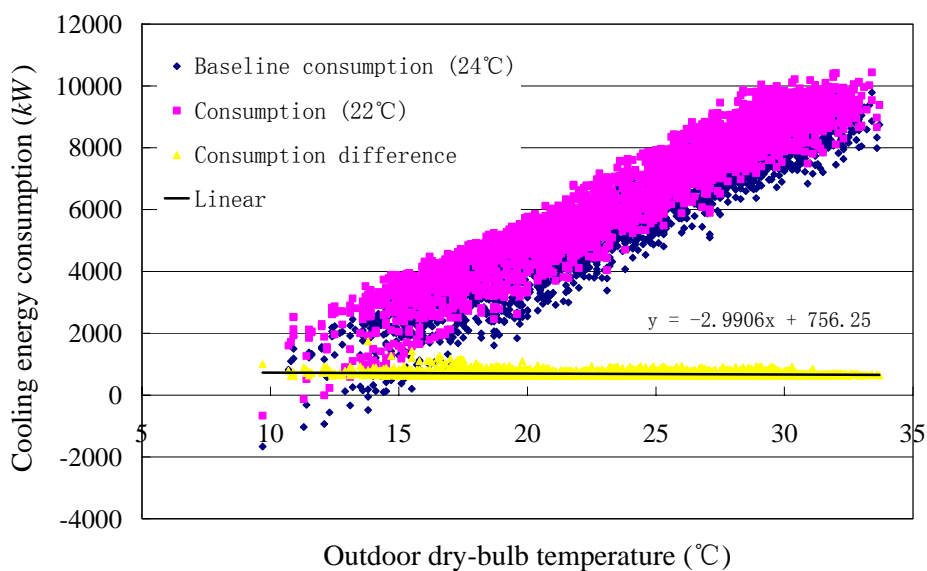
Figure 9.3 Comparison between baseline cooling energy consumption and the cooling energy consumption when the indoor temperature changed from 24℃ to 22℃

Figure 9.3 also shows that the difference between the baseline cooling energy consumption at baseline temperature 24℃ and the cooling energy consumption at the indoor temperature set point 22℃ is alike to a strip line which is parallel to the temperature axis. The regression line shows that the difference is about 760 *kW*.
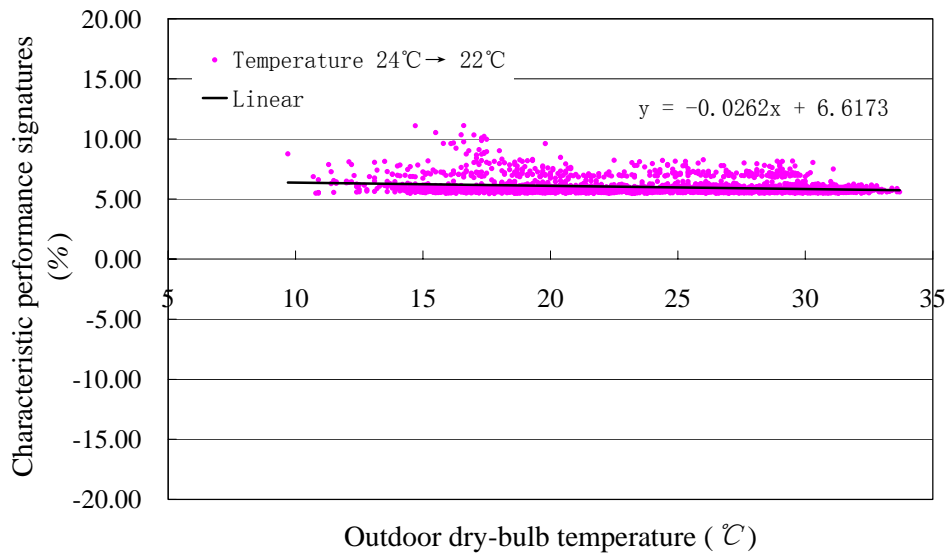
Figure 9.4 Characteristic performance signatures for indoor air temperature

The characteristic performance signatures for indoor temperature are calculated as Equation (9.2). Figure 9.4 presents the characteristic performance signatures. The regression linear line shows the characteristic performance signatures for indoor temperature, which are about 6.6%, are almost parallel to the temperature axis.

Figure 9.5 shows the characteristic performance signatures for internal heat gains. When the internal heat gains are 1.2 times the baseline internal heat gains, the cooling energy consumption difference is positive increase because more energy is needed to cool the increasing internal heat gains. The signatures are centralized and parallel to the temperature axis. The regression line deviates about 6.7% from the temperature axis. When the internal gains are 0.8 times the baseline internal heat gains, the cooling energy consumption difference is negative because less energy is needed. The regression line of the characteristic performance signatures is almost parallel to the

temperature axis. It deviates about -8.0% from the temperature axis.
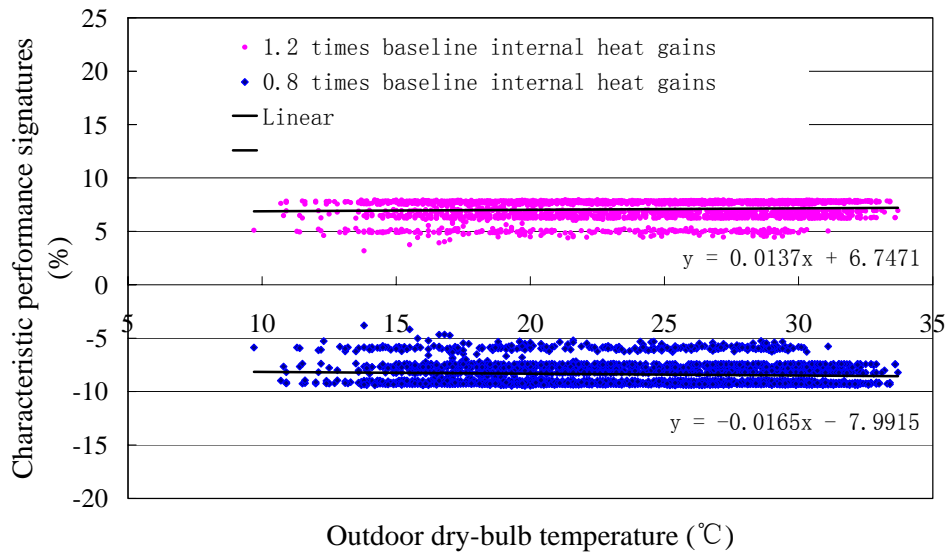
Figure 9.5 Characteristic performance signatures for internal heat gains
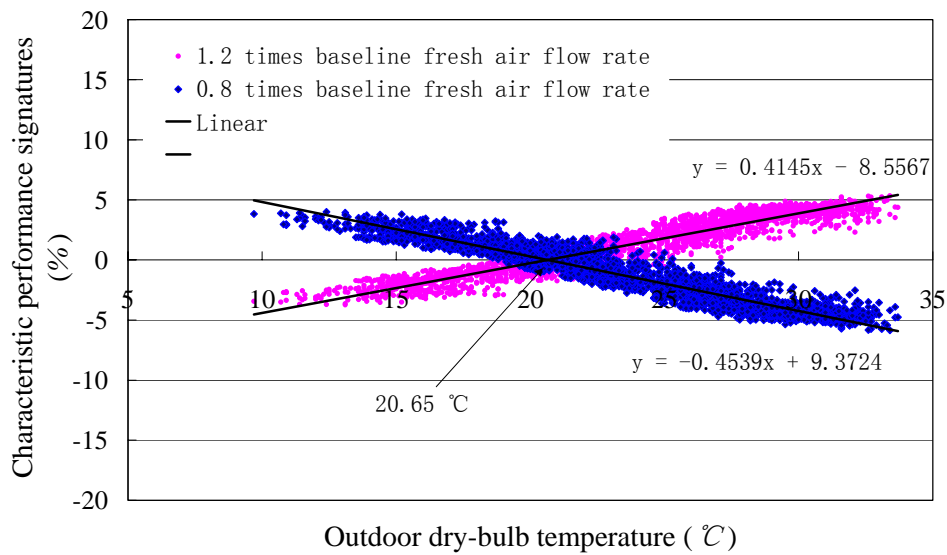
Figure 9.6 Characteristic performance signatures for fresh air

Figure 9.6 shows the characteristic performance signatures for fresh air. When the fresh air flow rate is 1.2 times the baseline fresh air flow rate, the characteristic

performance signatures are upward against the temperature axis. However, the characteristic performance signatures are downward against the temperature axis when the fresh air flow rate is 0.8 times the baseline fresh air flow rate. The regression linear lines can show the trends of the characteristic performance signatures more clearly against the temperature axis. The regression linear lines further reveal that there is a critical division region at about 20.6 ℃ for increasing or decreasing energy consumption. It can be described in details as follows.

For the case that the fresh air flow rate is 1.2 times the baseline fresh air flow rate, the cooling energy consumption difference (corresponding to the baseline cooling energy consumption) increases with the outdoor air temperature when the fresh air temperature is above about 20.6 ℃. More energy is consumed because more warm fresh air is introduced. However, when the fresh air temperature is below about 20.6 ℃, the cooling energy consumption difference is negative because more cool air is introduced to reduce cooling energy consumption.

For the case that the fresh air flow rate is 0.8 times the baseline fresh air flow rate, the situation is reverse. When the fresh air temperature is above about 20.6℃, the cooling energy consumption difference is negative and increases negatively with the outdoor air temperature because less warm fresh air is introduced. When the fresh air temperature is below about 20.6℃, the cooling energy consumption difference is positive because less warm fresh air is introduced for free cooling.

The characteristic performance signatures for fresh air are quite different from the

characteristic performance signatures for other building operation parameters. The characteristic performance signatures for fresh air flow rate have distinguishing slopes and intersection point with the temperature axis. The characteristic performance signatures for indoor air temperature and those for internal gains have similar features, i.e., parallel to the temperature axis.

9.4 Generation of cooling energy data using EnergyPlus

It is favorable to demonstrate the cooling energy consumption diagnosis process using the performance signature-based diagnosis strategy when the cooling energy consumption is measured from site for the whole year. However, the cooling energy consumption of the building was not measured for a year or large part of a year. To demonstrate the validity of the diagnosis strategy, EnergyPlus simulation program (a detail simulation model) is used to represent the tower building to produce the "measured" cooling energy consumption.

EnergyPlus is a detailed building energy simulation program for modeling building heating, cooling, lighting, ventilating, and other energy flows. Based on a user's description of a building from the perspective of the building's physical make-up, associated mechanical systems, etc., EnergyPlus calculates the heating and cooling loads necessary to maintain the indoor control set-points. It employs the heat balance based solution technique for determining building thermal loads, allowing simultaneous calculations of radiant and convective effects at both in the interior and exterior surfaces during each time step of simulation [EnergyPlus Archive 2003].

The current version of EnergyPlus (Version 1.2.1) is used to represent the real building of concern. Using EnergPlus to simulate the building, the chose algorithms, necessary input data, and the fitting process etc., are briefed as follows. The time step for simulation was chose as ten minutes while the output cooling energy load was extracted in the interval of an hour. The inside and outside convection algorithms were detailed. The heat balance algorithm was chose as CTF (conduction transfer functions) to calculate the heat transfer of building envelopes, floor, partitions, and furniture etc. The shading calculations (sun position, etc.) were performed every day to determine the sun position for calculating the solar radiation entering the building together with the global solar radiation read from the weather data file. The weather data was the typical Meteorological Year type data of Hong Kong (1989). The building was simulated for one year (8760 *hours*).

The necessary inputs for Energyplus simulation to represent the real building were detailed descriptions of building envelopes, floors and ceiling, design peak occupancy, lighting power and equipment power, and their corresponding pattern profiles for weekdays and weekend days, the set-points of indoor temperature and relative humidity, fresh air flow rate and infiltration etc. The furniture and carpets could not be described in detail. They were simplified as specific wood plate and specific carpet plate with certain areas respectively. The areas were used to tune the output cooling energy load to match the reference cooling load.

The measured cooling load for whole year was not available for the calibration

process. The simplified building energy model was used to produce the whole year's cooling load for reference, which is also the reference building energy model. The simplified building energy model can represent the real building, which was validated in *Chapter 7*. In the calibration process, the input building operation data, i.e., occupancy, lighting and equipment power, pattern profile, indoor control set points, fresh air were the same for the two simulation models (simplified model and detailed model-EnergyPlus). The weather condition was the same. The description of building envelopes was the same for the both models. The difference was the description of floors, ceilings, and furniture etc. (It is noted that the simplified building energy model consists of simplified models of building envelopes and the simplified model of internal mass. The parameters of the simplified model of building envelope were deduced from the detailed description of building envelope. The parameters of the simplified model of internal mass were identified from the recorded operation data.) The areas of the furniture and the carpet were used to tune the output cooling load of EnergyPlus simulation program (the detail model) to match the reference cooling load predicted using the simplified building energy model (the simplified model).

Figure 9.7 shows the outputs of the simplified model and the detail model against outdoor air temperature with same building operation data input. Figure 9.8 shows the residual between the outputs of both models. The comparisons demonstrate that the two models had good agreement of cooling energy consumption prediction although the detail model overestimated the cooling energy consumption at some

points. Therefore, the calibrated EnergyPlus simulation program can be used to represent the real building to produce the "measured" cooling energy consumption.
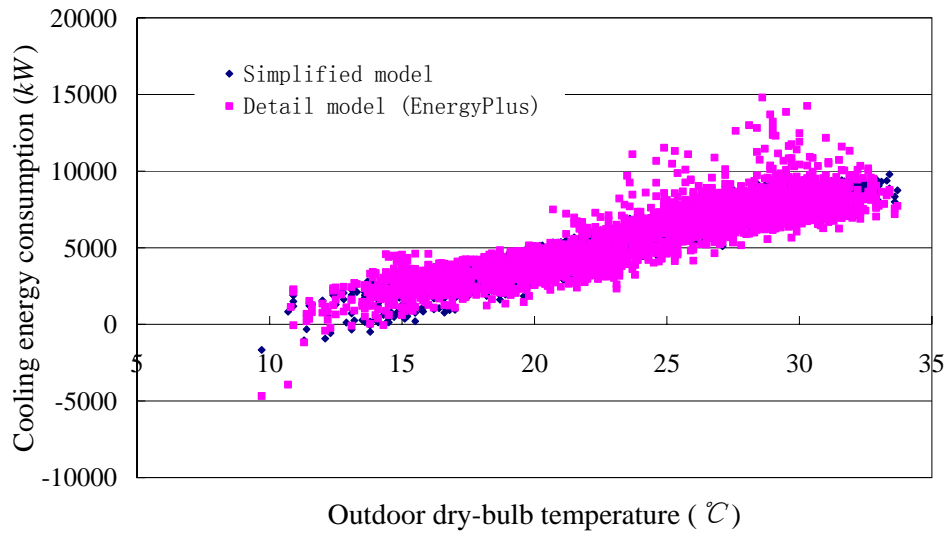
Figure 9.7 Outputs of the simplified model and the detail model (EnergyPlus)
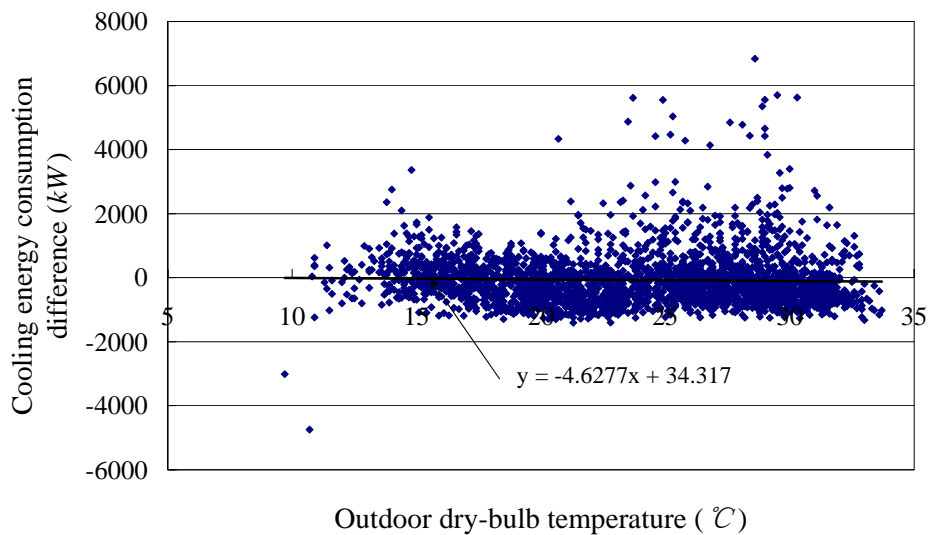
Figure 9.8 Residual between the outputs of the simplified model and the detail

model

9.5 Energy performance diagnosis of building system

According to the analysis of the characteristic performance signatures for these three building operation parameters, the characteristic performance signatures for fresh air are quite different from the characteristic performance signatures for indoor air temperature and internal heat gains. In the diagnosis process of building cooling energy consumption, fresh air should be considered first. Although the characteristic performance signatures for indoor temperature and those for internal heat gains have similar features, the indoor air temperature does not need to be diagnosed using the characteristic performance signatures for indoor temperature. The indoor air temperature can be easily available from BMS. The building internal heat gains can be diagnosed using the characteristic performance signatures for internal heat gains.

An example is presented to illustrate diagnosis process of the performance signature based diagnosis strategy. The characteristic performance signatures are used as reference for the observed performance signatures to diagnose the causes resulting cooling energy consumption deviation. The "measured" cooling energy consumption of the real building is produced using the detail model (EnergyPlus) with certain changes of these three building operation parameters deviating from their baseline values. The fresh air flow rate changed from baseline to 44.7 m^3/s (75% of the baseline). Indoor air temperature changed from baseline 24℃ to 22℃. Internal heat gains changed to 85% of the baseline, i.e., occupants 8540 *persons*, lighting power 1923 *kW*, equipment power 1923 *kW*. These changed values are shown in Table 9.1.

The changed values of these building operation parameters were introduced to the detail model (EnergyPlus) to obtain the "measured" cooling energy consumption of the building. The simplified building energy model was used to simulate the baseline cooling energy consumption with the baseline values of building operation parameters and to predict cooling energy consumption with changed values of building operation parameters. The "measured" data (Meas), simulation result using the simplified building energy model (Sim), the residuals (Res), observed performance signatures (Sign) for the "measured" cooling energy consumption were plotted versus outside air dry-bulb temperature as shown in Figure 9.9. The regression linear line of observed performance signatures was also presented. Figure 9.9 shows that the regression linear line of observed performance signatures had obvious slope, the observed performance signatures above the regression line scattered greatly. Therefore, we can infer that fresh air flow rate must have deviated from the baseline values.

First, the fresh air flow rate was diagnosed. In the characteristic performance signatures for fresh air as shown in Figure 9.6, the fresh air flow rate decreasing from baseline to 0.8 times the baseline fresh air flow rate can make the slope of the regression line to change from zero to about -0.45. Since the slope of the line is about -0.44, different values around 0.8 times the baseline fresh air flow rate were tested to reduce the slope to almost zero. 0.8 times the baseline fresh air flow rate (47.7 m^3/s) can make slope trend much smaller. With the estimated fresh air flow rate, the cooling energy consumption was simulated using the simplified building energy model. The observed performance signatures of the "measured" cooling energy consumption were

also calculated by comparing with the simulated cooling energy consumption using estimated fresh air flow rate. They were presented in Figure 9.10.
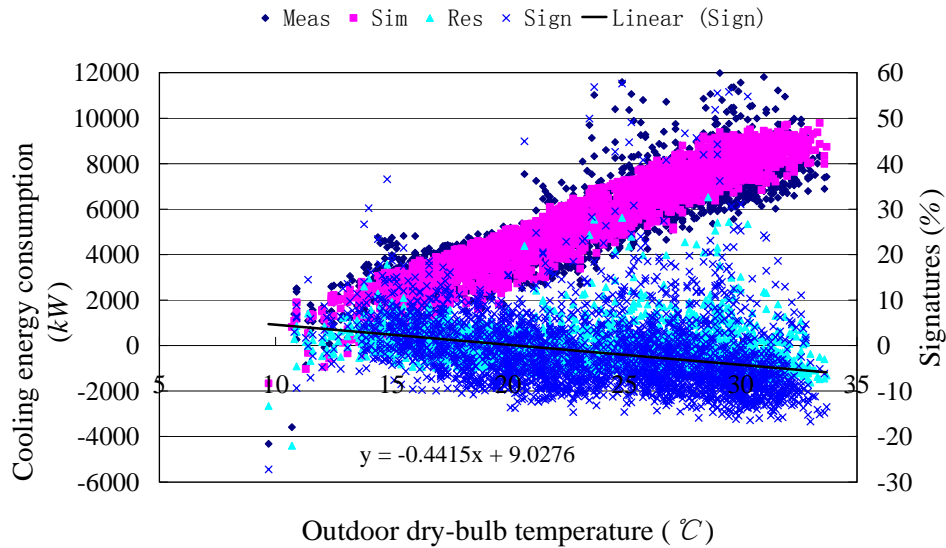
Figure 9.9 "Measured" and baseline cooling energy consumptions, residuals, and

observed performance signatures
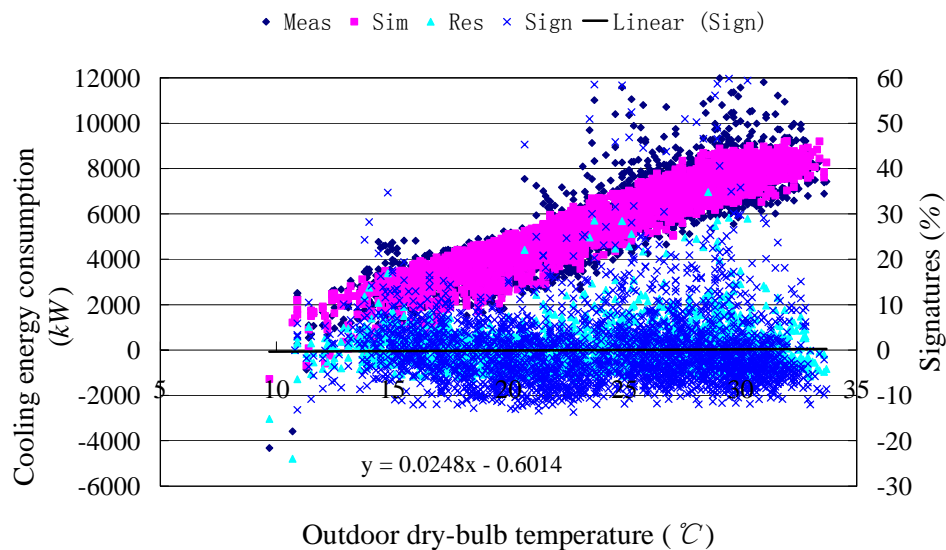
Figure 9.10 "Measured" and simulated cooling energy consumptions, residuals, and

observed performance signatures with estimated fresh air flow rate

After the estimated fresh air flow rate was used, the slope of the regression line dropped considerably to almost zero as presented in Figure 9.10. Although the regression line almost superposed over the temperature axis, it cannot indicate that there were not deviation of the indoor air temperature and internal heat gains from their baseline values. It is because reduced internal gains decreases cooling energy consumption while lower indoor air temperature increases cooling energy consumption. The indoor air temperature can be easily available from BMS. Assuming the "measured" indoor air temperature was 22.5℃. With the estimated fresh air flow rate and "measured" indoor temperature, the cooling energy consumption was simulated again using the simplified building energy model. Figure 9.11 shows the "measured" and simulated cooling energy, the residual and signatures.

After the estimated fresh air flow rate and "measured" indoor air temperature were used, the regression line, as shown in Figure 9.11, deviated significantly from the temperature axis. The regression line of the observed performance signatures was almost parallel to temperature axis and the intercept was -5.3. The deviation tells that the internal heat gains must have decreased from the baseline value when compared with the characteristic performance signatures for internal heat gains as shown in Figure 9.5. In the characteristic performance signatures for internal heat gains, the internal heat gains decreasing from baseline to 0.8 times the baseline internal gains can make the regression line of the characteristic performance signatures offset from the temperature axis to -7.99. By comparing the offset -5.3 of the regression line of the observed performance signatures with the offset -7.99 of the characteristic

performance signatures, around 0.86 times the baseline internal heat gain were tested

to reduce the offset to zero. After estimated 0.87 times the baseline internal gains (i.e.,

8745 *persons*, lighting power 1968 *kW*, equipment power 1968 *kW*.) were tested, the

result was satisfactory as shown in Figure 9.12.
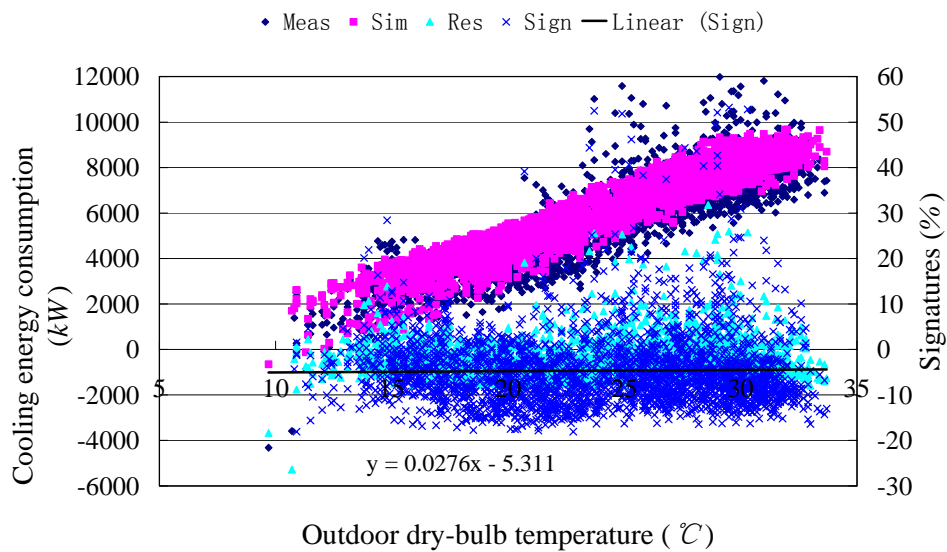
Figure 9.11 "Measured" and simulated cooling energy consumptions, residuals, and

observed performance signatures with "measured" indoor air temperature and

estimated fresh air flow rate

The performance evaluation and diagnosis results show the "measured" cooling energy consumption deviated greatly from the baseline cooling energy consumption. The diagnosis process further reveals that the deviation was caused by changed building operation parameters, i.e., the fresh air flow rate changing to 0.8 times baseline fresh air flow rate, the internal heat gains changing to 0.87 times baseline internal heat gains. Indoor temperature was "measured" changing from 24℃ to 22.5℃. These diagnosed causes are beneficial for further investigations. The baseline values to calculate the baseline cooling energy consumption, changed values to produce "measured" cooling energy consumption, and estimated values of these three building operation parameters in the diagnosis process are summarized in Table 9.1
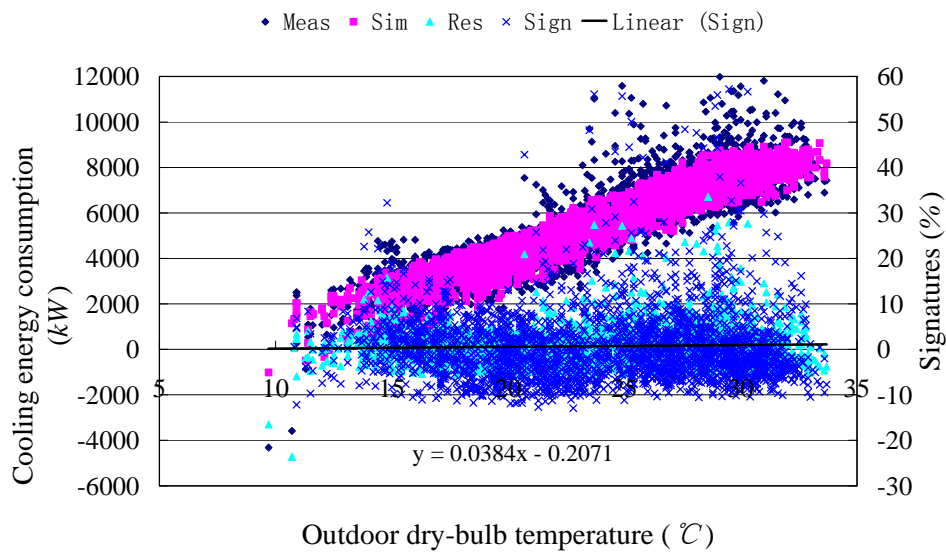
Figure 9.12 "Measured" and simulated cooling energy consumptions, residuals, and observed performance signatures with estimated fresh air flow rate, "measured" indoor air temperature and estimated internal heat gains

Table 9.1 Values of these three building operation parameters in different processes

Values	Baseline values		Changed values			Estimated values		
Process	calculate baseline cooling energy consumption		produce "measured" cooling energy consumption			diagnosis "measured" cooling energy consumption		
Fresh air flow rate	59.6 m^3/s		44.7 m^3/s (75% of the baseline)			47.7 m^3/s (80% of the baseline)		
Temperature	24.0 ℃		22.0 ℃			22.5 ℃ ("measured")		
Internal heat gain	Occupancy (*persons*)	10050	85% of the baseline	Occupancy (*persons*)	8540	87% of the baseline	Occupancy (*persons*)	8745
	Lighting power (*kW*)	2262		Lighting power (*kW*)	1923		Lighting power (*kW*)	1968
	Equipment power (*kW*)	2262		Equipment power (*kW*)	1923		Equipment power (*kW*)	1968

9.6 Summary

A performance signature-based diagnosis strategy based on the building global performance evaluation tool is developed for performance diagnose. This strategy was validated in a real building using the "measured" cooling energy consumption generated by EnergyPlus. The diagnosis process showed that the causes resulting in the "measured" cooling energy consumption deviating from the baseline can be identified qualitatively and quantitatively by comparing the observed performance signatures of the "measured" cooling energy consumption with characteristic performance signatures. These diagnosed causes are beneficial for further investigations of building system. The most important cause diagnosed using this strategy is fresh air flow rate deviation. When this cause is diagnosed, further survey should be carried out on entirely fresh air duct systems. And further measurement should be made on fresh air fan. Then the specific causes can be found and fixed finally.

CHAPTER 10 BUILDING PERFORMANCE EVALUATION WITH ALTERNATIVE CONTROL STRATEGIES FOR UPGRADING

A performance evaluation approach of alternative control strategies is presented in this chapter for energy performance evaluation with alternative control strategies at building level. This approach is based on performance prediction of the building global performance evaluation tool as described in *Chapter 2*. As the two elements of the building global performance evaluation tool, the simplified building energy model and the consolidation AHU model were validated in *Chapter 7* and *Chapter 8* respectively. Based on the energy performance prediction, this evaluation approach employs an enthalpy bin method to evaluate the energy performance of alternative control strategies for practical applications. The energy performance of a building with alternative control strategies was evaluated using the performance evaluation approach. This approach can be used to provide decision making consultation of air handling system retrofitting of buildings to use fresh air efficiently.

10.1 Introduction

In commercial buildings, various measurements can be applied to improve energy efficiency. High energy efficiency equipments in air conditioning system are common. VAV is an increasing popular configuration for energy efficient ventilation in buildings [Lorenzetti and Norford 1992, Englander and Norford 1992]. Enhanced

control strategies, such as resetting static pressure set point in VAV system and resetting supply air temperature set point of AHU system, etc., also contribute to energy savings. Economizer or demand controlled ventilation (DCV) can also reduce cooling energy consumption for AHU systems [Park and Kelly et al. 1984, May 1985, Lam and Hui 1995, Wang and Jin 1998, Wang 1999]. Generally, for energy consumption and indoor air quality consideration, four basic control strategies of fresh air can be exploited, i.e., conventional constant fresh flow rate control, temperature based economizer control, enthalpy based economizer control and DVC control.

The cooling energy consumption saving with alternative fresh air control strategies was demonstrated by some researches [Park and Kelly et al. 1984, May 1985, Lam and Hui 1995]. However, few reports address systematic methods to evaluate the energy performance of alternative fresh air control strategies for practical applications in terms of total electricity consumption savings which includes AHU fan energy consumption and chiller system energy consumption. To determine if alternative control strategies favor total electricity consumption savings, three main issues should be much concerned. First, building energy models are necessary to dynamically predict building cooling energy consumption. Second, chiller models and AHU models are necessary to predict the electricity consumption of chiller system and air handling systems respectively. Finally, suitable methods are necessary to evaluate energy performance of alternative control strategies based on the total energy consumption predictions. Obviously, these models should be calibrated with site measured data for ensuring the accuracy of performance prediction. Because of

limited measurement in many buildings, viewing the building as a whole or the air handling unit systems as a whole can make modeling simpler and calibration much easier as stated in *Chapter 2* and *Chapter 8*.

In this study, a performance evaluation approach of alternative control strategies is presented for energy performance evaluation of alternative control strategies at building level. This approach is based on performance prediction of the building global performance evaluation tool as described in *Chapter 2*. As the two elements of the building global performance evaluation tool, the simplified building energy model is used to predict cooling energy consumption resulting in electricity consumption of the chiller system. The consolidation AHU model is used to simulate the air side performance of AHU systems based on predicted sensible cooling energy consumption and fresh air flow rate. The two models have been validated in *Chapter 7* and *Chapter 8* respectively. Based on the energy performance prediction of the building system using the simplified building energy model and the consolidation AHU model, the performance evaluation approach employs an enthalpy bin method to evaluate the energy performance of alternative control strategies for practical applications. The enthalpy bin method facilitates energy performance evaluation by dividing performance prediction into a series of enthalpy bins. The energy performance of a high rising office building with alternative control strategies was evaluated using the performance evaluation approach. The results show that the optimal fresh air control strategy can easily be achieved for practical applications using the performance evaluation approach.

10.2 Performance evaluation approach of alternative control strategies
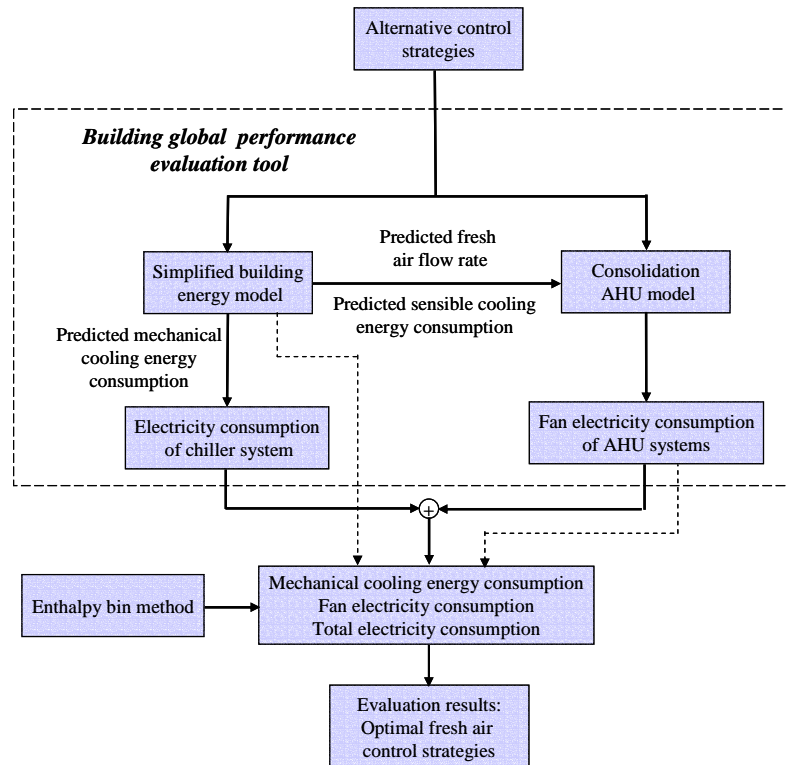
Figure 10.1 Illustration of the performance evaluation approach of alternative control strategies based on the building global performance evaluation tool

Figure 10.1 illustrates the performance evaluation approach of alternative control strategies. The approach is based on the building global performance evaluation tool. The approach uses the simplified building energy model and the consolidation AHU model for performance prediction at building level. Based on the performance prediction, approach employs an enthalpy bin method to facilitate performance evaluation of alternative control strategies. The procedure of the evaluation approach of alternative control strategies is briefed as follows.

To evaluate the energy performance of alternative control strategies (described in *Section 10.4*), the cooling energy consumption, the amount of introduced fresh air, and electricity consumption of HVAC systems in the building is needed to estimate. The simplified building energy model is used to reliably and accurately estimate the total cooling energy consumption and sensible cooling energy consumption caused by heat transfer of envelopes, solar radiation, occupants, lighting and equipments etc, except the heat transfer of introduced fresh air. When conventional fresh air control is exploited, the amount of fresh air is the design value or the site measurement. When temperature based economizer control is exploited, the amount of fresh air is estimated to counteract the sensible cooling energy consumption predicted by the simplified building energy model. When enthalpy based economizer control is exploited, the amount of fresh air is estimated to counteract the total cooling energy consumption. The amount of fresh air using temperature based and enthalpy based economizer controls is constrained between the minimum design value and the maximum capacity of fresh air delivery. When DCV control is exploited, the amount of fresh air is determined based on the estimated occupants.

With the heat transfer of introduced fresh air by alternative fresh air controls, the total mechanical cooling energy consumption as well as sensible cooling energy consumption can be estimated easily. The electricity consumptions of consolidation AHU model is calculated based on the sensible cooling energy consumption and the introduced fresh air flow rate as described in *Chapter 8*. Simplified chiller system models are favorable to estimate the chiller system electricity consumption. In the

evaluation approach, the chiller system electricity consumption is calculated using the overall COP of chilling system. The total electricity consumption is the summation of the chiller system electricity consumption and the fan electricity consumptions of AHU systems. The enthalpy bin method, which is described in *Section 10.3*, is employed for energy performance evaluation of alternative control strategies based on the energy performance prediction, i.e., mechanical cooling energy consumption, fan energy consumption and total electricity consumption.

10.3 Enthalpy bin method

"Bin" is not a new concept in academic fields. It is often used to divide a variable into a series of strips for facilitating analysis and simple applications. In HVAC field, the bin method was developed for energy calculations in heated and cooled buildings by dividing the outdoor air temperature into a series of bins [ASHARE 1981, Hanby 1995, Akbari and Konopacki 2005]. In this study, "bin" concept is borrowed for practical applications.

An enthalpy bin method is presented to evaluate the energy performance of alternative fresh air control strategies for practical applications by dividing the outdoor air enthalpy into a series of enthalpy bins as Equation (10.1). In each enthalpy bin, the fan electricity consumption, cooling energy consumption and total electricity consumption are accumulated respectively as Equation (10.2). These accumulated energy consumptions are plotted in charts or list in tables against enthalpy bins respectively. The charts and tables can lead to explicit comparison of energy

performance of alternative fresh air control strategies which may result in the best fresh air control strategy in a specific enthalpy bin. It is worth to note that enthalpy is used for bin division because enthalpy based economizer control performs better than temperature based economizer control (validated in *Section 10.6*).

$$En_i - \frac{1}{2}\Delta < En_j \leq En_i + \frac{1}{2}\Delta \tag{10.1}$$

$$E(bin(En_i)) = \sum_{j=1}^{n} E(En_j) \tag{10.2}$$

Where, *En* is enthalpy, En_i is the center of i-*th* enthalpy bin, Δ is the width of enthalpy bin. *E(En_j)* is the energy consumption against enthalpy En_j. *E(bin(En_i))* is accumulated energy consumption at the enthalpy bin *bin(En_i)*. The energy consumption can be cooling energy consumption, electricity consumption etc.

The whole year energy consumption *E* can be expressed as follows.

$$E = \sum_{i=1}^{m} E(bin(En_i)) \tag{10.3}$$

The width or interval of enthalpy bin can be determined as needed. The bins should cover the every hour enthalpy all the year of concern. In this study, the width of enthalpy bin is chosen as *5kJ/kg*.

10.4 Alternative Control strategies

In this section, various basic controls strategies about fresh air controls (i.e., conventional constant fresh flow rate control, temperature based economizer control, enthalpy based economizer control and DVC control) and adaptive comfort

temperature control (ACT) as well as their combinations are described in brief as follows.

10.4.1 Conventional fresh air control

In most air handling system, constant fresh air flow rate is introduced to dilute and exhaust odors and sensory irritant contaminants from occupants of space and their activities as well as from building system including furniture and furnishings etc. The introduced fresh air should achieve acceptable perceived indoor air quality. In this control mode, the fresh air flow rate or the fresh air damper position keeps unchanged regardless of the changed density of occupancy and weather condition.

10.4.2 Temperature based economizer control
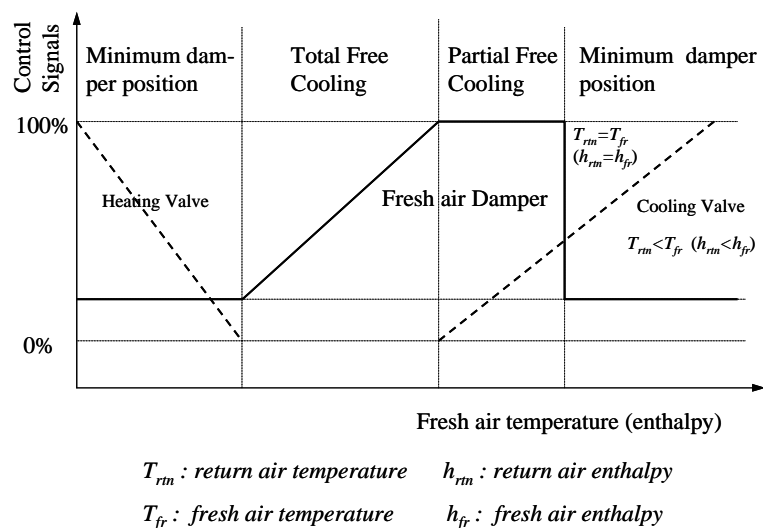
Figure 10.2 Temperature or enthalpy based economizer control

To save mechanical cooling energy, temperature based economizer control can be used to introduce more fresh air flow rate when the temperature is lower than return

air temperature. Figure 10.2 presents the relationship of fresh air control and fresh air temperature which is described and analyzed as follows.

In summer season or hot and humid weather condition, minimum fresh air is taken or the fresh air damper keeps at fixed position. When the outdoor air temperature decreases to be less than return air temperature, partial free cooling mode can be exploited to introduce maximum fresh air flow rate to relieve the sensible cooling energy consumption. At this moment, mechanical cooling is still in need.

When the outdoor air temperature decreases further and the sensible heat through building envelopes is also decreased consequently, fresh air can afford to all the sensible cooling energy consumption of the building system. This is the total free cooling process where the fresh air flow rate is between the maximum and minimum values. When heating is needed, the fresh air flow rate keeps at minimum to save heating energy consumption.

Although free cooling can reduce or even eliminate mechanical cooling energy consumption and improve indoor air quality, more fan electricity consumption is needed to deliver fresh air and exhaust air. It's noted that more mechanical cooling energy is consumed when latent heat of outdoor air is larger than that of return air even if the outdoor air dry-bulb temperature is less than return air dry-bulb temperature.

10.4.3 Enthalpy based economizer control

Enthalpy based economizer control is similar to temperature based economizer control, also shown in Figure 10.2. The main difference between both controls is that temperature or enthalpy is used to determine whether economizer control is adopted.

The same dilemma is faced by enthalpy based economizer control that it can save mechanical cooling energy consumption while consuming more fan electricity to deliver more fresh air and exhaust air.

10.4.4 DCV control

In conventional control mode, minimum fresh air is always taken. In economizer control, the minimum fresh air is introduced or the fresh air damper keeps at its minimum position when the system is in heating mode or hot and humid weather condition. In fact, in the aforementioned states, these control strategies result in over-ventilation providing the constant or design ventilation flow rate when the occupancy ratio is low and insufficient ventilation when the occupancy ratio is higher than the design or expected maximum occupancy. Certainly, these controls lead to energy waste or unsatisfied indoor air quality.

Demand controlled ventilation (DCV) control is a preferable method to achieve acceptable indoor air quality with minimum energy consumption in the aforesaid conditions. This control strategy determines the fresh air flow rate according to the actual occupancy load [ASHRAE 1999]. For office building, the ventilation rate of

fresh air shall be determined as Equation (4).

$$DVR = R_p P \tag{10.4}$$

Where R_p is the fresh air requirement per person, P is the actual number of occupants, DVR is the minimum fresh air flow rate demanded.

The number of occupants can be determined with the occupancy profiles, or determined with steady-state detection (suggested by 62-1989R [ASHRAE 1996]), or dynamic detection suggested by Wang and Jin [1998] which considers both the CO2 concentration and its change rate in real time control process. It can also be measured with occupancy sensors which are used widely in the control of lighting systems. For energy performance evaluation of system retrofittings etc., the number of occupants can be estimated based on site survey by representing as peak occupants and occupant profiles.
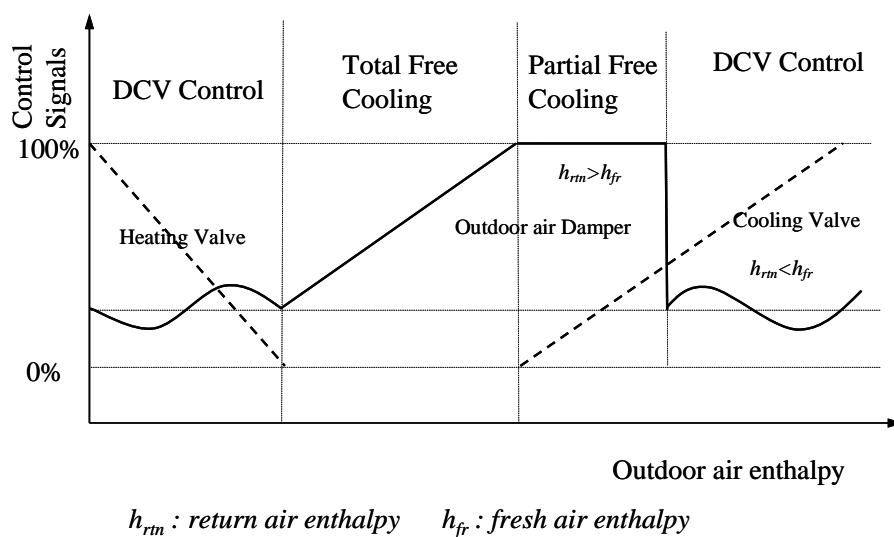
Figure 10.3 DCV+enthalpy based economizer control

DCV control is often combined with enthalpy based economizer control for practical application, as show in Figure 10.3. When the outdoor enthalpy is high or very low, fresh air is controlled at its minimum level acceptable for maintaining adequate indoor air quality using DCV control. Between these two extreme outdoor conditions, the fresh air is controlled at maximum flow rate (partial free cooling) or at proper level to cool the building using outdoor air only (total free cooling). As the outdoor air enthalpy in Hong Kong is high during large part of a year, DCV control in hot and humid weather condition is a typical fresh air flow rate control for the Hong Kong climate.

10.4.5 Adaptive comfort temperature control

Thermal comfort is a common sensation. It is defined in terms of the perception of satisfaction when a subject experiences in a given thermal environment [ASHRAE 1992]. Thermal comfort temperature (Neutral temperature) can be used as an indicator for thermal comfort [Brager and Dear 1998]. For the thermal comfort control in office buildings in Hong Kong, Mui [2002] established an adaptive comfort temperature model based on the results from site surveys. The adaptive comfort temperature (ACT) model relates indoor air temperature, at which a target percentage of satisfaction (80%) with thermal comfort is attained, with outdoor air temperature. The model is described as Equation (10.5).

$$\begin{cases} T_n = 19.1 & T_{out} < 5 \\ T_n = 18.303 + 0.158 T_o & 5 \le T_{out} < 41 \\ T_n = 24.8 & T_{out} \ge 41 \end{cases} \tag{10.5}$$

Where, T_n is thermal comfort temperature (indoor air temperature), T_{out} is outdoor air temperature.

It's obvious that the cooling energy consumption using ACT control is different from that using constant indoor air temperature control. The energy performance is also evaluated.

10.5 Description of building system and consolidation AHU

To demonstrate the performance evaluation approach of alternative control strategies for energy performance evaluation of alternative fresh air control strategies under different weather conditions, the tower office building of Chinese Resources Building described in *Chapter 7* is taken as the building prototype. The consolidation AHU model for the tower building described in *Chapter 8* is taken as the prototype of the air handling systems. Economizer control cannot be used in the original tower building to reduce energy consumption because of the shafts in the core only allowing for minimum fresh air intake and minimum exhaust air discharge. For the energy performance evaluation of economizer controls, the air handling systems are assumed to take fresh air locally and discharge exhaust air locally by the VAV and CAV system, which is also common in office buildings. Therefore, the modified consolidation AHU system as shown in Figure 10.4 is used to demonstrate the performance evaluation approach for energy performance evaluation of alternative control strategies. It is note that the energy performance is of concern while the control process is not addressed.
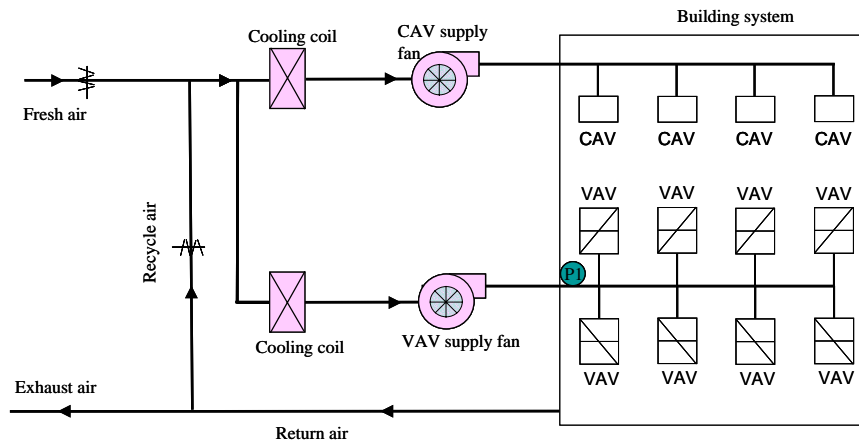
Figure 10.4 Schematics of the consolidation AHU model

10.6 Test results and performance evaluation

The performance evaluation approach of alternative control strategy was used to evaluate the energy performance of alternative fresh air control strategies in this section. The energy performance of alternative fresh air control strategies were conducted using constant indoor air temperature control and ACT control respectively. The constant indoor temperature was 24 ℃. Indoor air relative humidity was set at 55% for both temperature controls. Typical Meteorological Year type data sets used for these tests were the weather data for Hong Kong in 1989 for the whole year performance prediction. The fresh air control strategies are conventional control, temperature based economizer control, enthalpy based economizer control, DCV control, and DCV+enthalpy based economizer control. The energy performances of fresh air controls using constant indoor temperature control are presented and analyzed in detail using the performance evaluation approach in *Section 10.6.1*. The

energy performances of fresh air control strategies using ACT control are briefed and analyzed in *Section 10.6.2*.

10.6.1 Energy performance with constant indoor air temperature

The whole year outdoor air enthalpy is divided into 15 bins with the internal *5kJ/kg*. Figure 10.5 presents the mechanical cooling energy consumptions of alternative fresh air control strategies against outdoor air enthalpy bins. It shows that temperature based economizer control shared the same mechanical cooling energy consumption as conventional fresh air control when the bins were equal to and larger than 75 because constant fresh air was taken in. When the bins at 55, 60, 65, the mechanical cooling energy consumption of temperature based economizer control was much more than that of conventional fresh air control. In these three bins, plenty of fresh air with high humidity was introduced into indoor space leading mechanical cooling energy increase although the outdoor dry bulb temperature was lower than return air temperature. When the bins were lower than 50, temperature based economizer control introduced more fresh air to alleviate or eliminate mechanical cooling energy consumption.

Figure 10.6 presents fan electricity consumption of AHU systems using alternative fresh air control strategies against outdoor air enthalpy bins. The fan electricity consumption using temperature based economizer control was much more than that using conventional fresh air control when the outdoor air enthalpy bins were lower than 70 because plenty of fresh air was delivered into indoor space. The total electricity consumption including chiller system and air system is given in Figure 10.7.

Electricity consumption of chiller system was calculated by the product of mechanical cooling load and an overall COP of chilling system assuming 2.5 as constant. It shows that the total electricity consumption using temperature based economizer control was much higher than that using conventional fresh air control when in free cooling model. Table 10.1 shows that temperature based economizer control increased almost 19 % electricity consumption compared to conventional fresh air control. Therefore, temperature based economizer control didn't contribute to total electricity consumption saving in the study.
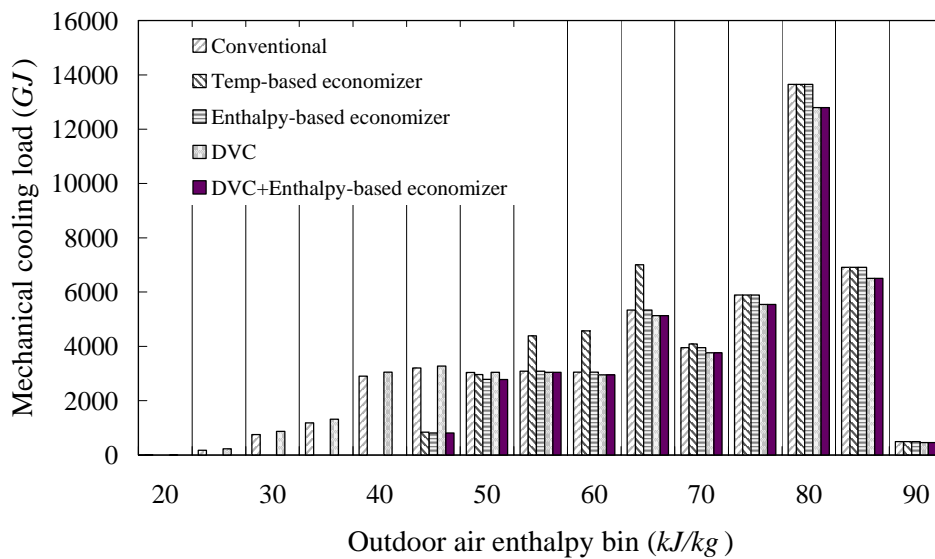
Figure 10.5 Mechanical cooling energy consumption against enthalpy bins
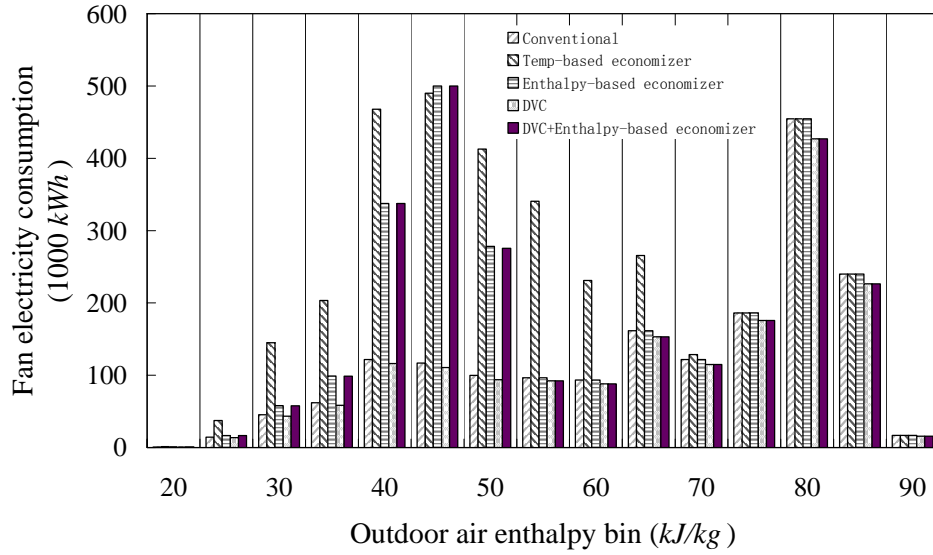
Figure 10.6 Fan electricity consumption against enthalpy bins
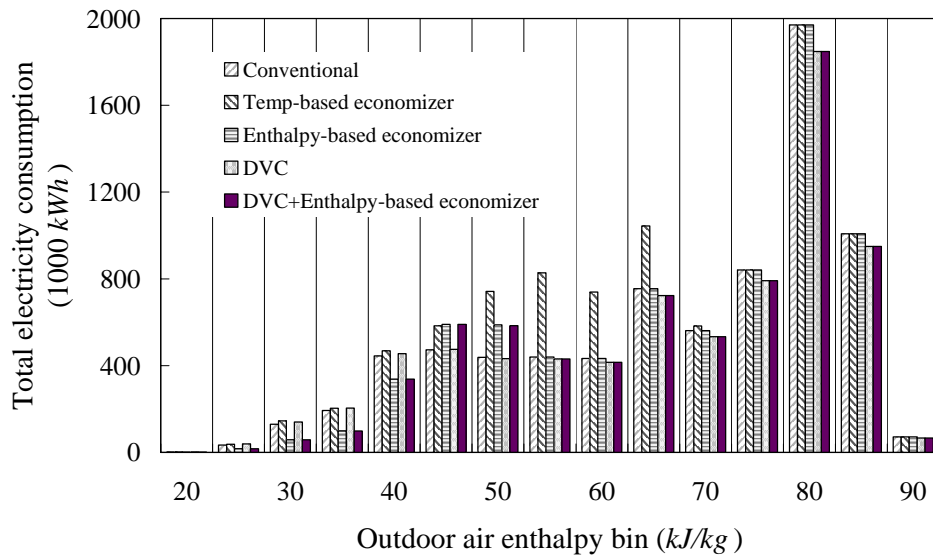
Figure 10.7 Total electricity consumption against enthalpy bins

Table 10.1 Total electricity consumption summary and comparison (constant

indoor temperature control)

Enthalpy bin (*kJ/kg*)	Total electriciry consumption of conventional fresh air control strategy (*kWh*)	Compared to conventional fresh air control strategy (*kWh*)				
		Temperature based economizer	Enthalpy based economizer	DVC	DCV+Enthalpy based economizer	Optimal
20	1180.83	-113.56	347.31	-419.01	380.98	380.98
25	33476.61	-3727.88	16907.26	-5265.83	17037.62	17037.62
30	128953.18	-15880.59	71065.80	-11055.78	71278.19	71278.19
35	193441.22	-9987.66	94758.66	-11224.96	94862.17	94862.17
40	444152.42	-23945.99	106495.71	-10894.55	106495.71	106495.71
45	472908.04	-110477.99	-117317.65	-1992.51	-117317.65	0.00
50	437687.85	-304112.62	-150191.11	5540.42	-146782.36	5540.42
55	439521.56	-388455.00	0.00	9139.26	9139.26	9139.26
60	432765.76	-305913.20	0.00	17185.44	17185.44	17185.44
65	754661.34	-289271.98	0.00	31653.03	31653.03	31653.03
70	560962.88	-21796.76	0.00	28115.65	28115.65	28115.65
75	840531.79	0.00	0.00	48657.37	48657.37	48657.37
80	1970976.67	0.00	0.00	122583.48	122583.48	122583.48
85	1007476.72	0.00	0.00	58068.20	58068.20	58068.20
90	71504.35	0.00	0.00	5270.99	5270.99	5270.99
Total	7790201.20	-1473683.23	22065.98	285361.19	346628.07	616268.51
Saving (%)	-	-18.92	0.28	3.66	4.45	7.91

When enthalpy based economizer control was applied, the mechanical cooling

energy consumption was the same as that using conventional fresh air control when

the bins were equal to and larger than 55 because constant fresh air was taken in, as

shown in Figure 10.5. When the bin is at 50, the mechanical cooling energy

consumption using enthalpy based economizer control was slightly less than that

using conventional fresh air control. The mechanical cooling energy consumption

using enthalpy based economizer control was much less when the bin was at 45.

When the bin was lower than 45, enthalpy based economizer control introduced

enough fresh air to eliminate mechanical cooling energy consumption. However, more

fan electricity was consumed to deliver plenty of fresh air into indoor space, as shown

in Figure 10.6. At the enthalpy bins of 40, 45, 50, multiple fan electricity was

consumed.

The total electricity consumption including chiller system and air system at each enthalpy bin is given in Figure 10.7 and Table 10.1. At the bins of 45 and 50, enthalpy based economizer control consumed more electricity compared to conventional fresh air control. When the bin was lower than 45, enthalpy based economizer control consumed less electricity. Table 10.1 shows that the potential of enthalpy based economizer control was very limited, about 0.28% compared to the total electricity consumption using conventional fresh air control.

When DCV control was applied alone, the mechanical cooling energy consumption was less than that using conventional fresh air control when the bins were larger than 50, as shown in Figure 10.5. It owed to that enough just enough fresh air was taken in preventing over-ventilation when the occupancy ratio is low. However, when the bins were less than 50, the mechanical cooling energy consumption using DCV control was slightly more than that using conventional fresh air control because more cool fresh air was prevented to be introduced. Figure 10.6 shows that fan electricity consumption using DCV control was slightly less than that using conventional fresh air control for the whole year. The total electricity consumption using DCV control alone is given in Figure10.7 and Table 10.1. It shows that DCV control consumed more electricity than conventional fresh air control when the bins were equal to and lower than 45 while DCV control consumed less electricity when the bins were higher than 45. The potential of electricity consumption savings

with DCV control alone was about 3.66% compared to conventional fresh air control.

When DCV control was applied together with enthalpy based economizer control, the potential of electricity saving was improved as shown in Figure 10.7 and Table 10.1. When the enthalpy bins were lower than 45, more fresh air was taken in to eliminate mechanical cooling energy consumption while increasing fan electricity consumption slightly. However, when the enthalpy bins were at 45 and 50, more fresh air was taken in to alleviate mechanical cooling energy consumption while increasing fan electricity consumption greatly. The total electricity consumption with DCV+enthalpy based economizer control was saved up to 4.45% compared to conventional fresh air control.

DCV+enthalpy based economizer control can be enhanced to control fresh air for improving electricity consumption saving. It's denoted as optimal fresh air control, i.e., only enthalpy based economizer control was applied when the bins were lower than 45, constant fresh air control applied when the bin was at 45, only DCV control applied when the bins were higher than 45. The electricity saving using optimal control was improved to about 8% compared to that using conventional fresh air control alone. The saving using optimal control was about 3.5% more than that using DCV+enthalpy based economizer control only.

10.6.2 Energy performance with ACT control

The energy performance of alternative fresh air control strategies using adaptive

comfort temperature (ACT) control was evaluated in this section. The detailed performance comparison and evaluation among various control strategies with ACT control are not presented because they are similar to those with constant indoor temperature control. Only conclusive evaluations are stated.

As shown in Table 10.2, temperature based economizer control increased electricity consumption about 15% compared to conventional fresh air control. Enthalpy based economizer control consumed more electricity energy compared to conventional fresh air control. DCV control reduced electricity about 4.86% compared to conventional fresh air control. However, DCV+enthalpy based economizer control only reduced electricity 3.00% because free cooling at bins 40 and 45 greatly increased fan electricity consumption.

Table 10.2 Total electricity consumption summary and comparison (ACT control)

Enthalpy bin (*kJ/kg*)	Total electriciry consumption of conventional fresh air control strategy (*kWh*)	Compared to conventional fresh air control strategy (*kWh*)				
		Temperature based economizer	Enthalpy based economizer	DVC	DCV+Enthalpy based economizer	Optimal
20	2567.80	3121.62	1318.98	-265.82	1318.98	1318.98
25	61030.17	55737.29	32888.48	-3438.02	32888.48	32888.48
30	201834.06	107103.15	93731.69	-7500.70	93731.69	93731.69
35	288770.86	3304.68	4973.89	-4982.42	4973.89	4973.89
40	616668.79	-195920.64	-205925.40	-546.71	-205925.40	0.00
45	626276.40	-360929.20	-87440.23	6680.92	-81979.22	6680.92
50	565537.93	-395131.72	0.00	14042.20	14042.20	14042.20
55	545790.47	-302809.05	0.00	16142.20	16142.20	16142.20
60	529178.45	-68589.44	0.00	24491.37	24491.37	24491.37
65	898951.29	0.00	0.00	41759.43	41759.43	41759.43
70	643146.50	0.00	0.00	34132.99	34132.99	34132.99
75	947426.58	0.00	0.00	56712.51	56712.51	56712.51
80	2125980.20	0.00	0.00	134965.60	134965.60	134965.60
85	1058085.03	0.00	0.00	60887.91	60887.91	60887.91
90	74966.72	0.00	0.00	5554.92	5554.92	5554.92
Total	9186211.25	-1154113.31	-160452.59	378636.41	233697.57	528283.11
Saving (%)	-	-14.81	-2.06	4.86	3.00	6.78

The electricity consumption was saved more by improving DCV+enthalpy based economizer control. It's also denoted as optimal fresh air control. The optimal fresh air control with ACT control is briefly described as follows. Only enthalpy based economizer control was applied when the bins were lower than 40. Constant fresh air control was applied when the bin was at 40 while DCV control applied when the bins were higher than 40. With the optimal fresh air control, the electricity saving was improved to 6.78%, as shown in Table 10.2, compared to that when conventional fresh air control was exploited alone. The saving was 3.78% more than that using DCV+enthalpy based economizer control only.

By comparing Table 10.1 with Table 10.2, it is shown that any control strategy with ACT control consumed more electricity energy than that with constant indoor air temperature control. It is because adaptive comfort temperature in Hong Kong is lower than constant indoor temperature set point (24℃). The lower indoor temperature not only increases mechanical cooling energy consumption as well as more fan electricity consumption, but also narrows the free cooling region to use free cooling sources.

10.7 Summary

A performance evaluation approach of alternative control strategies based on the building global performance evaluation tool is presented to evaluate the energy performance of alternative fresh air control under different weather conditions by dividing performance prediction into a series of enthalpy bins. The tests in a high

rising commercial office building in Hong Kong show that the approach can effectively evaluate the energy performance of alternative fresh air control strategies at different enthalpy bins. The tests also show that the optimal combinations of the basic alternative strategies can be easily achieved using the approach. For the studied building in Hong Kong, DCV control benefited total electricity consumption saving best for the enthalpy bins larger than 50*kJ/kg*. The conventional fresh air control benefited best for the enthalpy bin equal to 50*kJ/kg*. The enthalpy based economizer control benefited best for the enthalpy bins less than 50*kJ/kg*. The maximum potential using fresh air for total electricity consumption saving was about 8%.

CHAPTER 11 SUMMARY AND FURTHER WORK

Performance evaluation and faults detection and diagnosis are highly of value for building normal operation. Although various sophisticate fault detection and diagnosis method as well as intelligent optimal control have been developed for individual equipments or components, they can not be easily used in current building and HVAC systems because plenty of sensors are needed to be installed costly and it is also complicate to use those sophisticate methods and in real buildings. Usually, Kilowatt meter is needed for electricity consumption of the whole building or some part of a building, and cooling/heating energy consumption can often be measured at the central plant. Therefore, it is significant to develop cost effective methodology and technology to identify system fault and inefficiency at the building level with the easily available measurement. The methodology and technology are also highly valuable for performance evaluation with alternative control strategies to enhance building energy performance or environment performance.

Conclusions on Main Contributions

i. The achievements and original work's values of the PhD research are that a systematic methodology is presented for building performance evaluation and diagnosis viewing the building as a whole. The methodology involves the development of the building global performance evaluation tool for performance prediction of buildings and the developments of specific strategy and approach

for performance evaluation and diagnosis based on the tool performance prediction.

ii. The building global performance evaluation tool includes a simplified building energy model to estimate thermal energy consumption and a consolidation AHU model to estimate the air side performance of air terminals. GA estimators are developed for the parameter optimization of simplified building energy model. The electricity consumption of consolidation AHU VAV system is simplified to calculate the effective mechanical output power consumption. The robustness of the two models for performance prediction was validated in a real building in Hong Kong.

iii. Practical applications are the ultimate aims of the developed evaluation tool. A performance signature-based diagnosis strategy is developed for building performance evaluation and diagnosis based on "measurement" of the real building and prediction using the building global performance evaluation tool. The validation shows the diagnosis strategy can qualitatively and quantitatively diagnose the causes resulting in the "measured" cooling energy consumption deviating from the baseline.

iv. A performance evaluation approach of alternative control strategies is developed for building energy performance evaluation of alternative control strategies by dividing the outdoor enthalpy into a series of enthalpy bins based on performance prediction using the developed evaluation tool. The validation in a real building shows the optimal fresh air control strategy determined using this

approach can save electricity consumption significantly. The performance evaluation approach of alternative control strategies can provide decision making consultation of air handling system retrofitting of buildings.

Simplified Building Energy Model

The simplified building energy model is constructed as a hybrid building energy model, which is the compounding of simplified models of building envelopes and internal mass. The opaque building envelope is simplified as a simplified 3R2C model. The optimal nodal placement of 3R2C model is determined with a GA estimator which can make the frequency response characteristics of the simplified model match the theoretical frequency response characteristics as close as possible. This simplified model of building envelope was proved to perform better than the same order models with other configurations.

The internal mass is assumed the physical meanings of a 2R2C model because it is impossible to describe the physical characteristics of internal mass piece by piece. The simplified model of internal mass (2R2C) is partially data-driven. The parameters of this model are identified with the measured cooling energy consumption together the developed 3R2C models of building envelopes based on a GA estimator. The simplified building model consists of simplified models of building envelopes and internal mass was validated in different weather conditions. It was proved that the simplified building energy model can robustly predict thermal energy performance because it not only describes the thermal behaviors of building system but also

explains the building system physically.

Consolidation AHU Model

To simplify the modeling process and make model calibration much easier using the available measurements more efficient, a consolidation AHU model is presented to represent all the real AHU systems in a building to accomplish the basic functions of providing appropriate supply air temperature and flow rate to meet human thermal sensation requirement. A method is developed to predict the electricity consumption using the effective mechanical output power consumption of the consolidation AHU VAV system.

The efficiency of the consolidation AHU VAV system was identified with the monitoring electricity consumption and the model predicted effective mechanical output power consumption in a real building. The validation of the consolidation AHU model demonstrates that the consolidation AHU model can predict the electricity consumption of all the AHU VAV systems with acceptable accuracy. Consolidation AHU model can be used in design process to estimate the air side electricity consumption of all the AHU systems for budget. It is also can be used practically to estimate the energy consumption of the whole all-air systems for performance evaluation as well as for cost saving estimation in retrofitting process.

Building Performance Evaluation and Diagnosis

A performance signature-based diagnosis strategy based on the building global

performance evaluation tool is developed for performance diagnosis of cooling/heating energy consumption because the main causes resulting in performance deviation have distinguishing effects on cooling/heating energy consumption. Performance signatures of cooling energy consumption are a graphical representation of the difference between measured value and simulation value against outdoor air dry-bulb temperature. An existing office building was used to demonstrate the validity of the performance signature-based diagnosis strategy for cooling energy consumption performance diagnosis. The simplified building energy model, the core of the building global performance evaluation tool, is used as reference model for the building performance prediction. The diagnosis results of the "measured" cooling energy consumption show that the performance signature based diagnosis strategy can not only qualitatively detect the causes resulting in performance deviation of cooling/heating energy consumption, but also can quantitatively and efficiently identified the causes resulting in cooling/heating energy consumption deviation. These diagnosed causes are beneficial for further investigations of building system.

Building Performance Evaluation with Alternative Control Strategies

To evaluate the energy performance of alternative control strategies for practical applications such as retrofitting or upgrading, a performance evaluation approach of alternative control strategies based on the building global performance evaluation tool is presented. The approach employs the evaluation tool, i.e., the simplified building energy model and the consolidation AHU model, to reliably and dynamically predict

the building energy performance with alternative control strategies. Based on the predicted energy performance, the evaluation approach employs an enthalpy bin method to evaluate the energy performance of alternative fresh air control strategies by dividing outdoor enthalpy into a series of enthalpy bins where the estimated energy consumptions are accumulated. These accumulated energy consumptions are plotted in charts or list in tables against enthalpy bins respectively. The charts and tables can lead to explicit comparison of energy performance of alternative fresh air control strategies. They can also lead to the best fresh air control strategy in different enthalpy bins to exert the maximum potential of using fresh air efficiently.

The tests in an office high rising building in Hong Kong show that the performance evaluation approach can be used for optimal fresh air control decision. The optimal fresh air control strategy determined using the evaluation approach could save electricity consumption significantly rather than separate economizer control strategy and DCV control strategy. For the studied building in Hong Kong, DCV control benefited total electricity consumption saving best for the enthalpy bins larger than 50*kJ/kg*. The conventional fresh air control benefited best for the enthalpy bin equal to 50*kJ/kg*. The enthalpy based economizer control benefited best for the enthalpy bins less than 50*kJ/kg*. The maximum potential using fresh air for total electricity consumption saving was about 8*%*.

Further Work

As the supplement of the systematic methodology for building performance

evaluation and diagnosis, a consolidation chiller model is highly of value to be developed to simplify chiller system for performance prediction. The consolidation chiller model, which is similar to the consolidation AHU model, can represent all the equipments served for chiller system such as chillers, chilled water pumps, condensing water pumps and cooling towers, etc., according the system configuration. Such model can simplify modeling greatly and make calibration more easily with monitoring data.

More field case studies would be beneficial to increase the confidence of the systematic methodology for building performance evaluation and diagnosis. The methodology is highly of value to be used for building and system retrofitting evaluation for decision making. The methodology is also highly of value to be developed as application program which can be integrated with IBmanager (Intelligent Building manager) to provide remote service as active service provider (ASP) through internet. Field case studies will be carried out for decision making of alternative building retrofitting measures using the propose methodology.

REFERENCES

Akbari H and Eto J et al. (1993). Integrated Estimation of Commercial Sector End-Use Load Shapes and Energy Use Intensities in the PG&E Service Area. Final Report submitted to the California Energy Commission. LBNL Report No. 34263.

Akbari H and Konopacki S. (2005). Calculating energy-saving potentials of heat-island reduction strategies. Energy Policy, Vol.33(6), pp:721-756

Amin MG and Zhang Y. (2000). Direction finding based on spatial time-frequency distribution matrices. Digital Signal Processing, Vol.10(4), pp:325-339.

Anstett M and Kreider J (1993). Application of neural networking model to predict energy use. ASHRAE transactions, Vol.99(1) pp:505-517.

ASHRAE. (1981). Handbook of Fundamentals, 28.7-28.15. American Society of Heating, Refrigerating and Air-Conditioning Engineers, Atlanta, USA.

ASHRAE. (1992). ANSI/ASHRAE 55-1992, Thermal environmental conditions for human occupancy. Atlanta.

ASHRAE. (1993). Handbook of Fundamentals, American Society of Heating, Refrigerating and Air-Conditioning Engineers, Atlanta, USA.

ASHRAE. (1995). Building Operating Dynamic and Strategies. In 1995 ASHRAE Handbook-HVAC Applications, pp. 38.1. Atlanta: ASHRAE.

ASHRAE. (1995). ANSI/ASHRAE 55a-1992, Addendum to thermal environmental conditions for human occupancy. Atlanta.

ASHRAE Standard 62-1989R. Ventilation for acceptable indoor air quality (Public review draft). Atlanta: ASHRAE; 1996.

ASHRAE. (1997). Handbook of Fundamentals, American Society of Heating, Refrigerating and Air-Conditioning Engineers, Atlanta, USA.

ASHRAE. (1999). ASHRAE Standard 62-1999. Ventilation for acceptable indoor quality, Atlanta, 1999.

ASHRAE. (2001). Handbook of Fundamentals, American Society of Heating, Refrigerating and Air-Conditioning Engineers, Atlanta, USA.

Bahai H. and Esat I. (1994). A hybrid model for analysis of complex stress distribution in threaded connectors. Computers & Structures, Vol.52(1), pp:79-93.

Bliss R. (1961). Atmospheric radiation near the surface of the ground: A summary for engineers. Solar Energy, Vol.5(3), pp:103-120.

Bourdouxhe J, Grodent M and Lebrun J. (1999). HVAC 1 Toolkit – A toolkit for primary HVAC system energy calculation. ASHRAE. (CD-ROM Software)

Brager G and Dear R. (1998). Thermal adaptation in the built environment: a literature review. Energy and Buildings, Vol.27(1), pp:83-96.

Brandemunehl M, Gabel S and Andresen. (1993). HVAC 2 toolkit: Algorithm and subroutines for secondary HVAC system energy calculations. Altanta: American Society of Heating, Refrigerating and Air-conditioning Engineers, Inc.

Braun J and Montgomery K. et al. (2001). Evaluating the performance of building thermal mass control strategies. HVAC&R Research, Vol.7(4), pp:403-428.

Braun J and Chaturvedi N. (2002). An inverse gray-box model for transient building load prediction. HVAC&R Research, Vol.8(1), pp:73-99.

Building Systems Laboratory. (1999). BLAST 3.0 Users Manual. Department of Mechanical and Industrial Engineering, Building Systems Laboratory, University of Illinois, Urbana-Champaign, IL.

Butler P. and Letherman K.M. (1980). A criterion for the accuracy of modeling of transient heat conduction in plane slabs. Building and Environment, Vol.15, pp.143-149.

Carroll DL. (2001) FORTRAN Genetic algorithm (GA) driver. Version 1.7a. http://cuaerospace.com/carroll/ga.html, http://cuaerospace.com/carroll/gatips.html

Chen C.T. (1994). System and signal analysis, second edition. Saunder College Publishing, USA. pp.532.

Chen YM and Chen ZK. (2000). A neural-network-based experimental technique for determining z-transfer function coefficients of a building envelope. Building and Environment, Vol.35, pp:181-189.

Chen YM and Wang SW. (2001). Frequency-domain regression method for estimating CTF models of building multilayer constructions. Applied Mathematical Modelling, Vol.25(7), pp.579-592.

Chiles D and Sowell E. (1984). A count-intuitive effect of mass on zone cooling load response. ASHRAE Transactions, Vol.91(2A), pp:201-208.

Choi JM, Kim YC and Chung JT. (2004). An empirical correlation and rating charts for the performance of adiabatic capillary tubes with alternative refrigerants. Applied Thermal Engineering, Vol.24(1), pp:29-41.

Clark DR. (1985). HVACSIM+ buiding systems and equipment simulation program: Reference manual. NBSIR 84-2996, US, Department of Commerce, Washington DC.

Claridge D, Haberl J, and Sparks R et al. (1992). Monitored commercial building energy data: Reporting the results. Ashrae Transactions 98(1), pp:636-652.

Claridge D, Liu M and Haberl J. (1996). Can you achieve 150% of predicted retrofit savings? Is it time for recommissioning? Proceedings of 1996 ACEEE Summer Study on Energy Efficiency in Buildings, pp. 4.59-4.67, August 1996.

Claridge D, Liu M and Turner W. (1999). Whole Building Diagnostics. http://poet.lbl.gov/diagworkshop/proceedings

Claridge D, Culp C and Liu M et al. (2000). Campus-wide continuous commissioning

of university buildings. Proceedings of ACEEE Summer Study on Energy Efficiency in Buildings, pp. 3.101-3.112, Pacific Grove, CA, August 20-25, 2000.

Crawley and Drury B. (2000). EnergyPlus: energy simulation program. ASHRAE Journal, Vol. 42(4):49-56.

Davis L. (1991) Handbook of genetic algorithms. New York: Van Nostrand Reinhold.

Davies MG. (1997). Wall transient heat flow using time-domain analysis. Building and Environment, Vol.32(5), pp.427-46.

Davies M.G. (2003). A rationale for nodal placement for heat flow calculations in walls. Building and Environment, Vol.38:247-260.

Dear R, Schiller B and Cooper D. (1998). Developing an Adaptive Model of Thermal Comfort and Preference. ASHRAE Transactions 1998; SF-98-7-3, 4106, RP-884.

Deb K. (1996) Genetic algorithms for function optimisation. In Ferrera, F. and Verdegay, J.L.,editors. Genetic algorithms and soft computing. Heidelberg: Physica-Verlag, 3–29.

Deng SM and Burnett J. (1997). Performance monitoring and measurement for central air conditioning chiller plants in buildings in Hong Kong. HKIE Transactions, Vol.4(1), pp:7-12.

Deng S, Liu M and Turner W et al. (1998). Reducing pump power consumption by (1000 kW) 40% through improved pump management in a central plant. Proceedings of The Eleventh Symposium on Improving Building Systems in Hot and Humid Climates, pp. 403-409, June 1-2, 1998, Fort Worth. 33rd Intersociety Engineering Conference on Energy Conversion, August 2-6, 1998, Colorado Springs, CO.

Dhar A, Reddy T. and Claridge D. (1998). Modeling hourly energy use in commercial buildings with Fourier series functional forms. Journal of solar energy engineering, Vol.120, pp:217-223.

Dhar A, Reddy T. and Claridge D. (1999). A fourier series model to predict hourly heating and cooling energy use in commercial buildings with outdoor temperature as the only weather variable. Journal of solar energy engineering, Vol.121, pp:47-53.

DOE. 1980. DOE-2, Reference manual, part 1, Version 2.1. Lawrence Berkeley National Laboratory. Berkeley, Califonia.

Ed Kidd et al. (2001). DOE-2 Program Documentation, Energy Science & Technology Software Center, Oak Ridge, http://gundog.lbl.gov/dirsoft/d2getdoc.html

EIA. Energy Information Administration. (1995). U.S. Department of Energy. Commercial Buildings Energy Consumption and Expenditures 1992, Commercial Buildings Energy Consumption Survey.

Energy Information Administration. (1991). Energy Facts 1991, DOE/EIA-0469(91), Washington, DC.

Energy Systems Laboratory, University of Nebraska and Energy Systems Laboratory, Texas A&M University. (2002). Potential of On-line Simulation for Fault Detection and Diagnosis in Large Commercial Buildings with Built-up HVAC Systems. http://buildings.lbl.gov/hpcbs/Element_5/02_E5_P2_3_1.html

Energy User News. (1995). Vol. 20, Number 4, April. The Chilton Co., Radnor PA.

Englander SL and Norford LK. (1992). Saving fan energy in VAV systems-Part 1: analysis of a variable-speed-drive retrofit. ASHRAE Transactions, Vol.98(1), pp:3-17.

European standard. (1995). Thermal performance of buildings-internal temperatures without mechanical cooling-general criteria and calculation procedure. (Draft) ISO/DIS 13791, p.47.

Falconer D and Sowell E et al. (1993). Electronic tables for ASHRAE Load Calculation Manual. ASHRAE Transactions, Vol.99(1), pp:193-200.

Fels M. (1986). Measuring energy savings: The scorekeeping approach. Energy and Building, Vol.(9). (Total Volume 1:180)

Fels M. and Goldberg M. (1986). Refraction of PRISM results in components of saved energy. Energy and Building, Vol.(9):169-180.

Ferrano F and Wong K (1990). Prediction of thermal storage loads using a neural network. ASHRAE transactions, Vol.96(2) pp:723-726.

Finlayson E and Arasteh. (1993). Window 4.0: Documentation of calculation procedures. LBL-33943/UC-350. Lawrence Berkeley Laboratory, Energy & Environment Division, Berkeley, CA

García-Sanz M. (1997). A reduced model of central heating systems as a realistic scenario for analyzing control strategies. Applied Mathematical Modelling, Vol.21(9), pp.535-545.

Giebler T, Liu M and Claridge D. (1998). Evaluation of energy conversion measures by model simulation. The eleventh symposium on improving building systems in hot and humid climates proceedings, June 1-2, Fort Worth, Texes.

Goldberg D. (1989). Genetic algorithms in search, optimisation, and machine learning. New York: Addison-Wesley.

Gordon J and Ng K. (1994). Thermodynamic modeling of reciprocating chillers. Journal of applied physics. Vol.75, pp:2769-2774.

Gordon J, Ng K and Chua H. (1995). Centrifugal chillers: thermodynamic modeling and a diagnostic case study. International journal of refrigeration. Vol.18(4), pp:253-257.

Hanby V. (1995). Error estimation in bin method energy calculations. Applied Energy, Vol.52(1), pp:35-45.

Handy VI and Dil AJ. (1996). Error prediction in Markov models of building/HVAC systems. Applied Mathematical Modelling, Vol.20(8), pp.608-613.

Harris S and McQuiston F. (1988). A study to categorize walls and roofs on the basis of thermal response. ASHRAE Transactions, Vol.94(2), pp:688-715.

Haves P. (1999). Overview of diagnostic methods. http://poet.lbl.gov/diagworkshop/proceedings

HK-BEAM Society. (2003). An environmental assessment for new building developments, HK-BEAM Version 2003. HK-BEAM Society, Kowloon, Hong Kong.

Holland J. (1975). Adaptation in natural and artificial systems. University of Michigan Press, Ann Arbor, MI.

Holland J. (1992). Adaptation in natural and artificial systems. Cambridge, MA: MIT Press.

House J and Kelly G. (NIST). (1999). An overview of building diagnostic. http://poet.lbl.gov/diag-workshop/proceedings

House J and Smith T. (1991). Optimal control of a thermal system. ASHRAE Transactions, Vol.97(2), pp:991-1001.

IEA Annex 25. (1996). Building Optimization and Fault Diagnosis Source Book. Eds. J. Hyvärinen and S. Kärki, Technical Research Centre of Finland.

Kalogirou S, Neocleous C and Schizas C. (1997). Heating load estimation using artificial neural networks. In: Proc. CLIMA 2000 Conf., Brussels (Belgium).

Katipamula S. (1996). Great energy predictor shootout II: modeling energy use in large commercial buildings. ASHRAE Transactions 102:397-404.

Katipamula S and Claridge D. (1993). Use of simplified system models to measure retrofit energy savings. Journal of solar energy engineering, Vol.115, pp:57-68.

Kelin SA et al. (1990). TRNSYS – A Transient Simulation Program, User Manual Version 13.1. Madison: Engineering Experimentation Station, University of Wisconsin.

Kawashima M, Dorgan C and Michell J. (1995). Hourly thermal load prediction for the next 24 hours by ARIMA, EWMA, LR and an artificial neural network, ASHRAE transactions, Vol.101(1):186-200.

Kimura and Stephenson. (1968). Theoretical study of cooling loads caused by lights. ASHRAE Transactions, Vol.74(2), pp:189-197.

Kimbara A, Kurosu S and Endo R et al. (1995). On-line prediction for load profile of an air conditioning system. ASHRAE Transactions, Vol.101(2), pp:198-207.

Kissock JK. (1993). A methodology to measure retrofit energy saving in commercial buildings. PhD Thesis, Texas A&M University.

Kreider J and Wang X. (1991). Artificial neural network demonstration for automated generation of energy use predictors for commercial buildings. ASHRAE Transactions, Vol.97(1) pp:775-779.

Kusuda T. (1969). Thermal response factors for multilayer structures of various heat conduction system. ASHRAE Transactions, Vol. 75(1), pp.246-271.

Kusuda T. (1999). Early history and future prospects of buildings system simulation. Proceedings of Building Simulation '99, vol. I, Kyoto, Japan, Sep. 1999.

Lam C. and Hui C. (1995). Outdoor Design Conditions for HVAC System Design and Energy Estimation for Buildings in Hong Kong. Energy and Buildings, Vol.22, pp:25-43.

Lam J and Li H. (1996). Correlation between global solar radiation and its direct and diffuse components. Building and Environment, Vol.31(6), pp:527-535.

Lawrence Berkeley Laboratory. (1982). DOE-2 Engineering Manual Version 2.1C. Berkeley, CA, Lawrence Berkeley Laboratory.

Lebrun J. and Jokela M., et al. (1999). Annex 30: Bringing Simulation to Application – Final Report. International Energy Agency, University of Liege, Belgium, April 1999.

Lee W, House J and Kyong N. (2004). Subsystem level fault diagnosis of a building's air-handling unit using general regression neural networks. Applied Energy, Vol.77(2), pp:153-170.

Lee W, Park C and Kelly G. (1996). Fault detection in an air handling unit using residual and recursive parameter identification methods. ASHRAE Technical Data Bulletin, Vol.12(2).

Li HCH, Weis M, and Herszberg I et al. (2004). Damage detection in a fiber reinforced composite beam using random decrement signatures. Composite Structures, Vol.66, pp:159-167.

Liao Z. and Dexter AL. (2003). An inferential control scheme for optimizing the operation of boilers in multi-zone heating systems. Building services engineering research and technology, Vol.24(4), pp:245-256.

Liao Z. and Dexter AL. (2004). A simplified physical model for estimating the average air temperature in multi-zone heating systems. Building and environment, Vol.39, pp:1013-1022.

Liu M, Athar A and Claridge D et al. (1994). Reducing building energy costs using optimized operation strategies for constant volume air handling systems. Proceedings of the Ninth Symposium on Improving Building Systems in Hot and Humid Climates, Arlington, Texas, May 19-20, 1994, pp. 192-204.

Liu M and Claridge D. (1998). Use of calibrated HVAC system models to optimize system operation. Journal of solar energy engineering, Vol.120, pp:131-138.

Liu M, Claridge D and Bensouda N et al. (2003). Manual of Procedures for Calibrating Simulations of Building Systems. http://buildings.lbl.gov/hpcbs/ Element_5/02_E5_P2_3_2.html.

Liu M, Claridge D and Song L. (2002). Draft report-potential of on-line simulation for fault detection and diagnosis in large commercial buildings with built-up HVAC systems, submitted to California Energy Commission. June, 2002.

Liu M, Song L and Claridge D et al. (2002). Development of whole-building fault detection methods. http://buildings.lbl.gov/hpcbs/pubs/E5P23T1c.pdf

Liu M, Song L and Wei G et al. (2004). Simplified building and air-handling unit model calibration and applications. Journal of solar energy engineering, Vol.121, pp:601-609.

Liu X and Dexter A. (2001). Fault-tolerant supervisory control of VAV air-conditioning systems. Energy and Buildings, Vol.33(4), pp:379-389.

Lorenzetti DM and Norford LK. (1992). Measured energy consumption of variable-air-volume fans under inlet vane and variable-speed-drive control. ASHRAE Transactions, Vol.98(2), pp:371-379.

Lunde J. (1980). Solar thermal engineering: space heating and hot water systems. John Wiley & Sons, Inc. USA.

May W. (1985). Verification of Public Domain Control Algorithms For Building Energy Management and Control Systems. Nat. Bur. (US) NBSIR 85-3285.

Minoru K. and Charles D. et al. (1995). Hourly thermal load prediction for the next 24 hours by ARIMA, EWMA, LR and an artificial neural network. ASHRAE transactions, Vol.101(1), pp:186-200.

Mitalas G.P. (1968). Calculation of transient heat flow through walls and roofs, ASHRAE Transactions, Vol.74, pp:182-188.

Mitchell M. (1997). An introduction to genetic algorithm. Cambridge, MA: The MIT Press.

Mui KW. (2002). Building environmental performance model for variable air volume systems in air-conditioned high-rise buildings in sub-tropical climates. PhD Thesis, The Hong Kong Polytechnic University.

Muneer T and Saluja G. (1986). Correlation between hourly diffuse and global solar irradiation for the UK. Building services engineering and technology, Vol.7(1), pp:37-43.

Myers G.E. (1971). Analytical methods in conduction heat transfer. McGraw-Hill, NY, 1971.

Myers G.E. (1980). Long-time solutions to heat conduction transients with time-dependent inputs. Journal of heat transfer, Vol.102, pp.115-120.

Nizet JL, Lecomte L and Litt FX. (1984). Optimal control applied to air conditioning in building. ASHRAE Transactions, Vol.90(1B), pp:587-600.

Norford L, Wright J and Buswell R et al. (2002). Demonstration of fault detection and diagnosis methods for air-handling Units. HVAC&R Research, Vol.8(1), pp:41-72.

NTIS. (1986). HVACSIM+ Building Systems and Equipment Simulation Program Reference Manual. Washington, DC: National Technical Information Services, U.S. Department of Commerce 1986.

Ouyang K. and Haghighat F. (1991). A procedure for calculating thermal response factors of multi-layer walls – state space method. Building and environment, Vol.26(2), pp.173-177.

Padhy N. (2001). Unit commitment using hybrid models: a comparative study for dynamic programming, expert system, fuzzy system and genetic algorithms. International Journal of Electrical Power & Energy Systems, Vol.23(8), pp:827-836.

Park. C, Kelly G, and Kao J. (1984). Economizer Algorithms for Energy Management and Control System. Nat. Bur. (US) NBSIR 84-2832.

Petermeier H, Benning R and Delgado A et al. (2002). Hybrid model of the fouling process in tubular heat exchangers for the dairy industry. Journal of Food Engineering, Vol.55(1), pp:9-17.

Piette M and Gartland L et al. (1998). Development and Testing of an Information Monitoring and Diagnostic System for Large Commercial Buildings. Proceedings of the 1998 ACEEE Summer Study on Energy Efficiency in

Buildings. Pacific Grove, CA: August, 1998.

Piette M, Kinney S, and Haves P. (2001). Analysis of an Information Monitoring and Diagnostic System to Improve Building Operations. Energy and Buildings Vol.33(8), pp:783-791.

Pullman N.J. (1976). Matrix theory and its applications, selected topic. Marcel Dekker, INC.

Rabl A. (1988). Parameter estimation in buildings: methods for dynamic analysis of measured energy use. Journal of solar energy engineering, Vol.101, pp:52-66.

Reddy T. (1989). Application of dynamic building inverse models to three occupied residences monitored non-intrusively. Proceedings of the ASHRAE DOE/BTECC/CIBSE conference, Thermal performance of the exterior envelopes of building IV. Dec. 4-7. Orlando, Florida, pp:654-671.

Reddy T and Claridge D. (1994). Using synthetic data to evaluate multiple regression and principal component analyses for statistical modeling of daily building energy consumption. Energy and buildings, Vol.21, pp:35-44.

Reddy T, Kissock J and Ruch D. (1998). Uncertainty in baseline regression modeling and in determination of retrofit saving. Journal of solar energy engineering, Vol.120, pp:185-192.

Reddy T, Liu M and Katipamula S et al. (1998a). Extending the concept of energy delivery efficiency (EDE) of HVAC systems. ASHRAE Transactions, Vol.104(1), pp:13-23.

Reddy T, Liu M and Claridge D. (1998b). A study of energy use and satisfactory zone ventilation of different outdoor air ventilation strategies for terminal reheat variable air volume systems. Energy and buildings, Vol.29, pp:65-75.

Ruch D and Chen L et al. (1993). A change-point principal component analysis (CP/PCA) method for predicting energy usage in commercial buildings: The PCA Model. Journal of solar energy engineering, Vol.115, pp:77-84.

Ruch D. and Claridge D. (1991). A four parameter change-point model for predicting energy consumption in commercial buildings. Proceedings 1991 ASME-JSES-JSME Int. Solar Energy Conf. 433-440.

Ruch D and Claridge D. (1993). A development and comparison of NAC estimates for linear and chang-point energy models for commercial buildings. Energy and buildings, Vol.20, pp:87-95.

Salomon R. (1998). Resampling and its avoidance in genetic algorithms. In Porto, V.W. et al., editors, Evolutionary Programming VII: Proceedings, 7th International Conference/EP 98, San Diego, California, 25–27 March 1998. Berlin: Springer, 335–44.

Sat SK. (2003). Use of thermal performance line for assessing and controlling energy performance of commercial building in Hong. PhD Thesis, The Hong Kong Polytechnic University.

Seem J, Klein S and Beckman W et al. (1989). Transfer functions for efficient calculation of multidimensional transient heat transfer. Journal of heat transfer, Vol.111:5-12.

Stein J and Hydeman M. (2004). Development and testing of the characteristic curve fan model. ASHRAE Transactions, Vol.110(1), pp:347-356.

Stephenson D.G. and Mitalas G.P. (1967). Cooling load calculations by thermal response factors. ASHRAE Transactions, Vol.73, pp:III1.1-III1.7.

Stephenson D.G. and Mitalas G.P. (1971). Calculation of heat conduction transfer functions for multilayer slabs. ASHRAE Transactions, Vol.77, pp:117-126.

Sowell E. (1988(a)). Classification of 200, 640 parameteric zones for cooling load calculation. ASHRAE Transactions, Vol.94(2), pp:754-777.

Sowell E. (1988(b)). Cross-check and modification of the DOE program for calculation of zone weighting factors. ASHRAE Transactions, Vol.94(2), pp:737-753.

Sowell E. (1988(c)). Load calculations for 200, 640 zones. ASHRAE Transactions, Vol.94(2), pp:716-736.

Sowell E and Chiles D. (1984(a)). Characterization of zone dynamic response for CLF/CLTD tables. ASHRAE Transactions, Vol.91(2A), pp:162-178.

Sowell E and Chiles D. (1984(b)). Zone descriptions and response characterization for CLF/CLTD calculations. ASHRAE Transactions, Vol.91(2A), pp:179-200.

Spitler J and McQuiston F et al. (1993(a)). Development of a revised cooling and heating calculation manual. ASHRAE Transactions, Vol.99(1), pp:175-182.

Spitler J and McQuiston F et al. (1993(b)). The CLTD/SCL/CLF cooling load calculation method. ASHRAE Transactions, Vol.99(1), pp:183-192.

Subbarao K. and Burch J. et al. (1990). How to accurately measure the load coefficient of a residencial building. Sol Eng 1990 Twelfth Annu Int Sol Energ Conf, 1990, pp:419-425.

Subcommittee for Heating and cooling Loads, ASHRAE Task Group on Energy Requirements. (1975). Subroutine Algorithms for Heating and cooling Loads to Determine Building Energy Requirements, February, 1975.

Swider D, Browne M, and Bansal P et al. (2001). Modelling of vapour-compression liquid chillers with neural networks. Applied thermal engineering, Vol.21, pp:331-329

Thamilseran S and Haberl J. (1995). A bin method for calculating energy conservation retrofit savings in commercial buildings. Proceedings 1995 ASME-JSES-JSME Int. Solar Energy Conf. 111-124.

Virk GS, Cheung JY and Loveday DL. (1995). Practical stochastic multivariable identification for buildings. Applied Mathematical Modelling, Vol.19(10), pp.621-636.

Wang FL, Yoshida H and Miyata M. (2004). Total energy consumption model of fan subsystem suitable for continuous commissioning. ASHRAE Transactions,

Vol.110(1), pp:357-364.

Wang SW. (1999). Dynamic simulation of a building VAV air-conditioning system and evaluation of EMCS online control strategies. Building and Environment, Vol.34(6), pp.681-705.

Wang SW and Chen YM. (2001). A novel and simple building load calculation model for building and system dynamic simulation. Applied Thermal Engineering, Vol.21, pp:683-702.

Wang S and Jin X. (1998). CO2 based occupancy detection for on-line outdoor airflow control. Indoor Built Environment, 1998(7) pp:165-181.

Wang SW and Jin X. (2000). Model-based optimal control of VAV air-conditioning system using genetic algorithm. Building and Environment, Vol.35(6), pp:471-487.

Wang SW, John B and Chong H. (1999). Experimental validation of CO2 based occupancy detection demanded-controlled ventilation. Indoor Built Environment, 1999(8), pp:377-391.

Wang SW and Wang J. (2002). Automatic sensor evaluation in BMS commissioning of building refrigeration systems. Automation in Construction, Vol.11(1), pp:59-73.

Wang SW and Wang JB. (2002). Robust sensor fault diagnosis and validation in HVAC systems. T I MEAS CONTROL, Vol.24(3), pp: 231-262.

Wang SW and Xiao F. (2004). Detection and diagnosis of AHU sensor faults using principal component analysis method. Energy Conversion and Management, Vol.45(17), pp:2667-2686.

Wang SW and Xu XH. (2003). Hybrid Model for Building Performance Diagnosis and Optimal Control. International Conference for Enhanced Building Operations. October, 2003, California, USA

Wang SW and Xu XH. (2004). Optimal and robust control of outdoor ventilation

airflow rate for improving energy efficiency and IAQ. Building and Environment Vol.39, pp:763-773.

Waters J.R. and Wright A.J. (1985). Criteria for the distribution of nodes in multilayer walls in finite-difference thermal modeling. Building and Environment, Vol.20(3), pp.151-162.

Wei G, Liu M and Claridge D. (1998). Signatures of heating and cooling energy consumption for typical AHUs. Fort Worth, TX: Proceedings of the Eleventh Symposium on Improving Building Systems in Hot and Humid Climates.

Wright J. (1995). Summary and comparison of methods to calculate solar heat gain. ASHRAE Transactions Vol.101(1).

Wu TX. and Thompson D. (2002). A hybrid model for the noise generation due to railway wheel flats. Journal of Sound and Vibration, Vol.251(1), pp:115-139.

Yik WH. (1997). Survey of energy end-use in commercial buildings in Hong Kong. Workshop on methodologies and data for energy demand and supply outlook, March 17-19, 1997 Tokyo,asia Pacific Energy Reserch Center, Japan.

Yik WH, Chung T and Chan K. (1995). A method to estimate diffuse radiation in Hong Kong and its accurancy. Transactions of The Hong Kong Institution of Engineers, Vol.2, pp:23-29.

Yoshida H, Kumar S and Morita Y. (2001). Online fault detection and diagnosis in VAV air handling unit by RARX modeling. Energy and Buildings, Vol.33(4), pp:391-401.

Yu B, Paassen D and Riahy S. (2002). General modeling for model-based FDD on building HVAC system.Simulation Practice and Theory, Vol.9, pp:387-397.

Zarem A. (1963). Introduction to the utilization of solar energy. New York: McGraw-Hill, 1963.

Zhou Y and Xu B. (2003). Blind source separation in frequency domain. Signal Processing, Vol.83(9), pp: 2037-2046

Zmeureanu R. (1990). Assessment of the energy saving due to the building retrofit. Building and Environment, Vol.25(2), pp:95-103.

Zmeureanu R. (1992). A new method for evaluating the normalized energy consumption in office building. Energy, Vol.17(3), pp:235-246.

APPENDIX A DEDUCTION OF TRANSMISSION MATRIX

A1 Transmission matrix of heat transfer of monolayer homogeneous plane wall
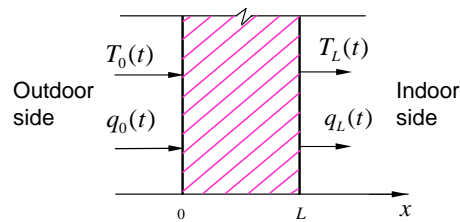
Figure A.1 Thermal system of monolayer homogeneous plane wall

Figure A.1 illustrates thermal system of monolayer homogeneous plane wall. Surface temperature and heat flow of both sides of the wall are the function of time t as follows.

Inside surface temperature $T(x,t)\big|_{x=L} = T_L(t)$

Inside heat flow $q(x,t)\big|_{x=L} = q_L(t)$

Outside surface temperature $T(x,t)\big|_{x=0} = T_0(t)$

Outside heat flow $q(x,t)\big|_{x=0} = q_0(t)$

There are four variables on both sides of the wall. Two of them are known functions while the other is to be solved. Assuming $T_0(t)$ and $q_0(t)$ are known, $T_L(t)$ and $q_L(t)$ are to be solved. Then the mathematic model of the binary linear

system is described as follows.

$$\begin{cases} \dfrac{\partial T(x,t)}{\partial t} = a\dfrac{\partial^2 T(x,t)}{\partial x^2} & (a) \\[2mm] q(x,t) = -\lambda\dfrac{\partial T(x,t)}{\partial x} & (b) \\[2mm] T(x,t)\big|_{t=0} = 0 & (c) \\[2mm] T(x,t)\big|_{x=0} = T_0(t) & (d) \\[2mm] q(x,t)\big|_{x=0} = q_0(t) & (e) \end{cases} \qquad (\text{A.1})$$

Laplace transform is used to solve the formula (A.1). Applying Laplace transform on the both sides of (a) in (A.1), we have

$$L\left[\frac{\partial T(x,t)}{\partial t}\right] = sL[T(x,t)] - T(x,0)$$
$$= sT(x,s) \qquad (\text{A.2})$$

and

$$L\left[a\frac{\partial^2 T(x,t)}{\partial x^2}\right] = a\int_0^{+\infty}\frac{\partial^2 T(x,t)}{\partial x^2}\cdot e^{-st}\cdot dt$$
$$= a\frac{\partial^2}{\partial x^2}\int_0^{+\infty} T(x,t)\cdot e^{-st}\cdot dt \qquad (\text{A.3})$$
$$= a\frac{\partial^2 T(x,s)}{\partial x^2}$$

where $L[T(x,t)] = T(x,s)$. It follows that:

$$sT(x,s) = a\frac{d^2 T(x,s)}{dx^2} \qquad (\text{Viewing } s \text{ as constant}) \qquad (\text{A.4})$$

Applying Laplace transform on the both sides of (b) in (A.1), we obtain equations (A.5) and (A.6).

$$L[q(x,t)] = q(x,s) \tag{A.5}$$

$$L\left[-\lambda \frac{\partial T(x,t)}{\partial x}\right] = -\lambda \frac{dT(x,s)}{dx} \tag{A.6}$$

then,

$$q(x,s) = -\lambda \frac{dT(x,s)}{dx} \tag{A.7}$$

Hence, the mathematic model of the binary linear system (A.1) is expressed in Laplace domain as follow.

$$\begin{cases} sT(x,s) = a \dfrac{d^2 T(x,s)}{\partial x^2} & (a) \\ q(x,s) = -\lambda \dfrac{dT(x,s)}{\partial x} & (b) \\ T(x,s)\big|_{t=0} = 0 & (c) \\ T(x,s)\big|_{x=0} = T_0(s) & (d) \\ q(x,s)\big|_{x=0} = q_0(s) & (e) \end{cases} \tag{A.8}$$

The expression (a) in (A.8) is a second order ordinary differential equation.

Letting

$$T(x,s) = e^{rx} \tag{A.9}$$

We find the general solution of (a) in (A.8)

$$T(x,s) = c_1' e^{x\sqrt{\frac{s}{a}}} + c_2' e^{-x\sqrt{\frac{s}{a}}} \tag{A.10}$$

With

$$\cosh(x\sqrt{\frac{s}{a}}) = \frac{1}{2}(e^{x\sqrt{\frac{s}{a}}} + e^{-x\sqrt{\frac{s}{a}}}) \tag{A.11}$$

$$\sinh(x\sqrt{\frac{s}{a}}) = \frac{1}{2}(e^{x\sqrt{\frac{s}{a}}} - e^{-x\sqrt{\frac{s}{a}}}) \tag{A.12}$$

and letting

$$c_1 = c_1' + c_2' \tag{A.13}$$

$$c_2 = c_1' - c_2' \tag{A.14}$$

The general solution of equation (a) in (A.8) is expressed in the form of hyperbolic functions as follows.

$$T(x,s) = c_1 \cosh(x\sqrt{\frac{s}{a}}) + c_2 \sinh(x\sqrt{\frac{s}{a}}) \tag{A.15}$$

Substituting the boundary condition (d) in (A.8) into (A.15), we get one coefficient.

$$c_1 = T_0(s) \tag{A.16}$$

Substituting the boundary condition (e) in (A.8) into (b) in (A.8),

$$\begin{aligned} q_0(s) &= -\lambda \frac{dT(x,s)}{x}\bigg|_{x=0} \\ &= -\lambda(c_1\sqrt{\frac{s}{a}}\sinh(x\sqrt{\frac{s}{a}}) + c_2\sqrt{\frac{s}{a}}\cosh(x\sqrt{\frac{s}{a}}))\bigg|_{x=0} \\ &= -\lambda c_2\sqrt{\frac{s}{a}} \end{aligned} \tag{A.17}$$

It follows that:

$$c_2 = -\frac{q_0(s)}{\lambda\sqrt{\dfrac{s}{a}}} \tag{A.18}$$

Therefore, the particular solution of (a) in (A.8) is yielded,

$$T(x,s) = T_0(s)\cosh(x\sqrt{\frac{s}{a}}) - q_0(t)\frac{\sinh(x\sqrt{\dfrac{s}{a}})}{\lambda\sqrt{\dfrac{s}{a}}} \tag{A.19}$$

Differentiating the equation,

$$\frac{dT(x,s)}{dx} = T_0(s)x\sqrt{\frac{s}{a}}\sinh(x\sqrt{\frac{s}{a}}) - q_0(t)\frac{\cosh(x\sqrt{\dfrac{s}{a}})}{\lambda} \tag{A.20}$$

Substituting the result into (b) in (A.4),

$$q(x,s) = -T_0(s)x\sqrt{\frac{s}{a}}\sinh(x\sqrt{\frac{s}{a}}) + q_0(t)\cosh(x\sqrt{\frac{s}{a}}) \tag{A.21}$$

We obtain the solutions of $T_l(t)$ and $q_l(t)$ when letting $x=L$. They are represented in matrix as follows.

$$\begin{bmatrix} T_l(s) \\ q_l(s) \end{bmatrix} = M(s)\begin{bmatrix} T_0(s) \\ q_0(s) \end{bmatrix} = \begin{bmatrix} A(s) & B(s) \\ C(s) & D(s) \end{bmatrix}\begin{bmatrix} T_0(s) \\ q_0(s) \end{bmatrix} \tag{A.22}$$

where $M(s)$ is the transmission matrix of thermal system of monolayer homogeneous plane wall, and

$$A = D = \cosh(L\sqrt{\frac{s}{a}}) \tag{A.23}$$

243

$$B = -\frac{\sinh(L\sqrt{\frac{s}{a}})}{\lambda\sqrt{\frac{s}{a}}} \tag{A.24}$$

$$C = -\lambda\sqrt{\frac{s}{a}}\sinh(L\sqrt{\frac{s}{a}}) \tag{A.25}$$

A2 Transmission matrix of heat transfer of multilayer homogeneous plane wall
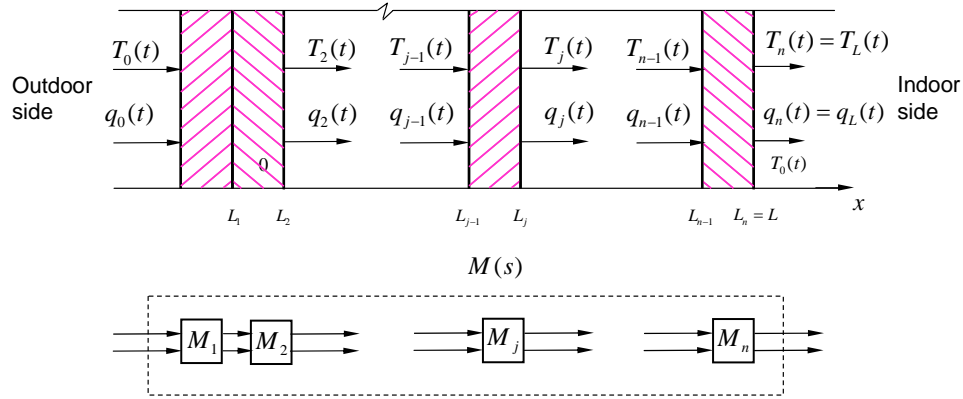
Figure A.2 Thermal system of multilayer homogeneous plane wall

Every layer of multilayer homogeneous plane wall contacts with each other tightly. Following the direction of heat flow, the response outputs of a certain layer are the inputs of next layer. Therefore, the total transmission matrix of thermal system of n-layer homogeneous plane wall can be expressed as follows.

$$M(s) = M_n(s)M_{n-1}(s)\cdots M_1(s) \tag{A.26}$$

A3 Transmission matrix of heat transfer of multilayer homogeneous plane wall with air films
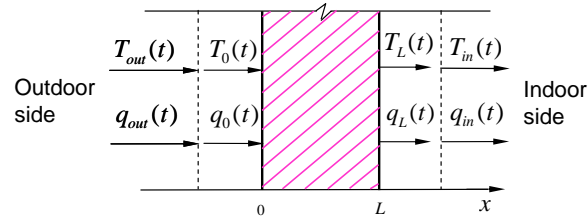
Figure A.3 Thermal system of multilayer homogeneous plane wall with air films

Air on both sides of wall contacts the both surfaces tightly. Heat exchange between air and wall's surface is conducted in an imaginary thin air film. Assuming air films are homogeneous, and their capacitors are neglected,

$$q_0(t) = q_{out}(t) \tag{A.27}$$

$$T_0(t) = T_{out}(t) - \frac{q_{out}(t)}{h_{out}} \tag{A.28}$$

Therefore, the transmission matrix of outside air film is

$$M_{out}(s) = \begin{bmatrix} 1 & -\dfrac{1}{h_{out}} \\ 0 & 1 \end{bmatrix} \tag{A.29}$$

Similarly, the transmission matrix of inside air film is

$$M_{in}(s) = \begin{bmatrix} 1 & -\dfrac{1}{h_{in}} \\ 0 & 1 \end{bmatrix} \tag{A.30}$$

The total transmission matrix of thermal system of n-layer homogeneous plane wall with air films on both sides can be read as follows.

$$M(s) = M_{in}(s)M_n(s)M_{n-1}(s)\cdots M_1(s)M_{out}(s) \tag{A.31}$$

APPENDIX B CALCULATION OF MATRIX POLYNOMIAL

Suppose an n-order square matrix A and a polynomial $f(\lambda) = \alpha_k \lambda^k + \alpha_{k-1} \lambda^{k-1} + \ldots + \alpha_1 \lambda + \alpha_0$ are given ($\alpha_k \neq 0$), and we want to evaluate $f(A) = \alpha_k A^k + \alpha_{k-1} A^{k-1} + \ldots + \alpha_1 A + \alpha_0$. Obviously, it may be difficult to do directly. However, one can use the Cayley-Himilton theorem to find $f(A)$.

Cayley-Hamilton Theorem [Pullman 1976]

If $Q(\lambda)$ is the characteristic polynomial of an arbitrary square matrix A, then $Q(A) = 0$.

Let $Q(\lambda)$ is the characteristic polynomial of the matrix A. If $f(\lambda)$ is divided by $Q(\lambda)$, one would obtain a quotient polynomial $p(\lambda)$ and a remainder $g(\lambda)$ such that for all λ,

$$f(\lambda) = p(\lambda)Q(\lambda) + g(\lambda) \tag{B.1}$$

where,

$$g(\lambda) = \beta_{n-1} \lambda^{n-1} + \beta_{n-2} \lambda^{n-2} + \ldots + \beta_1 \lambda + \beta_0 \tag{B.2}$$

The degree of $g(\lambda)$ is not larger than *n-1* because the degree of the divisor $Q(\lambda)$ is *n*. Therefore, by the Cayley-Hamilton theorem,

$$\begin{aligned} f(A) &= g(A) \\ &= \beta_{n-1} A^{n-1} + \beta_{n-2} A^{n-2} + \ldots + \beta_1 A + \beta_0 I \end{aligned} \tag{B.3}$$

Suppose the eigenvalues of A are $\{\lambda_1, \lambda_2, \cdots, \lambda_n\}$ and are distinct.

Let $\lambda = \lambda_i$, then obtain the system of equations

$$\begin{cases} \beta_0 + \beta_1 \lambda_1 + \ldots + \beta_{n-2} \lambda_1^{n-2} + \beta_{n-1} \lambda_1^{n-1} = f(\lambda_1) \\ \beta_0 + \beta_1 \lambda_2 + \ldots + \beta_{n-2} \lambda_2^{n-2} + \beta_{n-1} \lambda_2^{n-1} = f(\lambda_2) \\ \qquad\qquad \ldots \\ \beta_0 + \beta_1 \lambda_n + \ldots + \beta_{n-2} \lambda_n^{n-2} + \beta_{n-1} \lambda_n^{n-1} = f(\lambda_n) \end{cases} \tag{B.4}$$

Let:

$$\boldsymbol{\beta} = [\beta_0 \ \beta_1 \ \cdots \ \beta_{n-1}]^T \tag{B.5}$$

$$\boldsymbol{F} = [f(\lambda_1) \ f(\lambda_2) \ \cdots \ f(\lambda_n)]^T \tag{B.6}$$

$$\boldsymbol{Lamda} = \begin{bmatrix} 1 & \lambda_1 & \cdots & \lambda_1^{n-1} \\ 1 & \lambda_2 & \cdots & \lambda_2^{n-1} \\ \cdots & \cdots & \cdots & \cdots \\ 1 & \lambda_n & \cdots & \lambda_n^{n-1} \end{bmatrix} \tag{B.7}$$

The matrix **Lamda** is full rank. Therefore, the coefficients of the matrix polynomial are determined as follows.

$$\boldsymbol{\beta} = \boldsymbol{Lamad}^{-1} \cdot \boldsymbol{F}^T \tag{B.8}$$

APPENDIX C RUNGE-KUTTA ALGORITHM

To calculate the heat transfer of roof, external walls, and internal mass, the nodal temperature should be calculated first. The equations to represent the thermal transfer process of roof, external walls or the internal mass are the secondary order equations. They can be solved numerically with explicit Runge-Kutta algorithm.

For simplified 3R2C models of roof and external walls, they have the uniform form as illustrated in Figure 6.2. A simplified 3R2C model can be represented with the system of the secondary order differential equations as follows.

$$
\begin{cases}
C_2 \dfrac{dT_2(t)}{dt} = \dfrac{T_{out}(t) - T_2(t)}{R_1} - \dfrac{T_2(t) - T_4(t)}{R_3} \\
C_4 \dfrac{dT_4(t)}{dt} = \dfrac{T_2(t) - T_4(t)}{R_3} - \dfrac{T_4(t) - T_{in}(t)}{R_5}
\end{cases}
\tag{C.1}
$$

The system of linear ordinary differential equations can be rewritten as Equation (C.2) as follows.

$$
\begin{cases}
\dfrac{dT_2(t)}{dt} = \dfrac{-(R_1 + R_3)}{C_2 R_1 R_3} T_2(t) + \dfrac{R_1}{C_2 R_1 R_3} T_4(t) + \dfrac{R_3}{C_2 R_1 R_3} T_{out}(t) \\
\dfrac{dT_4(t)}{dt} = \dfrac{R_5}{C_4 R_3 R_5} T_2(t) + \dfrac{-(R_3 + R_5)}{C_4 R_3 R_5} T_4(t) + \dfrac{R_3}{C_4 R_3 R_5} T_{in}(t)
\end{cases}
\tag{C.2}
$$

This is also an inhomogeneous system of equations. The system is rewritten further as follows.

$$\begin{cases} \dfrac{dT_2}{dt} = a_{11}T_2 + a_{12}T_4 + a_{13}T_{out}(t) \\[2mm] \dfrac{dT_4}{dt} = a_{21}T_2 + a_{22}T_4 + a_{23}T_{in}(t) \end{cases} \qquad (C.3)$$

Where,

$$a_{11} = \frac{-(R_1 + R_3)}{C_2 R_1 R_3}, \quad a_{12} = \frac{1}{C_2 R_3} = \frac{R_1}{C_2 R_1 R_3}, \quad a_{13} = \frac{1}{C_2 R_1} = \frac{R_3}{C_2 R_1 R_3},$$

$$a_{21} = \frac{1}{C_4 R_3} = \frac{R_5}{C_4 R_3 R_5}, \quad a_{22} = \frac{-(R_3 + R_5)}{C_4 R_3 R_5}, \quad a_{23} = \frac{1}{C_4 R_5} = \frac{R_3}{C_4 R_3 R_5}.$$

This system of equations can be solved in discrete form with Runge-Kutta formula as follows.

$$\begin{cases} T_2(n+1) = T_2(n) + \dfrac{1}{6}(k_1 + 2k_2 + 2k_3 + k_4) \\[2mm] T_4(n+1) = T_4(n) + \dfrac{1}{6}(l_1 + 2l_2 + 2l_3 + l_4) \end{cases} \qquad (C.4)$$

Where,

$$k_1 = \Delta t[a_{11}T_2(n) + a_{12}T_4(n) + a_{13}T_{out}(n)] \qquad (C.5)$$

$$l_1 = \Delta t[a_{21}T_2(n) + a_{22}T_4(n) + a_{23}T_{in}(n)] \qquad (C.6)$$

$$k_2 = \Delta t\{a_{11}[T_2(n) + \frac{k_1}{2}] + a_{12}[T_4(n) + \frac{l_1}{2}] + a_{13}\frac{T_{out}(n) + T_{out}(n+1)}{2}\} \qquad (C.7)$$

$$l_2 = \Delta t\{a_{21}[T_2(n) + \frac{k_1}{2}] + a_{22}[T_4(n) + \frac{l_1}{2}] + a_{23}\frac{T_{in}(n) + T_{in}(n+1)}{2}\} \qquad (C.8)$$

$$k_3 = \Delta t\{a_{11}[T_2(n) + \frac{k_2}{2}] + a_{12}[T_4(n) + \frac{l_2}{2}] + a_{13}\frac{T_{out}(n) + T_{out}(n+1)}{2}\} \qquad (C.9)$$

$$l_3 = \Delta t \{ a_{21}[T_2(n) + \frac{k_2}{2}] + a_{22}[T_4(n) + \frac{l_2}{2}] + a_{23} \frac{T_{in}(n) + T_{in}(n+1)}{2} \} \qquad \text{(C.10)}$$

$$k_4 = \Delta t \{ a_{11}[T_2(n) + k_3] + a_{12}[T_4(n) + l_3] + a_{13}T_{out}(n+1) \} \qquad \text{(C.11)}$$

$$l_4 = \Delta t \{ a_{21}[T_2(n) + k_3] + a_{22}[T_4(n) + l_3] + a_{23}T_{in}(n+1) \} \qquad \text{(C.12)}$$

Where, Δt is time step and n indicate the time $n\Delta t$

When the nodal temperatures of 3R2C models of roof and external walls are to be calculated, the resistances and capacitances of the 3R2C model of roof or external walls replace the corresponding resistances and capacitances in Equation (C.1), the solar air temperature on the roof or the external walls replaces the outdoor air temperature T_{out}. Then the nodal temperatures can be calculated with Equation (C.4).

The procedure to calculate the nodal temperatures of the simplified 2R2C model of internal mass is similar to calculate those of simplified 3R2C models of roof and external walls. It is briefed as follows.

Equations (6.1) and (6.2) can be rearranged as follows.

$$\begin{cases} \dfrac{dT_{im,1}(t)}{dt} = -\dfrac{T_{im,1}(t)}{R_{im,1}C_{im,1}} + \dfrac{T_{im,2}(t)}{R_{im,1}C_{im,1}} + \dfrac{Q_{r,1}(t)}{C_{im,1}} \\ \dfrac{dT_{im,2}(t)}{dt} = \dfrac{T_{im,1}(t)}{R_{im,1}C_{im,2}} + \dfrac{-(R_{im,1}+R_{im,2})T_{im,2}(t)}{R_{im,1}R_{im,2}C_{im,2}} + \dfrac{Q_{r,2}(t)}{C_{im,2}} + \dfrac{T_{in}(t)}{R_{im,2}C_{im,2}} \end{cases} \qquad \text{(C.13)}$$

This is also an inhomogeneous system of equations. The system is rewritten as follows.

$$\begin{cases} \dfrac{dT_{im,1}}{dt} = a_{11}T_{im,1} + a_{12}T_{im,2} + a_{13}Y_{in1}(t) \\ \dfrac{dT_{im,2}}{dt} = a_{21}T_{im,1} + a_{22}T_{im,2} + a_{23}Y_{in2}(t) \end{cases} \qquad (C.14)$$

Where,

$$a_{11} = \frac{-1}{R_{im,1}C_{im,1}} \,, \quad a_{12} = \frac{1}{R_{im,1}C_{im,1}} \,, \quad a_{13} = 1 \,,$$

$$a_{21} = \frac{1}{R_{im,1}C_{im,2}} \,, \quad a_{22} = \frac{-(R_{im,1} + R_{im,2})}{R_{im,1}R_{im,2}C_{im,2}} \,, \quad a_{23} = 1 \,,$$

$$Y_{in1}(t) = \frac{Q_{r,1}(t)}{C_{im,1}} \,, \quad Y_{in2}(t) = \frac{Q_{r,2}(t)}{C_{im,2}} + \frac{T_{in}(t)}{R_{im,2}C_{im,2}}$$

This system can be solved with Runge-Kutta formula easily with Equation (C.4).

APPENDIX D DECOMPOSITION OF SOLAR RADIATION

To decompose the global solar radiation to diffusive radiation and direct normal solar radiation, solar angle and extraterrestrial solar radiation should be calculated first. The global solar radiation and extraterrestrial solar radiation refer to the solar radiation incident on horizontal surface. The calculation of solar angle and extraterrestrial solar radiation are given in **D1** and D**2** respectively. D**3** presents the calculation of diffusive solar radiation and direct normal solar radiation from the global solar radiation.

D1 Calculation of solar angle

Solar altitude angle is calculated as follows.

$$\sin(\alpha) = \cos(L)\cos(\delta)\cos(\omega) + \sin(L)\sin(\delta) \tag{D.1}$$

where, L is local latitude (degree) (+ for northern hemisphere, - for southern hemisphere), δ is solar inclination (degree), ω is hour angle (degree)

The following empirical equation can be used for calculation of solar inclination [Lunde 1980]

$$\delta = 23.45\sin[(\frac{DN-80}{370}) \times 360] \tag{D.2}$$

where, DN is the day number in the year (DN =1 for the 1st January)

Hour angle can be expressed as follows [Kimura 1977].

$$\omega = (t_s + \frac{L_s - L}{15} + e - 12) \times 15 \qquad \text{(D.3)}$$

where, t_s is hour expressed in local standard time (hour). L is local longitude (degree), for Hong Kong, east longitude $114^o10'$, Northern latitude $22^o18'$. (+ for west, - for east). L_s is longitude of the standard location of solar time (degree), equal to the product of time zone number multiplied by 15. For Hong Kong, the time zone number is -8 hours. e is the equation of time (hour)

The equation of time, which is an astronomical correction for irregularities in the earth's orbit, should be determined by the following table (Table D.1) (For northern hemisphere only) [Subcommittee for Heating and cooling Loads, ASHRAE Task Group on Energy Requirements, 1975].

Table D.1 Equation time for an astronomical correction

date	ET (equation of time, hours)
Jan. 21	-0.190
Feb. 21	-0.230
Mar. 21	-0.123
Apr. 21	0.020
May 21	0.060
Jun. 21	-0.025
Jul. 21	-0.103
Aug. 21	-0.051
Sept. 21	0.113
Oct. 21	0.255
Nov. 21	0.235
Dec. 21	0.033

D2 Calculate of hourly extraterrestrial solar radiation

Hourly extraterrestrial solar radiation is determined using Equation (D.4) as follows [Muneer and Saluja 1986].

$$I_0 = I_{sc} R \sin \alpha \qquad (D.4)$$

where, I_0 is hourly extraterrestrial radiation incident on a horizontal surface (Wh/m^2). I_{sc} is solar constant ($1370 Wh/m^2$) [ASHRAE 1993]. α is solar altitude angle at given time (degree). R is a parameter that accounts for the effect due to variation in the distance between the sun and earth in a year. It can be evaluated by the formula as Equation (D.5) [Muneer and Saluja 1986].

$$R = 1 + 0.033 \cos(2\pi \frac{DN}{365.24}) \qquad (D.5)$$

D3 Decomposition of solar radiation

Regression analysis was carried out by Lam and Li [1996] to correlate the ratio of diffuse solar radiation to global solar radiation (K) with the ratio of global solar radiation to extraterrestrial radiation (K_t) with Equation (D.4) for Hong Kong use. Table D.2 summarises the modelled regression equations for the three different periods.

$$K_t = \frac{I_{glob}}{I_0} \qquad (D.4)$$

Where, I_{glob} is global solar radiation.

Table D.2 Correlation between K and K_t

K_t region	Whole year	Cooling season	Heating season
$0.15 \geq K_t$	K=0.977	K=0.975	K=0.986
$0.15 < K_t \leq 0.7$	K=1.237-1.361 K_t	K=1.227-1.350 K_t	K=1.275-1.395 K_t
$0.7 < K_t$	K=0.273	K=0.272	K=0.280

The diffuse solar radiation can be calculated with Equation (D.5) when ratio of diffuse solar radiation to global solar radiation (K) is determined.

$$I_{dif} = K \cdot I_{glob} \qquad (D.5)$$

Where, I_{dif} is diffuse solar radiation, K is the ratio of diffuse solar radiation to global solar radiation, I_{glob} is global solar radiation

The direct normal solar radiation can be calculated as follows.

$$
\begin{aligned}
I_{dn} &= \frac{I_{glob} - I_{dif}}{\sin \alpha} = \frac{I_{glob} - K \cdot I_{glob}}{\sin \alpha} \\
&= \frac{(1-K)I_{glob}}{\sin \alpha}
\end{aligned}
\qquad (D.6)
$$

where, I_{dn} is direct normal solar radiation

APPENDIX E SOLAR AIR TEMPERATURE CALCULATION

Solar air (Sol-air) temperature is the temperature of the outdoor air that, in the absence of all radiation changes, gives the same rate of heat entry into the surface as would the combination of incident solar radiation, radiant energy exchange with the sky and other outdoor surroundings, and convective heat exchange with the outdoor air. Heat flux into an exterior sunlit surface can be expressed as follows according to heat balance at the sunlit surface.

$$q = \alpha I_t + h_o(T_o - T_s) - \varepsilon \Delta R \qquad (E.1)$$

where, q is heat flux into an exterior sunlit surface (W/m^2), α is absorptance of surface for solar radiation, I_t = total solar radiation incident on surface (W/m^2), h_o is coefficient of heat transfer by long-wave radiation and convection at outer surface ($W/(m^2 \cdot K)$), T_o is outdoor air temperature ($°C$), T_s is exterior surface temperature ($°C$), ε is hemispherical emittance of surface, ΔR is difference between long-wave radiation on surface from sky and surrounding and radiation emitted by blackbody at ourdoor air temperature (W/m^2).

Assuming the rate of heat transfer can be expressed in terms of the sol-air temperature T_{sol}.

$$q = h_o(T_{sol} - T_s) \qquad (E.2)$$

Substituting q in Equation (E.2) with Equation (E.1), the sol-air temperature can be solved as follows.

$$T_{sol} = T_o + \frac{\alpha I_t}{h_o} - \frac{\varepsilon \Delta R}{h_o}$$
(E.3)

Horizontal surfaces. For horizontal surfaces that receive long-wave from the sky only, an appreciate value of ΔR is about $63\ W/m^2$, so that if $\varepsilon = 1$ and $h_o = 17.0 W/(m^2 \cdot K)$, the long-wave correction term is about $-3.9\,°C$ (Bliss 1961).

Vertical surfaces. Because vertical surfaces receive long-wave radiation from ground and surrounding building as well as from sky, accurate ΔR values are difficult to determine. When the solar radiation intensity is high, surfaces of terrestrial objects usually have higher temperature than the outdoor air; thus, their long-wave radiation compensates to some extent for the sky's low emittance. Therefore, it's common practice to assume $\Delta R = 0$ for vertical surfaces [ASHRAE (a) 1997].

APPENDIX F CALCULATION OF WINDOW HEAT FLOW

To calculate the heat flow through windows, the angle of incidence (θ) of solar rays for any surface is calculated first as shown in **F1**.

F1 Calculation of the angle of incidence of solar rays for any surface

Solar azimuth ϕ measured from the due south is calculated in terms of declination, hour angle, and altitude as follows.

$$\cos\phi = \frac{\sin\alpha \sin L - \sin\delta}{\cos\alpha \cos L} \tag{F.1}$$

The azimuth position ϕ can also be given in terms of latitude, declination, and hour angle below [Zarem 1963].

$$tg\phi = \frac{\sin\omega}{\sin L \cos\omega - \cos(L)tg\delta} \tag{F.2}$$

The solar azimuth ϕ is positive for afternoon hours and negative for morning hours [ASHRAE 2001].

Surface solar azimuth γ is defined as follows.

$$\gamma = \phi - \psi \tag{F.3}$$

Where, ψ is the surface azimuth. Table F.1 gives the values for the surface azimuth ψ, applicable to the orientations of interest.

Table F.1 Surface orientations and azimuths, measured from south (degree)

Orientation	N	NE	E	SE	S	SW	W	NW
Surface azimuth ψ	180°	-135°	-90°	-45°	0°	45°	90°	135°

The angle of incidence θ for any surface is defined as the angle between the incoming solar rays and a line normal to that surface. For any surface, the incident angle θ is related to α, γ, and the tilt angle of the surface Σ by

$$\cos\theta = \cos\alpha\cos\gamma\sin\Sigma + \sin\alpha\cos\Sigma \qquad (F.4)$$

Where, Σ is the tilt angle of surface from horizontal.

When the surface is horizontal, $\Sigma = 0°$, and

$$\cos\theta_H = \sin\alpha$$

When the surface is vertical, $\Sigma = 90°$, and

$$\cos\theta_V = \cos\alpha\cos\gamma$$

F2 Calculation of window heat flow

Heat flows through windows via (1) conductive and convective heat transfer caused by the temperature difference between outdoor and indoor air; (2) solar radiation incident on the fenestration. The simplified basic equation can be used to calculate the instantaneous energy flow through a window as follows [ASHRAE 2001].

$$q = U_0 A_{pf}(t_{out} - t_{in}) + SHGC \cdot I_{dn} \cos\theta + SHGC_D \cdot I_{dif} \qquad \text{(F.5)}$$

Where, q is instantaneous heat flow (W), U_0 is overall coefficient of heat transfer (U-factor) ($W/(m^2K)$), T_{in} is interior air temperature ($^\circ C$), T_{out} is exterior air temperature($^\circ C$), A_{pf} is total projected area of a window (m^2), I_{dn} is direct normal solar radiation (W/m^2), I_{dif} is diffuse solar radiation (W/m^2), θ is the angle of incidence for any surface defined as the angle between the incoming solar rays and a line normal to that surface, $SHGC$ is solar heat gain coefficient for direct normal radiation (non-dimensional), $SHGC_D$ is solar heat gain coefficient for diffusive solar radiation (non-dimensional).

The center-glazing solar heat gain coefficients for single pane glass are given in Table H.2 [ASHRAE 2001]. The glazing SHGC values have been calculated using manufacturers' spectral data following methods developed by Finlayson and Arasteh [1993] and Wright [1995].

Table F.2 Glazing SHGC at specified incidence angles

Glass Thick (mm)	N 0°	N 40°	N 50°	N 60°	N 70°	N 80°	N 90°	H
3.2 Clear	0.86	0.84	0.82	0.78	0.67	0.42	0	0.78
3.2 Bronze	0.73	0.71	0.68	0.64	0.55	0.34	0	0.65
3.2 Green	0.70	0.68	0.66	0.62	0.53	0.33	0	0.63
3.2 Gray	0.70	0.68	0.66	0.61	0.53	0.33	0	0.63

Key: N=normal, H=hemispherical $SHGC= SHGC_D$

For angles other than those listed, straight-line interpolation can be used. SHGC is zero when the angle is 0 degree or the value other than 0~90 degree. For the convenience of calculation, the solar heat gain coefficient of the fenestration system uses the glazing SHGC.

PUBLICATIONS ORIGINATED FROM THIS STUDY

Journal Papers

2005   Shengwei Wang and Xinhua Xu. Simplified Building Model for Transient Thermal Performance Using GA-Based Parameter Identification. In print, International Journal of Thermal Sciences.

2005   Wangwei Wang and Xinhua Xu. Parameter Estimation of Internal Thermal Mass of Building Dynamic Models Using Genetic Algorithm. In print, Energy Conversion and Management.

2004   Wangwei Wang and Xinhua Xu. Optimal and robust control of outdoor ventilation airflow rate for improving energy efficiency and IAQ. Building and Environment, Vol.39, pp:763-773.

2004   Xinhua Xu, Shengwei Wang and Wen-zhong Shi. A robust sequencing control strategy for air-handling units. Building Services Engineering Research and Technology, Vol.25(2), pp:141-158.

2004   Xinhua Xu and Shengwei Wang. Optimal Nodal Placement of Simplified Models of Building Envelope Based on Frequency Domain Analysis. Submitted to Applied Thermal Engineering.

2004   Xinhua Xu and Shengwei Wang. A Simple Time Domain Calculation Method for Thermal Response Factors of Transient Heat Transfer Models. Submitted to Applied Mathematical Modeling.

2002   Shengwei Wang and Xinhua Xu. A robust control strategy for combining DCV control with economizer control. Energy Conversion and Management, Vol.43, pp:2569-2588.

Journal Papers under Preparation

2005   Shengwei Wang and Xinhua Xu. Performance signature-based diagnosis strategy for building performance evaluation and diagnosis.

2005   Shengwei Wang and Xinhua Xu. Building global energy evaluation tool for building energy performance evaluation of alternative fresh air control strategies.

2005   Shengwei Wang and Xinhua Xu. Semi-physical energy models for building performance benchmarking.

Conference Papers

2003   Shengwei Wang and Xinhua Xu. Hybrid Model for Building Performance Diagnosis and Optimal Control. International Conference for Enhanced Building Operations, 13-15/Oct. 2003, Berkeley California.

2003   Shengwei Wang and Xinhua Xu. Robust Ventilation Control for Building HVAC Performance Optimization. 3rd International Symposium on Heat Transfer Enhancement and Energy Conservation, Oct. 2003, Guangzhou.